THE FORMATION OF NEW ENGLAND COASTAL FRONTS

by

JOHN WILLIAM NIELSEN

B. S., Massachusetts Institute of Technology
(1984)

SUBMITTED TO THE DEPARTMENT OF
EARTH, ATMOSPHERIC, AND PLANETARY SCIENCES
IN PARTIAL FULFILLMENT OF THE REQUIREMENTS FOR
THE DEGREE OF

MASTER OF SCIENCE
IN METEOROLOGY

at the

MASSACHUSETTS INSTITUTE OF TECHNOLOGY

June 1987

Signature of Author_____
Department of Earth, Atmospheric, and Planetary Sciences
May 11, 1987

Certified by_____
Randall M. Dole
Thesis Supervisor

Accepted by_____
William F. Brace
Department Chairman

THE FORMATION OF NEW ENGLAND COASTAL FRONTS

by

JOHN WILLIAM NIELSEN

Submitted to the Department of Earth, Atmospheric, and Planetary Sciences
on May 11, 1987 in partial fulfillment of the requirements for the Degree of
Master of Science in Meteorology

ABSTRACT

Coastal fronts are a common late fall and early winter feature of the eastern New England weather pattern. Using data from a surface mesoscale network, we have been able to distinguish three specific types of coastal frontogenesis.

Type A coastal fronts form rapidly during cold air outbreaks as winds veer from offshore to onshore. The circulation is thermally forced, and differential friction may play a role in focusing the frontogenesis. Type B coastal fronts are also driven by heating from the ocean, but form during the evening as the land-sea contrast becomes large enough to support a circulation. Type C coastal fronts are forced by upstream blocking as a warm front approaches the Appalachian Mountains.

Coastal fronts are capable of persisting in coastal regions for days. A two-layer density current model has been constructed to investigate this behavior. Heating from the warm sea surface and increasing onshore winds were found to interact to produce quasi-stationary fronts for a wide range of environmental parameters.

Cold-air damming strengthens the temperature contrast and hinders inland movement of coastal fronts. A one-layer Lagrangian model was developed to simulate cold-air damming. Friction was found to play a critical role in the shape and flow patterns of the dammed air.

Coastal fronts should be expected to occur between 12 and 25 times a year in New England, and other parts of the world are also favorable for coastal frontogenesis. Guidelines for predicting the timing and location of coastal frontogenesis are presented.

Thesis Supervisor: Dr. Randall P. Dole

Title: Assistant Professor of Meteorology

CONTENTS

ACKNOWLEDGEMENTS

Rich Passarelli, Fred Sanders, and Speed Geotis helped to interest me in the problem of coastal frontogenesis. Many discussions with Peter Neilley and Steve Garner clarified the importance of the various mechanisms of coastal frontogenesis. Others who offered help when it was needed include Peter Baines and Kerry Emanuel, as well as Rob Black, Josh Wurman, Chris Davis, and Brad Lyon. My advisor, Randy Dole, was always ready with support and encouragement. But I dedicate this thesis to my parents, who believe in me.

This research was partially supported by NSF grants ATM-8209375 and ATM-8513935.

BIOGRAPHICAL NOTE

The author, John Nielsen, was born and raised near Richmond, Calif. He received his Batchelor's Degree from the Department of Earth and Planetary Sciences at MIT in June, 1984, and presently resides in Somerville, Mass. He had expected to complete this thesis long ago.

1. INTRODUCTION

1.1 Previous Observations of Coastal Fronts

The term 'coastal front' was given by Bosart *et al.* (1972) to an unusual late fall and early winter boundary layer feature in the New England area. They described coastal fronts as fronts which form locally near the coast and separate an easterly maritime air flow off the adjacent Atlantic from the cold northerly outflow of an anticyclone. They noted that coastal fronts often involve 10 K temperature contrasts over distances of 5-10 km. The fronts can be hundreds of kilometers long and typically persist for 12 hours in advance of East Coast cyclones, often separating frozen and non-frozen precipitation. Bosart *et al.* identified surface friction, orography, coastal configuration, and land-sea thermal contrast as being important factors to be considered in any theory of coastal frontogenesis.

Subsequent observations of New England coastal fronts have shown that the frontal temperature contrast can be as sharp as 5 K in 1 km (Clark, 1983; Sanders, 1983; Neilley, 1984). The frontal inversion levels off behind the surface front at an altitude of about 300-500 meters, comparable to the height of the adjacent Appalachian Mountains (Neilley, 1984), so that the cold air tends to be "trapped" between the front and the mountains. New England coastal fronts are most frequent in December, when the land-sea thermal contrast tends to be largest (Bosart, 1975). Coastal fronts have been associated with local enhancement of precipitation (Marks and Austin,

1979). Case studies of various New England coastal fronts are contained in Bosart *et al.* (1972), Bosart (1975), Marks and Austin (1979), Clark (1983), and Neilley (1984). Deformation calculations have consistently shown coastal frontogenesis to be an ageostrophic phenomenon.

Bosart *et al.* identified the Carolina and south Texas coasts as additional favored locations for coastal frontogenesis within the United States. A strong Carolina coastal front has been documented by Bosart (1981), and a Texas coastal front by Bosart (1984). Coastal frontogenesis can also occur in other parts of the world, such as the western edge of the Black Sea (Draghici, 1984), the southern coast of Norway (Fig. 6 of Bergeron, 1949), and the northwest coast of the Netherlands (Van den Berg, 1986). These locations all feature fairly straight or concave coasts, a climatological tendency for cold air to occasionally blow parallel to the coast with the warmer water on the left, and in most cases, higher terrain a short distance inland.

The critical mechanism for the onset of coastal frontogenesis in New England has been variously identified as differential friction (Bosart, 1975), differential heating (Ballentine, 1980), and upstream blocking by orography (Garner, 1986). A conclusive explanation has been impossible, however, due to the lack of observations of sufficient spatial and temporal density to resolve the 0.1-10 km scale aspects of coastal frontogenesis. The fronts, which can form within two hours and are generally about 1 km wide, often involve wind shifts of as little as 30 degrees and temperature differences of just 3 K. Such fronts can be entirely transparent to the regular hourly observing network in southern New England, and the Maine coast has but two regular hourly stations (PWM and NHZ). Coast Guard station observations improve the spatial resolution at the cost of temporal resolution, since observations are taken only every three hours.

1.2 The New England Winter Storms Experiment (NEWSEX)

Organized by the Massachusetts Institute of Technology (MIT), the New England Winter Storms Experiment took place between 1980 and 1983. The primary goals of NEWSEX were to obtain a better understanding of the organization of precipitation in winter storms and of the formation and behavior of coastal fronts.

The most extensive observing network of NEWSEX was operational during November and December of 1983. Fifteen PAM (Portable Automated Mesonet) stations were deployed across southeastern New England. Fig. 1.1 shows their locations, as well as the locations of hourly reporting stations, three-hourly Coast Guard stations, upper air stations, MIT, and other places mentioned in the text. The PAM stations have been assigned three-character codes, consisting of 'P' followed by a unique two-digit identifier which increases from north to south (tens digit) and from west to east (units digit).

The topography of the experimental region is shown in Fig. 1.2 . Observations were concentrated in a 150 km wide strip between the nearshore waters off the eastern coasts of New Hampshire and Massachusetts and the range of low mountains running southward through western New Hampshire into northeastern Connecticut. This range, 250-550 m high, will be referred to as 'the mountains' in the text. Note that the mountains run roughly parallel to the eastern coast of New England. This introduces an ambiguity into the discussion of coastal fronts; fronts which may be described as parallel to the coastline are also parallel to the mountains, potentially blurring the relationships between orographic features and frontal orientation.

The PAM stations transmitted data every five minutes via satellite to a base station, where the data were stored and made available for real-time analysis. Observations included peak wind speed, accumulated precipitation, and five-minute means of temperature, wet bulb temperature, wind speed,

wind direction, and station pressure. Wind measurements were made with a pair of propellers oriented north-south and east-west. The propellers were capable of measuring wind speed and direction even when sustained winds were less than 1 m/s. This sensitivity proved valuable for detecting circulation patterns on the cold air side of coastal fronts; winds were often so light that most hourly stations reported calm.

Also available through November and the first two weeks of December was an NCAR King Air, an airborne observing platform capable of higher speeds and longer flight times than the aircraft previously used by NEWSEX for studying coastal fronts. The King Air was used in part to make coastal front passes which were more extensive vertically and horizontally than those described by Neilley (1984). A rawinsonde launching site was established at MIT, but few launches were made due to a series of equipment failures. The MIT 10 cm Doppler radar was operational during NEWSEX, but the shallowness of coastal fronts prevented the radar from being used to directly observe frontal convergence patterns.

The NEWSEX mesoscale data set is superior to normally available data in two ways. First, the temporal resolution of the data makes it possible, for example, to determine to within an hour the time of frontal collapse. Until NEWSEX it had not been known whether coastal frontogenesis occurred within an established onshore airflow or as winds veered from offshore to onshore. This distinction is crucial for evaluating the importance of upstream blocking or frictional convergence. Second, analysis of the detailed structure of the frontal interface itself becomes possible. Direct observations by the King Air verify the density current nature of the coastal front. The temporal resolution of the PAM data during coastal front passages permits inference of the microscale surface wind and temperature structure. In principle, it should be possible as well to deduce from pressure data the shape of the coastal front inversion, but pressure perturbations associated with the coastal fronts which formed during NEWSEX (November and December, 1983) were weak.

1.3 Chapter Summary

This thesis will employ the NEWSEX mesoscale data set to examine coastal frontogenesis. Our objective is to determine the nature and causality of coastal frontogenesis in New England, in order to improve understanding and prediction of coastal fronts.

In Chapter 2, mesoscale analyses of three cases of coastal frontogenesis are presented to illustrate the characteristic types of New England coastal fronts and to show the process of coastal frontogenesis in greater detail than has previously been possible. Chapter 3 discusses the importance of a thermally direct coastal circulation in triggering most coastal frontogenesis events. In Chapter 4, the orographic influence of the Appalachian Mountains is described. The mountains slow the westward movement of land-breeze induced coastal fronts, and occasionally cause rapid "coastal" frontogenesis away from the coastline. Knowledge of the causes of coastal frontogenesis is applied in Chapter 5 to the problem of forecasting the formation and movement of coastal fronts. The principal conclusions are reviewed in Chapter 6, and application of the results to other geographical areas of coastal frontogenesis is discussed.

2. MESOSCALE ANALYSES OF COASTAL FRONT FORMATION

2.1 Introduction

Since the term 'coastal front' has not been explicitly defined in the literature, we adopted certain arbitrary criteria to distinguish coastal fronts from other fronts and from non-frontal systems. We required first that there be a clearly defined convergence zone, at most a few kilometers wide, separating two relatively homogeneous boundary layer air masses with differing winds and temperatures. The most unambiguous method of frontal detection was by observations of frontal passages at PAM stations, in which both temperature and wind changed rapidly within minutes. We required that the front be coherent and quasi-linear over a length of at least 100 km, with the front extending at least partly through the PAM network in eastern Massachusetts and southeastern New Hampshire. We required that the front form within 100 km of the Atlantic coast, and remain quasi-stationary within 100 km of the coast through most of its lifetime. Finally, we required that the temperature gradient across the front be positive toward the southeast; *i. e.*, that the warmer air be seaward.

During November and December of 1983, thirteen cases satisfied the above coastal front criteria. Approximately six coastal fronts were detected in real time with the help of the PAM network. The additional cases turned up in post-analysis.

Bosart (1975) classified New England coastal fronts according to five "synoptic categories" which represented the general synoptic situation at the time of frontogenesis. Since most coastal front cases share the common

feature of a cold anticyclone across northern New England, the synoptic categories were defined by the track and intensity of the advancing cyclones. Bosart constructed mean temperature and precipitation maps for the five categories and found, as might be expected, that temperatures and the pattern and amount of precipitation varied according to the type of storm. The temperature gradient pattern, the factor most directly affected by coastal fronts, varied little among the categories.

We abandon Bosart's classification system because our observations indicate that coastal frontogenesis bears little direct relationship with the characteristics of approaching cyclones. The classification system used throughout this paper was initially motivated by perceived differences in the location and timing of coastal frontogenesis relative to the establishment of an onshore airflow. It later became clear that there were dynamical differences as well.

The first type of coastal frontogenesis, most common among the thirteen frontogenesis events studied, takes place as gradient winds become onshore along the coast. The veering is ordinarily caused by the passage from west to east of a ridge of high pressure extending southward from a mobile anticyclone, although in two of the six cases the anticyclone passed directly over southern New England. During this "ridge passage" frontogenesis, also called type A, winds across inland New England remain northerly, setting up a convergence zone along the coast.

Type B or "evening onset" coastal frontogenesis occurs along the coast, as does type A, but it involves a different triggering mechanism. Prior to frontogenesis, winds are light and onshore (easterly or southerly) and temperature gradients are weak. As night falls, radiational cooling creates a temperature gradient along the coast. Inland winds back until they are northerly, and a coastal front soon forms. Type B coastal frontogenesis shares many common elements with the development of a land breeze; this relationship will be discussed in greater detail below.

The third and final type of coastal frontogenesis, termed type C or

"spontaneous" coastal frontogenesis, derives its name from the lack of an apparent triggering mechanism in the surface observations. The precursor environment is characterized by a warm southeasterly airflow which is not necessarily being heated by the adjacent coastal waters. The coastal front forms a few tens of kilometers inland, roughly halfway between the coastline and the first significant topographic ridge. The temperature difference across the front, weak at first, increases as a result of warm advection within the warm air.

Case studies of examples of all three types of New England coastal frontogenesis, selected for their representativeness as well as for the amount of data available, are given below. For completeness, we have reviewed previously published case studies of coastal fronts and attempted to categorize them on the basis of the available evidence. It appears that all cases analyzed in detail by Bosart *et al.* (1972), Bosart (1975), Clark (1983), and Neilley (1984) were ridge passage coastal fronts, with the exception of the spontaneous coastal front of December 4, 1968 in Bosart *et al.* The case studies presented below, which include PAM data, are the most detailed to date of New England coastal fronts.

In the mesoscale analyses (for example, Fig. 2.2), wind observations have been plotted at station locations in a nonstandard format: a long wind barb represents 1 m/s, a pennant represents 5 m/s. Temperatures are plotted adjacent to the station locations in degrees Fahrenheit. The pressure fields have been derived from reported altimeter settings and are subjectively analyzed in solid lines with a contour interval of 1 mb (100 Pa). To estimate systematic pressure errors, mean pressure maps were constructed from several periods with weak pressure and temperature gradients. The differences between the mean reported pressure at given stations and the interpolated mean pressure were taken to be systematic errors and have been subtracted from the observations. The errors were found to be typically 0.2 to 0.5 mb, and were consistent from week to week. The pressure analyses are based on the corrected altimeter settings, and the

NMC surface analyses have been used for guidance in data-poor regions and along the edges of the maps.

2.2 Ridge Passage (Type A) Coastal Front Formation

The synoptic weather situation at 0000 Dec. 4 (all times are GMT and all dates are 1983 unless otherwise specified) is shown in Fig. 2.1 . A large anticyclone was centered in southern Quebec just north of the border with New Hampshire and Vermont and had been moving eastward at about 15 m/s. The geostrophic wind direction in southern New England was northerly to northeasterly, parallel to the New Hampshire and eastern Massachusetts coasts, but was veering and developing an easterly component as the high progressed eastward. Skies over southern New England were clear to partly cloudy. A weak area of low pressure, which formed in the Gulf of Mexico, had moved to Kentucky. Frontal zones stretched eastward and southward from this system, but no fronts extended into the New England area at that time.

A mesoscale analysis of southern New England for the same time is shown in Fig. 2.2 . Winds were generally northwesterly in the eastern half of the map region and northerly in the western half. Winds along the coasts averaged twice the speed of winds inland. Some inland hourly stations were reporting calm conditions (indicated by a 'C'). At that time coastal regions were probably areas of divergence caused by the sudden change in surface friction across the coastline, but there is little offshore data available to confirm this. Temperatures were generally just above freezing along the coast and just below freezing inland, with lower temperatures to the north. The mesoscale pressure gradient was almost nonexistent; no half-millibar intermediate contours have been drawn because none could be found.

Three hours later (Fig. 2.3), as a consequence of the approach of the

anticyclone and the building of high pressure to the north, winds had veered substantially. The wind direction had become generally northeasterly across southwestern New England and Long Island, while winds were northerly at the Maine coast, Cape Cod, and BOS. Most of the remaining northwesterly winds were located along the eastern coasts of New Hampshire and Massachusetts, suggestive of a land breeze. Winds inland continued to be light. Temperatures have fallen by an average of 1-2 °C throughout the region.

By 0600 (Fig. 2.4), winds in the Long Island area had freshened and become uniformly northeasterly. Winds over eastern Massachusetts and New Hampshire, which had varied from westerly to easterly at 0300, now were more consistently from the north. Further inland, the wind was blowing down the Connecticut River Valley. The number of stations reporting calm conditions decreased from 11 to 3, but the bulk of that change was due to hourly stations shutting down for the night. Inland temperatures had fallen another degree or two, and small-scale temperature variations inland were becoming less apparent. Coastal and offshore temperatures had fallen little or remained steady, and a clear, systematic temperature gradient existed between coastal and inland regions.

A coastal front, depicted using the standard symbols for a stationary front, has been analyzed along the Gulf of Maine coast. The evidence within the 0600 observations for the existence of a coastal front is less than convincing: the windshift across the analyzed front is only about 40 degrees, there does not appear to be a consistent temperature gradient across the front, and it is necessary to include a suspicious-looking bend in the frontal position around the PAM observation at Gloucester. This frontal analysis is based primarily on data recorded during the succeeding several hours.

By 0900 (Fig. 2.5), the coastal front had become much more apparent. The coastal front was by that time west of the Gloucester PAM station. The windshift was greater than 90 degrees along the Massachusetts coast, and

the temperature difference across the front had reached 5 °C. Inland, wind speeds had increased substantially over three hours and had become almost uniformly northerly, a dramatic change from the disorganized breezes of 0300. Temperatures over land continued to become more uniform. Offshore winds were, on the average, almost easterly, and wind speeds offshore had also increased slightly.

During the next three hours, conditions on either side of the front changed little. At 1200 (Fig. 2.6), the front was located inland across Massachusetts, having just passed through Boston. Inland winds continued to blow from the north or north-northeast, parallel to the front and the mountains and down the pressure gradient, while offshore winds were more nearly in geostrophic balance. There had been a general slight increase in both wind speed and pressure gradient. The front in southern Maine was poorly observed, in part due to apparently erroneous wind observations at 26B and 447. The analyzed position is based primarily on temperatures. Observations with an instrumented aircraft three hours later, along the solid line running northwest-southeast through eastern New Hampshire in Fig. 2.6, revealed a well-developed frontal system near the Maine-New Hampshire border (Figs. 4.5-4.6).

Time series for selected stations (Figs. 2.7 and 2.8) reveal the details of the evolution of the flow patterns and the microscale structure of the surface front. (They also show many other interesting phenomena, but we shall limit our discussion to those features directly relating to the coastal front.) The wind velocity has been separated into two orthogonal components, designated u and v, with u positive toward 115 degrees and v positive toward 25 degrees. This system was based on the typical orientation of New England coastal fronts in the vicinity of the PAM network, and was designed so that u would be the wind component normal to coastal fronts.

Station P35 is included in both sets of time series and is representative of offshore conditions east of the coastal front. The wind at P35 veered steadily throughout the night from west-northwesterly to

easterly, and the temperature, except for variations on the order of minutes, was nearly constant at 1-2 °C. This was 3 °C cooler than the water temperatures at that time. Cold advection is being offset by increased surface heat fluxes caused by a lengthening overwater fetch. The surface pressure at P35 (not shown) reached a maximum, associated with the passage of the ridge, at 0400, at which time the wind direction at P35 was northerly.

The first definite coastal front passage in the PAM network was at station P25 (Fig. 2.7). The wind there, excluding frictional and other orographic effects, would have been expected to veer in a manner similar to the wind at P35. Friction would act to reduce wind speed and rotate the wind counterclockwise at P25 relative to P35 for westerly winds, while a similar rotation would occur at P35 for easterly winds. At 0000, the expected difference in wind direction can be seen. However, as the wind veered at P35, the difference increased, and by 0645 they differed by 70 degrees. During the next 50 minutes the wind at P25 proceeded to veer the entire 70 degrees, with more than half of the wind shift occurring in the final 15 minutes. The wind speed, 3.5 m/s before the shift, fell during the frontal passage to 1.5 m/s before recovering to 4 m/s as the wind became east-northeasterly. The frontal passage is indicated in the u wind component by a rapid change from 2 m/s to -2 m/s while the magnitude of the v component (not shown) decreased during the wind shift and recovered immediately afterwards. During the following hours, the winds at P25 and P35 again bore the expected similarities.

The temperature jump during the frontal passage coincides with the wind shift. This temperature jump, less than 1.5 K, is very small compared to most coastal front passages and most frontal passages in general. Before the frontal passage (see Fig. 2.4), P25 was warmer than any other station on the cold side of the coastal front. This anomalous warmth, and the resulting weak temperature gradient across the front, is a result of P25 being on a peninsula where air parcels in northerly flow must pass over water and be heated before reaching P25. The coastal front at that time was also only two

or three hours old, and the temperature gradient was still intensifying rapidly. There was also a hint of a frontal passage at 0455 at P25, suggestive of a coastal front in its infancy. The u wind component and temperature both deviated suddenly at that time those at P35 at that time.

The temperature change during the coastal front passage between 0910 and 0940 at station P34 (Fig. 2.8) was much sharper, almost 4 °C, because strong radiative cooling had been occuring at that station for several hours before the frontal passage. Otherwise, the frontal passage pattern is similar that at P25. The wind shift occurred at the same time as the temperature jump. Before the frontal passage, the wind direction was steady out of the northwest; after the wind shift, winds were stronger and began to veer gradually.

At about 0700, P34 had experienced a temperature jump of 3 °C. This was not another coastal front passage, though. The wind record shows that a half hour of 1.5 m/s wind from the north-northwest coincided with the temperature rise, and that after the wind died down again, the temperature fell. An extrapolation of the associated parcel trajectory shows that the warm air came from the direction of Massachusetts Bay, a heat source for boundary layer air during that night. The possibilities include an isolated blob of warm air advecting through the area, a temporary lowering of the nocturnal inversion to near ground level, or air turbulently mixed down from above the coastal front inversion.

The coastal front later passed stations P24 (Fig. 2.7) and P33 (Fig. 2.8) almost simultaneously. Conditions before and after frontal passage were nearly identical at the two stations. In both cases, the temperature rose 3.5 °C. The winds, nearly calm in both cases before frontal passage, concurrently developed a negative u component. The passage at P24 took 25 minutes, but the passage at P33 took 65 minutes, even though the front was moving faster at P33. This, combined with time series (not shown) from the adjacent hourly stations OWD and NZW, indicates that the frontal zone was broader at P33 than at P24. Crude estimates of the width of the frontal zone,

based on an assumed constant frontal speed between P25 and P24 and between P34 and P33, are 2.4 km at P24 and 7.8 km at P33. South of station P33 there is little surface data, but the hourly reports at PVD showed no sign of a frontal passage during the morning. The most intense part of the front was confined to the coastal areas north of Boston. During the morning, the southern portion of the front became broad and diffuse.

The 1200 Dec. 4 synoptic map is shown in Fig. 2.9. The anticyclone had moved to the northern tip of Maine, and geostrophic winds were southeasterly along the New England coast. The cyclone in the Midwest had reached Ohio, and a secondary low had formed along the Virginia-North Carolina border. Note that the New England coastal front was independent of the secondary low or the warm front, which both lay far to the south. Over the succeeding 18 hours, the secondary low deepened gradually and become the primary low. Instead of moving up the coast, it turned eastward and drifted out to sea, while the high in New Brunswick remained stationary. Consequently, the gradient wind in New England backed to northerly, and the coastal front, which had moved inland as far as P23 during the afternoon, proceeded back out to sea.

This coastal front is typical of the six coastal fronts during NEWSEX which formed along the coast as the winds became onshore. Analyses of these ridge passage coastal fronts share the following features:

* Air mass temperatures are colder than sea surface temperatures.

* The coastal front forms quickly (1-2 hours) as easterly winds develop offshore.

* Winds inland organize themselves parallel to the mountains during the first few hours of frontogenesis, changing little afterwards.

* The temperature difference across the front is due to the convergence of air parcels which have experienced differential heating.

* The fronts form locally along the coastline, are strongest in the vicinity of the New Hampshire coast, and tend to move inland after they form.

2.3 Evening Onset (Type B) Coastal Front Formation

At 1800 on Nov. 14 (Fig. 2.10), the center of a weak anticyclone was located just northeast of Maine. A low pressure center was east of Cape Hatteras, NC, and moving eastward without intensifying. A developing frontal system in the Midwest was also moving slowly eastward. Skies over New England were mostly cloudy, with light rain to the south.

The high north of New England had moved east from the Great Lakes region, following a route similar to that of the high associated with the devopment of the coastal front on Dec. 4 (compare with Fig. 2.1). A similar coastal front had formed at about 0200 Nov. 14 along the Gulf of Maine coast, between stations P13 and P14, east of P25, and between P34 and P35. The front moved inland during the night past P25 and P34, but traveled eastward past P14. During the morning of Nov. 14, the front dissipated *in situ* as the temperature gradient was destroyed by diurnal heating over land and winds on the inland side of the front veered from northerly to northeasterly.

Temperatures were fairly uniform across southern New England by that afternoon, as seen in the mesoscale analysis for 2100 (Fig. 2.11). The temperature gradients which did exist can be accounted for by differences in elevation and by differences in parcel trajectories, with air passing over the Gulf of Maine being heated two or three degrees before reaching eastern Massachusetts. Winds showed no sign of being deflected southward along the mountains and instead curved anticyclonically around the weak inverted ridge. Coastal winds were generally stronger than winds inland, and there was no evidence of confluence along the coast.

During the three hours ending at 0000 Nov. 15 (Fig. 2.12), temperatures fell by an average of 1 °C at the inland locations, but remained steady at those locations having an overwater fetch. Winds at most coastal locations had also varied little. Inland, however, winds had backed ten to

fifty degrees and were nearly parallel to the mountains. Wind speeds had decreased as well. The overall wind pattern bears a resemblance to the pattern of 0600 Dec. 4 (Fig. 2.4), but no front has been analyzed because there is no clear temperature discontinuity or windshift line and the available time series data (particularly at stations P25 and P33) does not support the existence of a frontal zone.

By 0300 (Fig. 2.13), inland winds, having continued to back, had become parallel to the mountains. Temperatures had fallen an additional degree in most inland locations. Offshore conditions, as represented by observations in Cape Cod and southeastern Massachusetts, remained unchanged. The coastal front had formed by this time. The sharp temperature gradient and wind shift from east to north which define the front lay between P13 and P14, P24 and P25, and P33 and NZW.

The front had not moved past any observing stations by 0600 (Fig. 2.14), and conditions immediately on either side of the frontal zone had changed little. Well inland, the development of the frontal circulation pattern had completed with the initiation of northerly winds at P23 and P31. Overall, temperatures had stabilized. During the next six hours (not shown), few changes of temperature or wind could be found on the cold side of the front, while the easterly airflow on the warm side of the front weakened somewhat. The coastal front itself drifted slowly seaward, passing PAM stations P14, P25, and (temporarily) P34.

On a larger scale (Fig. 2.15), the low to the south had moved eastward off the map and the frontal system in the Midwest had progressed toward the East Coast. But the high just north of New England had remained stationary, and the pressure gradient along the New England coast had not changed. This illustrates a characteristic of evening onset coastal frontogenesis: it is not dependent upon changes in or motions of synoptic-scale weather features.

The location of coastal frontogenesis, the subsequent motion of the front, and the wind patterns on both sides of the front were nearly identical

to the type A coastal front which had formed the previous night. But type A coastal frontogenesis occurs when a ridge passage causes the gradient wind to veer onshore. In this case, as in other type B coastal fronts, the front formed in preexisting onshore flow. The land-sea temperature contrast was initially very small and grew as a result of nocturnal cooling, with temperatures over land falling 2 to 3 °C while maritime temperatures remained constant. Coastal convergence was set up by an ageostrophic backing of inland winds until they blew roughly parallel to the mountains.

The evolution of the coastal front can be seen in Fig. 2.16 . Stations P22 and P34 have been selected because they show the differences between the landward and seaward sides of the coastal front most clearly. The plots run from midday of Nov. 14 to dawn of Nov. 15. During the evening, the temperature at P22 fell more than 2 °C, doubling the temperature difference between it and P34. The temperature leveled off at P22 at 0200. The change in wind direction lagged the temperature change, with the wind backing most rapidly between 0100 and 0600. Confluence about the axis of the coastal front existed from about 0100 onward. Just before 0900, the coastal front passed P34. The temperature fell 2.5 °C, and the wind shifted sharply. Winds at the two stations were now quite similar, and the temperature difference had become comparable to what it was before coastal frontogenesis. Two hours later, the coastal front moved back inland past P34, and the temperature and wind shifts were reversed. During the next few hours (not shown), the coastal front dissipated in a manner similar to the previous day's coastal front. The wind at P22 veered to easterly, and the temperature rose diurnally.

Evening onset coastal frontogenesis, such as the example above, occurred three times during NEWSEX. The common features are:

* Air mass temperatures during the day are comparable to marine air temperatures. This characteristic is required to either dissipate any coastal front which had formed earlier or to prevent the formation of a ridge passage coastal front if the ridge passage occurs during the day.

* Radiational cooling establishes a land-sea temperature contrast. The more nearly parallel the ambient winds are to the coastline, the sharper the temperature gradient will be and the more likely a coastal front will be to form. Stronger onshore winds lead to weaker temperature gradients.

* Winds inland back until they are northerly. There is some evidence that the backing occurs first near the frontogenetical region and propagates toward the mountains.

* The coastal front forms rapidly along the coast.

* Once formed, the front and associated circulation patterns are essentially indistinguishable from those of ridge passage coastal fronts.

It is one of our conclusions that evening onset coastal fronts form as a land-breeze-like circulation. On the other hand, the evening onset coastal front described above evolved so much like a land breeze that it is necessary to justify calling it a coastal front. The *a priori* justification is that what we are calling evening onset coastal fronts, once formed, are indistinguishable from ridge passage coastal fronts, and that ridge passage coastal fronts account for the majority of coastal fronts observed during NEWSEX and the vast majority of coastal fronts previously described in the literature. This alone does not, however, eliminate the possibility that such coastal fronts are simply misnamed land breezes. A more physical justification is that the mountains inland, while apparently irrelevant to the initial formation of the coastal front, have a strong effect on the flow of the cold air, the coastal front inversion, and the motion of the coastal front. This latter point will be discussed at length in Chapter 4.

2.4 Spontaneous (Type C) Coastal Front Formation

The most dramatic case of type C coastal frontogenesis during NEWSEX took place on Nov. 24-25. The weather pattern prior to frontogenesis is shown in Fig. 2.17 . Unlike the other two cases, this weather map features a

mature cyclone, which had deepened explosively over land while traveling northward up the Mississippi River and across the Great Lakes. A long cold front, with moderate amounts of precipitation ahead of it, lay from upstate New York along the Appalachian Mountains and into the Gulf of Mexico. An elongated ridge of high pressure was offshore at about 63W. Warm onshore flow prevailed along the entire Eastern Seaboard. A short warm front was analyzed north of New England. As with most warm fronts of similar form and location, the front was not easily detectible in the surface data east of the Appalachians.

At 1500 (Fig. 2.18), most southern New England locations had moderate southerly or southeasterly winds. The warmest temperatures were to the south and the coldest were in the interior and to the north. Anomalous regions include the Connecticut River Valley, where light drainage winds were blowing down the valley from the north, and the Maine coast, where remnants of a possible overnight land breeze remained.

The primary differences between this situation and conditions on Nov. 14 are: the ambient wind direction is from the south-southeast rather than the east-northeast, and the land temperatures are warmer, not slightly colder, than Gulf of Maine sea surface temperatures. The latter difference, in the absence of substantial nocturnal cooling, precludes formation of a thermally-driven coastal front along the shoreline like the one that formed on Nov. 15.

Three hours later (not shown), temperatures had increased 1-2 degrees Celsius and winds were unchanged. By 2100 (Fig. 2.19), though, a light northwesterly wind had developed at station P21, and the southerly component of the wind was significantly reduced at other inland stations such as ORH, P31, P22, and P23. Winds in the Connecticut River Valley remained northerly.

Similar winds existed at 0000 Nov. 25 (Fig. 2.20). Station P31 also was reporting northwesterly winds by this time. Despite nightfall, temperatures had risen in most of southern New England. The warm advection from the

south would continue for the next 15 hours. Temperatures had not risen and would not rise at those stations which had northerly or northwesterly winds.

There was by 0000 a convergent, confluent, quasi-linear zone east of P21 and P31 and stretching southeastward across central Connecticut. The temperature difference across the northern part of the confluence zone was 1.5 °C. This was the incipient coastal front. Time series data, part of which will be presented later, was used to determine at what time the convergence line became frontal in character (as defined in section 2.1). The PAM data indicates that no front had formed in Massachusetts by this time, but the situation in Connecticut is uncertain. Hourly observations are made only along the immediate coast and in the Connecticut River Valley, so it is difficult to distinguish local winds from frontal circulations. We make the conservative assumption that no front exists in Connecticut unless there is evidence of continuity with a front in adjoining regions which are not so data-sparse.

As a result, when the front does form in south-central Massachusetts by 0300 (Fig. 2.21), we have analyzed the front across central Connecticut as well. The uncertainty of the frontal location is indicated by the broken stationary front symbol, while the dashed line to the north indicates a convergence zone which had not yet collapsed into a front. East of the coastal front, temperatures had begun rising more rapidly than before, and the temperature jump across the front appears to be 5 °C. West of the front, temperatures had remained static. The moderate southeasterlies had become southerlies, with even some southwesterly winds present in the Long Island area. The anomalous observation at ORH is due to its 300 m elevation; the analyzed frontal position should be interpreted as the location of the surface front at valley level.

The front continued to develop rapidly, and at 0600 (Fig. 2.22) it extended well into Maine. The temperature difference across the front continued to grow as a result of increasing temperatures in the warm air

and unchanging temperatures in the cold air. The sea, at this time, was cooling the boundary layer air above it, and as a result temperatures were relatively cool on Cape Ann, the Isles of Shoals, and Cape Cod and the adjacent islands. Winds on the cold side of the coastal front had by this time become generally northwesterly; although they veered slightly the rest of the night, they never reached the mountain-parallel state of the other two coastal front cases.

On a larger scale, the cyclone north of the Great Lakes (not shown) had filled substantially. Its trailing cold front had reached the East Coast, and a secondary low had developed east of Virginia. This secondary would proceed to deepen explosively and track up the coast. The synoptic cold front moved east across New England between 1000 and 1300, eliminating the temperature difference across the coastal front and leading to the rapid disappearance of the coastal front.

The first set of time series (Fig. 2.23), from P31 and P32, shows the early stages of frontogenesis. Initially, conditions at the two stations were similar, with southwest winds of 2 m/s and 9 °C temperatures. Between 2100 and 2200, the wind shifted at both stations to much lighter, easterly winds. The strong warm advection began at P32 shortly before 2300. Over the following half hour, the winds at P32 returned to their prior state of southeasterly, while at P31, the wind became northerly. As the wind shifted at P31, the temperature dropped slightly, suggesting the passage of a newly-formed coastal front. Through the next few hours, the temperature graph at P31 is almost perfectly flat, while at P32, the temperature rose at the rate of over 1 degree per hour, so that by 0300 the two stations were 5.5 °C apart, despite being spatially separated by only 23 km. The front between the two stations eventually moved eastward, passing P32 at 1010 and causing the temperature there to fall 3.9 °C in 15 minutes.

Frontal passages involving the coastal front in various stages of formation can be seen in Fig. 2.24. The stations depicted are the northernmost row of PAM stations, in southeastern New Hampshire. During

the evening, the region of nearly stagnant, relatively colder air propagated eastward down the sloping terrain. The windshift at station P11 was gradual and occurred over a period of nearly two hours. As the shift began, the rate of temperature rise decreased by half. The windshift was complete at 0130, at which time the windshift began at station P12. This indicates that the convergence zone, still too broad to be called a front, was the size of the station separation, 15 km.

Instead of backing in a continuous manner, the wind at P12 backed to easterly, then decreased to nearly dead calm, then increased from the north. The duration of this transition was about 90 minutes. As the wind started backing, the rate of temperature rise decreased as it had at P11, and the temperature fell 0.5 °C suddenly as the wind picked up out of the north.

At station P13, the windshift took place between 0345 and 0445, a period of only one hour. The leading edge of the frontal zone also took longer to travel from P12 to P13, although the station separation is also 14 km. Assuming a smoothly changing frontal velocity, the monotonic decreases in windshift duration imply that the frontal zone was rapidly shrinking and would approach an absolute discontinuity between 0600 and 0700 (see Fig. 2.25). The windshift at P13 occurred in two nearly instantaneous phases. The first shift was from southeasterly to easterly and was accompanied by a 0.6 °C temperature drop. We regard this as the leading edge of the coastal front zone. The second shift was from easterly to northerly, and appeared to be related to a second, somewhat slower temperature decline.

The passage of the mature coastal front can be seen in the time series of P23 and P24 (Fig. 2.26). P23 undergoes the now-familiar gradual windshift from easterly to westerly between 0015 and 0350, while the temperature at P24, 25 km to the east, continued to rise. The temperature at P24 eventually reached 15.5 °C near 0700. The coastal front passage occurred at P24 at 0720, and was accompanied by a nearly instantaneous wind shift

from southerly to northwesterly and a temperature drop of 3.5 °C in fifteen minutes. After the frontal passage, winds at P24 and P23 were nearly identical. The temperature at P24 continued to decline and eventually approached that at P23.

Spontaneous coastal front events, such as the one described above, possess the following characteristics:

* Air temperatures are comparable to or warmer than sea surface temperatures.

* Large-scale warm advection is occurring, often accompanied by radiational cooling at the surface.

* The coastal front forms inland near the base of the mountains, tens of kilometers from the seacoast.

* The first manifestation of coastal frontogenesis is a sudden decrease of wind speed or reversal of wind direction at inland stations. The winds on the cold side of the coastal front tend to become northwesterly rather than northerly or northeasterly.

* The temperature difference is generated by warm advection on the warm side of the front.

* Frontal collapse takes place over a period of a few hours.

Common features of all three types of coastal fronts are:

* Large-scale winds are onshore; *i. e.*, between east-northeasterly and southerly.

* Inland winds suddenly change direction and become highly ageostrophic with respect to the large-scale pressure gradient.

* The formation of coastal fronts takes only a few hours, not one half to one day as stated by Bosart (1975, p. 977).

* The fronts are independent of any synoptic-scale frontal systems.

* Because of their small scale and slow speeds, coastal fronts might easily escape detection by a standard meteorological network.

3. RELATIONSHIP BETWEEN LAND-SEA BREEZES AND COASTAL FRONTS

3.1 Causes of Differences between Land and Sea Breezes

It has been suggested above that the initial stages of evening onset coastal frontogenesis are similar to a land breeze. A land breeze is generally regarded as the nighttime half of a diurnal circulation driven by radiative heating and cooling of a land surface adjacent to a body of water. Coastal fronts have elements in common with sea breezes as well, and we now briefly mention the primary differences between land and sea breezes and discuss causes for these differences.

Sea breezes, the term given to the daytime half of the circulation, are better documented than land breezes. Typical horizontal scales are 100-200 km and typical vertical scales are 1-2 km (Atkinson, 1981). Land breezes are the poor cousin of the sea breeze; they tend to be shallower and weaker, and have a smaller horizontal extent. Defant (1951) attributed this to two factors, one of which is relevant here: the difference in stability caused by surface cooling vs. surface heating.

Linear models of the land-sea breeze which specify symmetric, sinusoidal surface heating are antisymmetric about day and night, but they do indicate a relationship between the environmental static stability and certain characteristics of the diurnal circulation. Rotunno (1983) found, for inviscid linear models and mid- to high-latitudes, that the horizontal wind normal to the coast

$$U \approx N^{-1} (f^2 - \omega^2)^{-1/2} \qquad (3.1)$$

and the horizontal scale of the circulation

$$X \approx N h (f^2 - \omega^2)^{-1/2} \quad , \qquad (3.2)$$

where N is the Brunt-Vaisala frequency, f is the frequency of the pendulum day, ω is the frequency of the calendar day (the diurnal forcing), and h is the vertical scale of the heating (h also determines the vertical scale of the circulation, Z). Ueda (1983), using a viscous linear model, also found that U was inversely proportional to N, but that X varied with $N^{0.774}$ and that Z was independent of N. The inverse dependence of U on N has also been found in numerical simulations (*e. g.*, Patrinos and Kistler, 1977). A rough estimate of the relative strengths of land and sea breezes due to stratification differences can be made by taking the environmental stability to be the mean of the stabilities over land (N_1) and sea (N_2). If we assume N_2 is constant and N_1 varies between $N_1 = 0$ (sea breeze) and $N_1 = 2\ N_2$ (land breeze), we obtain

$$U_{\text{sea breeze}} = 3\ U_{\text{land breeze}} \quad . \qquad (3.3)$$

The simultaneous increase in horizontal scale and decrease in horizontal wind speed caused by an increase in N results in smaller gradients of wind and temperature and implies that sea breeze fronts should be more likely to occur than land breeze fronts. Indeed, in numerical models with no ambient wind and gradual diurnal heating variations, land breeze fronts tend to be nonexistent (Neumann and Mahrer, 1971; Gross, 1986).

Pearson (1975) generated land (sea) breeze fronts in a numerical

model by uniformly cooling (heating) a 1.25 km high by 82 km long rectangle of air. The resulting density currents were unequal despite equal (and opposite) amounts of heat transfer: the calculated maximum velocities at the edge of the rectangle were > 6 m/s for the sea breeze and < 4 m/s for the land breeze. The difference, Pearson showed, is due to differences in added potential energy. Heating a volume of air adjacent to the ground generates three times as much available potential energy than cooling.

A third cause for differences between land and sea breezes is the diurnal variation in eddy diffusivities implied by the difference between heating and cooling (Mak and Walsh, 1976). As the stability is increased at night, vertical transfer of heat is inhibited, which limits the vertical extent of the land breeze and the total magnitude of cooling. Also, the increased kinetic eddy diffusivity would reduce the magnitude of the velocities associated with the land breeze.

3.2 Comparison with Coastal Fronts

Directly or indirectly, all explanations for land-sea breeze differences are related to the fact that sea breezes are a result of adding heat to the boundary layer air and land breezes are a result of removing heat fron the boundary layer air. Because the density difference in type A coastal fronts is due to heating of the boundary layer, the appropriate analog is the sea breeze. Unlike an ordinary sea breeze, in which the heating occurs over land, type A coastal fronts involve air heated over water. As a result, the circulation is in the opposite direction. Hence, we describe type A coastal fronts as an inverted sea breeze. Similar heating-driven land breezes have been found over Lake Michigan (Passarelli and Braham, Jr., 1981; Ballentine, 1982).

Evening onset coastal fronts (type B) appear to occupy an intermediate position between land and sea breezes. The cooling of air over

land is the triggering mechanism. But two of the evening onset cases occurred less than eight hours after the passage of a ridge. Ridge passage frontogenesis had been suppressed at that time by diurnal heating over land, which reduced the temperature difference between land air and marine air. But even at the time of frontogenesis, the marine air had been over water only a few hours and was being heated from below. The third evening onset case was the one described in Chapter 2; although onshore flow had existed for 20 hours before frontogenesis, the flow was northeasterly and anticyclonic: according to observed wind directions, maritime air parcels reaching the Massachusetts coast had originated along the Maine coast, and their overwater trajectories were only 150-300 km.

Soundings taken during the first few hours of coastal frontogenesis of each of the three evening onset cases are shown in Figs. 3.1-3.3 . The air at Chatham is representative of conditions offshore. Parcels have advected there from the southern Gulf of Maine, and should be a couple of degrees warmer than parcels near the region of coastal frontogenesis because of slightly warmer sea surface temperatures and longer over-water trajectories. The Portland soundings show conditions a few miles inland of the frontogenesis region.

In all three cases, the boundary layer air at Chatham is neutrally bouyant (or nearly so) to a depth of about 1 km. Boundary layer air at Portland is also nearly neutral. The average stability $N = (g/\Theta_o \; d\Theta/dz)^{1/2}$ of the lowest 500m at Portland for the three cases is 0.57×10^{-2} sec^{-1}. Surface temperatures at Portland were lower than Gulf of Maine sea surface temperatures, and for one of the frontogenesis cases (Dec. 12), the air was still several degrees below the local sea surface temperatures by the time it reached Chatham, despite weak sea surface temperature gradients.

3.3 Null Cases of Coastal Frontogenesis

There were ten ridge passage events during NEWSEX. Six were associated with the immediate formation of a type A coastal front. Of the other four, two occurred during late morning under circumstances of boundary layer heating over land and over water. Evening onset coastal frontogenesis followed, and soundings for the two cases have been discussed in the preceding section. Coastal frontogenesis was not associated with the remaining two ridge passages (although spontaneous coastal frontogenesis did eventually take place in the onshore flow).

Soundings for one of the null ridge passages (Nov. 21) are presented in Fig. 3.4 . Unlike the evening onset cases (Figs. 3.1-3.3), the boundary layer temperature structure is stable. The bulk stability parameter N = 1.9 x 10^{-2} s^{-1} for the lowest 1 km. Portland has developed an inversion just above the surface, but the potential temperature of the air at the top of the inversion is as warm as nearby sea surface temperatures. This implies that the mean marine boundary layer temperature is at least as warm as the sea surface, so no heating can occur offshore. Any thermally driven coastal circulation that would form in this environment would have the character of a land breeze, driven by nocturnal cooling. No such circulation was observed by the station network, which is not surprising considering the comparative weakness of land breezes relative to sea breezes.

Unfortunately, the PAM data is incomplete for the Nov. 21 case, and it is impossible to perform a mesoscale analysis of the period in which the land breeze would have been developing. The other null ridge passage case occurred two days later, on Nov. 23, and it is that one which we present in detail here as an example of the evolution of the New England coastal boundary layer during the initial stages of onshore flow, in the absence of offshore heating.

The synoptic-scale ridge was directly over New England at 1800 Nov. 23 (Fig. 3.5). Sky conditions were clear or scattered, and the ridge was long

and broad, col-like, with weak pressure gradients: ideal conditions for radiative cooling that evening. Because of the light winds, any coastal circulation should have been easy to detect with the mesonetwork.

Due to the broadness of the high pressure center, the switch from offshore to onshore flow did not occur in an orderly fashion. Fig. 3.6 shows the conditions in southern New England at 1800. The map is unusual for the near total lack of temperature gradient. Between the northern and southern edges of the map the temperature changes by at most 2 °C. Stations experiencing onshore flow tended to be slightly colder than stations inland, unlike the situations before type A or type B coastal frontogenesis described in Chapter 2. Winds were generally northerly and light. Southerlies or southeasterlies were reported at BOS (Boston) and 25B (Portsmouth Harbor). These were not temporary, isolated eddies; by 2100 (not shown) the wind had become southerly or southeasterly across half of southern New England. In some cases, such as at station P25, the switch to southeasterlies came suddenly with a drop in temperature of 1 °C: a late November sea breeze!

At 0000 Nov. 24 (Fig. 3.7), the ridge line, as indicated by the winds and pressure, lay across western Maine and Cape Cod. Temperatures had already fallen by 4-8 degrees inland and by 2-3 degrees along the coast. At most stations in the interior of Massachusetts, Connecticut, and New Hampshire, wind speeds had dropped to less than 1 m/s. Despite the recently-developed coastal temperature contrast, there is no evidence of a land breeze.

Twelve hours later (Fig, 3.8), the southerly coastal wind speeds had increased, while inland the winds remained light and variable. In Maine, offshore winds had persisted throughout the night. This was probably a land breeze or slope breeze, but the lack of better than three-hourly observations along the Maine coast prevent investigation of the details of the circulation, such as whether there was a land breeze front. No land breeze existed in New Hampshire or Massachusetts. During the next three hours, the nocturnal inversion disippated and southerly winds were established at most inland locations (see Fig. 2.18).

Time series data for this null coastal front case is shown in Fig. 3.9 . Station P25 experienced the sea breeze front at 1910. After that time, the temperature at P25 was steady at between 7 and 8 °C, and the wind direction veered from easterly to southerly with gradually increasing wind speeds. The nearest inland station, P24, cooled rapidly during the early evening, reaching 0 °C at 0100. The temperature difference between P24 and P25 was larger than at any time during the Nov. 15 and Dec. 4 coastal fronts, but no northerly or northwesterly wind developed at P24. The nocturnal inversion was so strong at P24 that the sustained wind was not larger than 0.5 m/s at any time during the night. The light winds frequently caused only one of the two orthogonal propellers to turn, forcing the observed wind direction to be one of the four cardinal directions and causing the apparent rapid changes in wind direction. The sudden end to falling temperatures halfway through the night was probably related to the overcast conditions which developed across southern New England between 0300 and 0600.

The third station in the set of time series is P13. P13 was the only PAM station to show a persistent seaward wind during the night. Between 0500 and 1000, the wind at P13 was between 270 and 360 degrees at 1 m/s. This light seaward wind is a far cry from the organized coastal front circulations described earlier, and at 1000 the wind became calm again without any indication of a frontal passage. This may have been a land breeze, a drainage wind, or a combination of the two.

It would be difficult to find a more ideal situation for a land breeze to form in southern New England. The NEWSEX evidence suggests that pure land breezes do not often form along the southern New England coasts, and those that do, like the one possibly observed at P13 on Nov. 24, are not robust enough to organize themselves into coastal fronts. When the inland air starts out warmer than the marine air, as on Nov. 21 and Nov. 23, there appear to be two factors hindering the development of a land breeze coastal front. First, the overall static stability of the lower atmosphere is larger, which reduces the potential intensity of any direct coastal circulation.

Second, the inland surface air must undergo nocturnal cooling to a greater extent than would be necessary if the sea air were warmer, forming a stronger, shallower nocturnal inversion and creating isolated pools of shallow, stagnant cold air in low-lying areas.

3.4 Temperature and Wind Considerations

The heating of the boundary layer by the sea surface appears to be a key element in establishing a coastal temperature contrast and destabilizing the air on what will become the warm side of the coastal front. In cases of evening onset coastal frontogenesis, the final triggering mechanism is the cooling of the inland boundary layer during the early evening. A hybrid circulation then forms, which has the sense of a land breeze but otherwise more closely resembles a sea breeze. Evening onset coastal fronts therefore occur within a narrow range of onshore flow conditions. If the air is too warm, no breeze develops. If the air is too cold, a ridge passage coastal front forms immediately as the onshore flow begins. Finally, the onshore component of the wind must not be too strong, or the coastal temperature gradient would be spread out over such a broad area that no opposing thermally-direct circulation could develop.

For ridge passage coastal fronts, unlike evening onset coastal fronts, the land-sea contrast is already large enough to cause a direct circulation without the additional effect of radiative cooling. Sea breezes form under light offshore wind conditions when the temperature difference is as small as 1-3 °C (Watts, 1955). In southern New England, individual case studies of the vertical structure of sea breezes (Craig *et al.*, 1945; Fisher, 1960) have found well-developed sea breeze circulations with air temperature differences of 5 °C. This is at the low end of observed land-sea temperature differences during type A coastal frontogenesis (see Fig. 5.3).

The triggering mechanism for type A frontogenesis is the onshore veering of the ambient winds. Because the wind plays such an important role in initiating frontogenesis, we now examine the effects the ambient wind is known to have on sea breeze formation. The relationship is not as well understood as one might hope.

Some observational studies have seemed to indicate that the presence of a moderate ambient wind from any direction suppresses sea (or lake) breeze formation. Biggs and Graves (1962) obtained the semiempirical relationship that a lake breeze at the western end of Lake Erie will not form when

$$U^2 > \approx 3\, C_p\, \Delta T \quad , \tag{3.4}$$

where ΔT is the land-lake temperature difference, U is the ambient wind speed, and C_p is the heat capacity of air at constant pressure. They excluded cases with ambient winds coming off the lake. However, the local coastline is far from linear and the variations substantially reduce the temperature gradient even when the wind is parallel to the lakeshore.

Lyons (1972) applied Biggs and Graves' model to Lake Michigan. His observations were made in the central lakeshore regions, where the shoreline is nearly straight. Lyons found that lake breezes occurred on one or both sides of the lake when

$$U^2 < \approx 10\, C_p\, \Delta T \quad . \tag{3.5}$$

Winds parallel to both lakeshores were observed not to have as much of an inhibitory effect on lake breeze formation as winds blowing across the lakeshores. Lyons was able to improve the accuracy of the sea breeze index by multiplying any velocities within 30 degrees of the orientation of the shoreline by a factor of 3/8.

It seems plausible that coastline-parallel winds should have less of an impact on sea breeze formation than coastline-normal winds. In an inviscid model with a straight, infinitely long coastline, it is plain that a wind parallel to the coast can have no effect on the sea breeze circulation (Pearson *et al.*, 1983). Walsh (1974), in his linear model, found the observed U^2 relationship between wind speed and the existence of a sea breeze, but only when U was taken to be the speed of the offshore component of ambient wind. Variations in the coastline are potentially significant, however. McPherson (1970) found in his numerical study that with coastline-parallel winds, a bay increases the intensity of the sea breeze front upwind and decreases it downwind. The analogous situation for a coastal front would be a peninsula, such as Cape Ann or Cape Cod.

Walsh also found that offshore winds produce stronger temperature gradients and vertical velocities at the leading edge of the sea breeze, *i. e.*, a stronger sea breeze front. Conversely, a decreased response and decreased gradients are found in linear (Ueda, 1983) and non-linear (Physick, 1976) models to a following wind. Generation or enhancement of sea breeze fronts by offshore winds has often been observed (*e. g.*, Frizzola and Fisher, 1963; Helmis *et al.*, 1987) and calculated indirectly by numerical models (*e. g.*, Pielke, 1974), which because of lack of resolution determine frontal intensity indirectly by maximum vertical velocities and grid-point temperature differences. Estoque (1962) modeled sea breezes forming in calm conditions and with ambient geostrophic winds parallel to and normal to the coastline. The strongest front, which was slightly more intense than the front with no geostrophic wind, was associated with offshore winds. Onshore winds weakened the gradient considerably. Winds parallel to the coastline had little effect.

As for the relationship of the speed of the sea breeze front to the speed of the coastline-normal wind, Pearson *et al.* (1983) attempted to model that problem directly with an inviscid model and found gravity current behavior with constant c - u, where c is the speed of the front and u is the

speed of the normal wind. However, in Pearson *et al.*'s model the heating was turned off after only three hours. Two-dimensional models with a more realistic surface heating boundary condition, such as that of Kozo (1982), show that fronts tend to stall just onshore, with cross-shore velocities changing little in response to an increase in ambient wind speed.

The failure of Pearson *et al.* to correctly model the relationship between the speed of the ambient wind and the speed of the sea breeze front was due to the non-linear interaction between the heating, the location of the sea breeze front, and the frontal velocity. If the speed of the sea breeze front relative to the warm air is of the opposite sign and larger than the speed of the warm air, the sea breeze travels inland. The cold air behind the sea breeze comes in contact with the land surface and is heated from below, reducing the temperature difference across the front and causing a reduction of the relative speed. A stronger opposing wind can lead to a larger relative frontal speed because the front will not travel as far inland and the temperature difference across the front will be preserved. The air and sea temperatures set a maximum relative frontal speed for a given frontal depth, and no sea breeze can occur when the opposing winds are above this maximum.

Observations of sea and land breeze fronts have shown them to be density currents (Simpson, 1969; Mitsumoto *et al.*, 1983; Schoenberger, 1984). The speed of a density current relative to the earth can be written as the sum of the speed relative to the environmental air and the speed of the environmental air:

$$c = u_0 + c_r \quad . \tag{3.6}$$

The formula for a density current formed by a dense homogeneous fluid traveling through a lighter fluid is (Benjamin, 1968)

$$c_r = K (g h \Delta\rho / \rho)^{1/2} \quad , \tag{3.7}$$

where h is the depth of the density current, $\Delta\rho$ is the is the density difference between the two fluids, and ρ is the density of the heavier fluid. In the atmosphere the formula becomes

$$c_r = K (g^* h)^{1/2} \quad , \tag{3.8}$$

where g* is the 'reduced gravity' defined as

$$g^* = g \Delta\Theta / \Theta_0 \quad , \tag{3.9}$$

where Θ_0 is a reference potential temperature or virtual potential temperature, and $\Delta\Theta$ is the potential temperature difference across the density current. K is a proportionality constant which for inviscid theory is equal to $2^{1/2}$, but is generally between 0.6 and 1.3 for laboratory experiments and atmospheric density currents.

Neilley (1984) has made aircraft observations of two type A New England coastal fronts eight to ten hours after formation. He found that both coastal fronts had a density current structure. Neilley's estimates of K for the two fronts were 1.03 and 1.11.

3.5 A Two-layer, Density Current Model of Ridge Passage Coastal Frontogenesis

The above considerations lead us to hypothesize that ridge passage coastal fronts, like sea breezes, develop as density currents with speeds

relative to the ambient wind given by (3.8). We hypothesize that the rapid amplification of the temperature difference across such fronts is caused by a near-superposition of the coastal front and the discontinuity of diabatic heating at the coastline. We further hypothesize that the quasi-stationary behavior of ridge passage coastal fronts is caused by an approximate equilibrium between the intensifying onshore wind and the increasing temperature difference across the front.

To determine whether typical air temperatures, sea surface temperatures, and wind patterns are capable of interacting to form quasi-stationary type A coastal fronts like those observed during NEWSEX, a simple boundary-layer model has been constructed. The coastline is taken to be straight, infinitely long, and oriented north-south with the sea to the east. The topography is flat. The coastal front is assumed to be a density current whose speed in the eastward (positive x) direction is given by

$$c = u_2 + K (g h_1 (\Theta_2 - \Theta_1)/\Theta_2)^{1/2} \quad , \tag{3.10}$$

where subscripts 1 and 2 represent cold air and warm air values, respectively, and the other symbols are as in (3.8) and (3.9). The location X of the coastal front as a function of time is obtained by integrating

$$c\,dt = dX \quad . \tag{3.11}$$

This is done by calculating c for a given time t and frontal location X, stepping forward in time by an amount Δt:

$$t = t + \Delta t \quad , \tag{3.12}$$

and calculating the new location from

$$X_{(t+\Delta t)} = X_{(t)} + c\,\Delta t \quad . \tag{3.13}$$

The iteration is then repeated by calculating c from the values of temperature and wind speed at the new time and frontal location.

The warm air boundary layer is assumed to be well mixed in both potential temperature and wind up to a fixed height h_2. The assumption of a well-mixed boundary layer is consistent with sounding data from Chatham. For the warm air wind velocity, we take the simple case of constant wind speed U_2. To simulate the passage of a ridge, we take the wind direction to be westerly until time t = -L, to veer steadily through northerly to easterly until t = L, and to remain easterly for t > L. The component of wind normal to the front is therefore

$$u_2 = U_2 \quad , \quad t < -L \tag{3.14a}$$

$$u_2 = -U_2 \sin(\pi t / 2L) \quad , \quad -L <= t <= L \tag{3.14b}$$

$$u_2 = -U_2 \quad , \quad t > L \quad , \tag{3.14c}$$

while the component parallel to the front is

$$v_2 = -U_2 \cos(\pi t / 2L) \quad , \quad -L <= t <= L \tag{3.15a}$$

$$v_2 = 0 \quad , \quad \text{otherwise} \quad . \tag{3.15b}$$

Vertical heat fluxes are taken to be zero over land (x < 0). The vertical heat fluxes over water are assumed to decrease linearly with height to zero at the top of the boundary layers, so that the thermodynamic equation for both the warm and cold air is

$$d\Theta/dt = 0 \quad , \quad x < 0 \tag{3.16a}$$

$$d\Theta/dt = Q_{z=0}/h \quad , \quad x >= 0 \tag{3.16b}$$

In integral form,

$$\Theta - \Theta_0 = \int (Q/h)\, dt \quad , \tag{3.17}$$

where the limits of integration are determined by the time the air parcel is over water.

The surface heat flux parameterization is based on Deardorff's (1972) formulation for an unstable planetary boundary layer. Calculation of Deardorff's friction and heat transfer coefficients for ranges of h, Θ, and u found in coastal front situations indicated that Deardorff's Eq. 27 can be approximated to within about 15 percent as

$$Q \approx (A + B\,U)(\Theta_s - \Theta) \tag{3.18}$$

with appropriate selection of the constants A and B (see Table 3.1, below), and where Θ_s is the sea surface temperature.

To obtain an expression for the potential temperature of the warm air, we combine (3.16) and (3.18):

$$d\Theta_2/dt = h_2^{-1} (\Theta_s - \Theta_2)(A + B\,U) \tag{3.19}$$

Rearranging,

$$d(\ln(\Theta_s - \Theta_2)) = -h_2^{-1} (A + B\,U_2)\, dt \quad . \tag{3.20}$$

We integrate (3.20) from t_0, the time the warm air first crossed the coast, to t_c, the time the air recrossed the coast (or the current time, if the air is still

over water) :

$$\ln(\Theta_s - \Theta_2) - \ln(\Theta_s - \Theta_o) = -h_2^{-1} (A + B U_2) (t_c - t_o) \quad , \qquad (3.21)$$

where Θ_o is the initial potential temperature of the air over land. Solving for Θ_2,

$$\Theta_2 = \Theta_s - (\Theta_s - \Theta_o) \exp \{ h_2^{-1} (A + B U_2) (t_c - t_o) \} \quad . \qquad (3.22)$$

Because of the simplicity of (3.14), t_c and t_o may be obtained directly for any t and X. Thus, the temperature of the warm air can be determined analytically at any time and location. The temperature gradient implied by (3.22) is always positive toward positive X, and at t = 0 the entire gradient is offshore, with maximum temperature gradient adjacent to the coast. As t increases, the temperature gradient is advected in the negative X direction toward the density current, while the heating offshore continues.

Determination of the temperature of the cold air requires further approximations. The total wind speed within the cold air U_1 is needed to solve (3.17), and the component of the wind normal to the front u_1 is needed to determine the limits of integration of (3.16). We assume a constant vertical cold air velocity profile. From PAM observations of ridge passage coastal fronts over water, we take

$$v_1 = v_2 \quad . \qquad (3.23)$$

For the eastward component of the cold air wind we employ a relation representing an average of laboratory and atmospheric data for density currents, obtained from Simpson and Britter (1980, Fig. 4):

$$u_1 = 1.2\,c - 0.2\,u_2 \quad . \tag{3.24}$$

In order to simulate the thermally forced offshore flow at the coast and to simplify the integration, we specify a minimum value for u_1:

$$u_1 >= u^o_1 \quad . \tag{3.25}$$

This constraint affects the motion of the coastal front indirectly, by ensuring that a constant supply of cold air reaches the coastal front during the first few hours of integration. Without (3.25), the front initially moves offshore, but the cold air is quickly heated to the temperature of the warm air and the 'front' is then passively advected downwind. We assume that in the atmosphere, differential heating behind the front, acting on nearly stationary air, would induce a direct circulation and reinforce the front.

The bulk of the computation time is used for integrating (3.17) numerically for the temperature of the cold air when the coastal front is over water. This is done using (3.24)-(3.25) and subject to the condition

$$\Theta_1 = \Theta_0 \quad , \quad x < 0 \quad . \tag{3.26}$$

To perform the integration, the previously calculated values of u_1 and U_1 must be stored in one-dimensional arrays.

The model is initialized at t = 0 with the position of the coastal front X = 0. In other words, the front is taken to be located at the coastline at the moment ambient winds are precisely parallel to the coastline. No starting temperature difference is imposed across the front, but a temperature difference rapidly forms and the front moves offshore during the first hour of integration. The parameters of the model, with the values used in the

'control' model run, are given in Table 3.1.

TABLE 3.1

Control run parameters, density current model

A	0.004 m sec^{-1}	Δt	10 sec
B	0.015	U_o	7.5 m sec^{-1}
h_1	300 m	$u^o{}_1$	1.0 m sec^{-1}
h_2	1000 m	Θ_o	270 K
K	1.0	Θ_s	277.5 K

With a Δt of 10 seconds, a 24 hour model integration requires an average of 3 minutes of CPU time on a MicroVax II computer. To check the sensitivity of the model to the time step, a run was made with Δt = 100 seconds. The increased time step had little effect; the difference in position of the coastal front after 18 hours compared to the control run was less than a tenth of a kilometer. We conclude that little accuracy is being lost with our discretization of time.

The values for h_1 and K are based on the airplane observations of two coastal fronts by Neilley (1984). Neilley found coastal front depths of 300m - 350m. A similar coastal front depth was found for the Dec. 4 case (see Chapter 4). Here we use the low value of 300m because it appears that the upper portion of the cold air is modified by turbulent exchange with the overlying warm air. We take K to be 1.00 both for simplicity and as a minor adjustment toward Simpson's (1969) average sea breeze value of K = 0.62. Simpson and Britter (1980, see their Fig. 3) show a relationship between K and u_2. It has been stated (Seitter, 1986) that their results imply that u_2

should be multiplied by 0.62 in (3.10); however, the relationship is not a linear one and for $u_2 < 0$ (as is the case with coastal fronts), the multiplier approaches 1.

The depth of the warm air boundary layer h_2 is an average value taken from rawinsonde observations during NEWSEX. The veering time L is a typical value. Θ_0 was kept fixed at 270 K for all model runs while Θ_s was varied. Since the important parameter is $\Theta_s - \Theta_0$, similar results would have been obtained had Θ_0 been allowed to vary instead. Also varied over a wide range was U_2.

A similar density current model has been constructed by Simpson *et al.* (1977) to compare to observations of a sea breeze front. Simpson *et al.* specified the temperature of the warm air to conform with observations, and for the cold air they assumed a sinusoidal surface heating function whose amplitude was specified to result in temperatures which agreed with observations. The cold air wind speed was taken to be constant, an assumption which was justified by the data. The density current phase speed equation was integrated numerically, and the computed frontal positions were in general agreement with the observed frontal motions. In particular, Simpson *et al.* confirmed their hypothesis that an observed slowing of the sea breeze front at midday was due to rapid heating of the cold air over land.

The modeled frontal speed and position, using the control parameters, are shown in Fig. 3.10. Despite the simplicity of the model and the smooth variation in the onshore wind, the modeled coastal front exhibits some rather complicated behavior. The front initially moves offshore as the surface heating establishes a temperature difference. After 3.2 hours, the front has come to a stop 3.3 km offshore, as the onshore wind increases at a faster rate than the speed of the coastal front. The front retreats and crosses the coast at 7.9 hours. By this time, the temperature difference across the

front (not shown) is 4.4 K, which is more than half of the 7.5 K land-sea temperature difference.

Alhough the onshore wind becomes steady at -7.5 m/s, the speed of the coastal front relative to the warm air begins to increase because the heating of the warm air continues. The maximum inland penetration of the coastal front, 2.3 km, occurs at 11.0 hours. The front recrosses the coast at 13.7 hours with a temperature difference of 5.8 K. As the front proceeds offshore, the temperature difference begins to weaken as the cold air is heated by the water. By 24 hours, the front is 15.8 km offshore, the warm air is up to 277.0 K, and the cold air is 271.3 K. The front is moving into a -7.5 m/s wind with a speed of 0.3 m/s, so its relative speed is 7.8 m/s.

A feature of this and many other model runs is that the front stays within 10 km of the coast for well over 12 hours, despite the fact that onshore winds and frontal temperatures have both changed rapidly. This is possible because the winds and frontal temperatures are acting in opposite directions on the frontal speed. To accomplish near-stationarity, the speed of the front relative to the warm air, as given by (3.6), must increase from near zero to near 7.5 m/s toward the east as the warm air winds increase to a comparable speed in the opposite direction. Without the headwind, the front would move quickly offshore; a front with U_2 = 0.1 m/sec and the other parameters the same as in the control run moves 36.5 km offshore during the first two hours.

If the model were permitted to run indefinitely, the coastal front would approach a stationary position offshore. This position is the place at which the cold air has been heated just enough to give the front a warm-air-relative speed which is precisely the magnitude of the opposing wind. This location, as a function of the warm air wind speed and the land-sea temperature difference, is

$$X_{t=\infty} = h_1 \, [B + A/\max(0.2\, U_2, 1)] \;\; \ln \{ K^2 \, g \, h_1 \, (\Theta_s - \Theta_o) / (\Theta_s \, U_2^2) \} \qquad (3.27)$$

If the logarithm is negative, no stationary location is possible. Instead, the front approaches a constant speed given by

$$c = K (g h_1 (\Theta_s - \Theta_o) / \Theta_s)^{1/2} - U_2 \qquad (3.28)$$

For the control run, the logarithm is positive, and the asymptotic frontal position is X = 25.6 km .

Model runs were made for a variety of sea surface temperatures, holding the other parameters fixed (Figs. 3.11-3.14, note changes in scale). As the land-sea temperature difference is increased, the coastal front speed also increases. With a small temperature difference (Fig. 3.11), the coastal front only travels 1.4 km offshore, and crosses the coast at 3.1 hours. The front proceeds inland at speeds of between -2.0 and -3.2 m/s, and has reached a distance of 100 km from the coast at 14.0 hours. With a 6 K temperature difference (Fig. 3.12), the front stays offshore until 5.8 hours and eventually stalls between 14 and 26 hours at 25-30 km inland. The model coastal fronts associated with larger temperature differences (Figs. 3.13 and 3.14) move slowly offshore for the first 6-10 hours and then move out to sea at speeds of up to about 1 m/s.

Holding the initial temperatures constant and varying the warm air wind speed produces analogous results (not shown). Weak winds permit the front to move offshore, while strong winds drive the front onshore, where it either stalls (with winds of about 6.5 m/s) or continues moving inland (with stronger winds).

Further variations in frontal motions can be obtained by altering L, the length of time at which the winds veer completely onshore. Fig. 3.15 shows the results of a model run using the control parameters, except with L decreased to 5 hours. The more rapid veering results in a stronger headwind for the first 10 hours, driving the front almost 40 km inland before it reverses direction and heads back out to sea. The frontal position at large

time is still given by (3.26). A separate model run (Fig. 3.16) was made with L = 20 hours and Θ_s = 275 K. The front remained offshore for 15 hours before moving inland at about -0.5 m/s.

The effect of changing other parameters is straightforward and predictable. Increasing h_1 or K increases the speed of the coastal front relative to the warm air and result in fronts which are farther east. Increasing h_2 slows the heating of the warm air, reducing the frontal speed and moving the fronts farther west. Increasing the surface heat flux parameters A or B tends to keep coastal fronts closer to the coast.

Fig. 3.17 shows the coastal front positions after 18 hours for a range of U_2 and Θ_s. For comparison, coastal front positions calculated assuming no heat flux and a temperature discontinuity of constant magnitude (assumptions analogous to those made by Pearson *et al.*, 1983) are shown in Fig. 3.18. The effect of surface heat flux is to tend to hold the fronts much closer to the coast. For the sake of this discussion, we define quasi-stationary fronts to be modeled fronts which in eighteen hours have traveled at an average speed of less than 1 m/s. For U_2 = 5 m/sec, the full density current model predicts quasi-stationary fronts for an 8.7 K range of $\Theta_s - \Theta_o$, and the range expands to 14.1 K when U_2 = 10 m/sec. Without surface heating, the corresponding ranges of $\Theta_s - \Theta_o$ are 1.6 K and 3.3 K, respectively.

We have demonstrated the importance of surface heating to the motion of type A coastal fronts. Densiy currents which would otherwise travel far- out to sea are driven back toward the coast by heating of the cold air. As the onshore wind increases, the warm air temperature increases as well, and the effects tend to offset each other. With no external influences other than heat fluxes from the ocean and backing winds, the model correctly predicts that thermally-driven coastal fronts should remain near

the coastline.

The predictive power of the density current model was tested by running it using parameters valid on Dec. 4 (the type A case described in Chapter 2): Θ_s = 281 K, U_2 = 8.0 m/s, h_2 = 1200 m, and L = 6 hours. The result (Fig. 3.19) is in rough agreement with reality, as shown in Fig. 2.7 . Taking t = 0 (the time that winds were parallel to the coastline) to be 0500 Dec. 4, the model predicts the front crossing the coast by 0800, consistent with the weak frontal passage observed at P25. At t = 7 hrs, the time the real front passed station P24 with a temperature jump of about 3 K, the predicted temperature difference across the front is 5.2 K. The predicted frontal location at that time is 11.8 km from the coast; the actual distance between P24 and P25 is 25.1 km. We attribute the discrepancy in the model to the effect of the curved coastline in the real atmosphere. The warm air is not over the water as long as the model supposes, and the model therefore overestimates the temperature of the warm air and the relative speed of the front.

If this model were to be used as a forecasting tool, certain additional improvements would be desirable. The model might easily be modified to accept observed vertical temperature structures by making the warm air boundary layer height a function of the boundary layer temperature. Incorporating forecasted warm air winds is possible, but would more than double the run time of the model by requiring numerical integration of (3.17) instead of the analytical solution (3.22). A final modification might be to hypothesize that the density current is composed of a finite amount of air trapped between the coast and the mountains, and make the height of the density current a reciprocal function of the distance between the front and the mountains, with the height of the mountains being an upper bound on the depth of the density current. This would keep fronts closer to the coast, making an even higher percentage of fronts quasi-stationary. However, as discussed in Chapter 4, the possible influence of the mountains on inland-moving fronts is not so simple.

3.6 The Possible Effect of Friction

The preceding discussion of coastal frontogenesis during veering large-scale winds made no mention of surface friction. However, the confluence and convergence induced by the difference in surface drag across the coastline is an additional factor which may trigger or accelerate type A coastal frontogenesis.

Roeloffzen *et al.* (1986) have used a two-dimensional numerical model with the coast represented as a jump in mixing length from 0.1 mm to 10 cm to calculate the ageostrophic motions in the coastline-normal plane for a 360 degree range of geostrophic wind directions. They found that for geostrophic wind directions which make an angle of 15-22 degrees with the coast (corresponding in eastern New England to a geostrophic wind from the northeast), an ageostrophic frontogenetical circulation develops 15-20 km offshore. A geostrophic wind speed of 20 m/s produces a 1 km deep circulation, with the size of the circulation reduced for smaller wind speeds. A similar front can form about 20 km inland in onshore flow incident at an angle of 20-28 degrees to the coast. Other wind directions, while they may induce coastal convergence, cannot cause frontal collapse because air parcels advect quickly through the convergence zones.

Roeloffzen *et al.* found that differential friction acting on onshore winds at suitable angles to the coast can create stationary coastal fronts which produce substantial convective precipitation along the Netherlands coast during cold-air outbreaks. According to Van den Berg (1986), about ten strong coastal fronts occur in the Netherlands per year. Those which occur in the early fall tend to be caused by frictional frontogenesis, while those which occur in late fall and early winter are generally induced by land breezes.

Prolonged periods of geostrophic winds at an angle of 20 degrees to the coastline, in either the Eulerian or Lagrangian sense, are much less

common in New England than in the Netherlands. During ridge passage events, the geostrophic winds tend to be within the proper range of angles for only an hour or so. Frictional frontogenesis may serve to focus the temperature gradient and help generate the land-breeze front 15-20 km offshore during the early stages of type A coastal frontogenesis. However, we suspect that differential friction is secondary in importance to the land breeze mechanism in most cases of ridge passage coastal frontogenesis.

Due to the curved configuration of the coastline, prolonged frictionally frontogenetical winds must be strongly cyclonically curved, so would tend to occur in northern New England only when a cyclone is stationary near Cape Cod. Since this would also likely be a circumstance of heavy rain or snow for coastal areas, purely frictional coastal fronts, if they form at all in New England, would have a significant effect on precipitation patterns in coastal regions. Unfortunately, there were no cases of intense, slow-moving cyclones just off the coast during NEWSEX, so we cannot investigate the validity of the above speculation here.

One of the earliest attempts to account for coastal frontogenesis was the so-called Sanders hypothesis. According to the hypothesis as stated by Bosart (1975), the horizontal pressure gradient across the coast is balanced by differential friction. The differential friction serves to pack the isotherms together, much like synoptic-scale deformation in classical frontogenesis. Bosart discussed the hypothesis in terms of a geostrophic flow perpendicular to the coastline.

The calculations of Roeloffzen *et al.* indicate that frictional frontogenesis is most effective when the geostrophic wind is at an angle of 20 degrees with the coast, not 90 degrees, and the observations described in this study indicate that those few fronts which form along the coast within onshore winds are essentially land-sea breezes. If friction plays a role in coastal frontogenesis, it is when the wind is nearly parallel to the coast, not when it is nearly perpendicular. The concept of coastal fronts generally forming within onshore flow rather than as onshore flow develops appears

to have been an incorrect and misleading one.

3.7 Summary

In this chapter we have discussed the physical processes which led to the formation of nine of the thirteen coastal fronts observed during NEWSEX. Three of the nine, termed evening onset coastal fronts, developed as land breezes, although the stability characteristics of the lower atmosphere permitted them to rival sea breezes in intensity. The other six coastal fronts were driven primarily by heating from the sea surface, so that in a sense they formed as inverted sea breezes. A simple density current model of ridge passage coastal fronts was developed, in order to determine what effect heat fluxes and veering winds would have on frontal motion. It was found that for a wide range of commonly observed temperatures and wind speeds, the fronts remained quasi-stationary through 18 hours. The simulated fronts possessed many characteristics of observed coastal fronts.

It is appropriate at this point to discuss Ballentine (1980), the only three-dimensional modeling study of the New England coastal front published to date. Ballentine's initial conditions corresponded to generally northeasterly geostrophic winds at the surface, and he imposed an approaching 700 mb trough, which forced the surface geostrophic winds to veer to southeasterly during the integration. The initial temperatures over water, however, are extrapolated from observed land temperatures. The lack of an initial temperature gradient along the coast is therefore compensated by unrealistically large air-sea temperature differences. These initial conditions prevent the model from correctly simulating the initial stages of ridge passage coastal frontogenesis, including determining the relative importance of differential friction and differential heating. The resulting coastal front becomes a cross between type A (driven entirely by heating)

and type B (forming within an onshore air flow) coastal fronts. For the stated initial conditions, Ballentine found that heating and a veering onshore wind were of primary importance in forming a coastal front. When heating was suppressed, no coastal front formed. When veering was suppressed, the central portions of the coastal front moved offshore and were weaker, in agreement with the density current model developed above. The motion of the modeled coastal front is unfortunately affected by Ballentine's lateral boundary conditions, which forced the front to remain stationary at the coastline on the margins of the model grid. Direct comparisons of frontal motions calculated by Ballentine and by the density current model are therefore impossible. Ballentine's model is also unsuitable for investigating the effect of orography on frontal motion.

4. RELATIONSHIP BETWEEN UPSTREAM BLOCKING AND COASTAL FRONTS

4.1 Introduction

The land-sea breeze mechanism does not account for the four fronts which have been called spontaneous coastal fronts. Land-sea temperature differences were small or of the wrong sign. The spontaneous fronts formed well inland rather than along the coast.

Ridge passage or evening onset coastal fronts also tend to interact closely with topography during their lifetimes. Previous observers and researchers have found a tendency for coastal fronts in Massachusetts to become stationary along a line from Boston to Providence, near the hills of Arlington, or along the northern portions of Route 128. While some coastal fronts simulated with the model of Chapter 3 became stationary temporarily onshore, such stalling is much more common than the model predicts.

Bosart *et al.* (1972) noted that

> " A key synoptic feature in coastal front formation is the presence of a cold anticyclone over northern New England. This anticyclone usually takes the form of a pressure ridge east of the mountains. "

Such pressure ridges, also known as wedges, were studied by Baker (1970), who called the phenomenon "damming". Baker showed that the characteristic inverted ridge pressure pattern along the eastern side of the Appalachians was the surface signature of a dome of partially or completely

blocked cold air. Bosart (1981), Neilley (1984), and Forbes *et al.* (1987) have shown that the coastal front inversion forms the upper margin of the dammed air both in the Carolinas and in New England.

4.2 Orographic Blocking of a Continuously Stratified Fluid

Cold-air damming, wedging, and upstream blocking are different names for the same type of process involving the flow of discretely or continuously stratified fluid over orography. The relevant non-dimensional parameter for such flows is the Froude number (Fr), which in this paper shall be defined as

$$Fr = N H / U \tag{4.1}$$

for a continuously stratified fluid, and

$$Fr = (g^* / h)^{1/2} H / U \tag{4.2}$$

for a two-layer fluid, where H is the height of the orographic obstacle, h is the depth of the lower fluid, g^* is the reduced gravity, as defined in (3.9), and other symbols have their usual meanings.

Laboratory and theoretical studies have indicated that blocking occurs in continuously stratified, deep, non-rotating fluids passing over a two-dimensional obstacle when Fr is order one or greater. Linear theory (Pierrehumbert, 1984), if extrapolated beyond its range of validity, predicts that fluid becomes completely blocked when Fr becomes greater than about 2. Recent laboratory experiments with a variety of obstacle shapes and a simulated upper boundary radiation condition (Baines and Hoinka, 1985) have exhibited blocking with Fr larger than about 2, with the depth of the blocked fluid increasing as Fr is increased. Minor dependence on the shape

of the obstacle was found. The most efficient obstacle for blocking had a steep windward side and a gradually sloping leeward side.

Numerical simulations of the non-rotating, inviscid case with a Gaussian mountain (Pierrehumbert and Wyman, 1985; here abbreviated PW) found three critical values of Fr. When Fr > 0.75, columnar wavelike disturbances propagated upstream, decelerating the fluid near the surface. PW related this cutoff value to the existence of wave breaking over the mountain. Baines and Hoinka found columnar modes and upstream influence when Fr > 0.3, a discrepancy which PW attributed to the non-hydrostaticity of the laboratory simulation. Stagnant fluid was first formed upstream of the mountain when Fr = 1.5 . When Fr > 2.0, as suggested by the simulation of Baines and Hoinka, the region of completely blocked fluid expanded upstream indefinitely. The depth h of the blocked fluid increased as Fr increased, and the calculations suggested that the depth adjusted itself so that

$$N(H-h)/U \approx 1.5 \quad . \tag{4.3}$$

The addition of even a small amount of rotation, as discussed by PW, substantially affects the long term behavior of blocked flows. First, while blocking in a non-rotating fluid permanently modifies the fluid speeds far upstream by amounts comparable to the initial flow speed, rotation prohibits finite modification of the flow infinitely far upstream. Second, steady solutions cannot have zeroes in u, because the ambient pressure gradient in the y direction (which is driving the blocked flow) would indefinitely increase v. As a result, any blocking which occurs is unsteady, and is associated with a mountain-parallel jet, also known as a barrier wind (*e. g.*, Parish, 1982).

The parameter which determines the importance of rotation to the flow is the local Rossby number,

$$Ro = U / f L \quad , \tag{4.4}$$

where L is the length scale of the windward mountain slope and U is the speed of the incident wind. For small Ro, semigeostrophic theory (Pierrehumbert, 1985) indeed predicts that the flow is never completely blocked. The top of the decelerated region, for large RoFr, slopes back from near the top of the mountain, intersecting the ground at a distance proportional to

$$(Ld\, L)^{1/2} = (RoFr)^{1/2}\, L \quad . \tag{4.5}$$

The existence of such unblocked, steady solutions was verified by PW's model.

The simulations of PW indicate that for Ro >= 1, there is persistent unsteadiness. It is in this parameter range that the orography of New England falls; onshore flows over the mountains typically have 1.5 <= Ro <= 5.0 . Although totally blocked fluid did develop in the simulations and persist for advective time scales of 1 to 6 (corresponding to dimensional times in New England of 3-5 hours), it is not clear that blocked fluid would have formed if the fluid had been started from rest gradually rather than impulsively.

Garner (1986) recognized that the presence of warm advection in a rotating, stratified flow past orography could lead to enhanced blocking and frontogenesis. As such a flow is decelerated at low levels by the mountains, the orographically-induced vertical shear increases Fr by increasing the static stability in the shear region. This in turn enhances the blocking. Because the magnitude of the perturbation velocity decreases upwind, the temperature gradient perpendicular to the mountains leads to frontogenesis at the leading edge of the blocked region.

Garner used a Lagrangian model to determine the blocking characteristics of flows with 1 <= Fr <= 1.5 , Ro > 2 , a parameter range for

which PW predict no blocking. The parameter describing the advecting temperature gradient is, in Garner's notation, β, which for $\partial V/\partial x = 0$ is

$$\beta = \partial V/\partial z \, N^{-1} \quad , \tag{4.6}$$

where V is the wind component in the y-direction (parallel to the mountain). Garner considered a north-south oriented mountain range with flow from the east, so negative β implies warm advection. The mountain shape was similar to that found by Baines and Hoinka (1985, see above) to be favorable for blocking at low Fr.

The blocking criterion as a function of β, Fr, and Ro as calculated by Garner is shown in Fig. 4.1a. The mountain profiles used are LK: $z = x/(1+x^2)$ and B5: Gaussian profile with downwind length scale five times the upwind length scale. The B5 profile more closely resembles the orography of New England, although neither is a close match. It can be seen that the addition of warm advection causes blocking in the model for Fr near 1. For ease of interpretation, Fig. 4.1b shows the blocking criterion as a function of $\partial V/\partial z$, U, and $\partial\Theta/\partial z$ for scales applicable to New England: $\Theta_0 = 280$ K, $f = 1 \times 10^{-4}$ s^{-1}, H = 500 m, and L = 35 km. Garner's model with warm advection, contrary to the theory and model of PW with no warm advection, predicts total blocking for commonly observed winds and temperatures.

The model also predicts frontogenesis at the leading edge of the blocked region. Fig. 4.2 shows a simulation for $\beta = -0.8$, Ro = 5.0, and Fr = 1.2, well within the range for blocking, after non-dimensional time t = 30. Since the onset of blocking, the region of strong surface temperature gradient had moved slowly away from the foot of the mountain and intensified. Garner noted that the front tended to lie at a distance of roughly Lr from the mountain. Additional simulations showed that reducing the lee width of the mountain had little effect, and that the addition of a north-south temperature gradient (a feature usually present during coastal

frontogenesis) increased the strength of the perturbation circulation.

The use of a crude surface friction parameterization substantially affected the perturbation wind patterns, especially the wind component parallel to the obstacle (see Fig. 4.3). Friction reduced its magnitude and elevated the maximum wind to near the top of the blocked region. Mason and Sykes (1978) have modeled two-dimensional flow with rotation and surface friction over an obstacle and also found flow separation for Fr $\approx$ 1 and Ro $\approx$ 5. Because they do not include temperature advection, the separation regions do not develop into density discontinuities.

4.3 Comparison with Observations

A comparison of the predictions of Garner's frontogenesis mechanism was made with the Nov. 25 spontaneous coastal frontogenesis case. As was described in Chapter 2, the front formed apparently free from significant diabatic influences. The frontogenesis occurred initially in Massachusetts and propagated northward. The wind perturbation formed prior to the establishment of a significant temperature gradient, which then intensified as a result of differential warm advection, consistent with the orographic model of frontogenesis. The front formed two to four half-widths from the mountain ridge line and slowly moved away from the mountains. This behavior is also seen in Garner's model, but it is not known to what extent the motion of the atmospheric coastal front was affected by variations in the warm air flow.

The most stringent comparison of theory with observations is an analysis of the parameters β, Ro, and Fr (or, equivalently, U, $\partial V/\partial z$, and $\partial \Theta/\partial z$) at the onset of coastal frontogenesis. If Garner's theory is correct, the parameters should have been below the critical values for blocking prior to frontogenesis (which are shown in Fig. 4.1b), but should have risen above

the critical values just before or during the observed onset of frontogenesis.

The sounding most representative of conditions prior to frontogenesis was taken at PWM at 0000 Nov. 25 (Fig. 4.4). Synoptic and mesoscale maps at or near 0000 have been presented earlier (Figs. 2.17 and 2.20). Steady rain was occurring at PWM at the time of the sounding, and the rain persisted in southern New England throughout the frontogenesis event. Consistent with that observation, the sounding at PWM shows near-saturation through the entire lower troposphere. The planetary boundary layer, well-mixed in equivalent potential temperature, extended up to 930 mb (~ 700 m above ground level). It was capped by a warm-frontal inversion 80 mb thick, through which the temperature increased by 4 K. Above the warm front, the atmosphere was nearly moist-adiabatic.

The temperature structure at CHH (not shown) included a shallow (30mb) inversion at the ground, topped by a deep moist-adiabatic layer with similar properties to that at PWM. This sounding, in combination with other soundings and surface data, indicates that a broad warm frontal zone was at the surface near CHH at 0000, and that the frontal inversion sloped upward toward the north. In addition, surface data shows that the zone of strongest temperature gradient was progressing northward. We therefore assume that the cross-mountain flow can be represented by the three atmospheric layers observed at PWM, with the heights of the two interfaces decreasing toward the south and in time.

The calculated magnitudes of the relevant parameters are given in Table 4.1. We have oriented our coordinate system so that U is positive toward 300 degrees and V is positive toward 30 degrees. Since the atmosphere was saturated and precipition was occurring, the stratification was calculated using the wet bulb potential temperature. These values are to be compared with Fig. 4.1b. The neutral boundary layer is theoretically unblocked, but the warm front layer falls above the blocking cutoff. Inhomogeneities in the ambient flow are not considered by Garner, but since the inversion was deeper than the mountains (700m vs. 500m), it is

plausible to assume that frontogenesis would have been initiated when the bulk surface-to-ridge-top parameters approached the neighborhood of the cutoff criterion; *i. e.*, when the base of the inversion reached 100-300 m above sea level.

TABLE 4.1

Blocking parameters, PWM 0000 25 Nov. 1983

LAYER	U	$\Delta V/500m$	$\Delta\Theta/500m$
20 m - 730 m	5.1 m/sec	6.9	0.7
730 m - 1440 m	2.6 m/sec	5.3	4.6
1440 m - 2150 m	-6.2 m/sec	-1.1	0.7

As well as can be determined from the PAM data, this was indeed the case. Confluence was first noted at PAM stations at the same time as the initiation of the rapid temperature rises east of the front denoting the arrival of the warm frontal zone. This is seen especially clearly in Fig. 2.24 , in which steady confluence between P31 and P32 and the rapid temperature rise at P32 both commence at 2315. The observed northward propagation of coastal frontogenesis is accounted for by the south-to-north tilt and gradual lowering of the warm frontal inversion. Thus, the coastal frontogenesis event of 25 Nov. is well explained by the orographic frontogenesis model of Garner (1986).

Similar parameter calculations were made for the other three cases of spontaneous coastal frontogenesis during NEWSEX. As in the 25 Nov. case, coastal frontogenesis occurred during the approach of synoptic-scale warm fronts, implying locally large values of $\partial V/\partial z$ and $\partial\Theta/\partial z$. The case of 21 Nov.

involved parameter sizes similar to 25 Nov. In the remaining two cases, parameters measured at PWM and CHH approached but did not exceed the blocking cutoff. However, large spatial variations in the temperature and wind structure make it difficult to estimate the temperature and wind structure in eastern Massachusetts and New Hampshire during those events, although in both cases there is evidence that the orographic frontogenesis forcing is stronger than estimated.

The final check of the theory is confirmation that it did not incorrectly predict the formation of a coastal front when none occurred. Since it is unlikely that the blocking criterion is often satisfied ooutside of warm frontal inversions, the check consisted of a search through the NMC surface weather maps for all instances of a warm front within 300 km south of New England. All such warm fronts were found either to be associated with one of the four spontaneous coastal fronts or to have approached New England while a ridge passage or evening onset coastal front was already present. We conclude that the theory of orographic coastal frontogenesis is a valid explanation for spontaneous coastal frontogenesis.

4.4 Observations of Mature Coastal Front Structure

After initial frontogenesis, soundings, aircraft data, and surface observations indicate that coastal fronts evolve into a boundary between relatively cold air trapped against the mountains and warmer air overriding the cold air and flowing over the mountains. This is true even for ridge passage and evening onset coastal fronts, whose initial formation was independent of the mountains.

The most complete aircraft observations of a New England coastal front were made during NEWSEX on Dec. 4, 1983. The coastal front, described in Chapter 2, was a type A coastal front which had formed near 0600. Between 1400 and 1600, the NCAR King Air made multiple passes through the

front near PSM.

In order to construct a cross section from the aircraft data, it was necessary to adjust the data for changes in the coastal front which occurred while the observations were being made. All observations were projected onto an x-z plane normal to the coastal front. The orientation of the coastal front was obtained from analysis of the PAM, hourly, and Coast Guard data. Observations taken near the surface front were corrected for the motion of the front to obtain a front-relative cross section. The speed of the coastal front was obtained from multiple low-level aircraft passes. Data taken at different times at adjacent x-z points were used to estimate systematic changes in temperature and wind in both the warm and cold air during the two hours of observations, and these changes were subtracted from the raw data. Surface elevations were taken to be the 75th percentile of elevations within a 20 km band along the flight track.

The resulting cross-section of potential temperature, valid at 1500 Dec. 4, is shown in Fig. 4.5a. The coastal front is prominent as a near-discontinuity of temperature 250-300 m above the surface. Vertical temperature gradients through the frontal zone average greater than 0.04 K/m. Beneath the inversion, the stratification is weak, about 1 K / 500 m ($N = 0.85 \times 10^{-2}\ s^{-1}$). East of the coastal front, the oncoming warm air, having been heated by the sea surface, is neutral or slightly unstable through the lowest 1 km. The temperature gradient within the warm air above the frontal inversion has most likely been advected there from offshore, although mixing may have cooled the warm air near the inversion.

The front-normal winds (Fig. 4.5b) also have a near-discontinuity at the leading edge of the coastal front and along the frontal inversion. Twenty-five kilometers west of the front, the Richardson number ($N^2 / (\partial V/\partial z)^2$) along the inversion is estimated to be 0.3 . Except for near the ground, the cold air is blowing weakly toward the mountains. The air over the inversion appears to be accelerating toward the west, which is to be expected since its vertical extent is limited by the coastal front below and a

warm front above located at about 1.2 km. Some deceleration of warm air is evident near the surface just ahead of the coastal front.

The front-parallel winds (Fig. 4.6a) do not exhibit a discontinuity at the frontal interface. The wind is essential continuous across the surface frontal zone. At the frontal inversion, the front-parallel winds reach a maximum, with the strongest winds coinciding with the steepest slope of the inversion. This is consistent with thermal wind balance across the interface (Lettau and Schwerdtfeger, 1967).

The speed of the coastal front was determined from multiple airplane passes to be northwestward at 1.1 m/sec. A front-relative stream function (Fig. 4.6b) was constructed from the vertical gradient of the difference between the front-normal winds and the speed of the front, which was determined from multiple airplane passes to be 1.1 m/s. The basic assumption of the stream function is that there is no along-front variation in the front-parallel wind, and the significance of a front-relative stream function is unclear over regions of sloping topography. Two circulation centers are seen, a primary one about 20 km behind the front, and a smaller one 2-3 km wide just behind the front. The warm air is thrust upward by the coastal front at speeds of 1-3 m/s (verified by aircraft measurements of vertical velocity) and undergoes a rapid vertical displacement of up to 300 m, which decreases with initial height. The streamlines appear to penetrate the frontal inversion from above; this has been both observed and modeled in other density currents by Garratt and Physick (1987), and is due to turbulent heat fluxes between the warm and cold air.

The Dec. 3 cross sections are consistent with those made by Neilley (1984) of the region within 20 km of two 1983 coastal fronts. All three cross sections show an elevated 'head' at the leading edge of the front, with a vortex in front-relative velocity beneath it. These are characteristics of density currents. A calculation of the theoretical speed of the Dec. 4 front using (3.5)-(3.6) using $u_2 = -8.0 \pm 0.2$ m/s, $\Delta\Theta = 4.3$ K, $\Theta = 271$ K, $h_1 = 285 \pm 20$

m, and c = -1.1 m/s yields K = 1.04 ± 0.07, which is consistent with Neilley's results and consistent with the ridge passage coastal front model employed in Chapter 3.

The front is shallower than typical cold fronts. The intense front analyzed by Sanders (1955) was 700 m above ground level (AGL) at a distance of 75 km from the front, while this coastal front was only 300 m AGL at the same distance. The vertical gradients of potential temperature at that distance are comparable; Sanders found mean gradients of 0.05 K/m. Recent tower measurements in Colorado (Shapiro *et al.*, 1985; Young and Johnson, 1984), which because of the slope of the front could only observe the first 13 km of the frontal zone, found the vertical temperature gradient to be 0.05 to 0.08 K/m at that range. Cold frontal inversions tend to weaken with distance from the front (see, for example, Sanders, 1955), but there was no evidence of a weakening of the vertical temperature gradient in the above coastal front case over the 80 km extent of the data.

4.5 The Two-fluid Problem: Theory

The Dec. 4 front has been shown to have been caused by the coastal surface temperature discontinuity interacting with a large-scale veering air flow. The only source of the strong temperature gradient of the frontal inversion in such a circulation is advection of the boundary between the heated and unheated air. The process is essentially one of vertical shear deformation converting a horizontal temperature gradient into a vertical one. The time scale of the inversion formation is essentially the time required to advect the heated air over the top of the unheated air. Neglecting thermally-driven 'return flow' circulations, the speed of propagation of the temperature inversion is roughly given by the speed of the oncoming warm air near the surface coastal front. For the observed

winds in the Dec. 4 case, assuming coastal front formation at 0500, the weak leading edge of the inversion should have reached the mountains (a distance of 110 km) in 7-8 hours, 2-3 hours before the aircraft cross sections were made.

The propagation of the coastal front inversion was modeled successfully by Ballentine (1980). Fifteen hours after the initiation of his mesoscale model with the initial condition of a warm ocean but little initial temperature gradient, an inversion had formed between about 300 to 500 m AGL, with the thickness of the inversion (200 m) comparable to the vertical grid spacing.

Ballentine stated that the coastal front inversion forms "as warm air from the ocean is forced up over the shallow cold air between the Appalachians and the coast". Ballentine's model did not extend westward to the ridge line, so it is not known whether the modeled inversion would have ascended over the ridge or intersected the ground. While there have been no direct observations of a New England coastal front inversion intersecting the ground below the ridge line, observations from ORH provide indirect data. ORH is located atop a ridge in central Massachusetts at an elevation of 300 m. In about half the coastal front cases observed by the author over the past several years, ORH was located in the warm air, implying that the inversion reached the ground somewhere below ORH. An example of this, for a type C coastal front, can be seen in Fig. 2.22 .

The motion of coastal fronts inland depends upon the effect of cold-air damming on the height of the cold air. Given the narrowness of the inversion and the much more nearly neutral stratification above and below, we take as an appropriate model for the interaction of the coastal front with the mountains a two fluid system. The theory of non-rotating two-layer flow over topography has been developed by Baines (1984). The governing parameters are, in Baines' notation,

$$\text{the inverse Froude number} \qquad Fo = u / (g^* d_1)^{1/2} \quad , \qquad (4.7)$$

the relative obstacle height $H = h/d1$, (4.8)

and the relative fluid depth $r = d_1/d$, (4.9)

where d_1 is the depth of the lower fluid, d is the total depth of the two fluids, and h is the depth of the obstacle. Flow regime diagrams are presented in Baines' Fig. 8. Briefly, the conditions for totally blocked fluid require that the lower fluid be less deep than the obstacle, and there is an inverse Froude number cutoff that increases with decreasing r and for r = 0.35 (similar to the Dec. 4 case) is roughly Fo < 0.4 . The results are qualitatively similar to the laboratory Froude number cutoff for continuous stratification, with blocking favored with low u, shallow lower fluid, high orography, and high density contrast.

As the upper fluid becomes deep (r -> 0), the behavior of the lower fluid approaches that of the one-layer case with g replaced by g* (Long, 1970; Baines and Davies, 1980). Under such conditions, the criterion for complete blocking becomes (Long, 1970)

$$Fr = u / (g^* d_1)^{1/2} < (H-1)((H+1)/2H)^{1/2} \quad , \qquad (4.10)$$

where H is defined in (4.8). In the case of, for example, a fluid half as deep as the obstacle, (4.10) reduces to $Fr < 0.75^{1/2}$. In terms of an inverse Froude number defined by the obstacle height rather than the fluid depth, $Fo < 0.375^{1/2}$. This is again similar to laboratory observations discussed earlier for the continuously stratified fluid, which found that $Fo < 0.25^{1/2}$ for complete stagnation of part of the flow.

Like the continuous case, the addition of rotation to the two-dimensional inviscid problem prevents steady blocked solutions. With the component of wind toward the mountain forced to equal zero, nothing can balance the pressure gradient along the mountains but an acceleration of the wind along the mountains. If variations in the fluid along the

mountain are permitted, the pressure gradient may be balanced locally by an corresponding gradient in the height of the fluid along the obstacle. Indeed, cold air domes associated with coastal fronts in the Carolinas are often analyzed to have zero along-mountain surface pressure gradients for several hundred kilometers, implying that changes in the depth of the cold air are exactly balancing the north-south pressure gradient above the inversion.

The coastal front problem is further removed from the irrotational two-fluid theory by inherent time-dependence. Rather than a semi-infinite fluid approaching an obstacle with constant velocity, the coastal front problem is formally one of the evolution of a finite two-dimensional fluid started from rest against an obstacle, and affected by a gradually increasing pressure gradient acting to geostrophically drive the fluid over the obstacle. The problem is non-linear and time-dependent.

We shall consider the equations of motion for a two-dimensional, homogeneous layer of fluid with a rigid lower boundary and a free upper interface with a less-dense, neutrally stratified fluid. With $\partial/\partial y = 0$ in the lower fluid, the equations are

$$Du/Dt - fv = -(1/\rho)\,\partial p/\partial x - g^*\,\partial h/\partial x - g^*\,\partial s/\partial x + F(u) \qquad (4.11)$$

$$Dv/Dt + fu = -(1/\rho)\,\partial p/\partial y + F(v) \qquad (4.12)$$

$$Dh/Dt + h\,\partial u/\partial x = 0 \quad , \qquad (4.13)$$

where $h(x)$ is the height of the top of the fluid above the lower topography $s(x)$, $p(x,y)$ is the external pressure imposed by the upper fluid, ρ is the density of the lower fluid, F is an as yet unspecified frictional force, and

$$D/Dt = \partial/\partial t + u\,\partial/\partial x \quad . \qquad (4.14)$$

A simple case occurs under the assumption of steady state ($\partial/\partial t = 0$),

with no external pressure gradient ($\partial p/\partial(x,y) = 0$), no friction ($F = 0$), and no topography ($s = 0$). Eqs. (4.11)-(4.13) reduce to

$$u = 0 \tag{4.15}$$

$$f v = g^* \partial h/\partial x \quad . \tag{4.16}$$

To solve for v, we employ the Bernoulli condition

$$0.5\, g^* h + 0.5\, v^2 = \text{constant} \tag{4.17}$$

and, requiring that $h_{x=\pm\infty} = 0$, we obtain

$$v = -f(x - x_0)/2 \tag{4.18}$$

$$h = H_0 - (f(x - x_0))^2 / 4 g^* \quad , \tag{4.19}$$

with the solution only meaningful when $h > s$.

The fluid is an inverted parabola in geostrophic balance, with the horizontal distance between $h = H_0$ (the maximum height of the fluid) and $h = 0$ given by twice the Rossby radius of deformation

$$2 Lr = 2 (g^* H_0)^{1/2} / f \quad . \tag{4.20}$$

The same solution may be obtained by requiring Lagrangian steadiness, *i. e.*, $D/Dt = 0$. The addition of surface topography does not affect the shape of the upper surface. The solution becomes

$$v = -f(x - x_0)/2 \tag{4.21}$$

$$h + s = H_0 - (f(x - x_0))^2 / 4 g^* \tag{4.22}$$

The parabolic dome of fluid may be stationary even on sloping terrain.

If we now impose a nonzero external pressure gradient in the y direction, no steady Eulerian ($\partial/\partial t = 0$) solution is possible. Eqs. (4.11)-(4.13) would become

$$u\,\partial u/\partial x - f v = -g^* \partial h/\partial x - g^* \partial s/\partial x \tag{4.23}$$

$$u\,\partial v/\partial x + f u = -(1/\rho)\,\partial p/\partial y \tag{4.24}$$

$$u\,\partial h/\partial x + h\,\partial u/\partial x = 0 \quad . \tag{4.25}$$

Eq. (4.25) implies that at the left-hand edge of the fluid ($x = x_1$), where $h = 0$ and $\partial h/\partial x > 0$, $u = 0$. A short distance to the right, where $x = x_1 + \delta x$, $h = \delta h$ and $\partial h/\partial x > 0$, (4.25) implies that u and $\partial u/\partial x$ are of opposite sign, which is impossible. So from (4.25), $u = 0$. But (4.24) becomes $0 = -(1/\rho)\partial p/\partial y$, which contradicts the condition that $\partial p/\partial y$ is not equal to 0.

In a Lagrangian sense, a steady solution is possible with flat topography ($s = 0$): a parabolic blob of fluid being advected at constant geostrophic u:

$$u = -(f\rho)^{-1}\,\partial p/\partial y \tag{4.26}$$

$$v = -f(x - x_0 - u t) \tag{4.27}$$

$$h = H_0 - (f(x - x_0 - u t))^2/2\,g^* \quad . \tag{4.28}$$

Stationary topography and nonzero u are inconsistent with a steady solution.

A steady solution for a fluid blocked by topography is possible when friction is included. If we use the crude frictional parameterization

$$F(u) = -C_d u \quad ; \quad F(v) = -C_d v \tag{4.29}$$

and assume the fluid is blocked by some obstacle so that u = 0, the time-independent equations are

$$-f v = -g^* \partial(h+s)/\partial x \tag{4.30}$$

$$0 = -(1/\rho) \partial p/\partial y - C_d v \quad . \tag{4.31}$$

For clarity, we substitute $f U_g = -(1/\rho) \partial p/\partial y$. The solution is

$$v = f U_g / C_d \tag{4.32}$$

$$h + s = f^2 U_g (x - x_o) / C_d g^* \quad . \tag{4.33}$$

The top of the fluid has constant slope with the same sign as Ug, and v is now an antitriptic wind.

The condition from (4.32)-(4.33) for blocking in the lee of an obstacle, where $U_g \partial s/\partial x > 0$, is

$$|\partial s/\partial x| > \partial s/\partial x_{crit} \tag{4.34}$$

where

$$\partial s/\partial x_{crit} = \partial(h+s)/\partial x = f^2 U_g / C_d g^* \quad . \tag{4.35}$$

Substituting $U = |U_g|$ and $H/L = |\partial s/\partial x|$, the condition becomes

$$Ro\, Fr / Re^{1/2} > 1 \quad , \tag{4.36}$$

where

$$Ro = U/fL \tag{4.37}$$

$$Fr = (g^* H)^{1/2} / U \tag{4.38}$$

$$Re = C_d L / U \quad . \tag{4.39}$$

The stronger the drag, the more likely the flow is to be blocked.

4.6 A One-layer Lagrangian Model of Upstream Blocking

To examine the time-dependent behavior of a finite, two-dimensional, dense, homogeneous fluid interacting with an obstacle, we have developed a one-layer Lagrangian model. An Eulerian model, such as that employed by Baines (1986) for studying the flow of an infinite fluid over a shallow obstacle, would have difficulty with the horizontal margins of the fluid. The finite element equations were derived from (4.11)-(4.13), employing the condition that each element of fluid has equal two-dimensional area A. Each element has some location X and velocities U and V. The height of the fluid is proportional to the inverse of the distance between the elements. The external pressure gradient and the bottom topography (s) are specified as functions of X. The equations of motion for the i'th fluid element are:

$$\begin{aligned}(U_{i(new)} - U_i) / \Delta t \;=\; & f V_i \\ & - 2 A g^* \{ (X_{i+1} - X_i)^{-1} - (X_i - X_{i-1})^{-1} \} (X_{i+1} - X_{i-1})^{-1} \\ & - \partial p/\partial x_i / \rho \quad - g^* \partial s/\partial x_i \quad - C_d U_i \end{aligned} \tag{4.40}$$

$$(V_{i(new)} - V_i) / \Delta t \;=\; f U_i \;-\; \partial p/\partial y_i / \rho \;-\; C_d V_i \tag{4.41}$$

$$(X_{i(new)} - X_i) / \Delta t = U_i \tag{4.42}$$

The height gradient terms at the edges of the lower fluid are handled crudely by setting the height of the fluid to zero at a distance equal to half the finite element spacing. For example, the equations corresponding to (4.40) for the leftmost (i = 1) fluid element is

$$(U_{1(n+1)} - U_{1(n)})/\Delta t = f V_1 - A g^* (X_2 - X_1)^{-2} - \partial p/\partial x_1 / \rho - g^* \partial s/\partial x - C_d U_1 \tag{4.43}$$

Because of the Lagrangian nature of the model, discontinuous initial conditions may be used without adverse numerical effects. For the model runs without topography, the initial conditions were

$$U_i = 0 \tag{4.44}$$

$$V_i = 0 \tag{4.45}$$

$$X_i = A\, i\, \Delta X / H \quad , \tag{4.46}$$

which is a stationary rectangular blob of fluid of depth H. For runs with topography, an element spacing was selected which resulted in an approximately flat upper surface to the fluid (Fig. 4.7).

Simulations (not shown) with zero external pressure gradient and blobs a few hundred meters high, a few hundred kilometers long, and g* a few tenths of a m s^{-2} exhibited anticipated characteristics. When $C_d = 0$ and the fluid is sufficiently more narrow than its Rossby radius of deformation, the fluid undergoes an inertial oscillation. As C_d is increased, the magnitude of the oscillation rapidly decreases, and $1/C_d$ is the time scale of the decay of

the oscillation. For times larger than $1/C_d$, the fluid has parabolic shape, but the width of the parabola gradually increases as friction drives fluid away from the center. A parabolic shape is attained, as in (4.22), even if the fluid is on a slope. The addition of an external pressure gradient causes the fluid to self-advect in the expected direction.

Simulations were then performed with the fluid resting against a slope designed to resemble the east-facing topography of east-central New England. Initial and boundary conditions for the 'basic' run are given in Table 4.2 and Fig. 4.7 . Subsequent runs were performed with all but one of the parameters identical to those of the basic run. In the figure, the interface height has been calculated between fluid elements only, so the graph does not intersect the lower boundary.

TABLE 4.2

Parameters for 'basic' run, damming model

$$\partial p/\partial y = 1.0 \text{ mb} / 100 \text{ km}$$
$$g^* = 0.2854 \text{ m s}^{-2}$$
$$f = 1 \times 10^{-4} \text{ s}^{-1}$$
$$C_d = 8 \times 10^{-5} \text{ s}^{-1}$$
$$\Delta t = 10 \text{ s}$$

All simulations shared many features with the basic simulation. During the first 3-5 hours of the simulations, the right side of the fluid flowed out rapidly. Then, the combination of an inertial oscillation (for small friction) and the external pressure gradient (if one existed) brought the fluid back toward its initial position. Meanwhile, the left side of the fluid, responding to the pressure gradient, began climbing the obstacle. As the entire fluid moved westward, weak hydraulic jumps formed near the

base of the slope and propagated eastward. By ten hours, the jumps had generally reached the eastern edge of the fluid. The fluid which remained east of the obstacle approached the equilibrium slope of (4.33). If the pressure gradient was sufficient, other fluid spilled over the top of the obstacle and continued streaming westward at a velocity determined by the pressure gradient and the friction. In none of the simulations was fluid observed to flow back eastward over the step.

The position of the fluid interface in the basic simulation after 12 hours is shown in Fig. 4.8. The fluid height can be directly calculated only between elements, so the graph of the interface does not intersect the surface. The upper part of the fluid has just begun to flow over the top of the obstacle. The remaining fluid is at most 250 m deep. The hump at the top of the step is larger when more fluid is flowing over the top. It is similar to the hump seen in the 1 1/2 layer model of Baines (1986) and is due to the westward acceleration of the fluid after it crosses the step. The depth of fluid at the top of the hump is less than its depth over the nearby slope.

The magnitude of the u component of wind within the air below the step is generally less than 0.5 m/sec by this time. The v component upwind of the step varies between -10.9 and -11.2 m/sec. It had been steadily becoming more negative through the simulation, but had only fallen 1 m/sec during the previous two hours. The upper surface forms nearly a straight line, almost identical in slope to the theoretical steady-state slope of -0.0039 . The 'final' state of this system would have the sloping interface intersecting the ground right at the top of the step, with the excess fluid having flowed over the step toward the left.

The effect of varying the pressure gradient can be seen in three simulations which were otherwise identical to the basic run. With no pressure gradient, the fluid flowed freely outward toward the right and had attained a shallow parabolic shape by twelve hours (Fig. 4.9). The eastern edge of the fluid was 160 km from its starting position. Beyond twelve hours, the fluid continued to spread out gradually. A pressure gradient of 0.5

mb/100km (Fig. 4.10) kept the fluid trapped against the slope; as expected, both the slope of the top of the fluid and the v wind component are half the magnitude of the basic simulation because the pressure gradient is half. Finally, a pressure gradient of 2.0 mb/100km (Fig. 4.11) causes most of the fluid to flow over the obstacle, since the equilibrium slope is nearly the slope of the obstacle. At long time, a small amount of fluid would remain trapped behind the slope. The criterion (4.34) for blocking by the obstacle in the model is violated when the pressure gradient is greater than 2.56 mb/100km and the other parameters are as given in Table 4.2 .

An increased density contrast leads to a shallower equilibrium slope by (4.33), and this effect can be seen in Fig. 4.12 . The parameters are identical to the basic case, except that the density difference is doubled. This results in a fluid shape after twelve hours almost identical to Fig. 4.10, which is again expected from (4.33). The primary difference is an increase of 'turbulent' energy (as shown by waves along the interface and in u) caused by the more violent fluid motions. The v component is doubled.

Two other simulations were run to examine the effect of changing the friction parameter C_d. The first run, with C_d halved (Fig. 4.13), permitted much of the fluid to escape over the obstacle, and also led to an increase in wave activity. The second run was made with Cd_d doubled (Fig. 4.14). The increased diffusion damped out the wave motions almost completely, allowing the fluid interface to become almost perfectly straight. The slope of the interface, as predicted by (4.33), is identical to the slope of Figs. 4.10 and 4.12 .

While the above model was intended to capture the basic aspects of a homogeneous, rotating fluid blocked by a barrier, various assumptions and shortcomings prevent the results from being interpreted in any sort of quantitative manner. Effects of the lower fluid on the upper fluid were neglected, as were such interactions as Reynolds stresses on the fluid interface and density current effects on the fluid edges. The initial

conditions were intentionally unrealistic, primarily because it is not known what the proper initial conditions would be for the coastal front/dammed fluid problem. The neglect of density variations, such as non-neutral stability in the lower or upper fluid or mixing across the interface, is not expected to be as detrimental as the other approximations mentioned above, but a complete model would have to include them.

Friction was shown to be crucially important for balancing the along-mountain wind and controlling the amount and shape of the blocked fluid, but the friction parameterization employed in the model is extremely crude. An attempt to improve the model's representation of surface drag was made by taking

$$F(u) = C_u (u^2+v^2)^{1/2} u / h \qquad (4.47)$$

$$F(v) = C_u (u^2+v^2)^{1/2} v / h \quad . \qquad (4.48)$$

In general, the effect of this change on the overall shape of the fluid was minor. A simulation with C_u = 0.0018 (Fig. 4.15), for example, is quite similar to the basic simulation (see Fig. 4.8), although the equilibrium fluid interface is no longer a straight line. Because of the reciprocal dependence on h, the shallower margins of the fluid are retarded. We expect the model to be least valid in those regions due to neglect of density current effects and turbulent mixing. Also, rather than being constant, v varies considerably and reaches a maximum where the fluid is deepest.

To attempt to consider density current effects, the equation for the u component of wind for the rightmost fluid element was taken to be the equation for the speed of a density current (3.6)-(3.7), with K = 1. Because this is a diagnostic equation, the righthand side of the model quickly reaches an equilibrium density current height instead of gradually accelerating outward. The density current equation puts a further constraint on the blocking ability of the obstacle: not only must the u = 0

fluid slope be shallower than the maximum slope of the topography, but the trapped fluid must be deep enough to support a density current moving at a phase speed equal to and opposing the wind speed of the upper layer, which we shall take to be the geostrophic wind speed. This constraint would prevent any fluid from being permanently trapped in the simulation of Fig. 4.15, for example; the maximum fluid height was 250 m, while the density current height required for no motion is 280 m.

A density current fluid which is completely blocked is shown in Fig. 4.16 . The only parameter which has been altered from those in Fig. 4.15 is C_u, which has been increased to 0.005 . The edge of the density current is near the lowest inflection point of the topography, and the slope of the fluid is steeper than the topography, implying that some fluid could escape over the top without destroying the equilibrium. After twelve hours, the fluid has just barely reached the top of the obstacle. The shape of the fluid interface continues to be nearly a straight line. The simulation bears at least a superficial similarity to the observed Dec. 4 coastal front (Fig. 4.5). We will not attempt a specific simulation of the Dec. 4 coastal front case because the inherent inaccuracies of the model discussed on these pages lead us to expect that a close agreement of the model with a specific case would likely be due to a fortuitious cancelling of the errors and neglected parameters.

A final difficulty involves the assumption of two-dimensionality. The Appalachian Mountains of New England are approximately 425 km long. Fluid traveling southward at 10 m/s would pass from one end to the other in less than 12 hours. As a result, the behavior of the fluid blob in time cannot be interpreted as a representation of the motion of a coastal front interface at a given location. It is more appropriate to think of the model as representing the coastal front interface in a frame of reference moving southward with the lower fluid, although this not only violates the two-dimensional assumption but places great importance on the initial conditions for the form of the northern portions of the coastal front.

With a non-varying 'entrance region' at the northern margin of the cold air, steady-state conditions would be easy to achieve. Even situations which when considered two-dimensionally lead to no permanently blocked fluid, such as the basic model simulation (Fig. 4.8), would not necessarily prevent a coastal front from running the length of New England, although the front would be expected to lie closer to the mountains to the south as some of the cold air escapes over the ridge. It is probably not a coincidence that this tendency is indeed commonly observed, but no direct observations of cold air flow over the mountains in southern New England have been made.

Due to the above considerations, we feel that a satisfactory theoretical description of the interaction of coastal fronts in New England with orography is not possible without consideration of the fully three-dimensional problem.

5. PREDICTING COASTAL FRONTS

5.1 Generality of the NEWSEX Observations

How representative with respect to coastal fronts were conditions in New England during November and December, 1983? Type A and B coastal fronts require onshore winds and a land-sea temperature difference, while type C coastal fronts require onshore winds and an approaching warm front. According to monthly land and sea climatological data (National Climate Data Center, 1984; National Weather Service, 1984), the mean land-sea temperature contrast in east-central New England was 0.8 °C above normal. This slightly enhanced contrast would make ridge passage coastal fronts more likely to form. Spontaneous coastal fronts, which cannot form if a coastal front already exists, should be less common under enhanced temperature contrast conditions. The net effect should be a slight increase in the total number of coastal fronts.

Precipitation data is also available (NCDC, 1984), and a check of monthly totals revealed that the two months of NEWSEX were 44% wetter than normal. What this implies regarding coastal front frequency is not clear, however. Inasmuch as onshore winds in the New England wintertime generally occur in advance of mobile cyclones, the large amount of precipitation implies that storms were relatively frequent and that there may have been more episodes of onshore winds than normal. A direct comparison of the winds of the two month period with the climatological mean winds, or a comparison of storm tracks, have not been performed, although they would make an estimate of the relative expected frequency of

coastal fronts more accurate. From the available evidence, it appears likely that there should have been an above-normal incidence of coastal frontogenesis during NEWSEX.

The best available climatology of New England coastal fronts was made by Bosart (1975). Bosart scanned nine years (excluding May-August) of NMC surface maps for the occurrence of coastal fronts. His objective criteria for the existence of a coastal front, which had to be satisfied on two consecutive three-hourly maps, were:

1. 5 C or more surface temperature difference between BOS-ACK, BOS-CON, or BOS-PWM.

2. 40 degrees or more difference in surface wind direction between the same pair(s) of stations satisfying 1.

The station pair BOS-BDL was used occasionally to resolve marginal cases. Teletype data was employed for case verification when availiable. Bosart found a total of 30 coastal fronts in nine Novembers and Decembers, which averages out to 3.3 per November-December, much lower than the observed 13 coastal fronts of November-December, 1983.

The discrepancy could be due to more frequent occurence of costal fronts during 1983, imperfect detection of coastal fronts by Bosart, or a combination of the two. Imperfect detection is likely because Bosart did not have access to a mesoscale station network and only employed five stations in his coastal front search. To assess how well Bosart's method detects coastal fronts, the above objective criteria were applied to the NMC surface maps for November-December, 1983. The search uncovered a mere four possible coastal fronts, only three of which were confirmed to be coastal fronts with the PAM data. According to this synoptic map search, November-December 1983 was a period of average coastal front frequency.

New England coastal fronts are certainly more plentiful than the 6.3

per year Bosart's climatology implies. We hesitate to boldly extrapolate the 3 or 4 versus 13 discrepancy found for the two months of NEWSEX, though, since the land-sea contrast and precipitation data suggest more favorable than normal conditions for coastal frontogenesis. We therefore suggest that the average annual frequency of coastal fronts is between twelve and twenty-five coastal fronts per year.

The tendency for coastal frontogenesis was surprisingly robust during NEWSEX. The surface geostrophic wind direction at Boston, based on NMC six-hourly analyses, was estimated for the two-month period of NEWSEX. It was found that coastal fronts occurred during all ten periods of onshore winds at Boston, where a period of onshore winds was defined as at least two consecutive six-hourly analyses in which the geostrophic wind direction lay between east-northeast and south-southwest. Two or three coastal fronts occurred sequentially during two of those periods, so all thirteen observed coastal fronts are accounted for. It appears that, at least during that time of year when the sea is much warmer than the land, the simple presence of onshore wind can be confidently used to determine whether a coastal front should be expected to form.

Bosart (1975) constructed a mean surface pressure map for the time of onset of his 57 cases. The map, shown in Fig. 5.1, provides a means of assessing the representativeness of the sample of 13 coastal fronts from NEWSEX. Accordingly, for each of the 13 coastal fronts, the three-hourly NMC surface pressure analyses valid $\approx$3 hours before and $\approx$3 hours after the estimated time of coastal front collapse were reduced to a 2 degree latitude by 2 degree longitude grid. Means of the 'before' and 'after' pressure fields were then calculated. The resulting composites (Fig. 5.2) are almost identical to Bosart's composite map. The closest resemblance is with the 'after' map (Fig. 5.2b), which is to be expected since the PAM network can be used to detect coastal frontogenesis earlier than the hourly stations used by Bosart. It appears that the coastal fronts of NEWSEX were on the whole simliar to the

nine years of fronts which made up Bosart's climatology, and therefore representative of New England coastal fronts in general.

5.2 Conditions for Coastal Front Formation

While the composite maps discussed above were useful for determining the overall consistency between two sets of coastal front cases, they are not particularly useful for Bosart's intended purpose: to isolate prominent recurring synoptic features. As has been shown in this study, coastal fronts form under three distinct synoptic situations:

A. Ridge passage coastal fronts are associated with the passage of an anticyclone or inverted ridge from west to east across New England and the related veering of geostrophic surface winds from offshore to onshore.

B. Evening onset coastal fronts occur during the evening immediately following either the passage of a ridge or the dissipation of a ridge passage coastal front. Typically, the inverted ridge lies a few hundred kilometers to the east.

C. Spontaneous coastal fronts form when a warm front approaches from the south during onshore flow. The specific location of a ridge or anticyclone is irrelevant.

To illustrate these distinctions and to show the features common to each type, the gridded pressure data has been stratified by coastal front type and three sets of composites have been constructed. The composites of the latter two types, being composed of three and four cases each, do not necessarily represent the mean pressure field one would obtain from a larger sample. Detailed individual case studies have been presented in Chapter 2.

Ridge passage coastal fronts are in principle the easiest type of coastal front to forecast. They have a simple environmental requirement (an air-sea temperature difference) and a simple triggering mechanism (a wind shift from offshore to onshore). Aside from predicting the time of onset of onshore winds, which may done quite well by inspection of any of the currently operational numerical forecasts, the primary forecasting consideration should be an estimate of the magnitude of the temperature difference. Obviously, zero temperature difference or water cooler than air would prevent ridge passage coastal frontogenesis, while sufficiently large temperature contrast would favor frontogenesis.

One estimate of the critical magnitude of temperature difference necessary for coastal frontogenesis may be made from Fig. 3.17, which shows the location of a density current after 18 hours as a function of wind speed and temperature difference. Those model fronts which are advected more than 100 km inland by eighteen hours are comparatively weak relative to the strength of the mean flow. We therefore hypothesize that they would be unlikely to form in the first place or to retain their frontal characteristics for an extended period of time. Using Fig. 3.17, this criterion can be approximated as

$$\Delta T_{min} = 3\,|U|^2/40 + 0.3 \quad . \tag{5.1}$$

For a wind speed of 10 m/s, for example, the formula requires a difference between sea temperatures and land air temperatures of at least 4 K.

The observed ridge passage events indicate that this relationship underestimates the temperature difference required for type A coastal frontogenesis. Fig. 5.3 shows estimates of ΔT, $|U|$, and ΔT_{min} for all ten onsets of onshore wind. Ridge passages associated with type A coastal frontogenesis are denoted with dots, while other ridge passages are denoted

with open circles. The most inconsistent point is for the Nov. 10 ridge passage, in which a coastal front formed even though the temperature difference was 1 K. A close examination of that case showed that it was the only ridge passage event which took place near sundown, and that temperatures over water were 3-4 K warmer than sea surface temperatures. If the air temperature over water is used rather than the sea surface temperature, the point moves into the parameter space of expected coastal fronogenesis.

The composite surface pressure maps before and after ridge passage coastal frontogenesis (Fig. 5.4) illustrate the principal feature of this type of frontogenesis: a mobile anticyclone travelling across northern New England. The critical difference between the two maps is the change in wind direction along the southeast New England coast: in Fig. 5.4a, the geostrophic wind is very light and northerly, while in Fig. 5.4b, it is slightly stronger and southeasterly. The surface wind directions implied by these pressure patterns are northwesterly and easterly, respectively. The stationary, inverted ridge extending southward from New England along the east side of the Appalachians is the signature of strong cold-air damming (Baker, 1970) and is symptomatic of the cold air circulating around the anticyclone. When this pressure pattern occurs along the southern part of the Eastern Seaboard, it is normally associated with the existence of a Carolina coastal front. In Fig. 5.4b, a secondary low appears along the trough east of the mountains. Such lows typically form near the intersection between warm fronts and coastal fronts as primary cyclones approach the mountains from the west, and often intensify rapidly and grow to dominate the system. All of these mesoscale features are generally associated with the same synoptic-scale pressure pattern which produces ridge passage coastal fronts: a large, cold anticyclone moving eastward across the coast, and the implied approach of a cyclone from the west or southwest.

Type B coastal fronts form as a result of an enhanced nighttime temperature contrast in the presence of light onshore winds. A necessary condition, therefore, in addition to light onshore winds, is daytime temperatures over land comparable to sea surface temperatures. If land temperatures are too cold, a ridge passage front will already exist. If land temperatures are too warm, nocturnal cooling might not be strong enough to reverse the temperature gradient and set up a coastal front. As could best be determined, all three type B NEWSEX fronts formed between 5 PM and 8 PM local time, or during the hours immediately after sunset. With higher land temperatures or less rapid radiational cooling, coastal fronts would be expected to form a bit later in the evening.

The composite surface pressure maps for evening onset coastal frontogenesis (Fig. 5.5) are grossly similar to the ridge passage maps (Fig. 5.4) but contain some significant differences. In the type B composites, winds along the New England coast are light and onshore both before and after coastal frontogenesis. One would not expect any significant systematic change in the local pressure pattern such as is associated with type A frontogenesis. Also, the inverted ridge along the Appalachians is much less apparent. This is indicative of the generally warmer air temperatures associated with evening onset frontogenesis. The weak cyclone in the Atlantic appearing in the composites is due to a single case (Nov. 14-15) and is not representative of type B events.

Prediction of spontaneous coastal frontogenesis would ideally be made through the application of Fig. 4.1b using forecasted values of wind velocity, horizontal temperature gradient, and vertical stratification. In practice, however, it may prove to be more expeditious to simply base forecasts on the expected location and motion of warm fronts, since conditions theoretically suitable for spontaneous coastal frontogenesis tend to occur in warm frontal zones. The converse also seems to be true: warm fronts pronounced enough to have been analyzed on an NMC surface map

tend to imply favorable conditions for type C coastal frontogenesis. Forecasting frontogenesis is thereby reduced to forecasting the approach of warm fronts. From the case study of Chapter 2 and from theoretical considerations, frontogenesis should begin at about the time the northern edge of the surface frontal zone reaches the mountains. Since the warm front on a synoptic weather map represents the southern, warm edge of the frontal zone, the analyzed front should still lie some distance to the south at the time of frontogenesis. The exact distance depends on the vertical thickness of the frontal zone and the slope of the front, both of which can be estimated from a pair of soundings through the frontal zone.

The composite maps (Fig. 5.6) reflect the fact that spontaneous coastal frontogenesis is brought about by an entirely different process than the other two types of frontogenesis. The surface cyclone is much closer to New England, and the onshore winds are relatively strong. The net warm frontal trough position is near 39.5N before frontogenesis, and has moved to 40.5N six hours later. Meanwhile, the cold frontal trough has reached the eastern seaboard. Spontaneous coastal fronts tend not to last as long as other coastal fronts because winds become offshore again sooner.

5.3 Location and Motion of Coastal Fronts

The initial location of coastal frontogenesis is consistent and easy to predict. Fig. 5.7 shows the preferred locations of coastal frontogenesis as observed in NEWSEX, stratified by type of coastal front. Ridge passage and evening onset coastal fronts first appear just off the coast, extending from the Boston area northward to possibly beyond Portland, Maine. The four spontaneous coastal fronts formed along a band stretching between the Connecticut-Massachusetts-Rhode Island triple point and a point about 10-15

km north of Portsmouth, New Hampshire. Possible northward and southward extensions are uncertain, due to lack of data.

Predicting the motion of coastal fronts is more difficult. The density current model of Chapter 3 showed the tendency of most land-breeze coastal fronts to stay a short distance offshore. Generally, the onshore wind speed increases with time, driving the front back inland. At some point the cold air begins interacting with the mountains, hindering the further retreat of the cold air and affecting the shape of the coastal front. Coastal fronts which move inland do so most readily across southeastern Massachusetts, and they tend to stall along a line running south-southwest from the Maine coast to Providence or northeastern Connecticut. While changes in the temperature difference will affect the motion of the front, with a decrease of the difference helping push the front inland, the primary variable controlling frontal motion is the warm air wind. If and when the wind shifts so that it is parallel to the front or blowing offshore, the front can be expected to quickly slide out to sea, leaving sharp temperature falls and possible freezing conditions in its wake.

All three types of coastal front are worthy of forecasting consideration. Ridge passage coastal fronts are most likely to have a significant impact on the local weather. They are potentially the longest lived, and because they often separate below-freezing cold air from air which has been heated by the sea surface, they frequently delineate changes in precipitation type. They often separate rain from freezing rain or accumulating snow from melting snow, and thus can cause dangerous, rapid changes in driving or flying conditions. Evening onset fronts, because the temperature difference is weaker, tend to be somewhat less severe. The cold air behind spontaneous coastal fronts is usually above freezing, but because they form at a time of strong warm advection, they can quickly generate substantial temperature discontinuities over a short distance.

6. DISCUSSION

6.1 Conclusions

Coastal fronts are a common late fall and early winter feature of southern New England. Coastal fronts existed during at least part of every onshore flow episode during November and December 1983. We estimate, based on a two-month sample and comparison with an earlier climatology (Bosart, 1975), that an average of 12-25 coastal fronts per year form in eastern New England. Bosart's estimate of coastal front frequency is too low because many weak coastal fronts escape detection by standard meteorological observations.

We found three clearly distinguishable modes of formation. Type A, or ridge passage, coastal fronts form as part of a thermally direct circulation driven by heating of relatively cold air by the adjacent sea surface. Frontogenesis occurs as winds veer from offshore to onshore as a result of the passage of a surface high pressure ridge from west to east. Inland winds remain parallel to the coast, and the front initially forms a few kilometers offshore, possibly as a consequence of differential friction. Most case studies of coastal fronts in the literature are of type A coastal fronts. To investigate the tendency for type A fronts to remain near the coast, we have modeled them using a one-dimensional density current model. The tendency was found to be due to the interaction of veering winds and differential heating.

Type B (evening onset) coastal frontogenesis occurs in a preexisting onshore airflow when the diurnal variation of temperature over land is such that a strong land-sea temperature gradient can exist at night but not during the day. As temperatures fall over land during the evening, winds

back to northerly and a coastal front forms along the coast, much like a land breeze. Once formed, type A and type B coastal fronts are indistinguishable, except that type A fronts are inherently capable of having larger temperature discontinuities. Neither type A nor type B frontogenesis require the existence of a cyclone, and both may persist for days under suitable onshore wind conditions.

Type C (spontaneous) coastal fronts are caused by upstream blocking of a warm-advective, stable airflow by the Appalachian Mountains, as has been modeled by Garner (1986). This process is not dependent on the existence of a nearby coastline. As the stable zone (commonly a warm front) descends to the level of the orography, the air is partially blocked and decelerated. Differential warm advection enhances the blocking by increasing the vertical stratification. The coastal front forms near the base of the mountains.

Although the inland mountains have but a secondary influence on type A or type B frontogenesis by channeling the cold air winds, they dam the dome of cold air which becomes isolated beneath the coastal front inversion. We have expressed the cold-air damming problem as one of an isolated layer of dense fluid forced geostrophically against a two-dimensional obstacle. A Lagrangian model showed that the density difference, the ambient pressure gradient, and the surface friction governed the degree of damming and the extent of the trapped air in a simplified system.

6.2 Coastal Frontogenesis in Other Areas

Coastal fronts similar to those in New England should be expected in geographical areas with similar orographic elements. For example, a favored location for type A and type B coastal fronts would have a long, nearly straight coastline with few bays, and frequent cold air outbreaks

with the land on the right relative to the cold airflow in order to favor frictional convergence. In the Northern Hemisphere, this implies a north- or east-facing coastline. In the contiguous United States, these conditions are satisfied by the eastern New England coast, the Atlantic coastline from central North Carolina southward to central Florida, and to a lesser extent the south Texas coast. These areas indeed experience coastal frontogenesis (Bosart *et al.*, 1972). Long-lived type A or B fronts require cold-air damming to reinforce the temperature gradient and hinder the inland movement of the front. Again, New England satisfies this condition, as does the Carolina coast.

An additional factor in the Carolinas is the presence of the Gulf Stream, which introduces differential surface heating over the ocean. Thermally-driven coastal fronts form along the north wall of the Gulf Stream (Riordan *et al.*, 1985), much as a type A front would form along the coastline. Such fronts are usually not observed directly until they move across the coastal waters and onshore. Also, the damming aspect ratio (the height of the ridge line divided by the distance from the locus of coastal frontogenesis) is .0025 for the Carolinas, compared to .006 for New England. As was derived in Section 4.5, the slope of the dammed cold air is independent of the height of the obstacle, and therefore we should expect the margin of cold air damming to lie further inland in the Carolinas compared to New England.

There is some evidence that the inland motion of the coastal front to the margin of the dammed air in the Carolinas is accomplished by the front decaying along the coast and reforming inland. George (1960) discusses warm fronts which 'jump' from one location to another, and gives as an example what we would now call a coastal front jumping from the Carolina coast to the Piedmont. Also, preliminary analysis of GALE (Genesis of Atlantic Lows Experiment) data from March 13 shows such a process occurring. Fig. 6.1, a surface map constructed with preliminary PAM data and other surface data, shows the inland front within hours of its initial

appearance. The southern portion of the offshore coastal front had vanished, and winds became easterly along the entire coastal plain, without any apparent frontal passages, during the subsequent few hours.

Type C frontogenesis is dependent upon a steep mountain range, not directly abutting a warm body of water, which experiences warm frontal passages. In the Northern Hemisphere, this would imply mountains with at least some southward exposure. In the contiguous United States, this includes most of the Appalachians, the Sierra Nevada, and certain ranges in the Rocky Mountains. Indeed, the term 'coastal front' is a misnomer for type C fronts, and it would be more appropriate to use another name to refer to them, such as orographic fronts, blocked warm fronts, or Garner fronts.

6.3 Other Topics

Not considered in this study are coastal fronts caused by so-called zipper lows (Clark, 1983; Keshishian and Bosart, 1987). None were observed during NEWSEX. Unlike type A fronts, the frontogenetical forcing ahead of zipper lows is largely geostrophic. It is not known whether zipper low coastal fronts are confined to the boundary layer like other types of coastal fronts or extend through the lower troposphere.

We suggest that future work on coastal fronts be concentrated on investigating their interactions with synoptic-scale weather systems. Coastal fronts may act as low-level hyperbaroclinic zones favorable to small-scale cyclogenesis, or the frontal surface may serve to decouple the cold air from the lower troposphere, producing an effect similar to a rigid orographic feature. We expect that the unprecented three-dimensional coastal front data set available from GALE may be used to investigate this problem, and to clarify the similarities and differences between Carolina coastal frontogenesis and New England coastal frontogenesis.

BIBLIOGRAPHY

Atkinson, B. W., 1981: Meso- Scale Atmospheric Circulations. Academic Press, London, 495 pp.

Baines, P. G., 1984: A unified description of two-layer flow over topography. *J Fluid Mech.* **146** : 127-167.

_____, 1986: The effects of rotation on disturbances upstream of cold fronts approaching south-eastern Australia. *Preprint Volume Second International Conference on Southern Hemisphere Meteorology,* American Meteorological Society, Boston, Mass., no. 3.6 .

_____, and P. A. Davies, 1980: Laboratory studies of topographic effects in rotating and/or stratified fluids. *Orographic Effects in Planetary Flows,* GARP Publication Series No. 23, WMO-CSU, Chap. 8.

_____, and K. P. Hoinka, 1985: Stratified flow over two-dimensional topography in fluid of infinite depth: a laboratory simulation. *J Atmos. Sci.* **42** : 1614-1630.

Baker, D. G., 1970: A study of high pressure ridges to the east of the Appalachian Mountains. Ph. D. thesis, Massachusetts Institute of Technology, Cambridge, Mass., 127 pp.

Ballentine, R. J., 1980: A numerical investigation of New England coastal frontogenesis. *Mon. Wea. Rev.* **108** : 1479-1497.

_____, 1982: Numerical simulation of land-breeze-induced snowbands along the western shore of Lake Michigan. *Mon. Wea. Rev.* **110** : 1544-1553.

Benjamin, T. B., 1968: Gravity currents and related phenomena. *J Fluid Mech.* **31** : 209-248.

Bergeron, T., 1949: The problem of artificial control of rainfall on the globe. II: the coastal orographic maxima of precipitation in autumn and winter. *Tellus* **1(3)** : 15-32.

Biggs, W. G., and M. E. Graves, 1962: A lake breeze index. *J Appl. Meteor.* **1** : 474-480.

Bosart, L. F., 1975: New England coastal frontogenesis. *Quart. J Roy. Meteor. Soc.* **101** : 957-978.

_____, 1981: The Presidents' Day Snowstorm of 18-19 February 1979: a subsynoptic-scale event. *Mon. Wea. Rev.* **109**: 1542-1566.

_____, 1984: The Texas coastal rainstorm of 17-21 September 1979: an example of synoptic-mesoscale interaction. *Mon. Wea. Rev.* **112** : 1108-1133.

_____, C. J. Vaudo, and J. H. Helsdon, Jr., 1972: Coastal frontogenesis. *J Appl. Meteor.* **11** : 1236-1258.

Clark, D. A., 1983: A comparative study of coastal frontogenesis. M. S. thesis, Massachusetts Institute of Technology, Cambridge, Mass., 86 pp.

Craig, R. A., I. Katz, and P. J. Harney, 1945: Sea breeze cross sections from psychometric measurements. *Bull. Amer. Meteor. Soc.* **26** : 405-410.

Deardorff, J. W., 1972: Parameterization of the planetary boundary layer for use in general circulation models. Mon. Wea. Rev. **100** : 93-106.

Defant, F., 1951: Local Winds. *Compendium of Meteorology,* T. F. Malone, ed., American Meteorological Society, Boston, pp. 655-672.

Draghici, I., 1984: Black Sea coastal frontogenesis. *Nowcasting II: Mesoscale Observations and Very-Short-Range Weather Forecasting.* European Space Agency. pp. 75-79.

Estoque, M. A., 1962: The sea breeze as a function of the prevailing synoptic situation. *J Atmos. Sci.* **19** : 244-250.

Fisher, E. L., 1960: An observational study of the sea breeze. *J Meteor.* **17** : 645-660.

Forbes, G. S., R. A. Anthes, and D. W. Thomson, 1987: Synoptic and mesoscale aspects of an Appalachian ice storm associated with cold-air damming. *Mon. Wea. Rev.* **115** : 564-591.

Frizzola, J. A., and E. L. Fisher, 1963: A series of sea breeze observations in the New York City area. *J Appl. Meteor.* **2** : 722-739.

Garner, S. T., 1986: An orographic mechanism for rapid frontogenesis. Ph. D. thesis, Massachusetts Institute of Technology, Cambridge, Mass., 222 pp.

Garratt, J. R., and W. L. Physick, 1986: Numerical study of atmospheric gravity currents. I: simulations and observations of cold fronts. *Beitr. Phys. Atmos.* **59** : 282-300.

George, J. J., 1960: Weather Forecasting for Aeronautics. Academic Press, New York, 673 pp.

Gross, G., 1986: A numerical study of the land and sea breeze including cloud formation. *Beitr. Phys. Atmos.* **59** : 97-114.

Helmis, C. G., D. N. Asimakopoulos, G. D. Deligiorgi, and D. P. Lalas, 1987. Observation of sea-breeze fronts near the shoreline. *Bound. Lay. Meteor.* **38** : 395-410.

Keshishian, L. G., and L. F. Bosart, 1987: A case study of extended East Coast frontogenesis. *Mon. Wea. Rev.* **115** : 100-117.

Kozo, T. L., 1982: A mathematical model of sea breezes along the Alaskan Beaufort Sea coast: part II. *J Appl. Meteor.* **21** : 906-924.

Lettau, H. H., and W. Schwerdtfeger, 1967: Dynamics of the surface-wind regime over the interior of Antarctica. *Antarc. J United States* **2** : 155-158.

Long, R. R., 1970: Blocking effects in flow over obstacles. *Tellus* **22** : 471-480.

Lyons, W. A., 1972: The climatology and prediction of the Chicago lake breeze. *J Appl. Meteor.* **11** : 1259-1270.

Mak, M. K., and J. E. Walsh, 1976: On the relative intensities of sea and land breezes. *J Atmos. Sci.* **33** : 242-251.

Marks, F. D., Jr., and P. M. Austin, 1979: Effects of the New England coastal front on the distribution of precipitation. *Mon. Wea. Rev.* **107** : 53-67.

Mason, P. J., and R. I. Sykes, 1978: On the interaction of topography and Ekman boundary layer pumping in a stratified atmosphere. *Quart. J Roy. Meteor. Soc.* **104** : 475-490.

McPherson, R. D., 1970: A numerical study of the effect of a coastal irregularity on the sea breeze. *J Appl. Meteor.* **9** : 767-777.

Mitsumoto, S., H. Ueda, and H. Ozoe, 1983: A laboratory experiment on the dynamics of the land and sea breeze. *J Atmos. Sci.* **40** : 1228-1240.

National Climatic Data Center, 1984: Climatological data, 1983 annual summary, New England. Asheville, N. C.

National Weather Service, 1984: Oceanographic monthly summary, Nov. - Dec. 1983. Washington, D. C.

Neilley, P. P., 1984: Application of a density current model to aircraft observations of the New England coastal front. M. S. thesis, Massachusetts Institute of Technology, Cambridge, Mass., 64 pp.

Neumann, J., and Y. Mahrer, 1971: A theoretical study of the land and sea breeze circulation. *J Atmos. Sci.* **28** : 532-542.

Parish, T. R., 1982: Barrier winds along the Sierra Nevada mountains. *J Appl. Meteor.* **21** : 925-930.

Passarelli, R. E., Jr., and H. Boehme, 1983: The orographic modulation of pre-warm-front precipitation in southern New England. *Mon. Wea. Rev.* **111** : 1062-1070.

_____, and R. R. Braham, Jr., 1981: The role of the winter land breeze in the formation of Great Lake snow storms. *Bull. Amer. Meteor. Soc.* **62** : 482-491.

Patrinos, A. A. N., and A. L. Kistler, 1977: A numerical study of the Chicago lake breeze. *Bound. Lay. Meteor.* **12** : 93-123.

Pearson, R. A., 1975: On the asymmetry of the land-breeze sea-breeze circulation. *Quart. J Roy. Meteor. Soc.* **101** : 529-536.

_____, G. Carboni, and G. Brusasca, 1983: The sea breeze with mean flow. *Quart. J Roy. Meteor. Soc.* **109** : 809-830.

Physick, W., 1976: A numerical model of the sea-breeze phenomenon over a lake or gulf. *J Atmos. Sci.* **33** : 2107-2135.

Pielke, R. A., 1974: A three-dimensional numerical model of the sea breezes over south Florida. *Mon. Wea. Rev.* **102** : 115-139.

Pierrehumbert, R. T., 1984: Linear results on the barrier effects of mesoscale mountains. *J Atmos. Sci.* 41 : 1356-1367.

_____, 1985: Stratified semigeostrophic flow over two-dimensional topography in an unbounded atmosphere. *J Atmos. Sci.* **42** : 523-526.

_____, and B. Wyman, 1985: Upstream effects of mesoscale mountains. *J Atmos. Sci.* **42** : 977-1003.

Riordan, A. J., S. SethuRaman, J. M. Davis, and S. Viessman, 1985: Measurements in the marine boundary layer near a coastal front. *Geophys. Res. Let.* **12** : 681-684.

Roeloffzen, J. C., W. D. Van Den Berg, and J. Oerlemans, 1986: Frictional convergence at coastlines. *Tellus* **38A** : 397-411.

Rotunno, R., 1983: On the linear theory of the land and sea breeze. J *Atmos. Sci.* **40** : 1999-2009.

Sanders, F., 1955: An investigation of the structure and dynamics of an intense surface frontal zone. *J Meteor.* **12** : 542-552.

_____, 1983: Observations of fronts. *Mesoscale Meteorology - Theories, Observations, and Methods,* D. K. Lilly and T. Gal-Chen, eds., pp. 175-203.

Schoenberger, L. M., 1984: Doppler radar observations of a land-breeze cold front. *Mon. Wea. Rev.* **112** : 2455-2464.

Seitter, K. L., 1986: A numerical study of atmospheric density current motion including the effects of condensation. *J Atmos. Sci.* **43** : 3068-3076.

Shapiro, M. A., T. Hampel, D. Rotzoll, and F. Mosher, 1985: The frontal hydraulic head: a micro - α scale (~ 1 km) triggering mechanism for mesoconvective weather systems. *Mon. Wea. Rev.* **113** : 1166-1183.

Simpson, J. E., 1969: A comparison between laboratory and atmospheric density currents. *Quart. J Roy. Meteor.* Soc. **95** : 758-765.

_____, and R. E. Britter, 1980: A laboratory model of an atmospheric mesofront. *Quart. J Roy. Meteor. Soc.* **106** : 485-500.

_____, D. A. Mansfield, and J. R. Milford, 1977: Inland penetration of sea-breeze fronts. *Quart. J Roy. Meteor. Soc.* **103** : 47-76.

Ueda, H., 1983: Effects of external parameters on the flow field in the coastal region - a linear model. *J Clim. Appl. Meteor.* **22** : 312-321.

Van Den Berg, W. D., 1986: Coastal frontogenesis in the Netherlands: observations and modelling. Ph. D. thesis, University of Ultrecht. Discussed in Roeloffzen et al., 1986.

Walsh, J. E., 1974: Sea breeze theory and applications. *J Atmos. Sci.* **31** : 2012-2026.

Watts, A. J., 1955: Sea-breeze at Thorney Island. *Meteor. Mag.* **84** : 42-48.

Young, G. S., and R. H. Johnson, 1984: Meso- and microscale features of a Colorado cold front. *J Clim. Appl. Meteor.* **23** : 1315-1325.

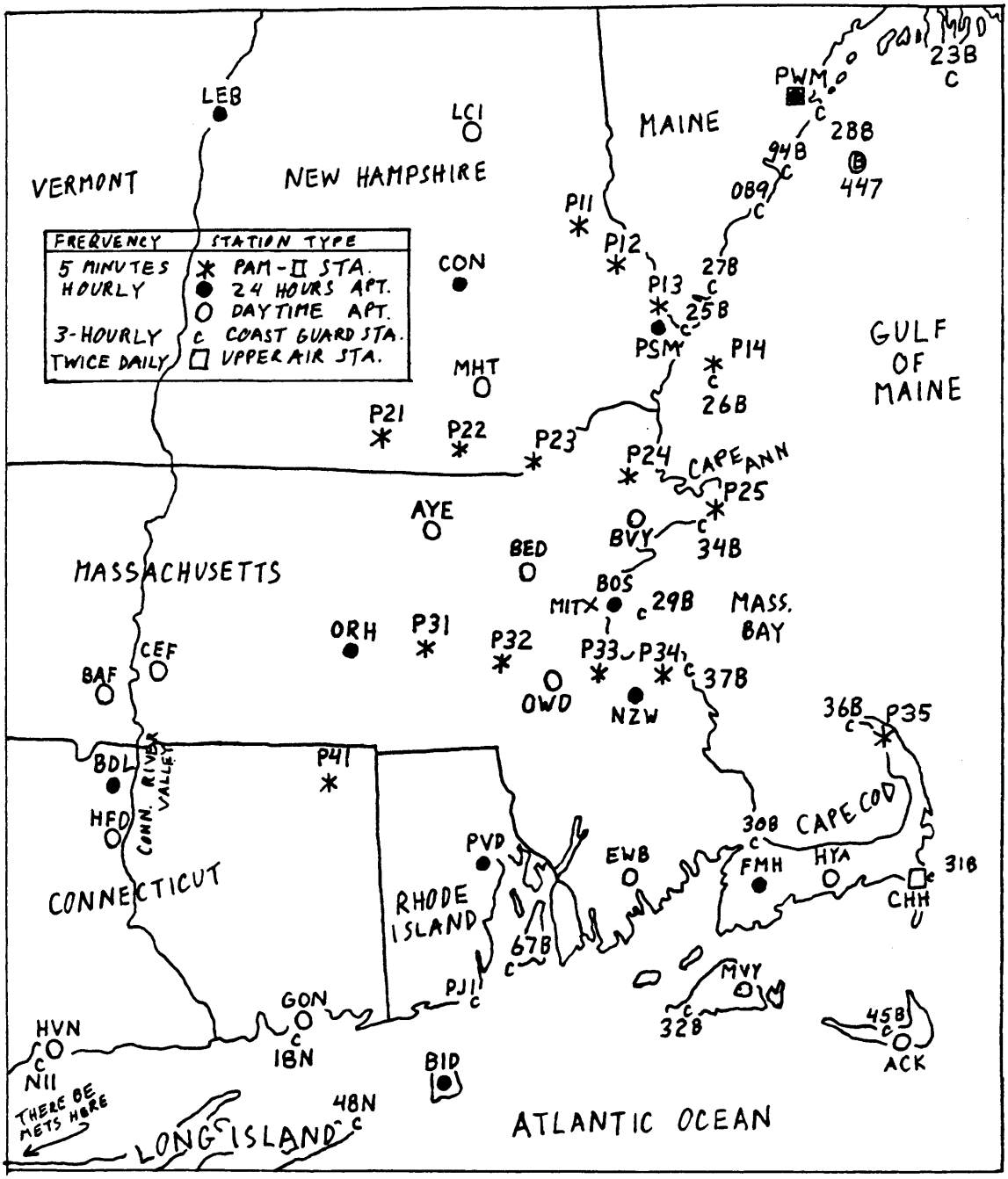

Fig. 1.1 Map of southeastern New England, showing locations of PAM stations (asterisks), hourly stations (circles, filled if station reports 24 hours a day), Coast Guard stations (c's), and upper air sounding sites (squares).

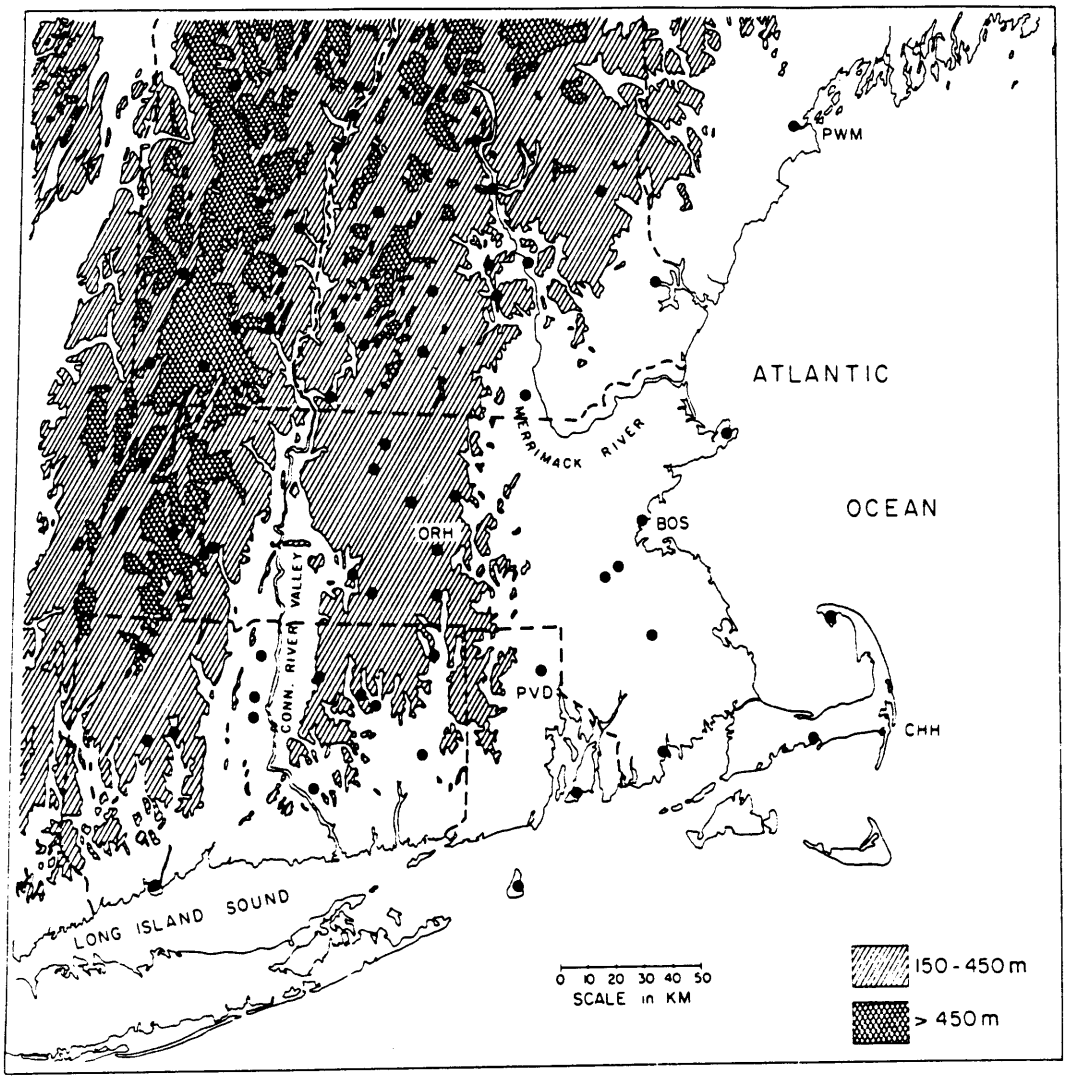

Fig. 1.2 Surface elevations across southern New England (from Passarelli and Boehme, 1983).

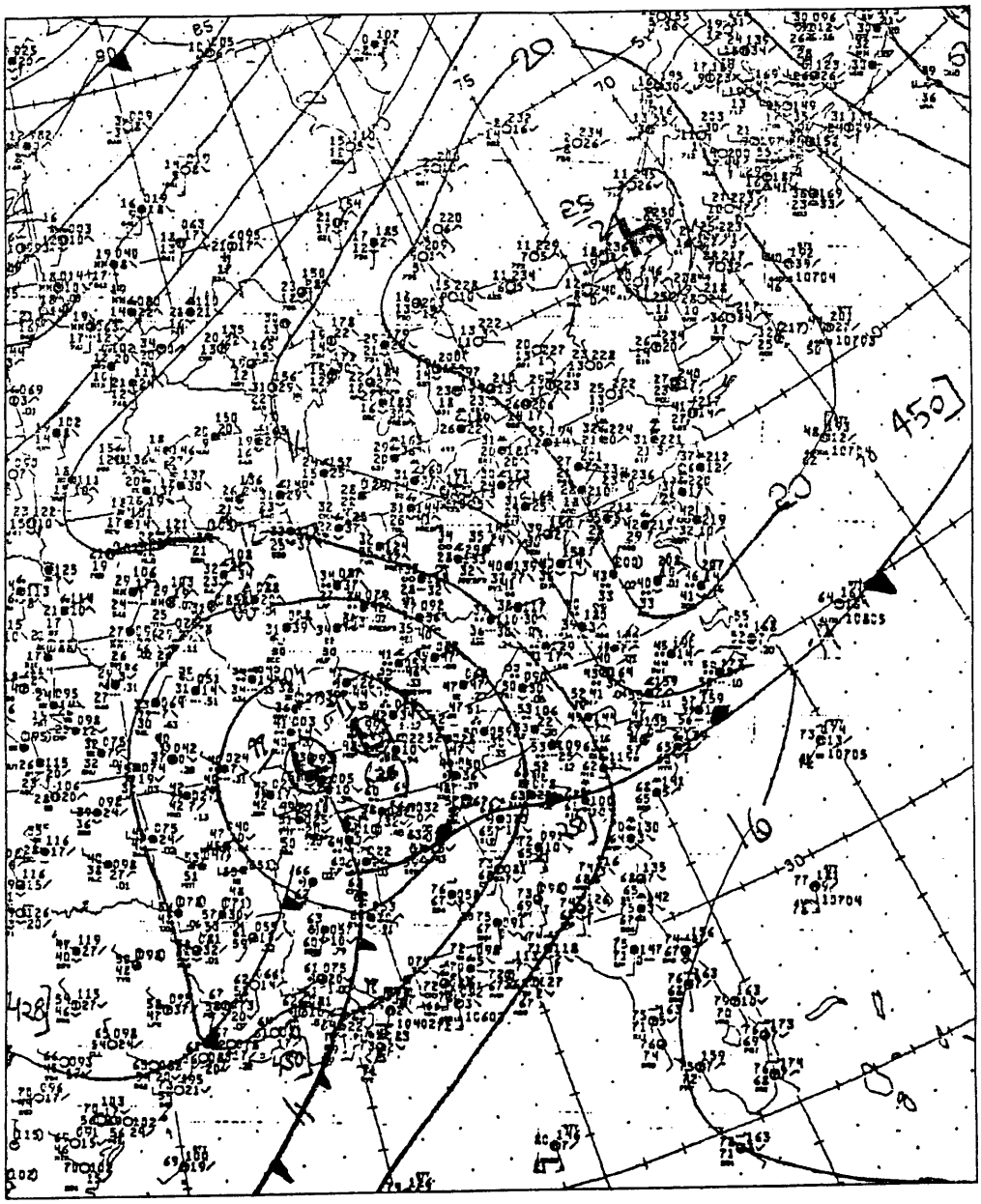

Fig. 2.1 National Meterological Center (NMC) operational surface analysis, eastern United States, 0000 4 Dec 1983.

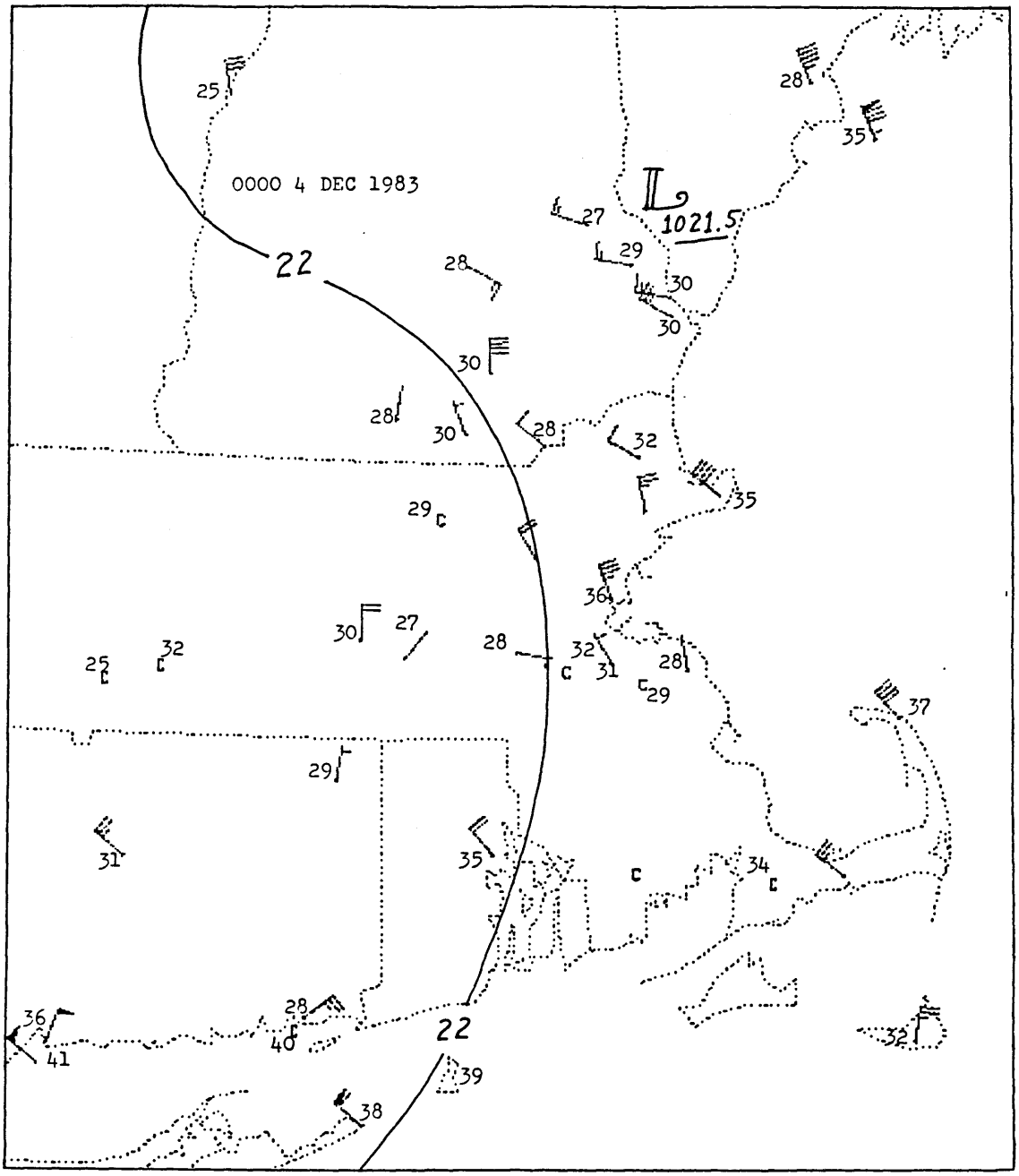

Fig. 2.2 Mesoscale analysis of southeastern New England, 0000 4 Dec 1983. Wind directions are indicated in the conventional manner, and speeds are plotted using pennants (5 m/s), barbs (1 m/s), and half-barbs (0.5 m/s). Temperatures are plotted in degrees Fahrenheit. The surface pressure analysis (contour interval = 1 mb = 100 Pa, first two digits dropped from contour labels) is from corrected altimeter settings. See text for details.

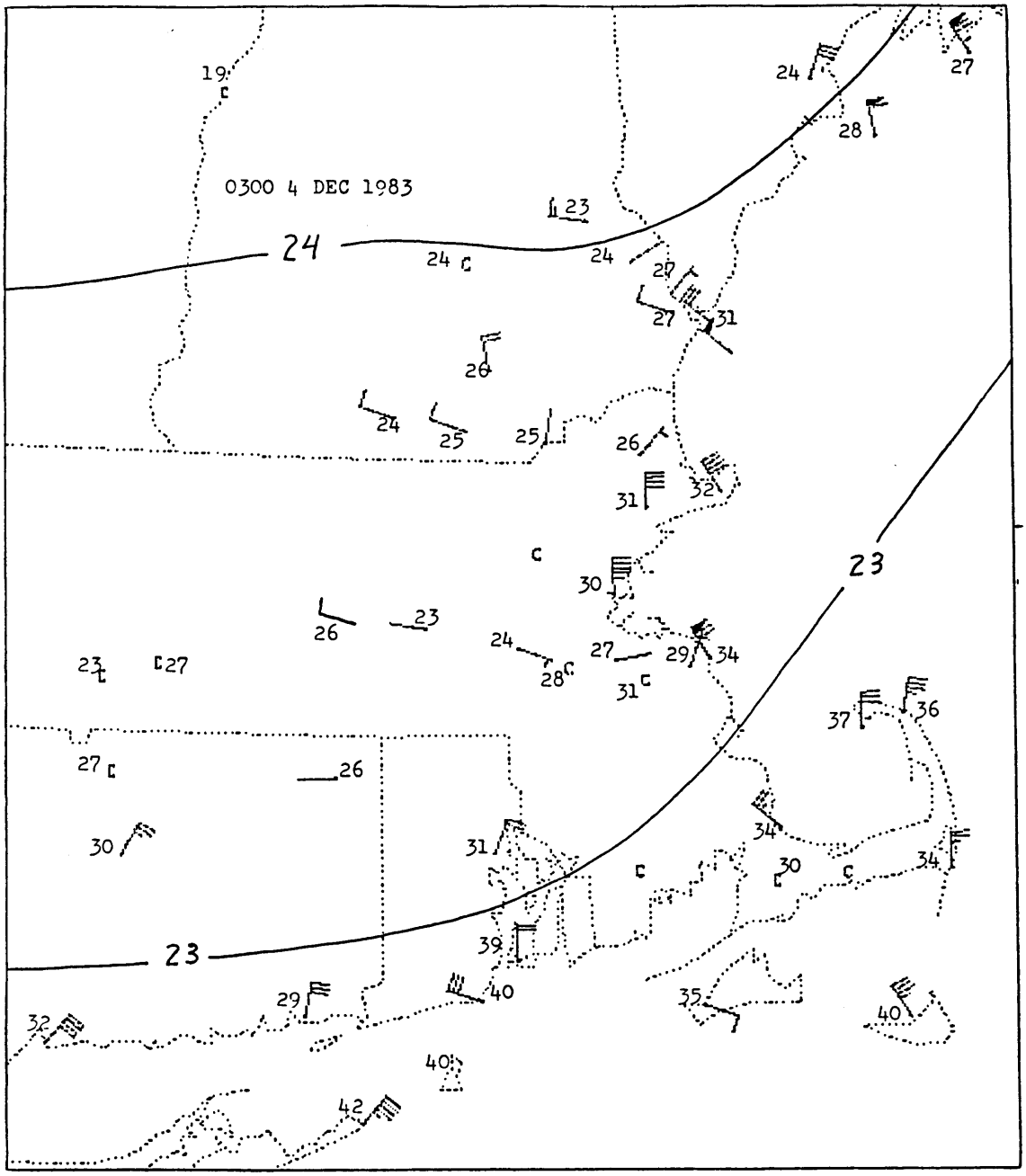

Fig. 2.3 Mesoscale analysis (as in Fig. 2.2), 0300 4 Dec 1983.

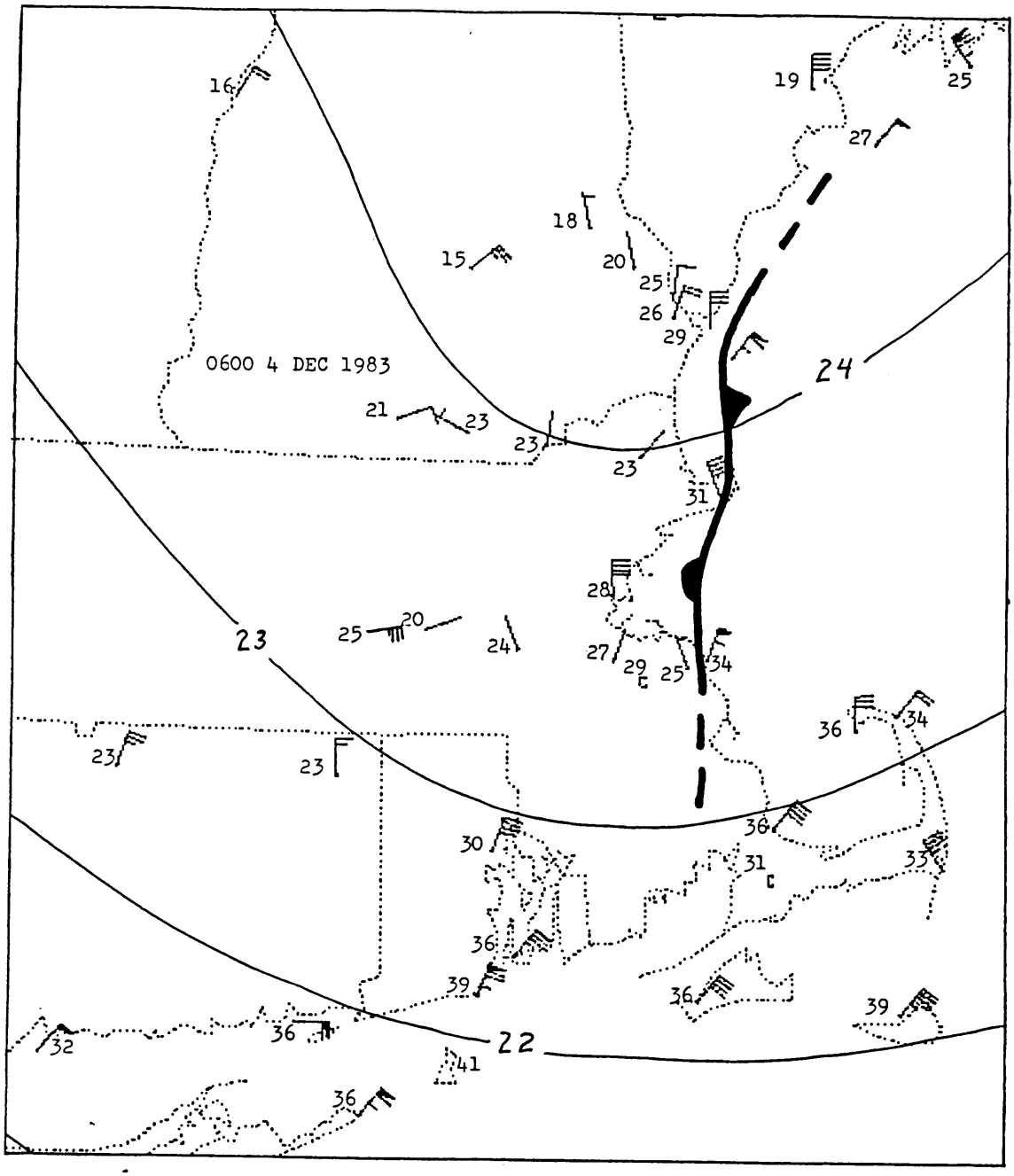

Fig. 2.4 Mesoscale analysis (as in Fig. 2.2), 0600 4 Dec 1983.

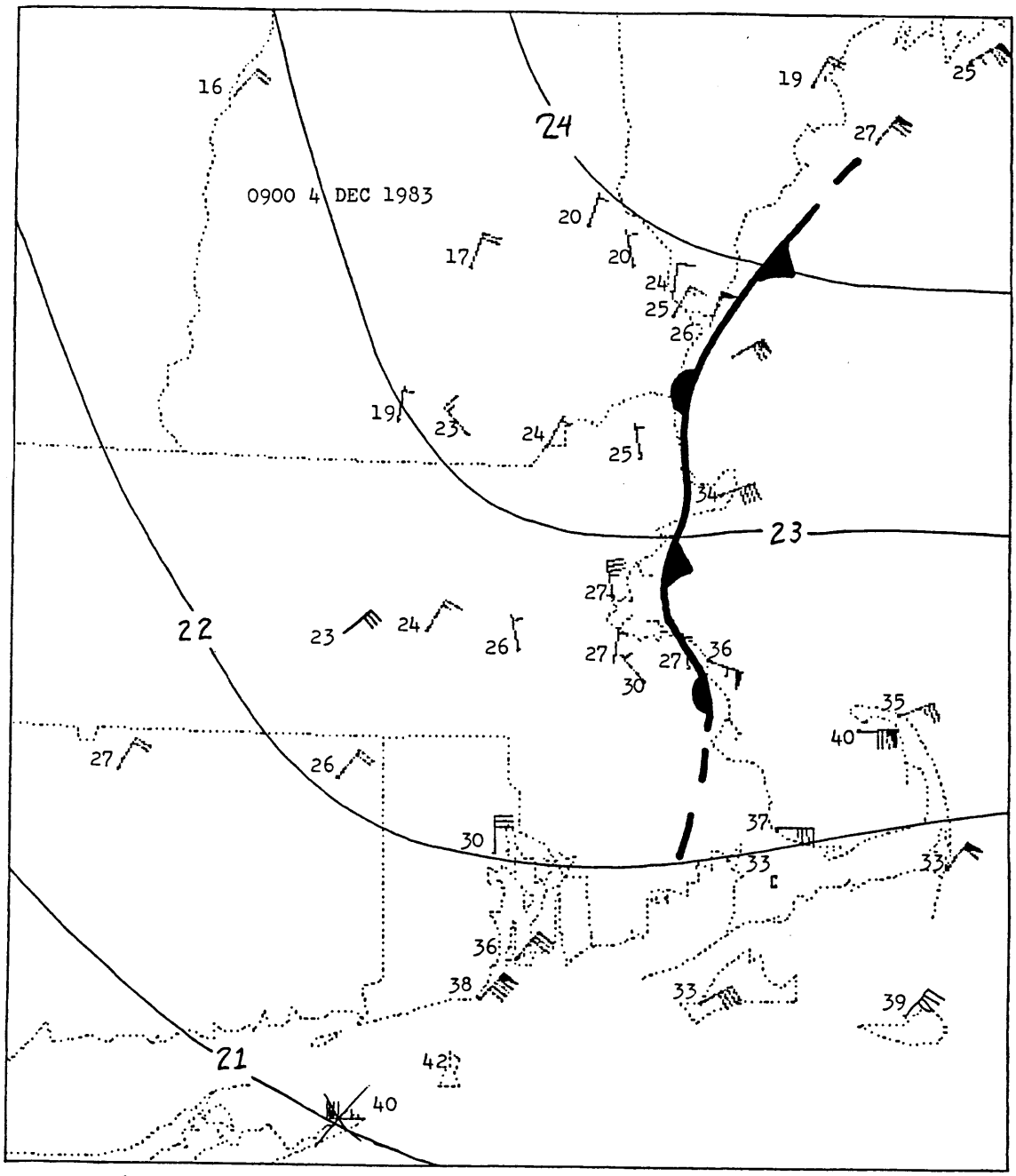

Fig. 2.5 Mesoscale analysis (as in Fig. 2.2), 0900 4 Dec 1983.

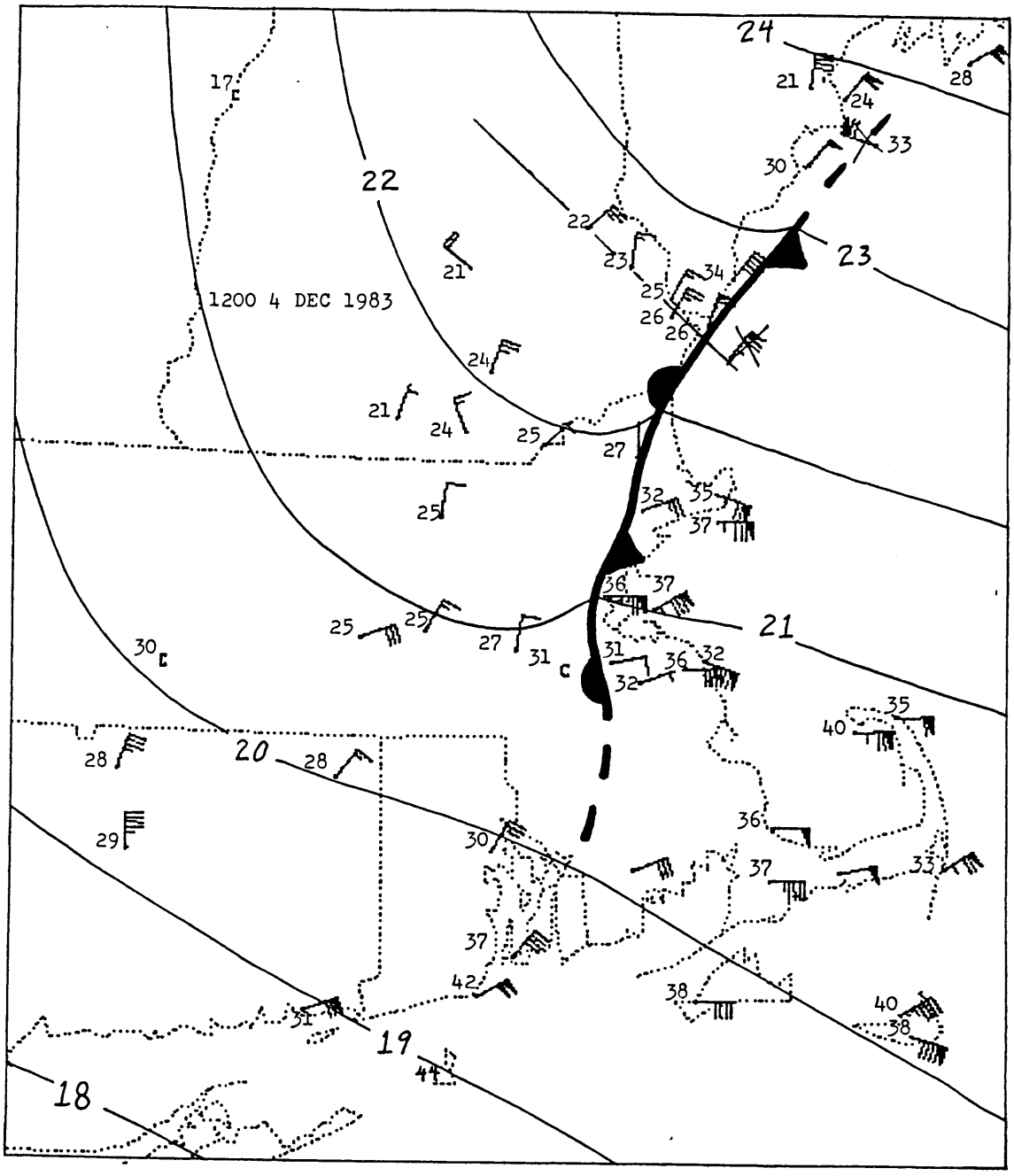

Fig. 2.6 Mesoscale analysis (as in Fig. 2.2), 1200 4 Dec 1983.

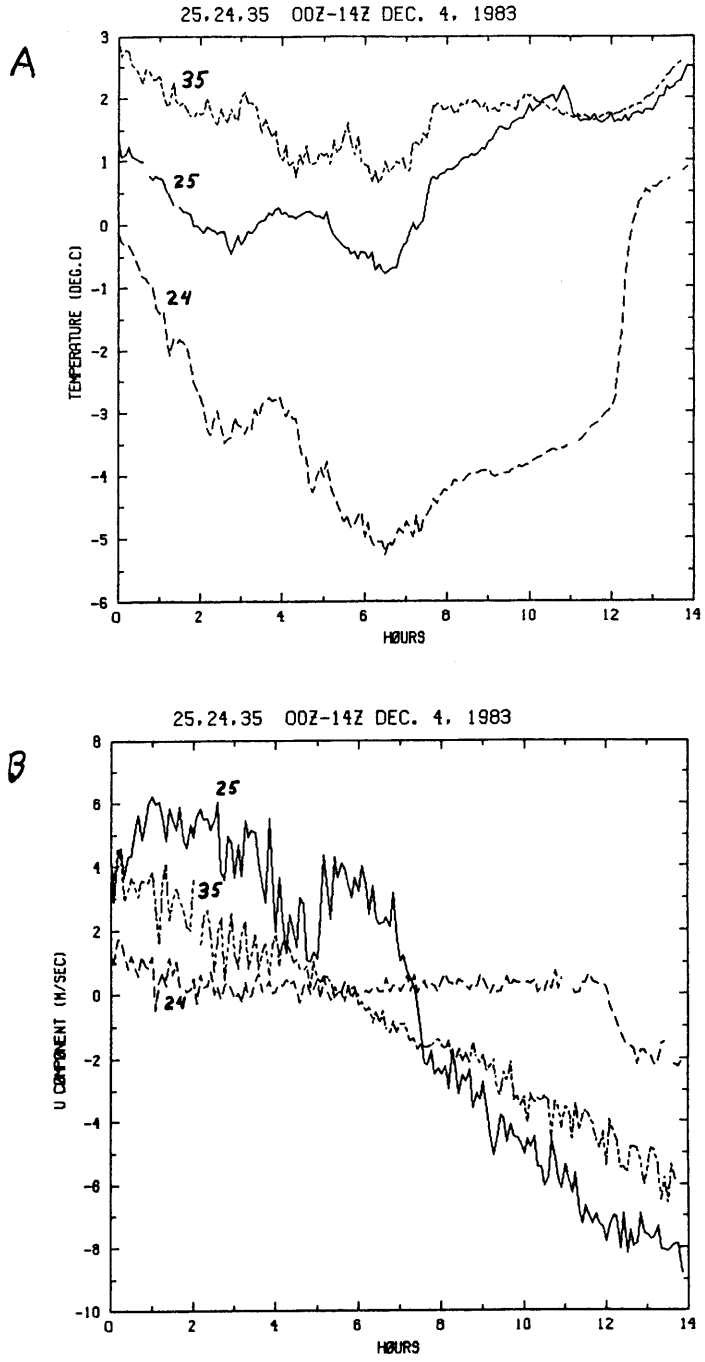

Fig. 2.7 Time series, stations P24, P25, and P35, 0000 4 Dec 1983 - 1400 4 Dec 1983. a) Temperature, degrees Celsius b) Wind component positive toward 115 degrees, m/s c) Total wind speed, m/s d) Wind direction, degrees (negative directions = degrees - 360)

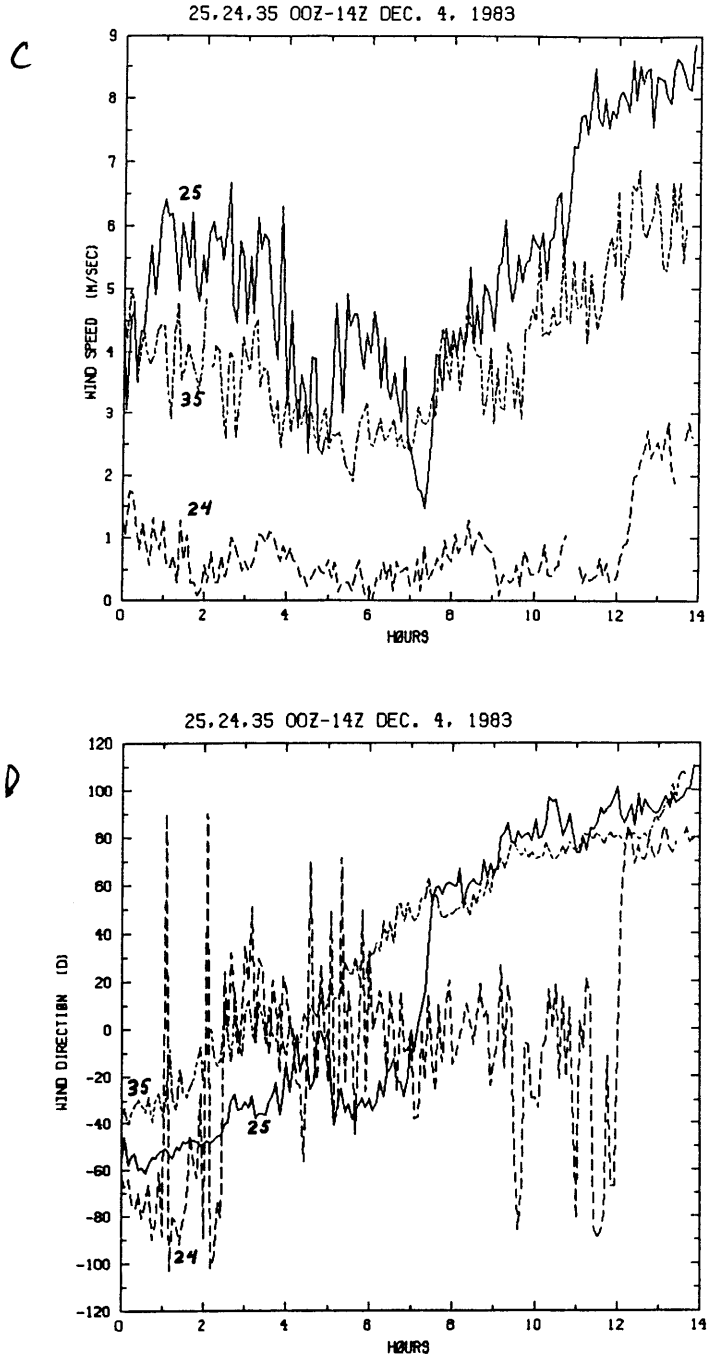

Fig. 2.7 (continued)

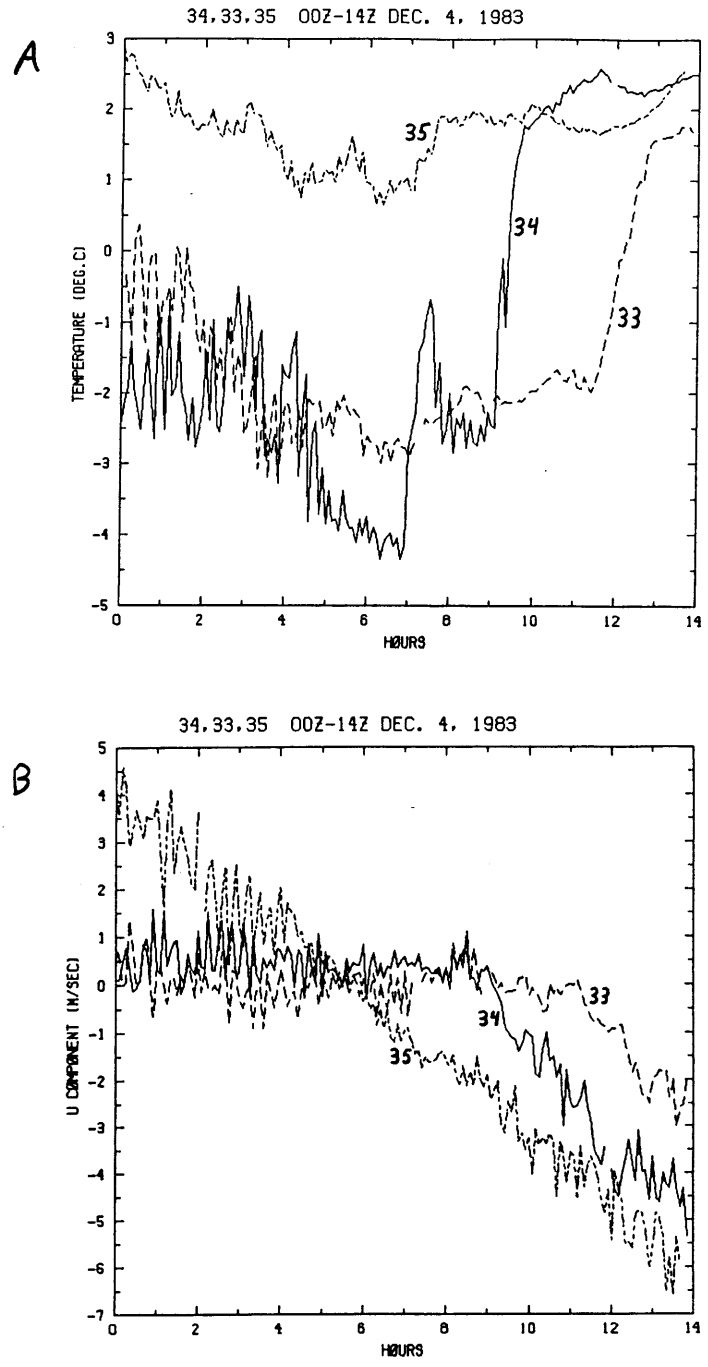

Fig. 2.8 Time series, as in Fig. 2.7, but for stations P33, P34, and P35.

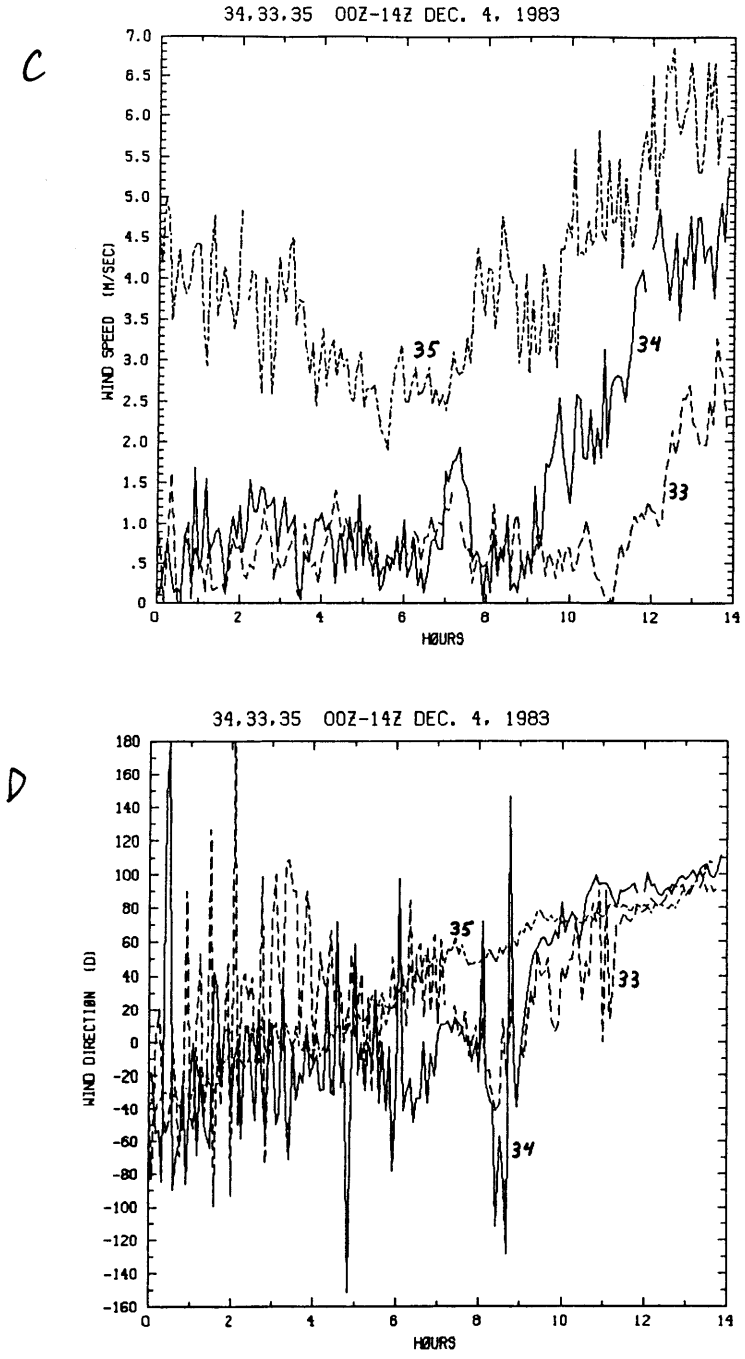

Fig. 2.8 (continued)

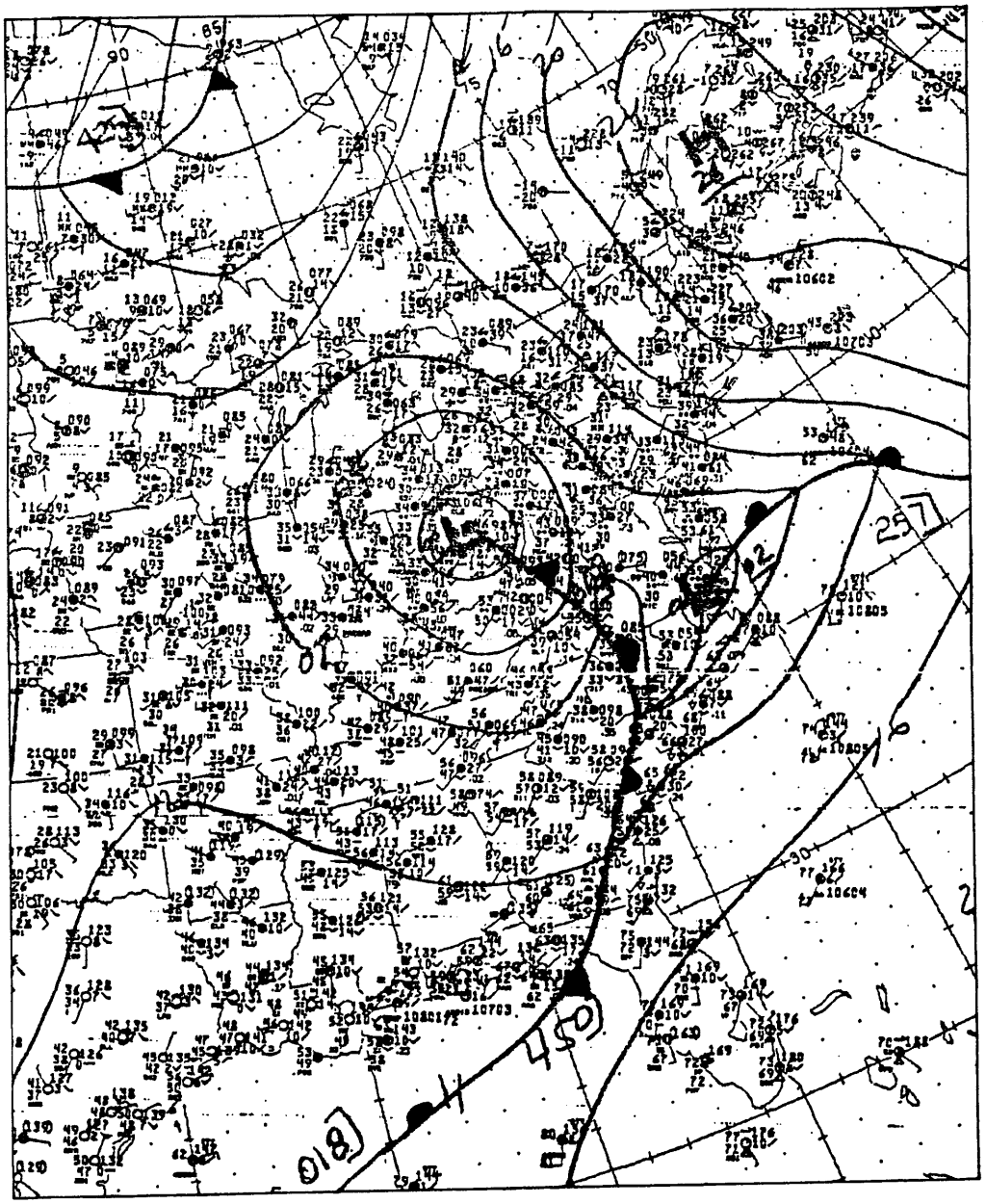

Fig. 2.9 NMC surface analysis, 1200 4 Dec 1983.

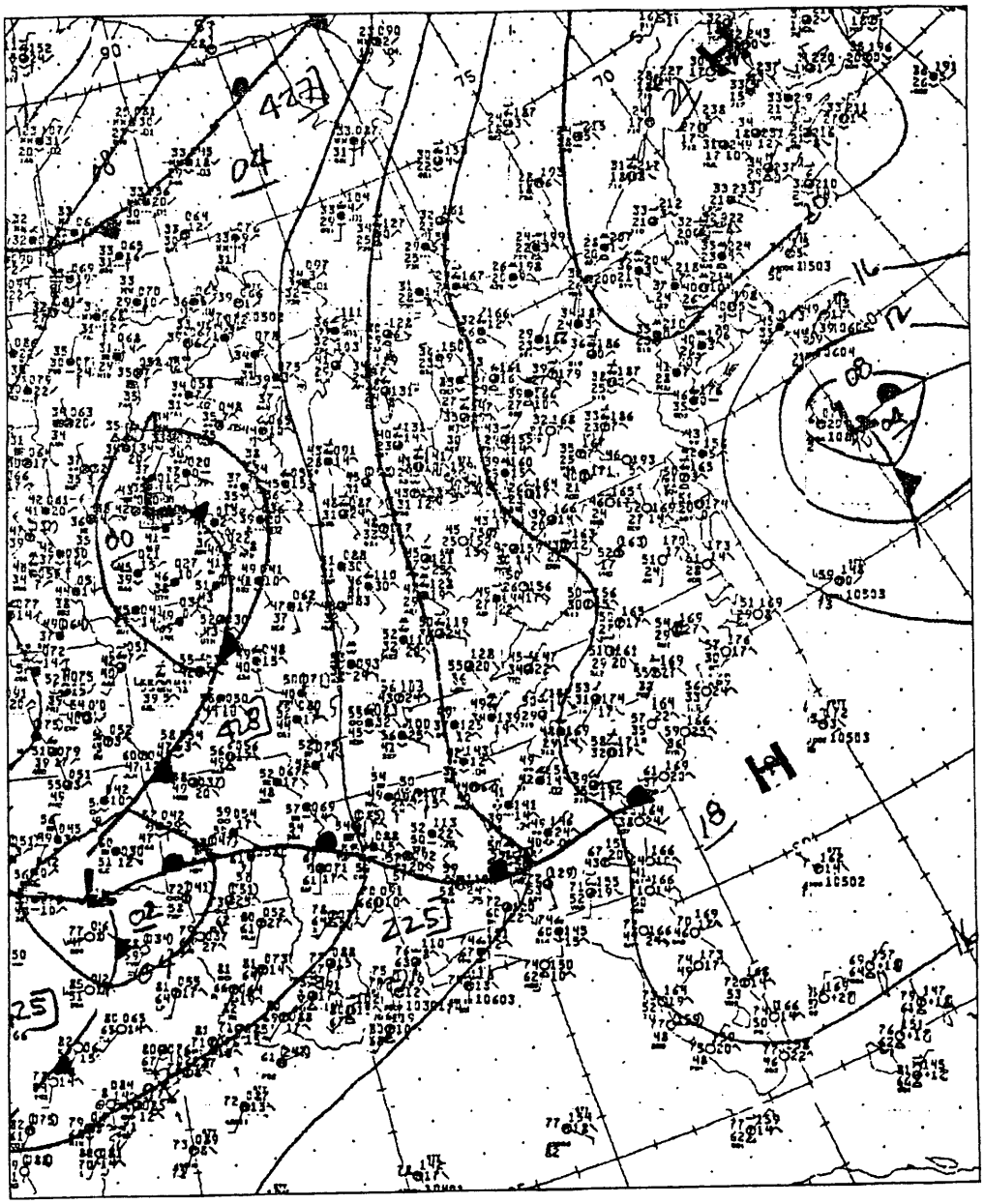

Fig. 2.10 NMC surface analysis, 1800 14 Nov 1983.

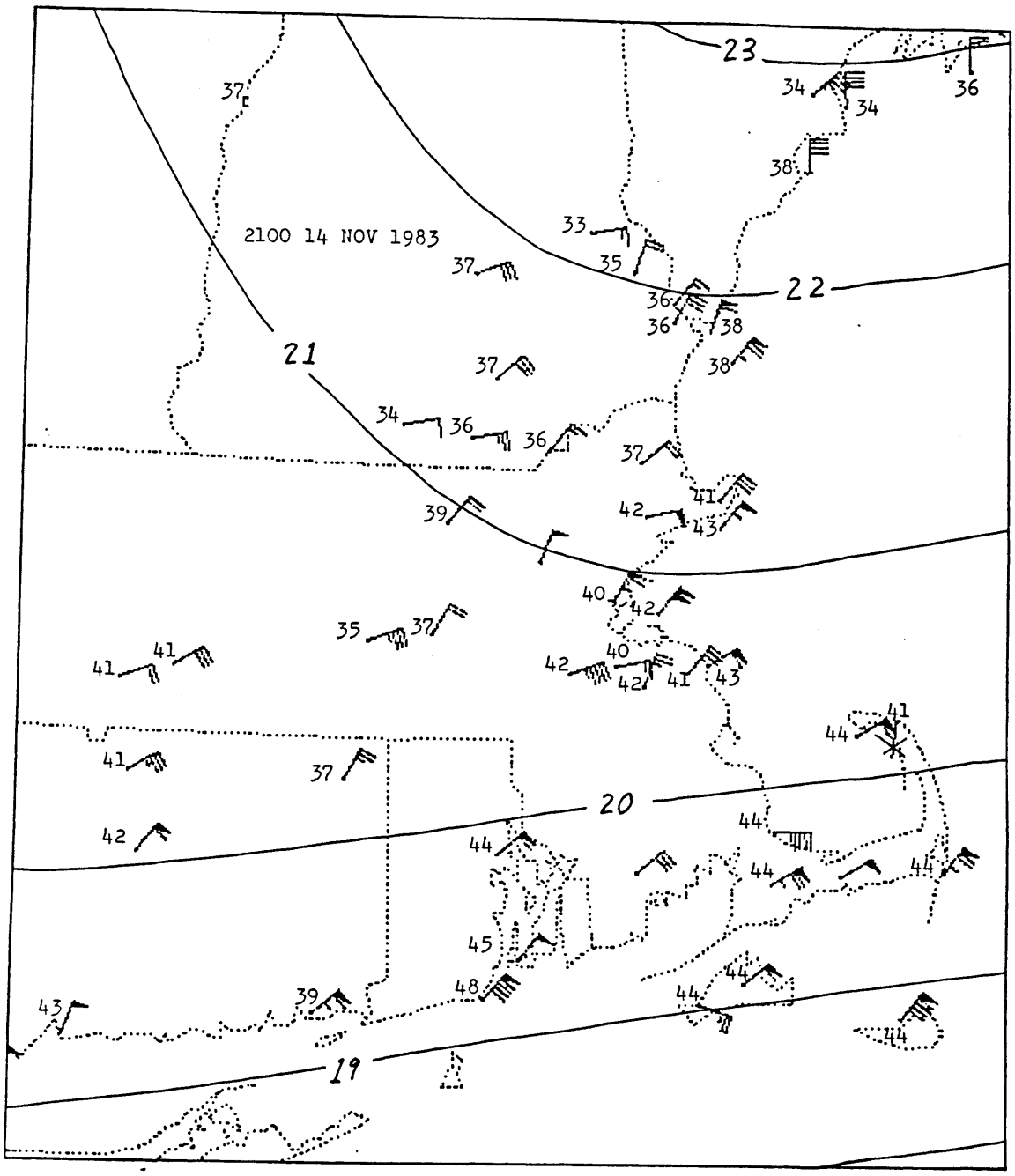

Fig 2.11 Mesoscale analysis (as in Fig. 2.2), 2100 14 Nov 1983.

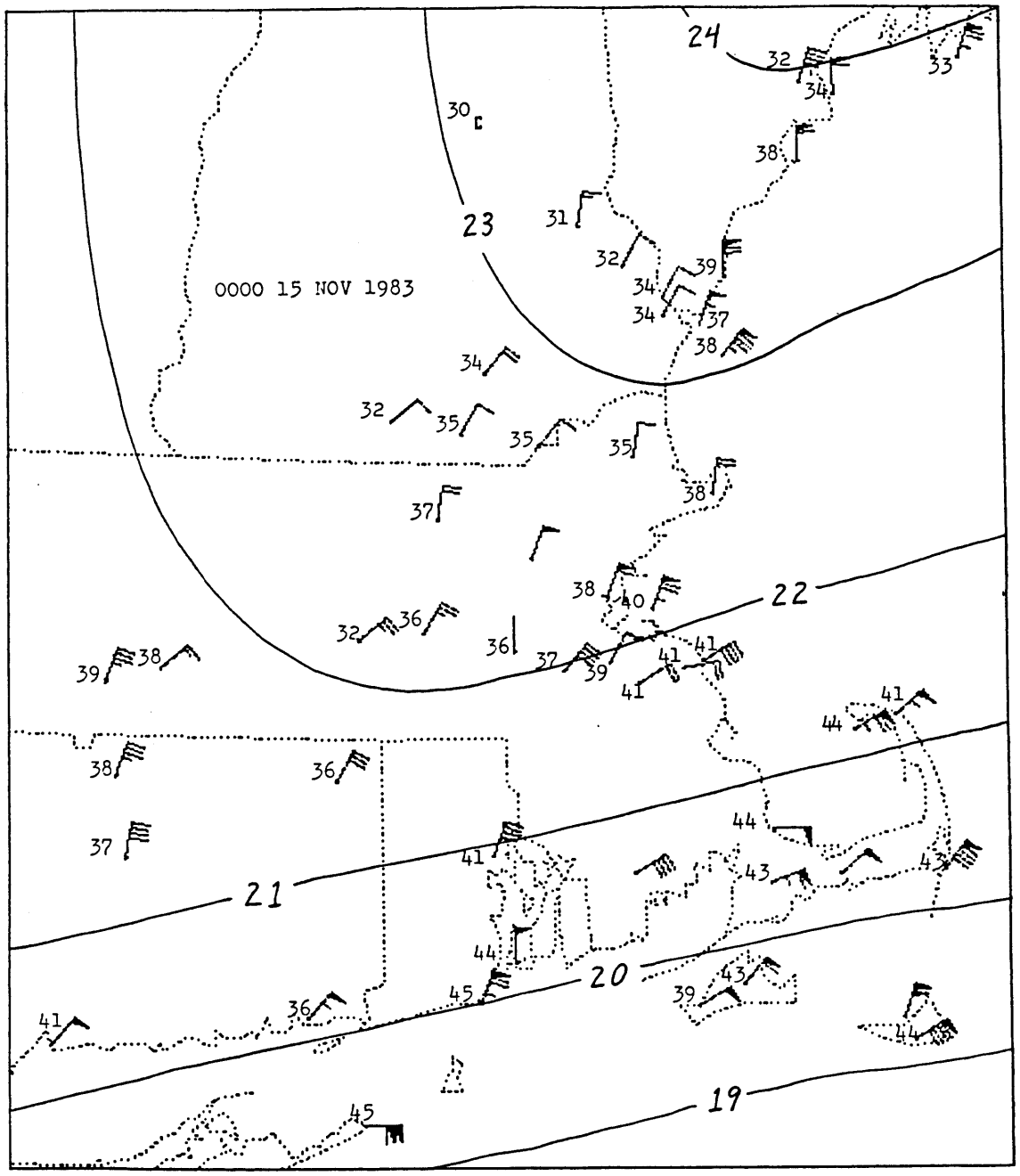

Fig. 2.12 Mesoscale analysis (as in Fig. 2.2), 0000 15 Nov 1983.

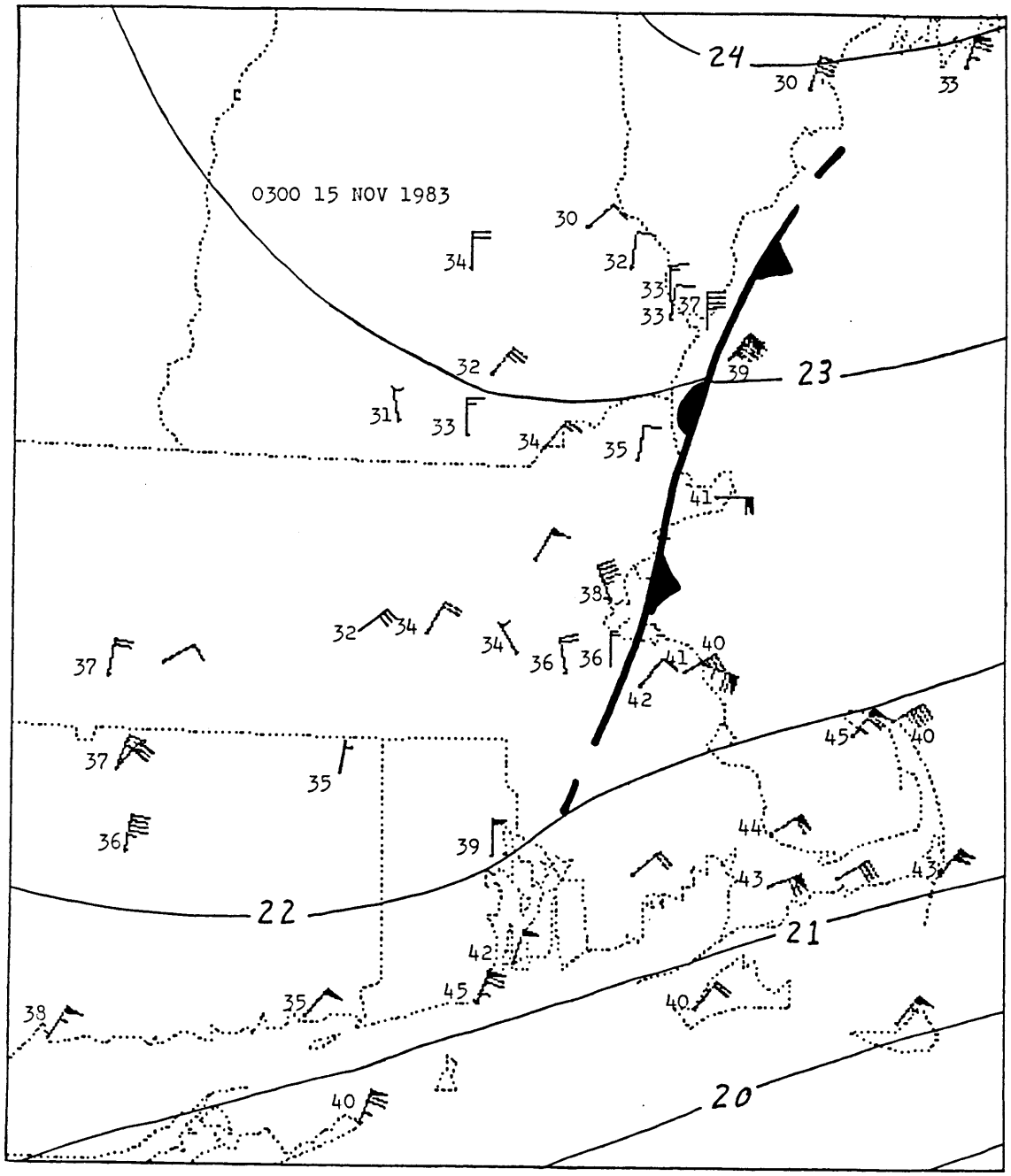

Fig. 2.13 Mesoscale analysis (as in Fig. 2.2), 0300 15 Nov 1983.

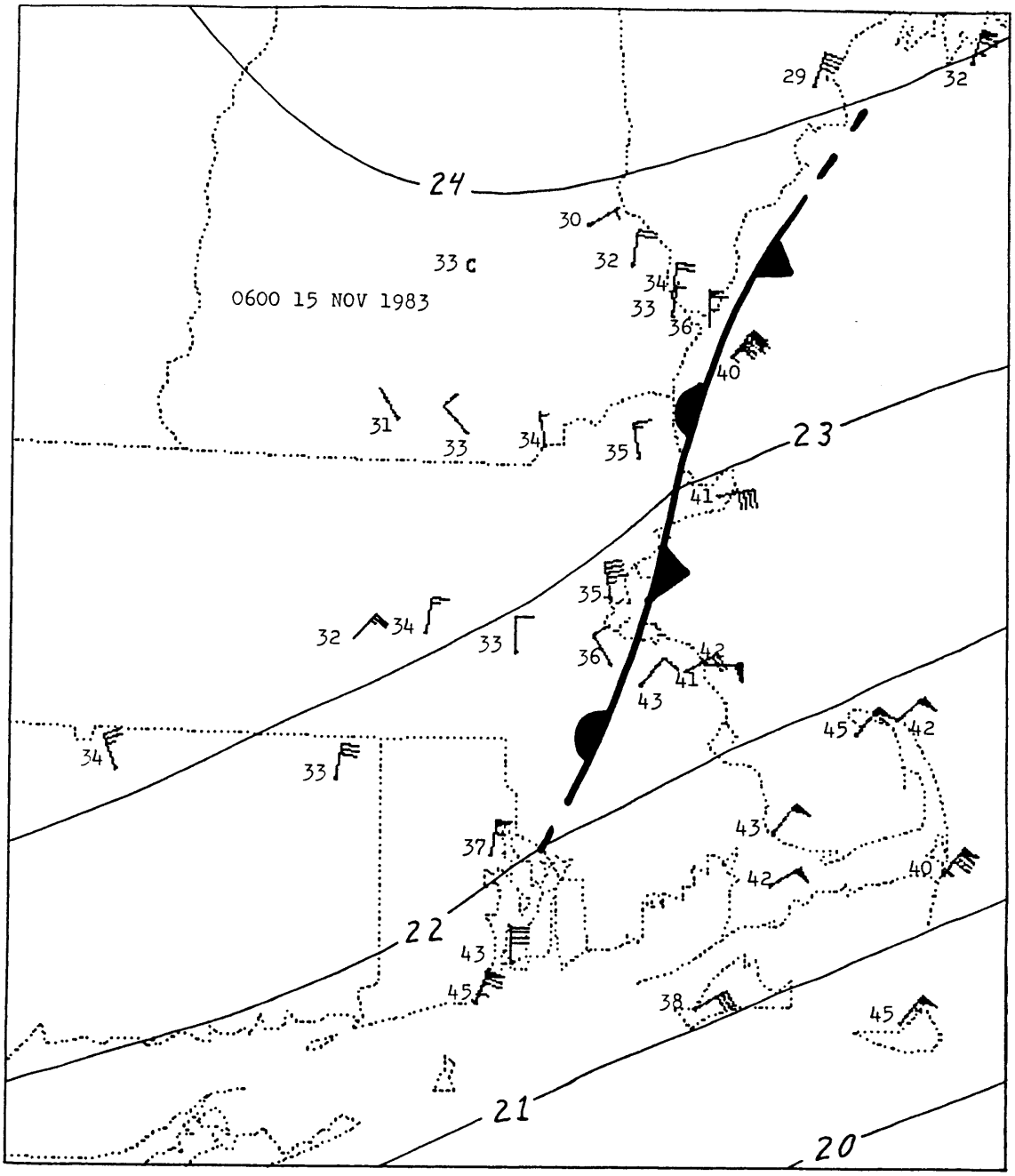

Fig. 2.14 Mesoscale analysis (as in Fig. 2.2), 0600 15 Nov 1983.

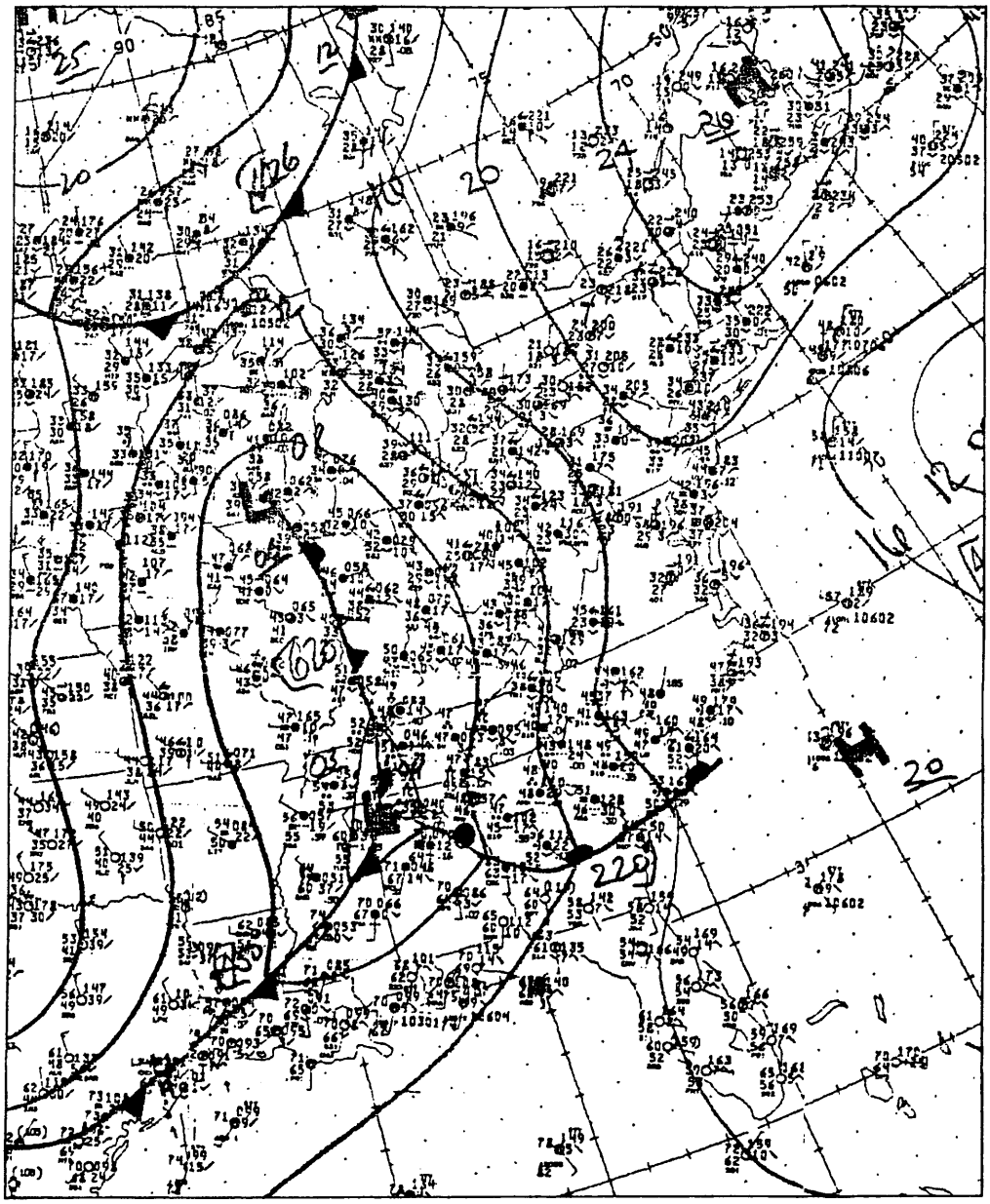

Fig. 2.15 NMC surface analysis, 0600 15 Nov 1983.

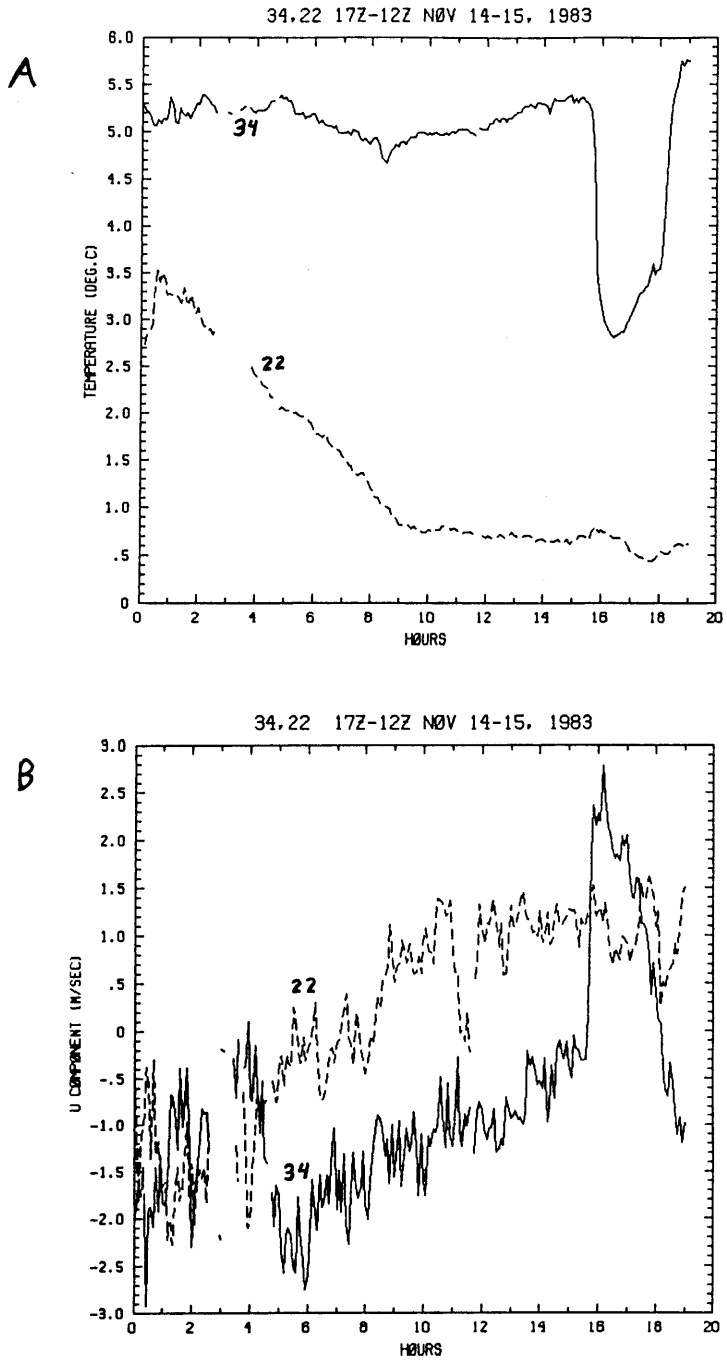

Fig. 2.16 Time series, as in Fig. 2.7, but for stations P22 and P34, 1700 14 Nov 1983 - 1200 15 Nov 1983.

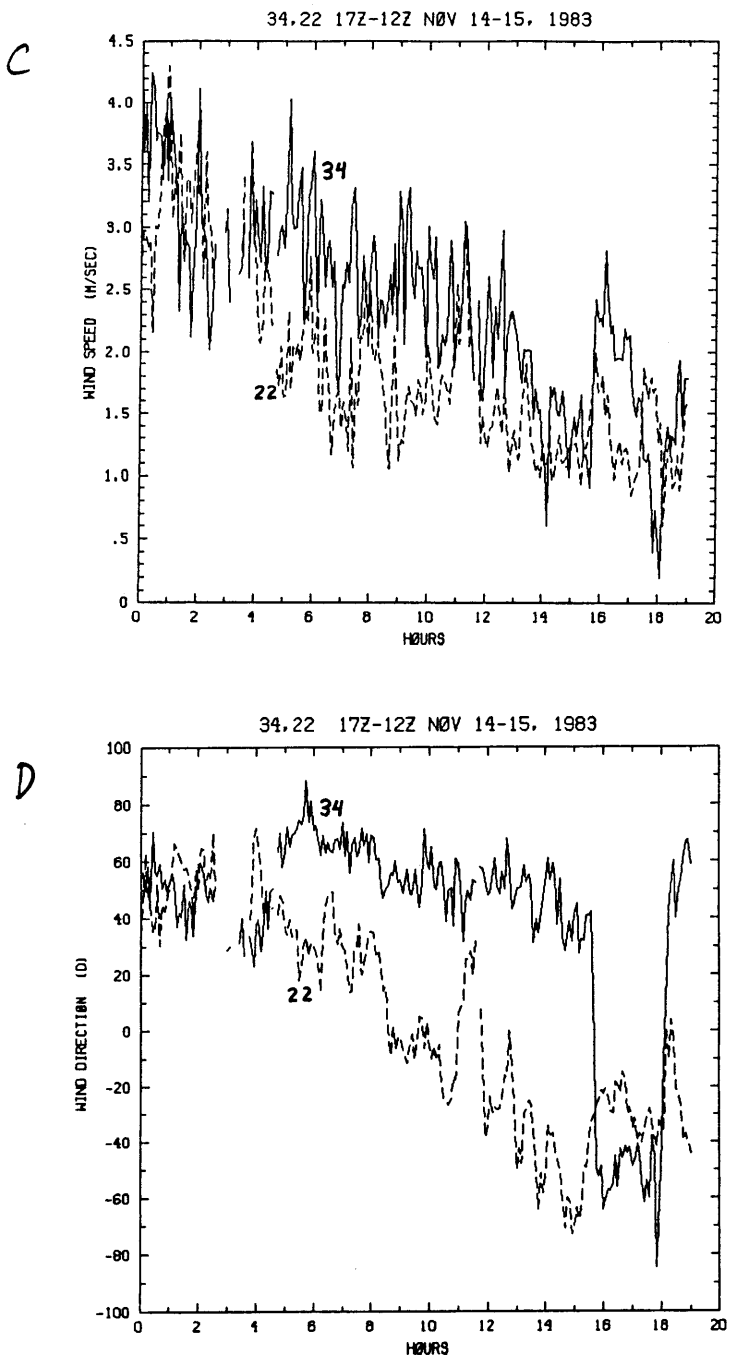

Fig. 2.16 (continued)

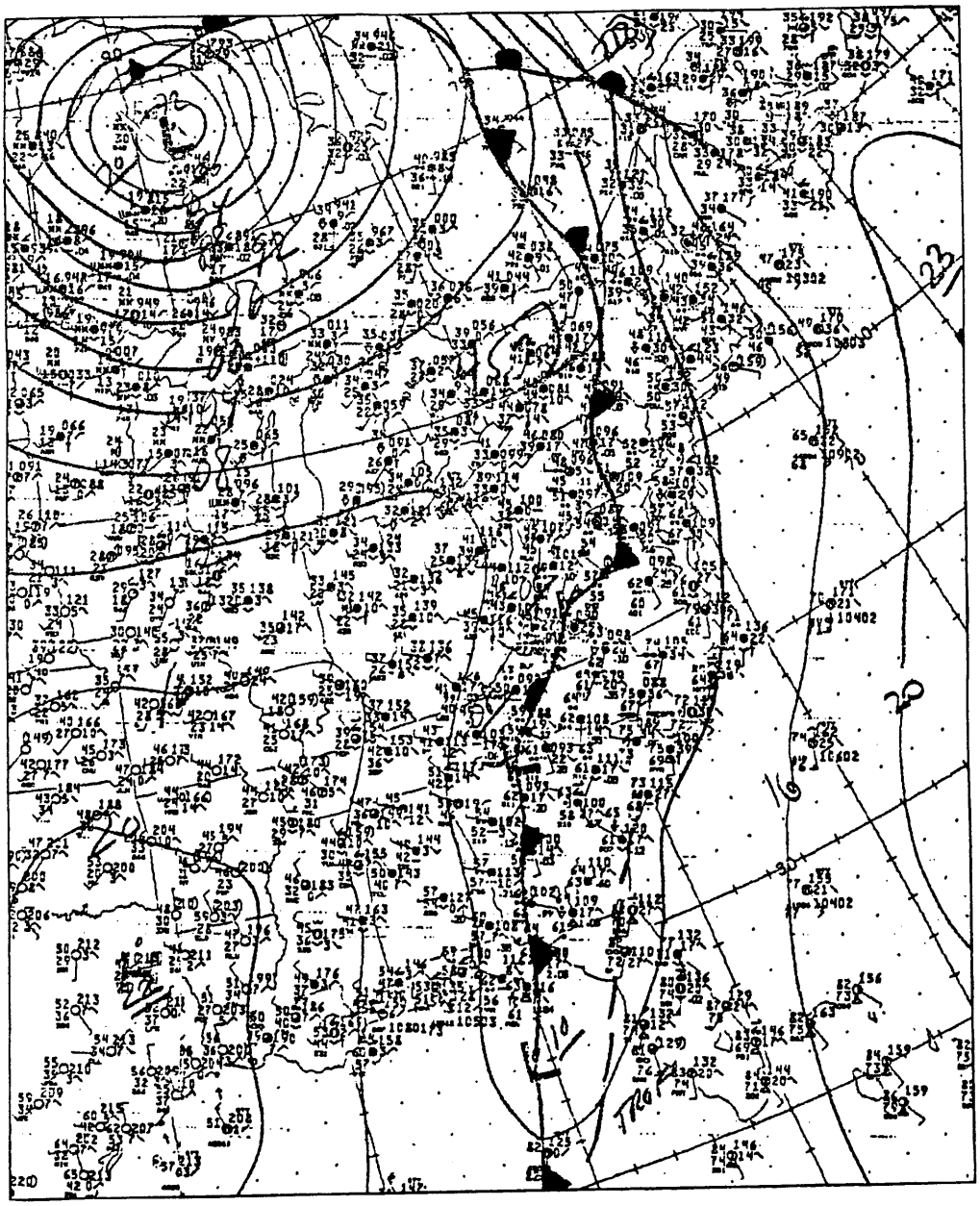

Fig. 2.17 NMC surface analysis, 1800 24 Nov 1983.

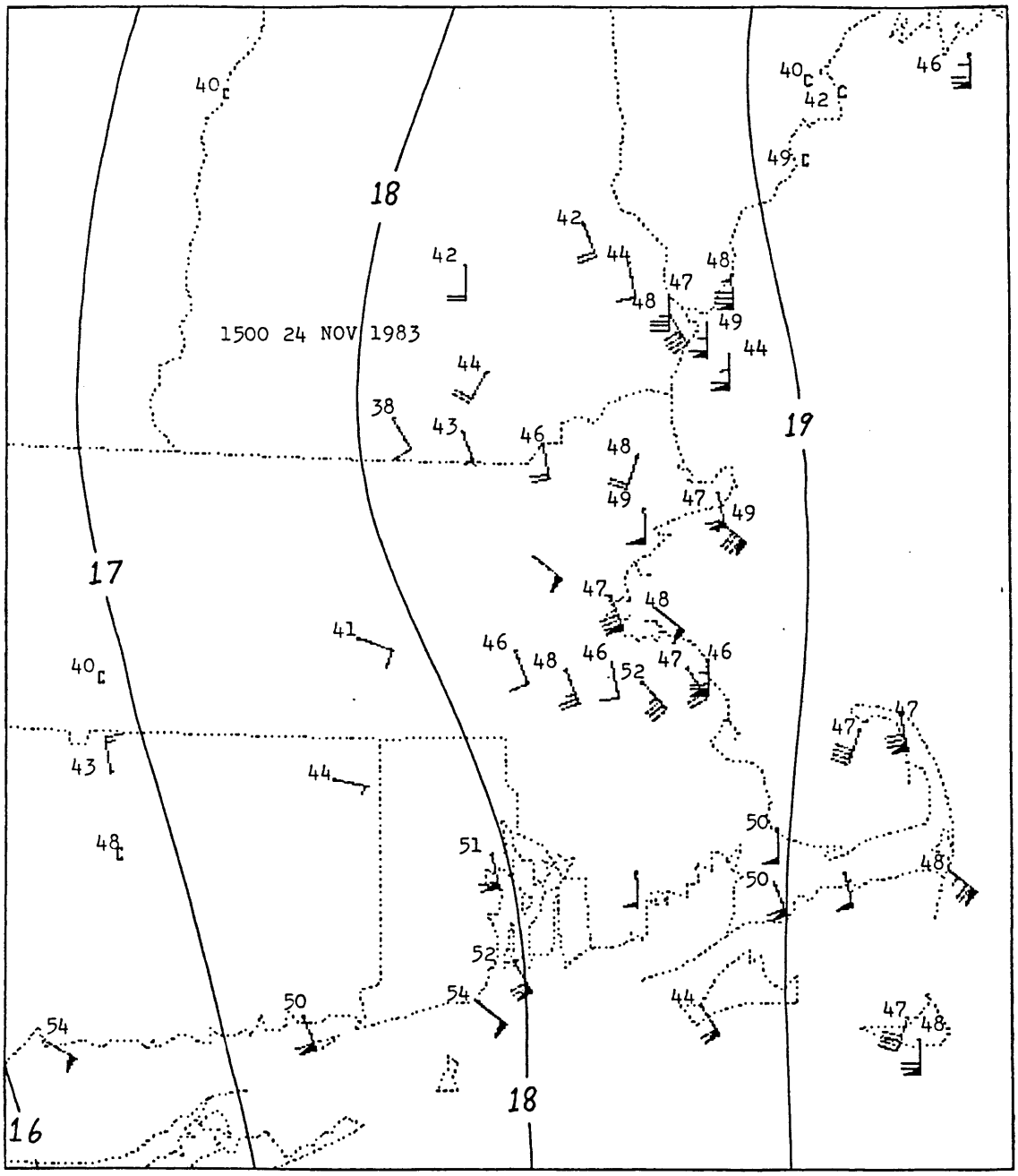

Fig. 2.18 Mesoscale analysis (as in Fig. 2.2), 1500 24 Nov 1983.

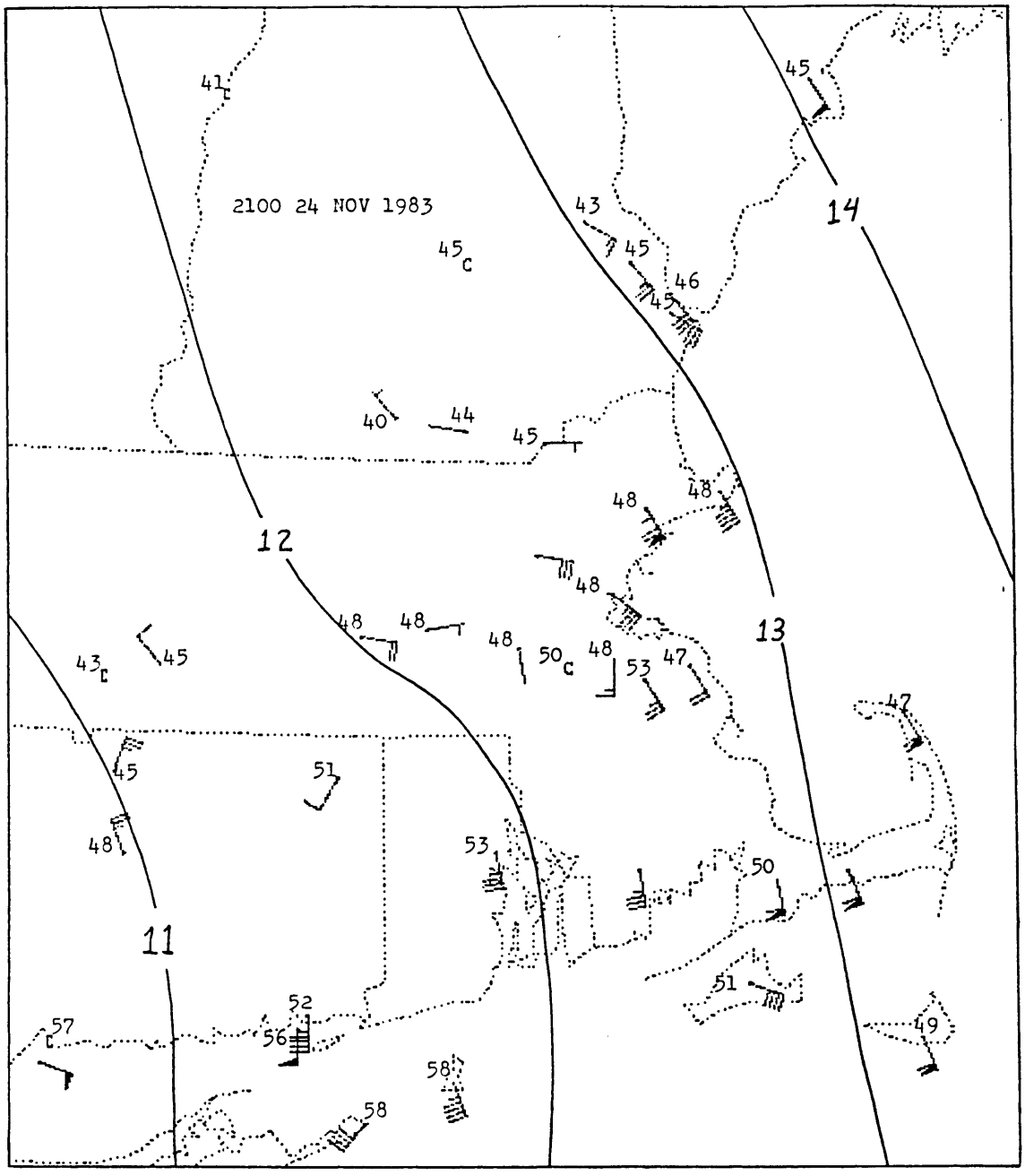

Fig. 2.19 Mesoscale analysis (as in Fig. 2.2), 2100 24 Nov 1983.

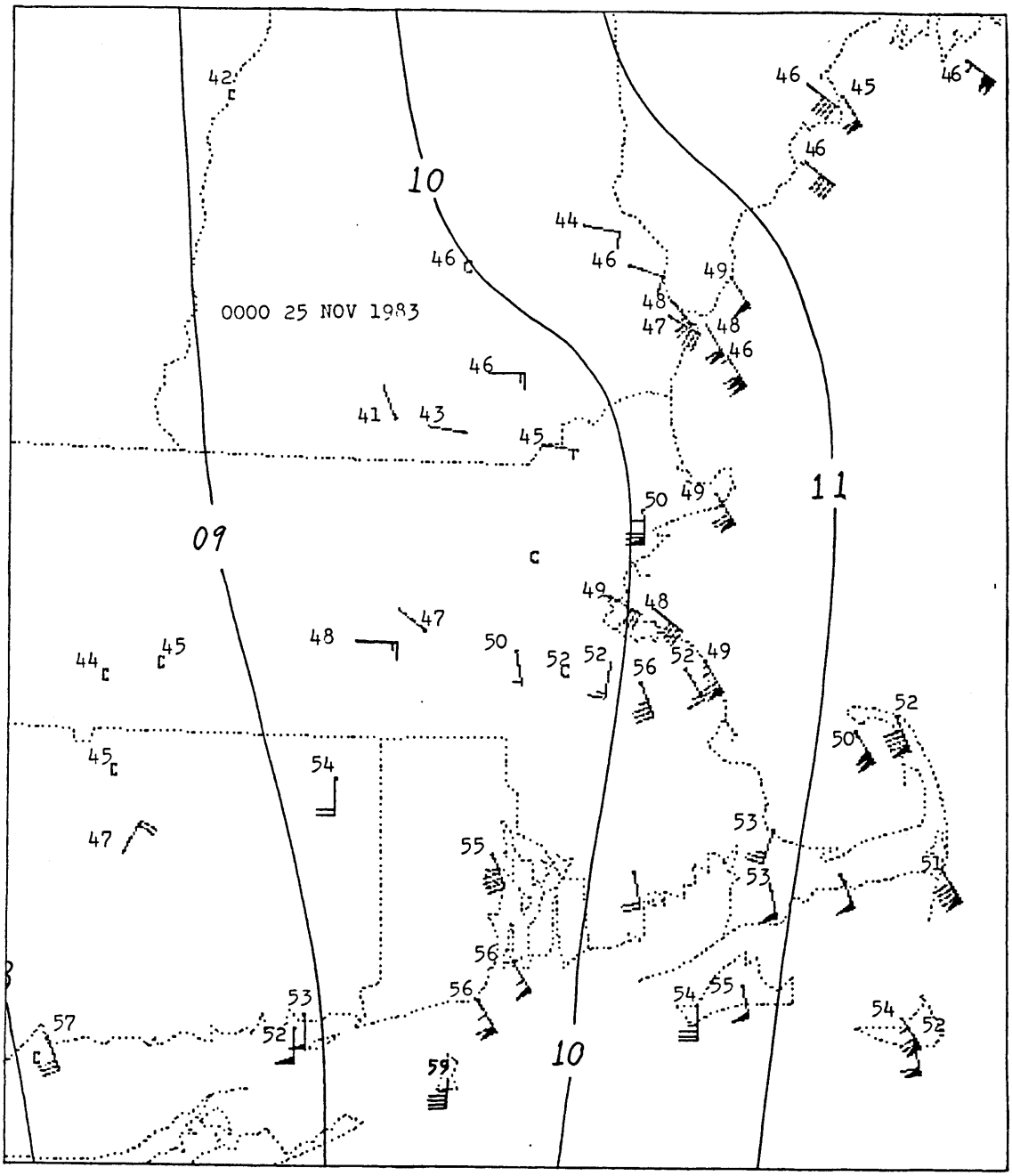

Fig. 2.20 Mesoscale analysis (as in Fig. 2.2), 0000 25 Nov 1983.

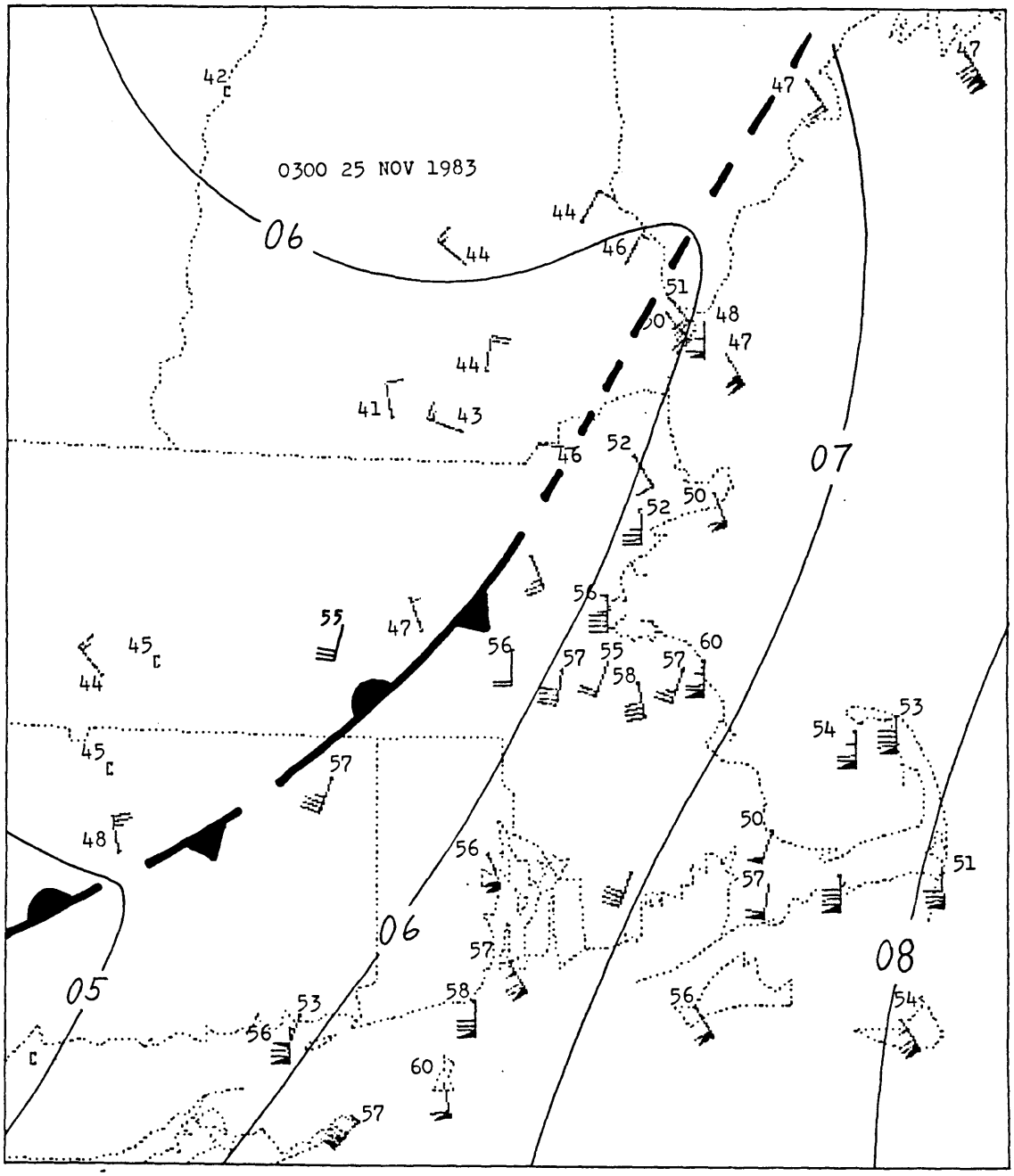

Fig. 2.21 Mesoscale analysis (as in Fig. 2.2), 0300 25 Nov 1983.

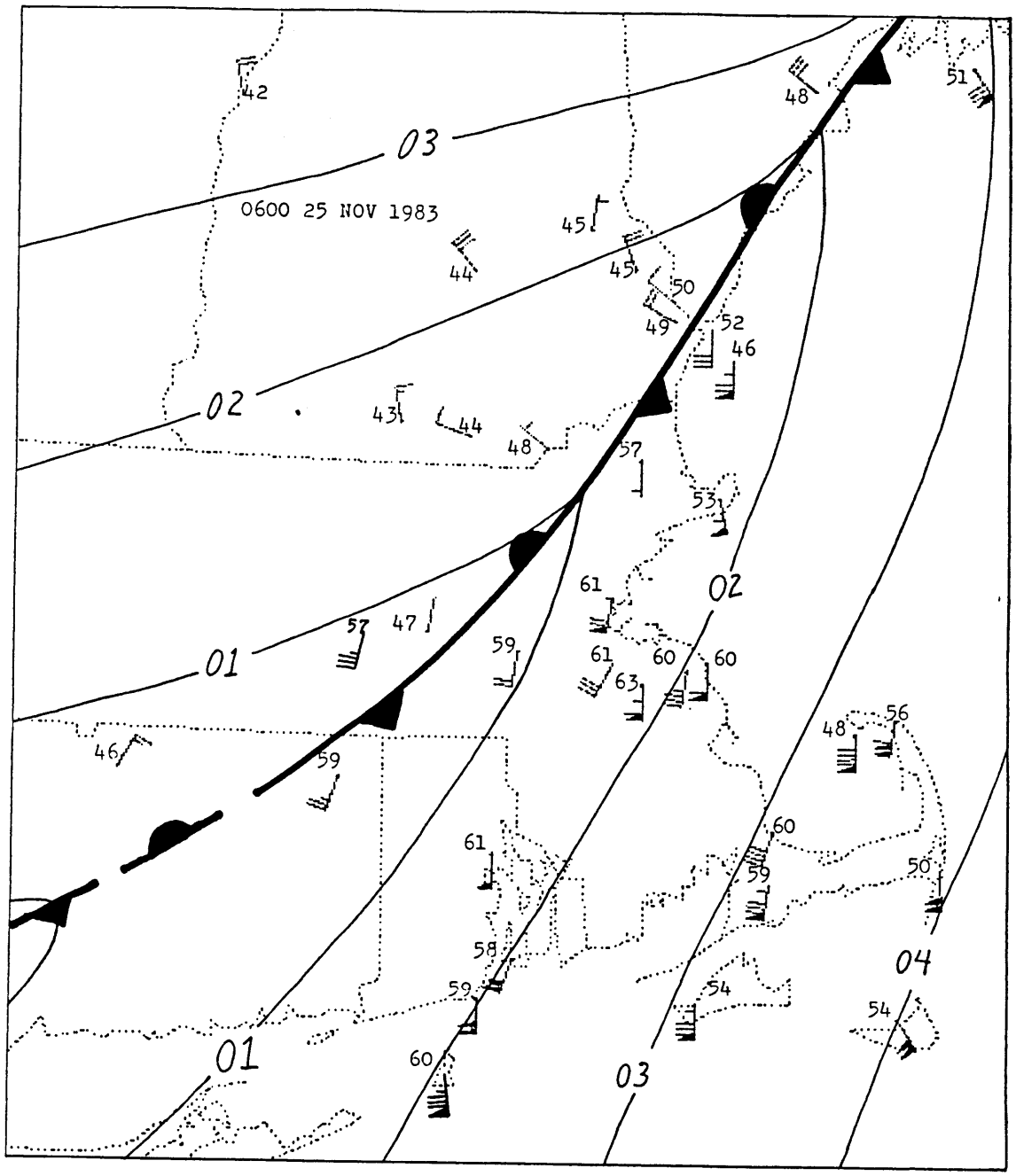

Fig. 2.22 Mesoscale analysis (as in Fig. 2.2), 0600 25 Nov 1983.

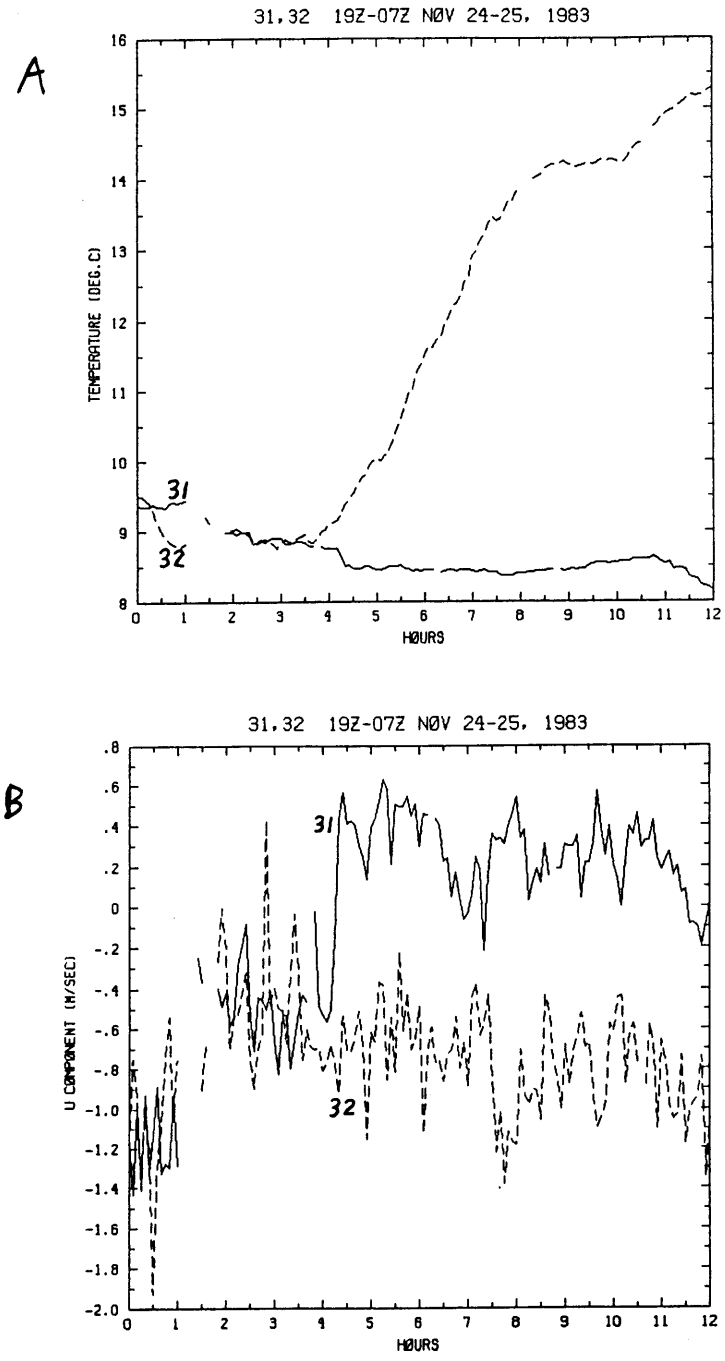

Fig. 2.23 Time series, as in Fig. 2.7, but for stations P31 and P32, 1900 24 Nov 1983 - 0700 25 Nov 1983.

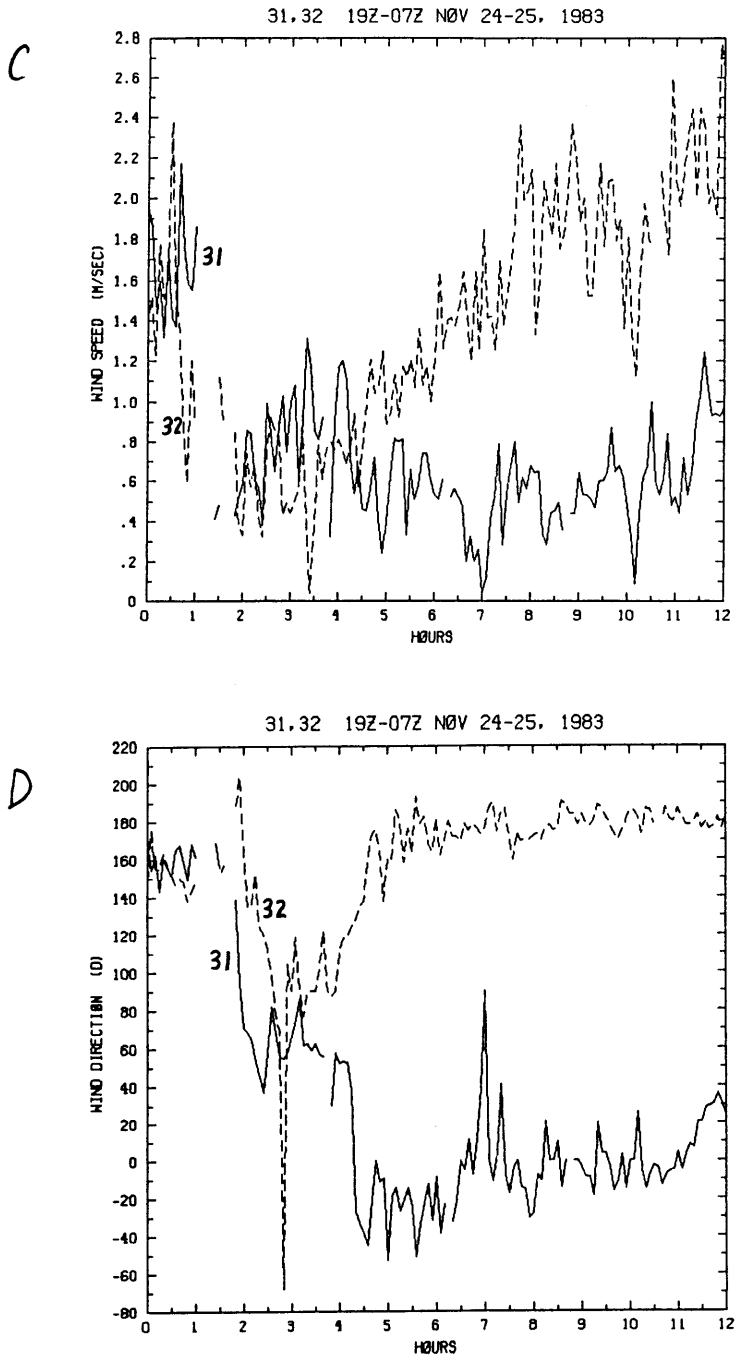

Fig. 2.23 (continued)

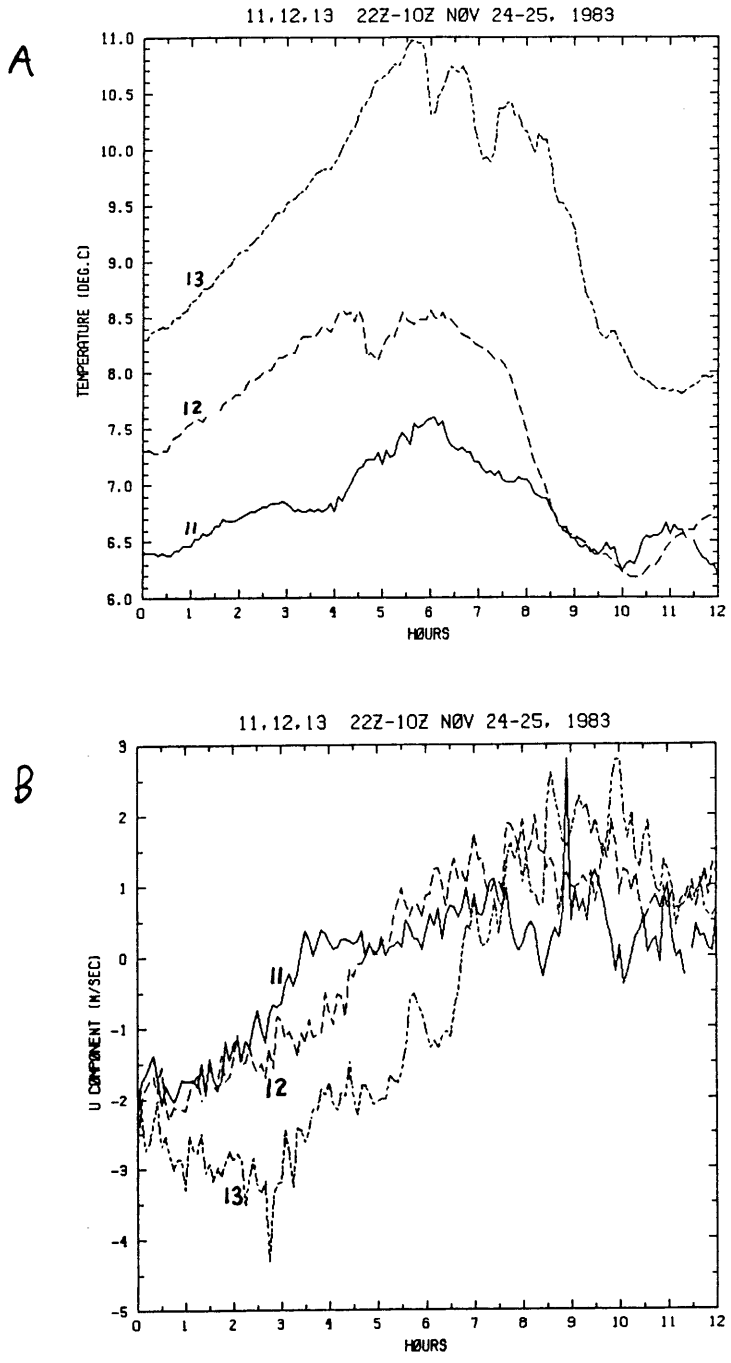

Fig. 2.24 Time series, as in Fig. 2.7, but for stations P11, P12, and P13, 2200 24 Nov 1983 - 1000 25 Nov 1983.

C

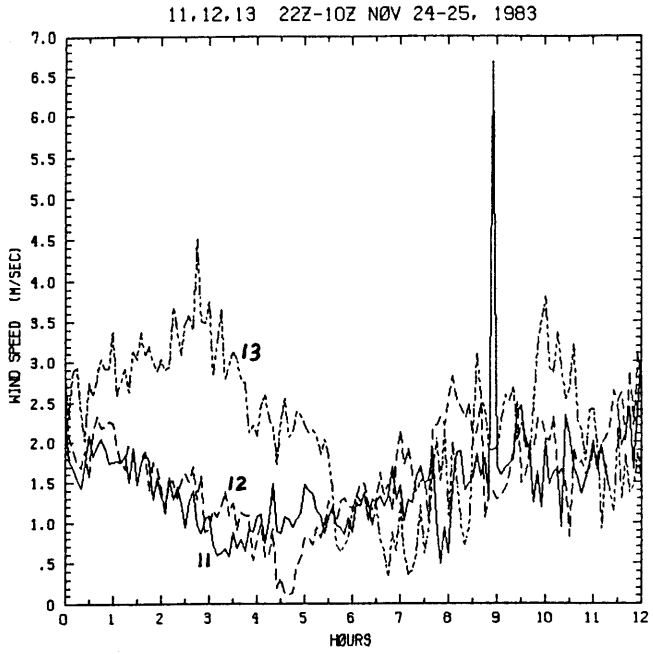

D

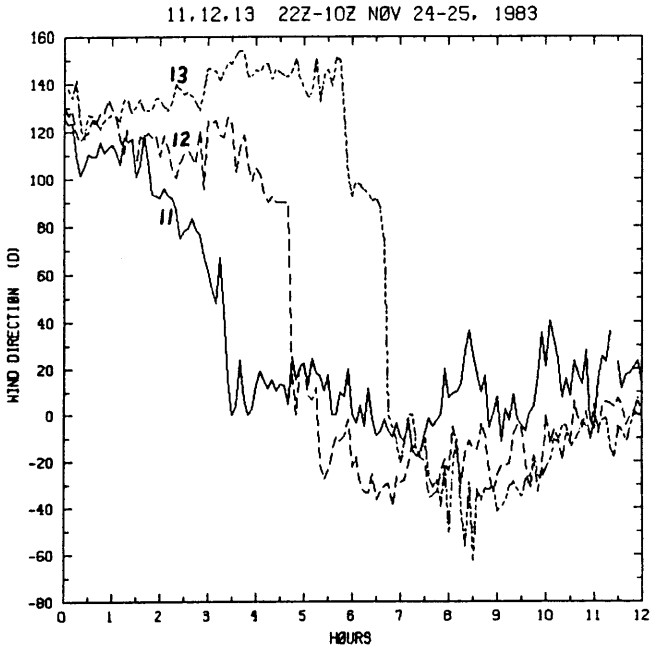

Fig. 2.24 (continued)

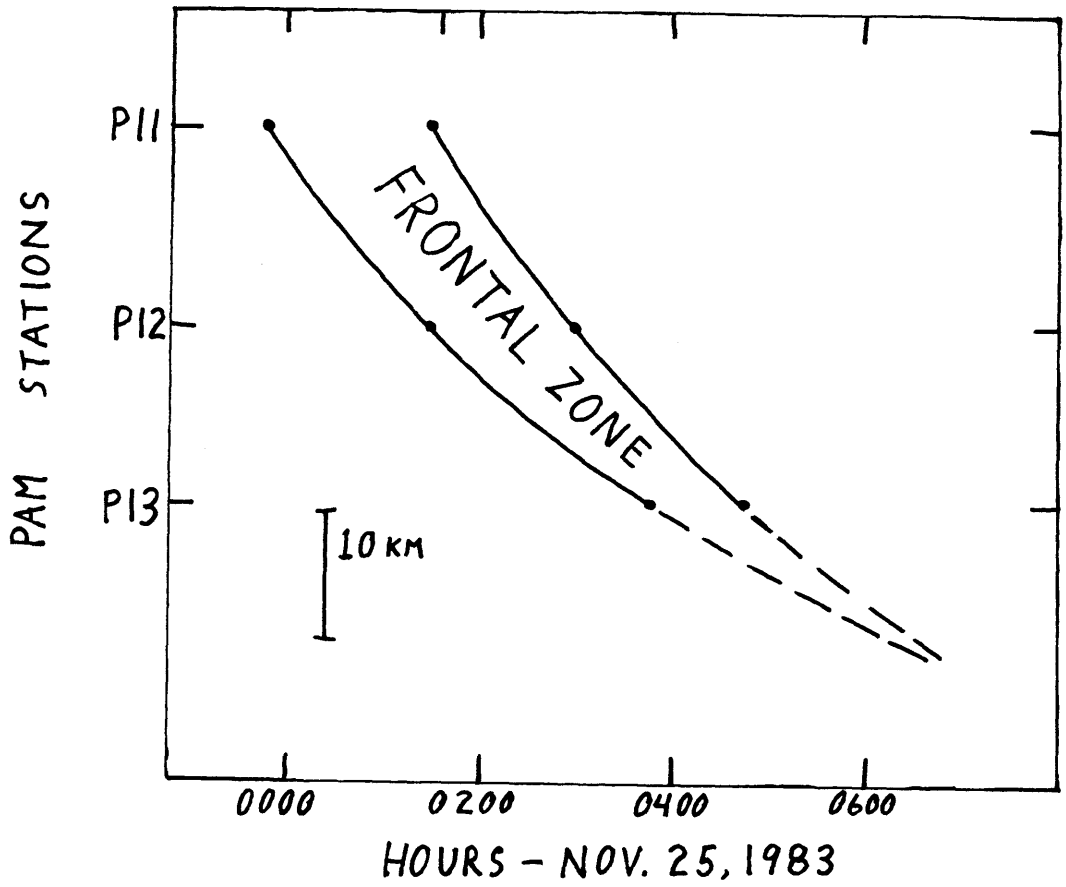

Fig. 2.25 Position of frontal zone with respect to stations P11, P12, and P13 as a function of time, showing crudely extrapolated location and time of frontal collapse.

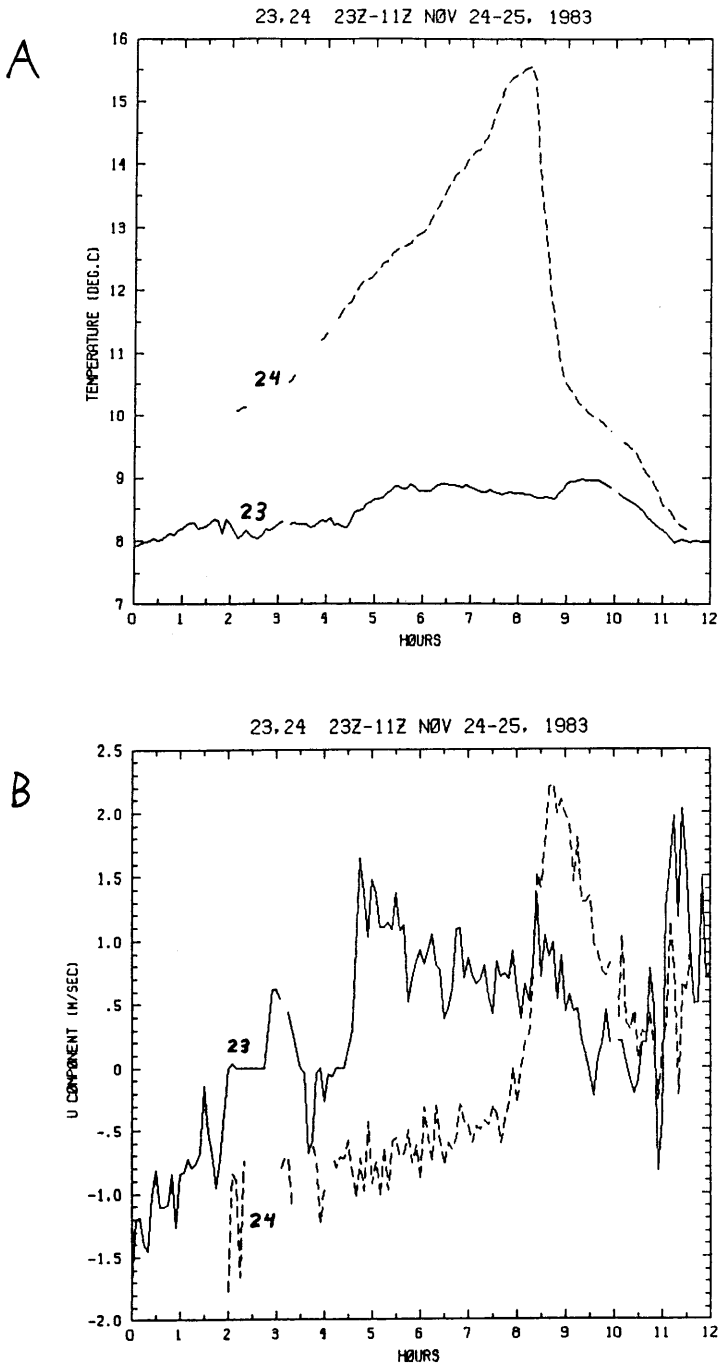

Fig. 2.26 Time series, as in Fig. 2.7, but for stations P23 and P24, 2300 24 Nov 1983 - 1100 24 Nov 1983.

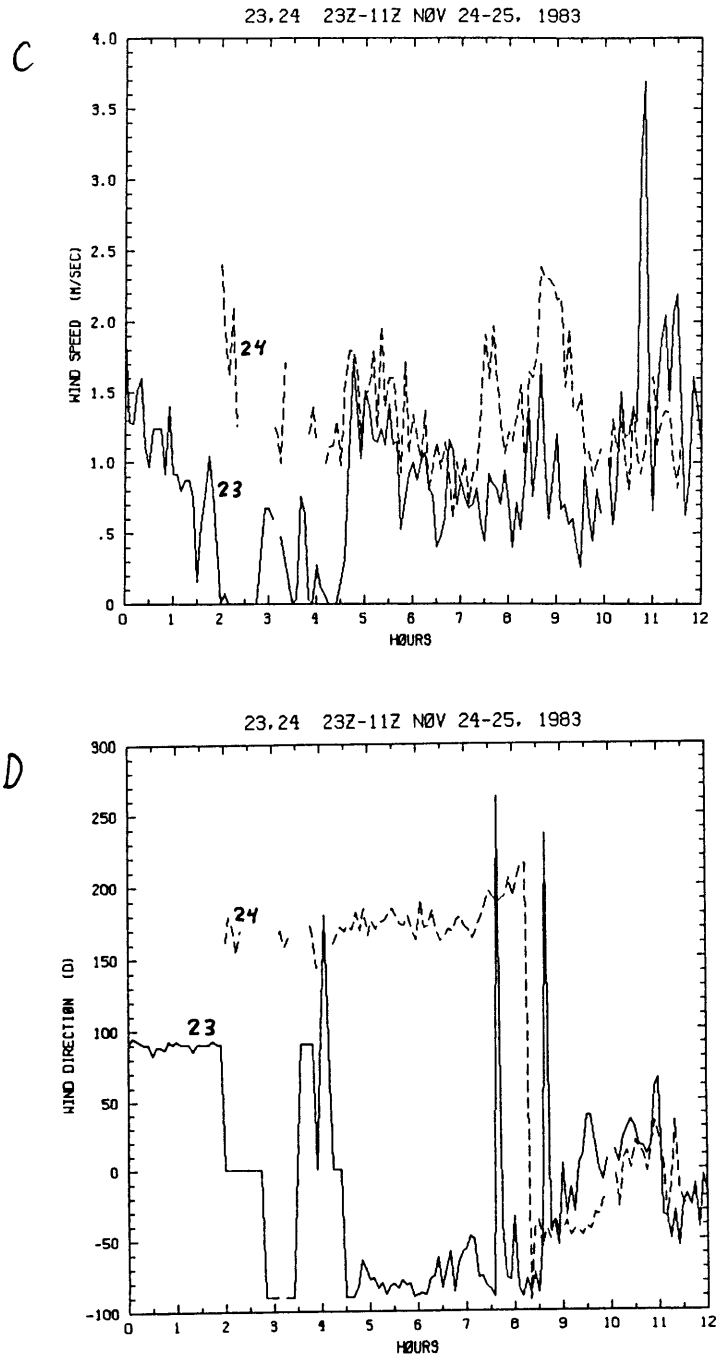

Fig. 2.26 (continued)

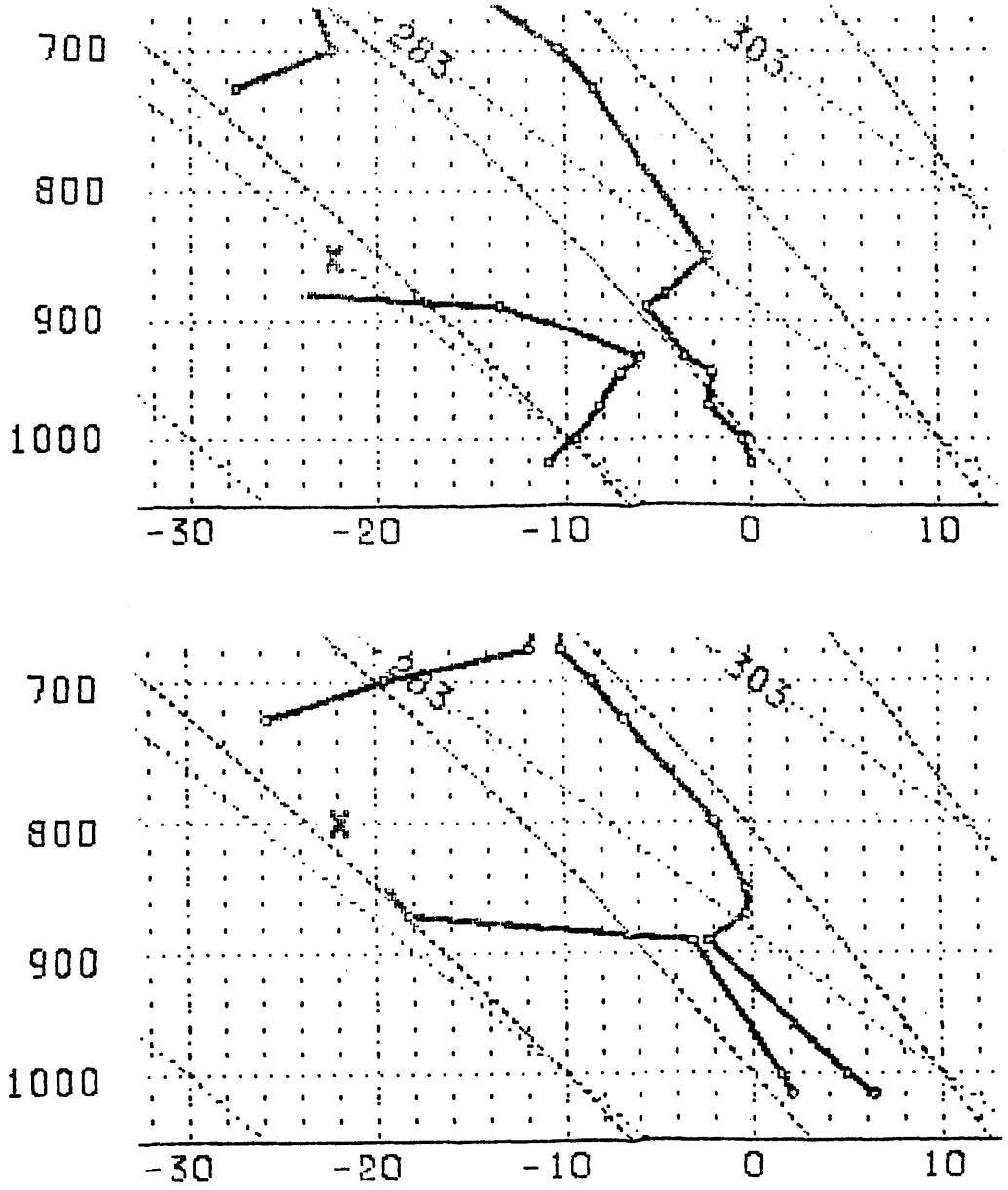

Fig. 3.1. Low-level temperature (solid right-hand line) and dew point (solid left-hand line, 'dry' dew point indicated by 'X') soundings, 0000 15 Nov 1983. Vertical axis is pressure (labeled in millibars), horizontal axis is temperature (labeled in degrees Celsius), sloping straight lines are dry adiabats (spacing, 10 K), sloping curved lines are moist adiabats (spacing, 10 K) a) Portland, Maine (PWM) b) Chatham, Mass. (CHH)

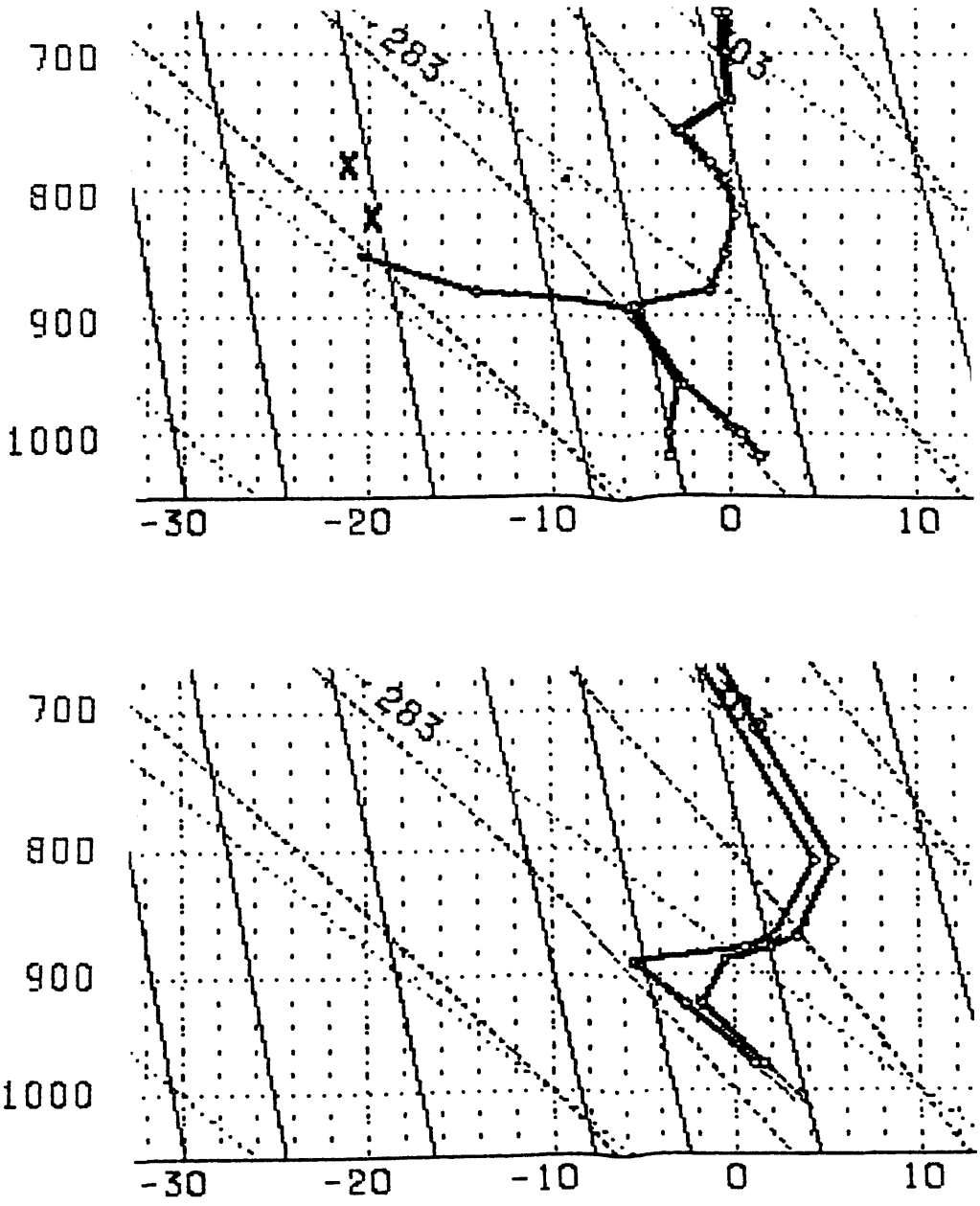

Fig. 3.2 Low-level soundings, as in Fig. 3.1, but for 0000 29 Nov 1983. Steeply sloping straight lines are lines of constant mixing ratio.

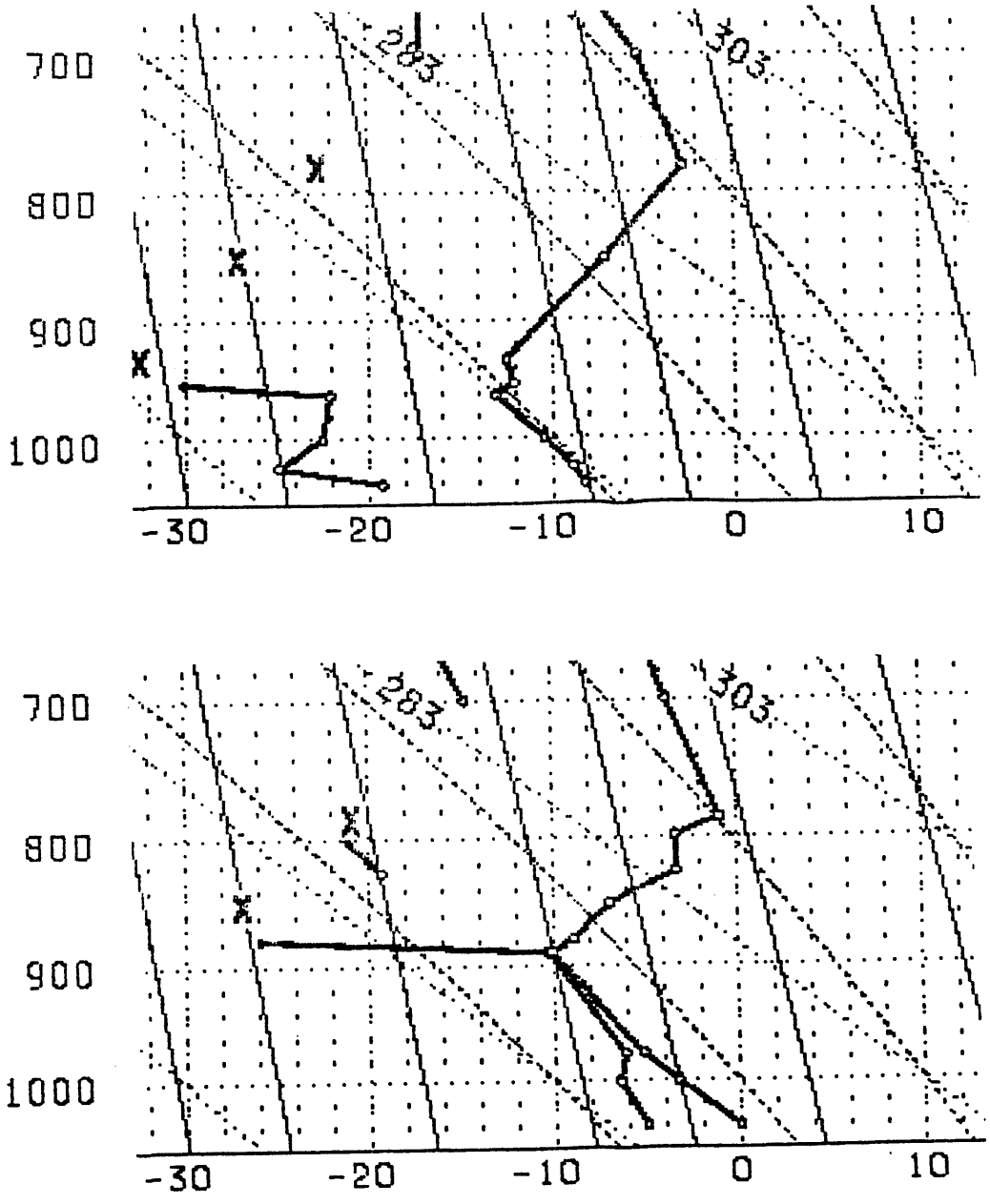

Fig. 3.3 Low-level soundings, as in Fig. 3.2, but for 0000 12 Dec 1983.

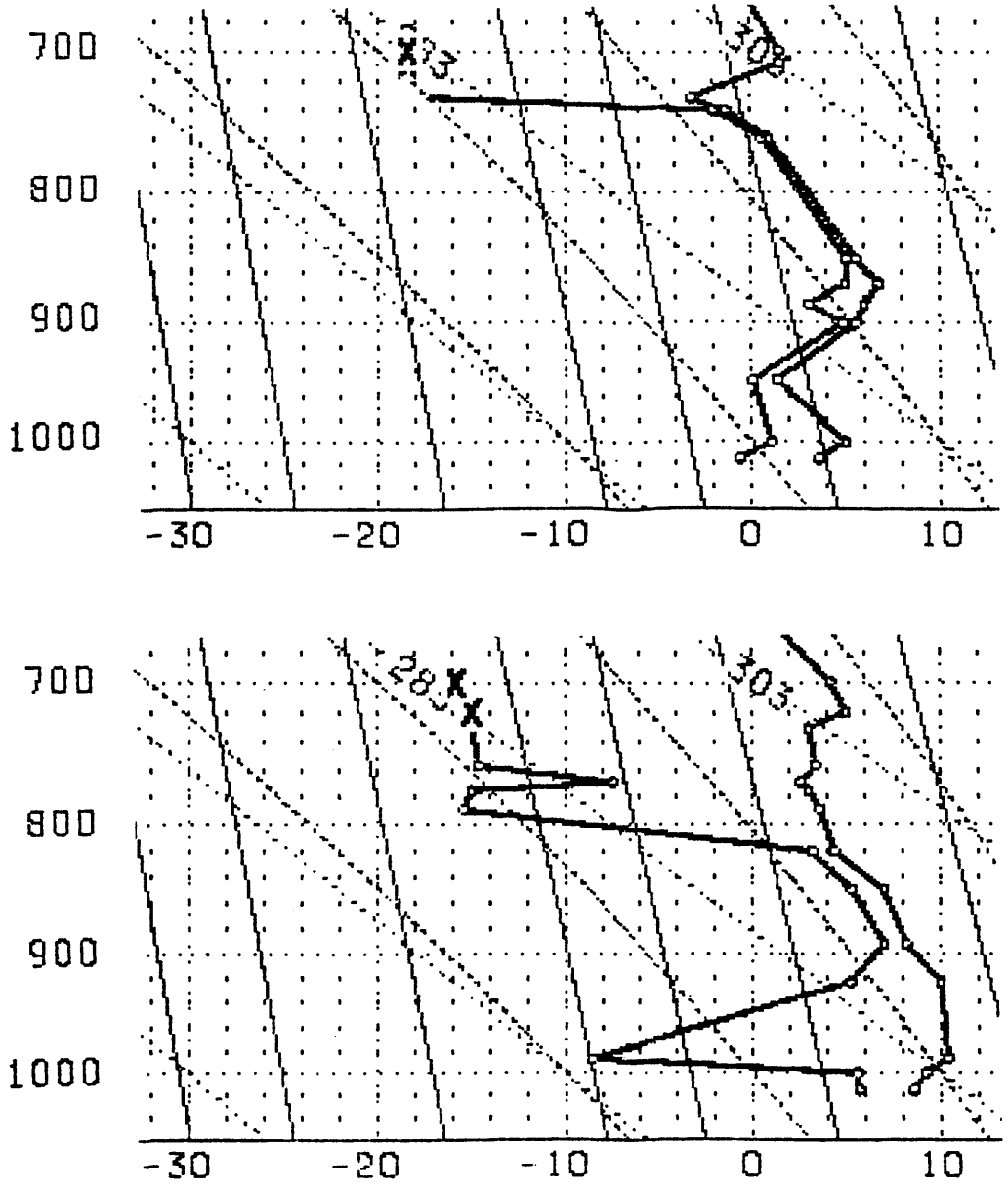

Fig. 3.4 Low-level soundings, as in Fig. 3.2, but for 0000 21 Nov 1983.

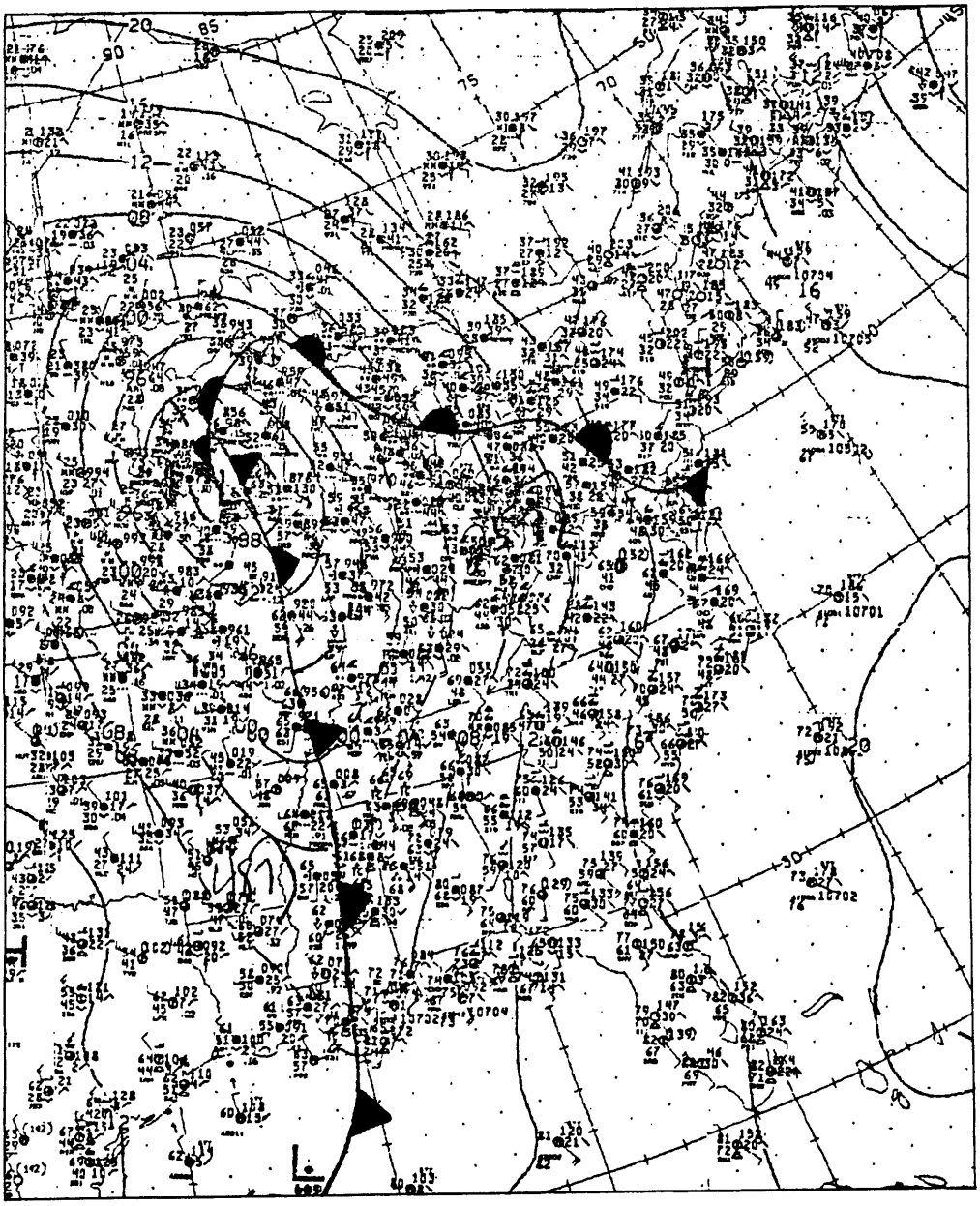

Fig. 3.5 NMC surface analysis, 1800 23 Nov 1983.

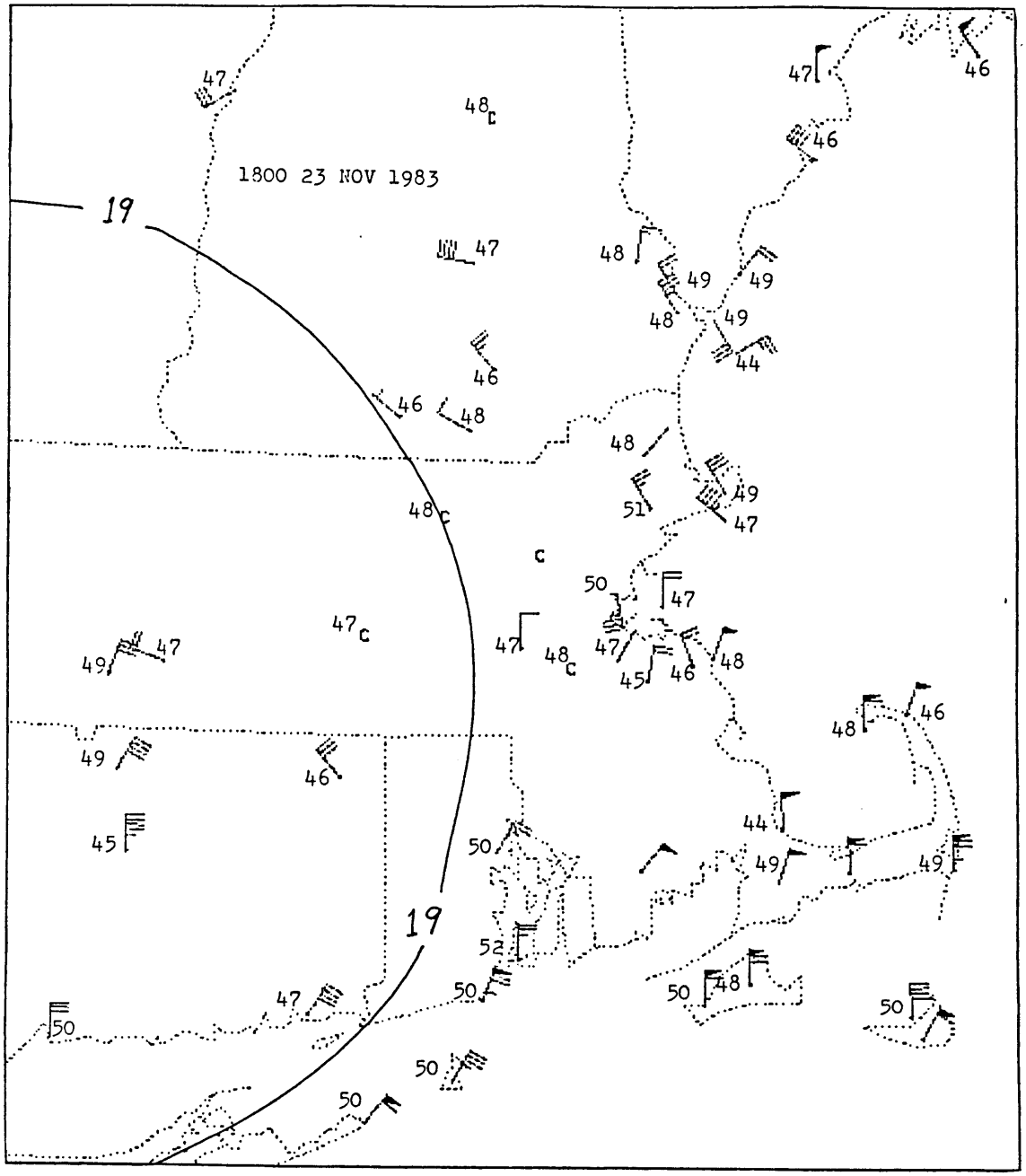

Fig. 3.6 Mesoscale analysis (as in Fig. 2.2), 1800 23 Nov 1983.

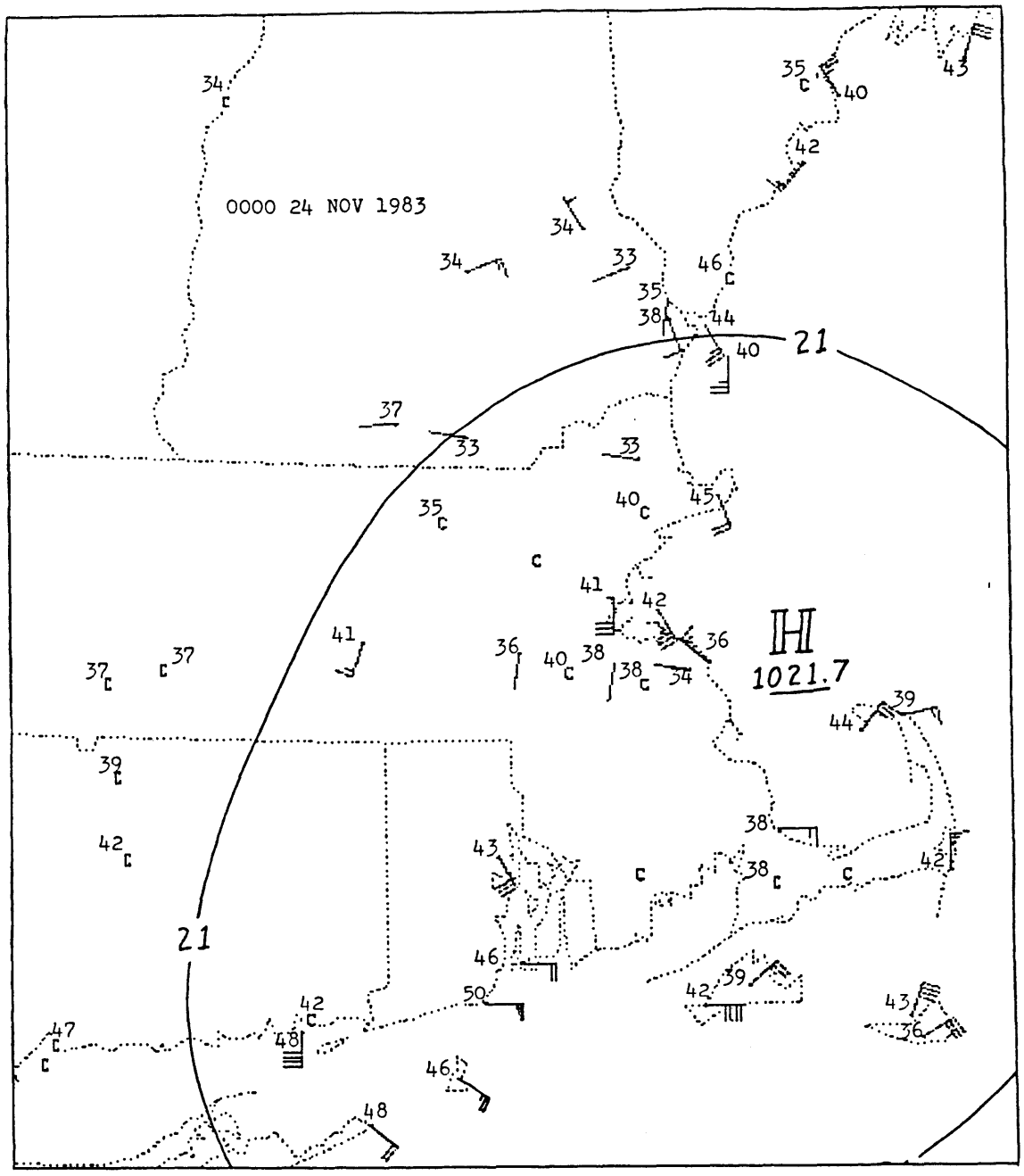

Fig. 3.7 Mesoscale analysis (as in Fig. 2.2), 0000 24 Nov 1983.

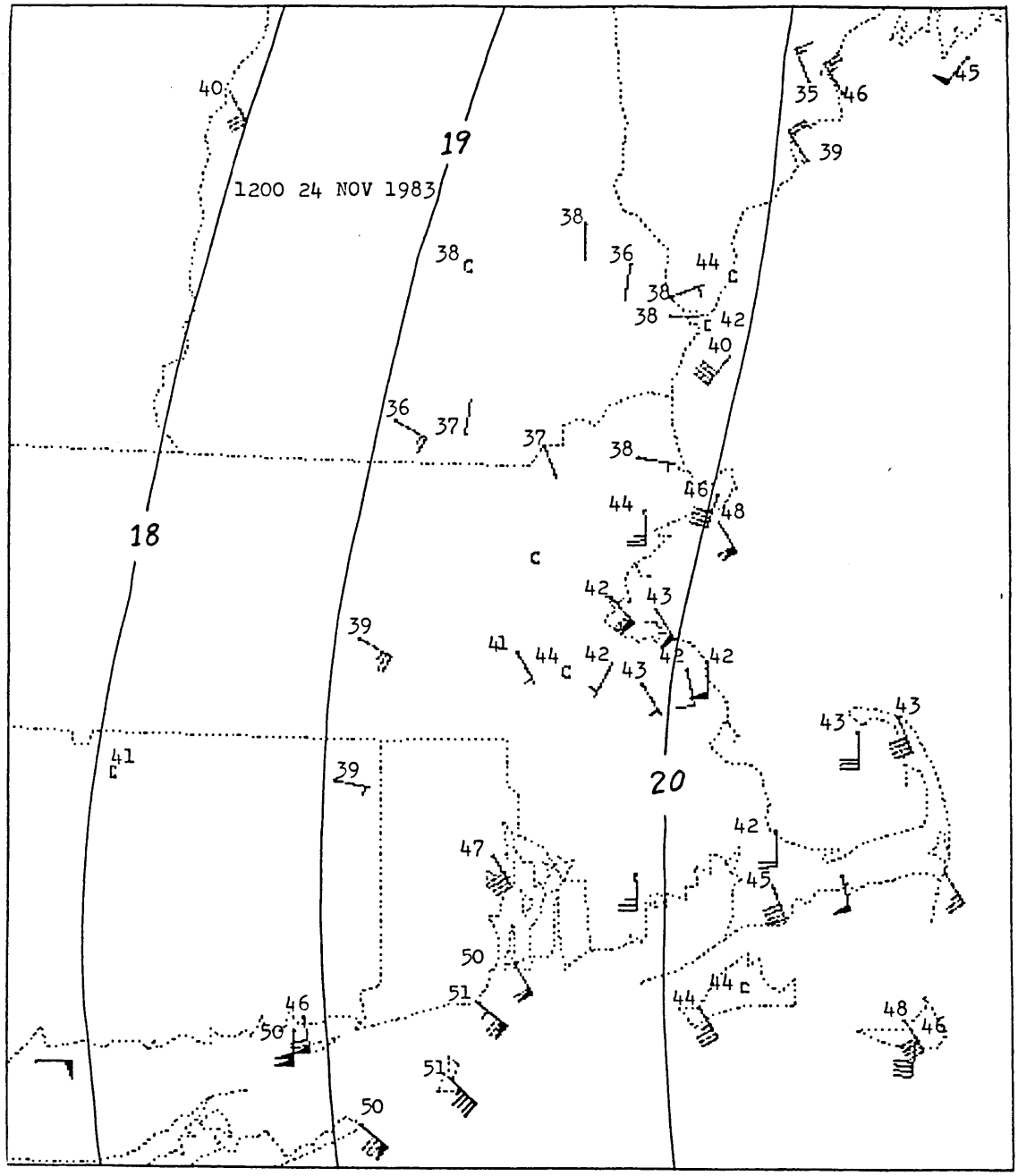

Fig. 3.8 Mesoscale analysis (as in Fig. 2.2), 1200 24 Nov 1983.

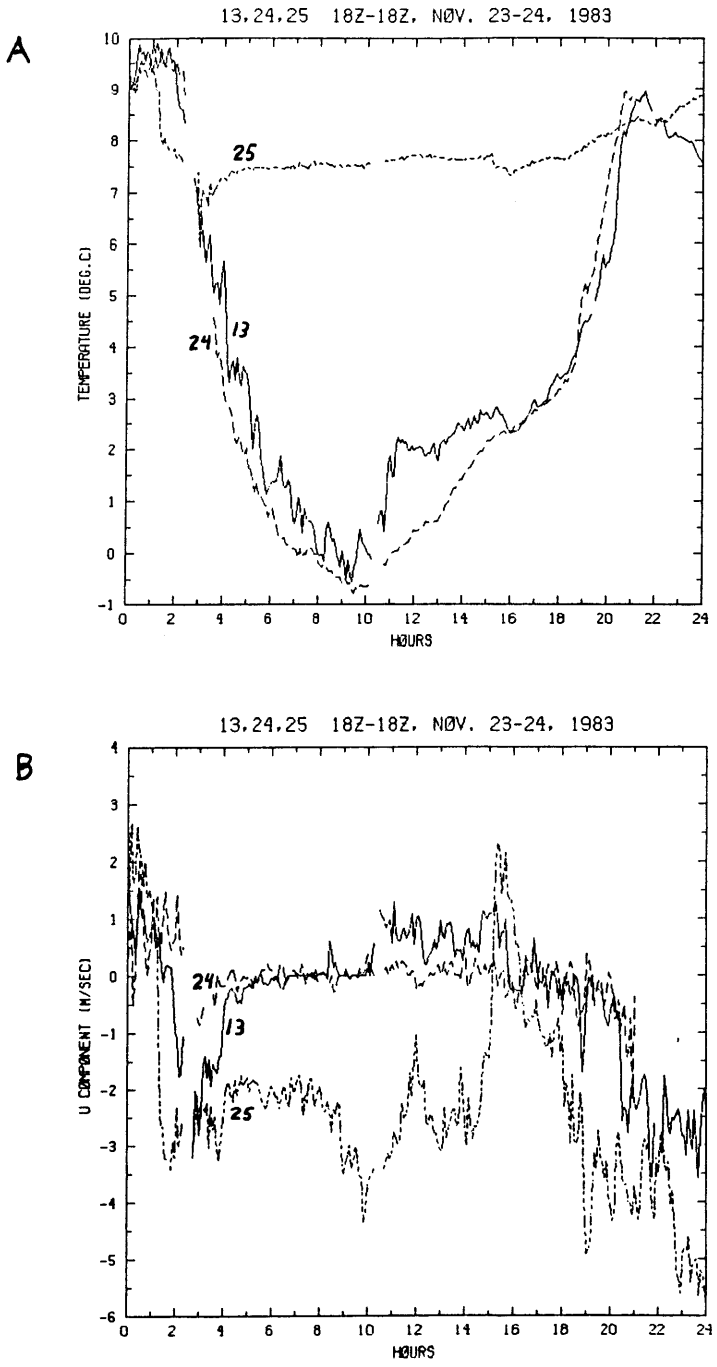

Fig. 3.9 Time series, as in Fig. 2.7, but for stations P24 and P25, 1800 23 Nov 1983 - 1800 24 Nov 1983.

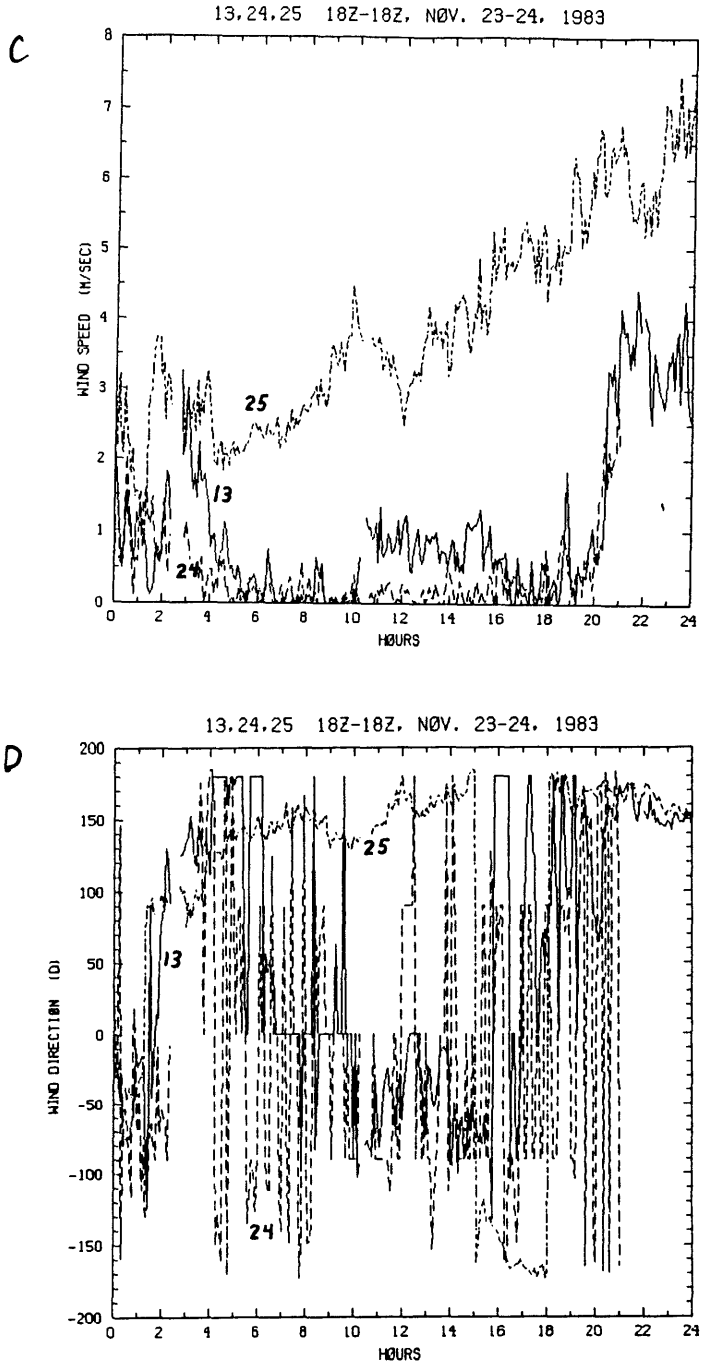

Fig. 3.9 (continued)

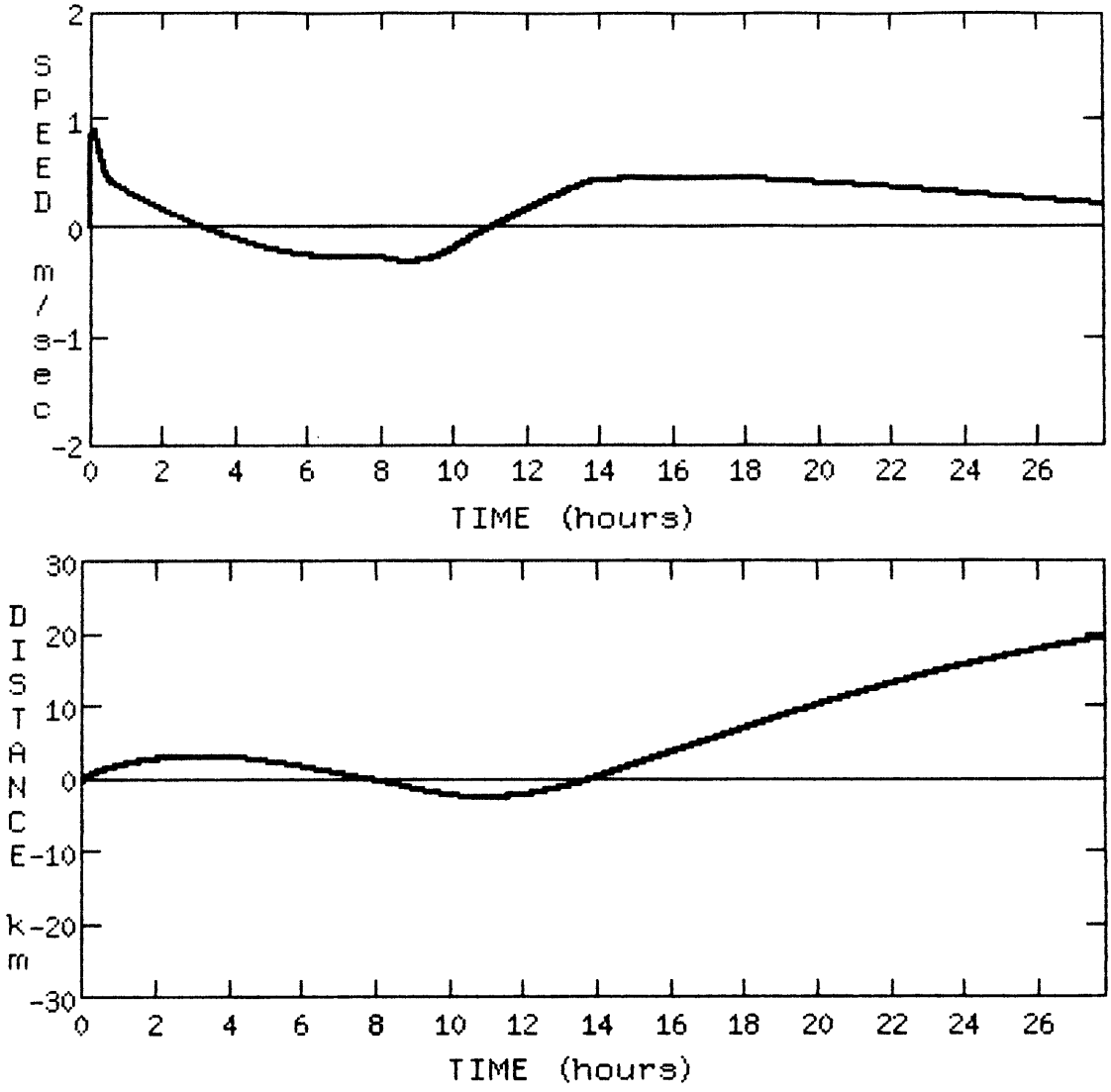

Fig. 3.10 Speed (m/s) and position (m, positive offshore) of density current as a function of time (hours), using density current model control parameters. See text for details.

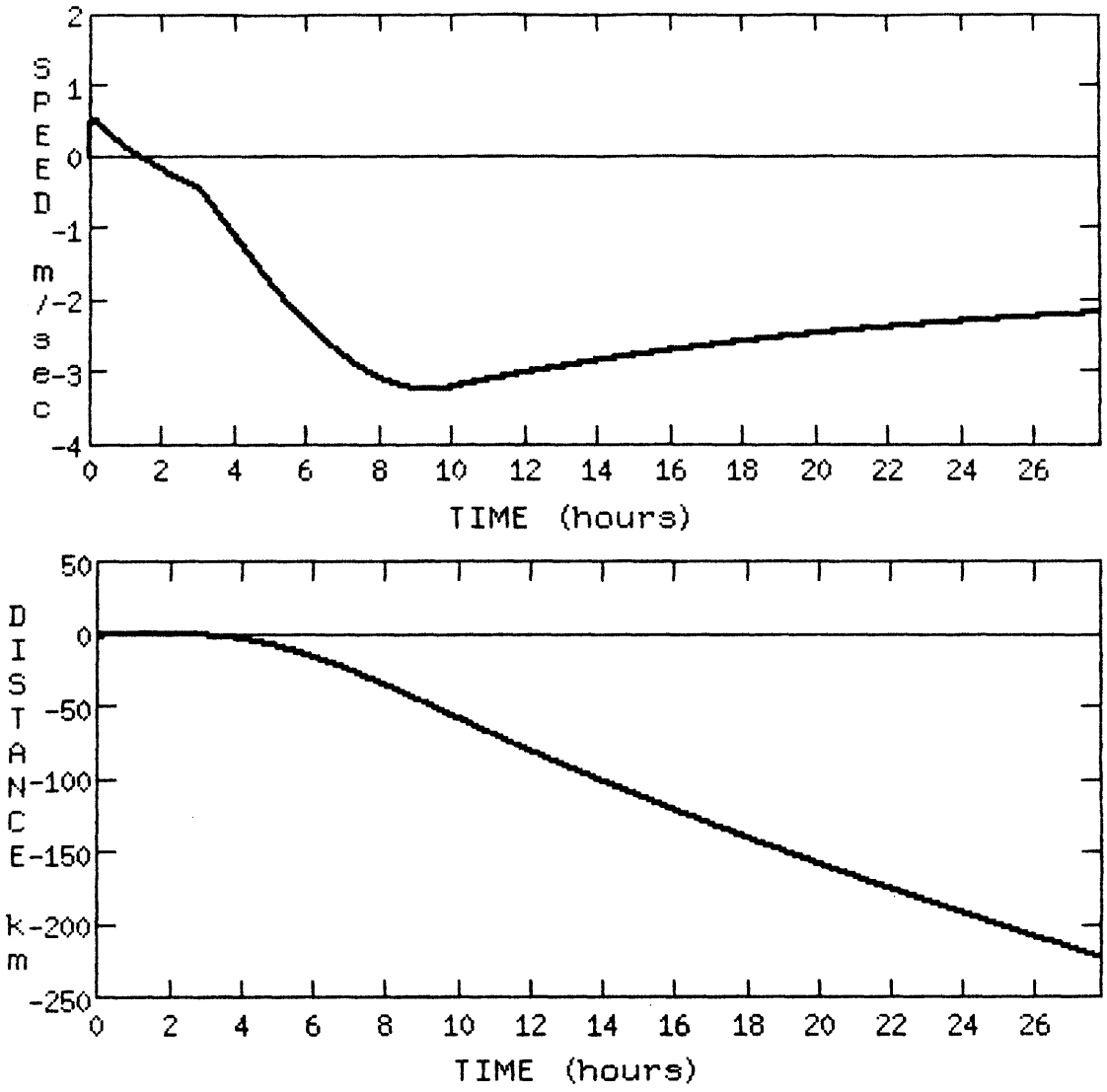

Fig. 3.11 As in Fig. 3.10, but with air-sea temperature difference of 3 K.

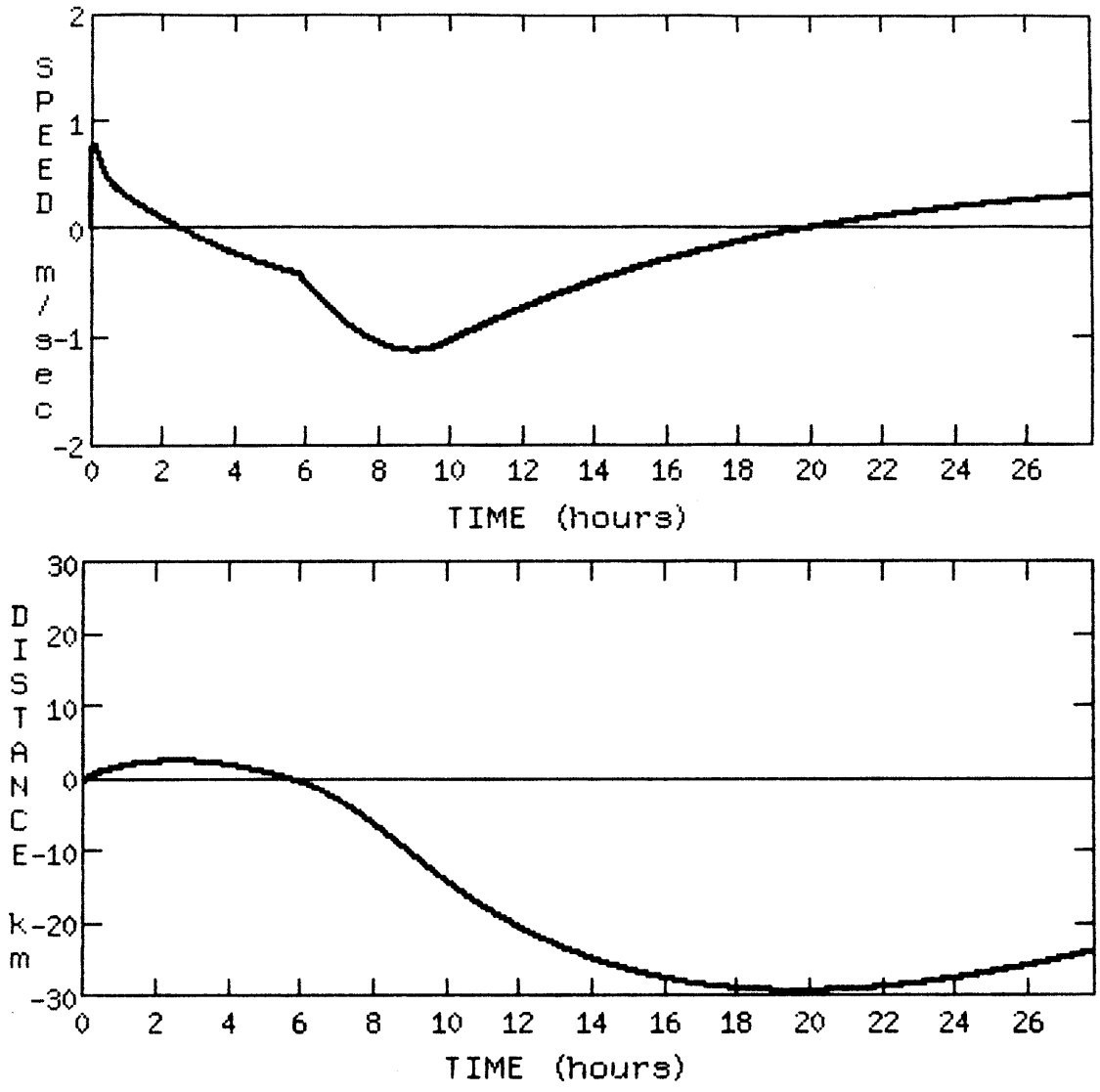

Fig. 3.12 As in Fig. 3.10, but with air-sea temperature difference of 6 K.

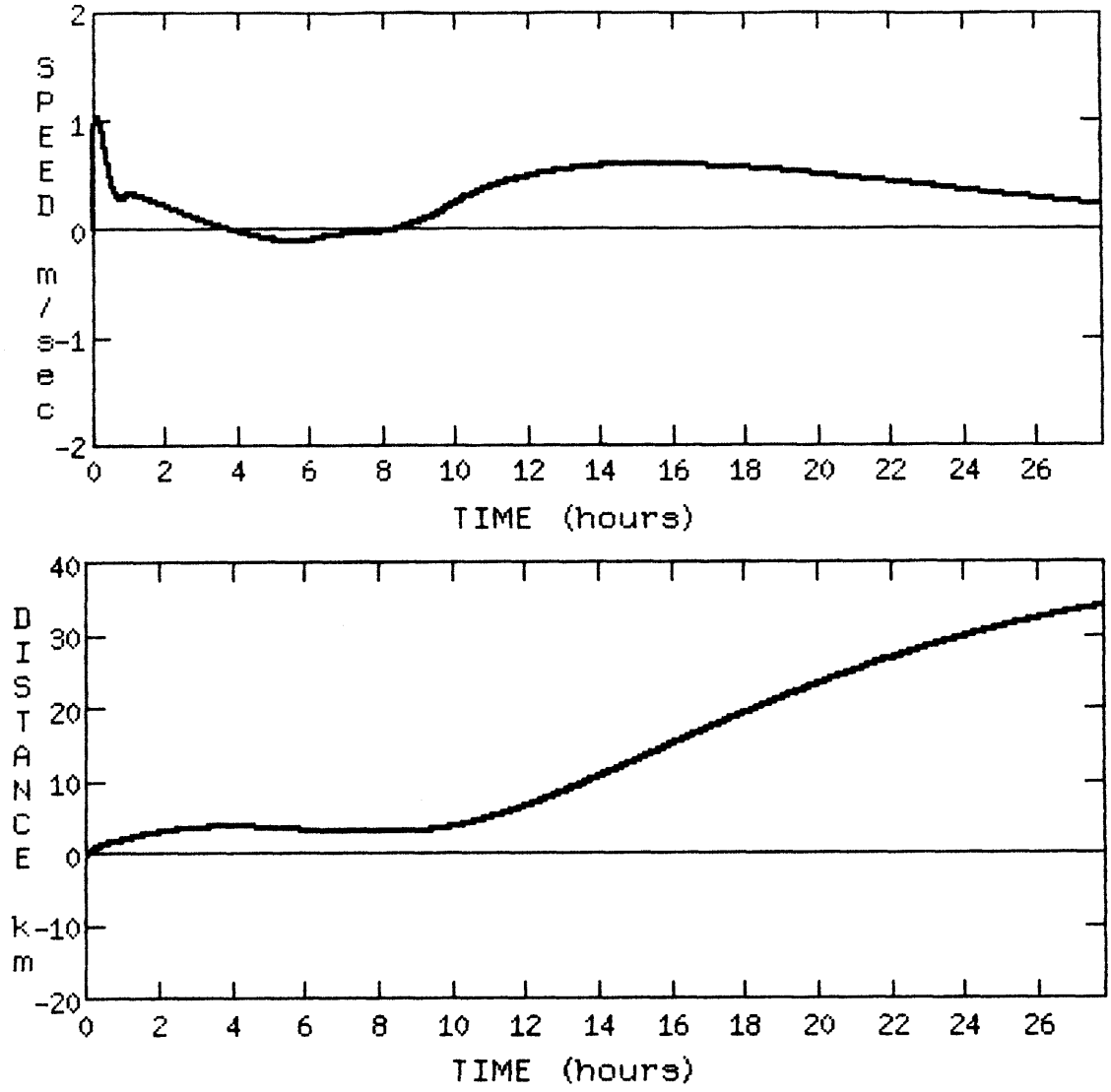

Fig. 3.13 As in Fig. 3.10, but with air-sea temperature difference of 9 K.

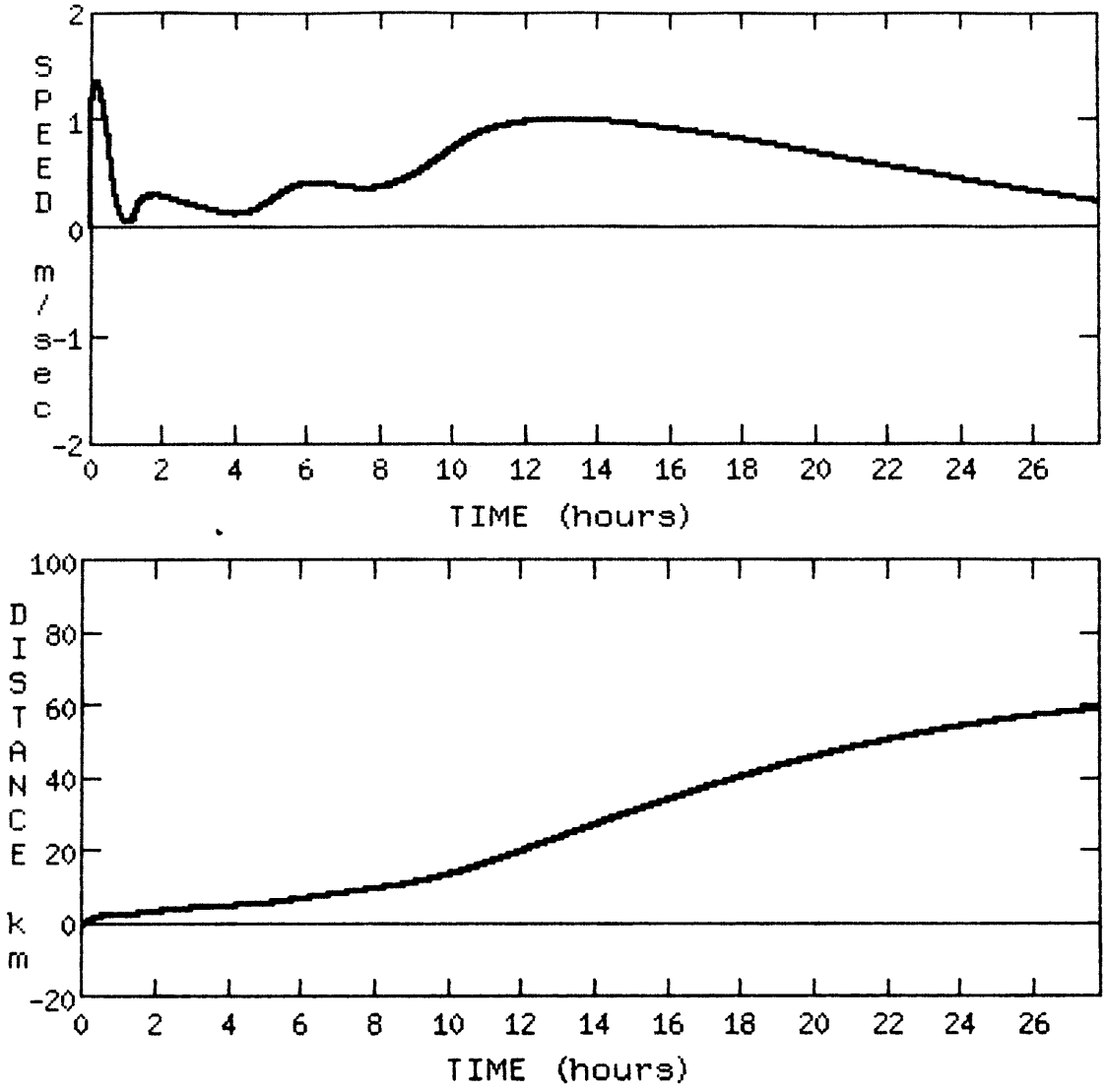

Fig. 3.14 As in Fig. 3.10, but with air-sea temperature difference of 12 K.

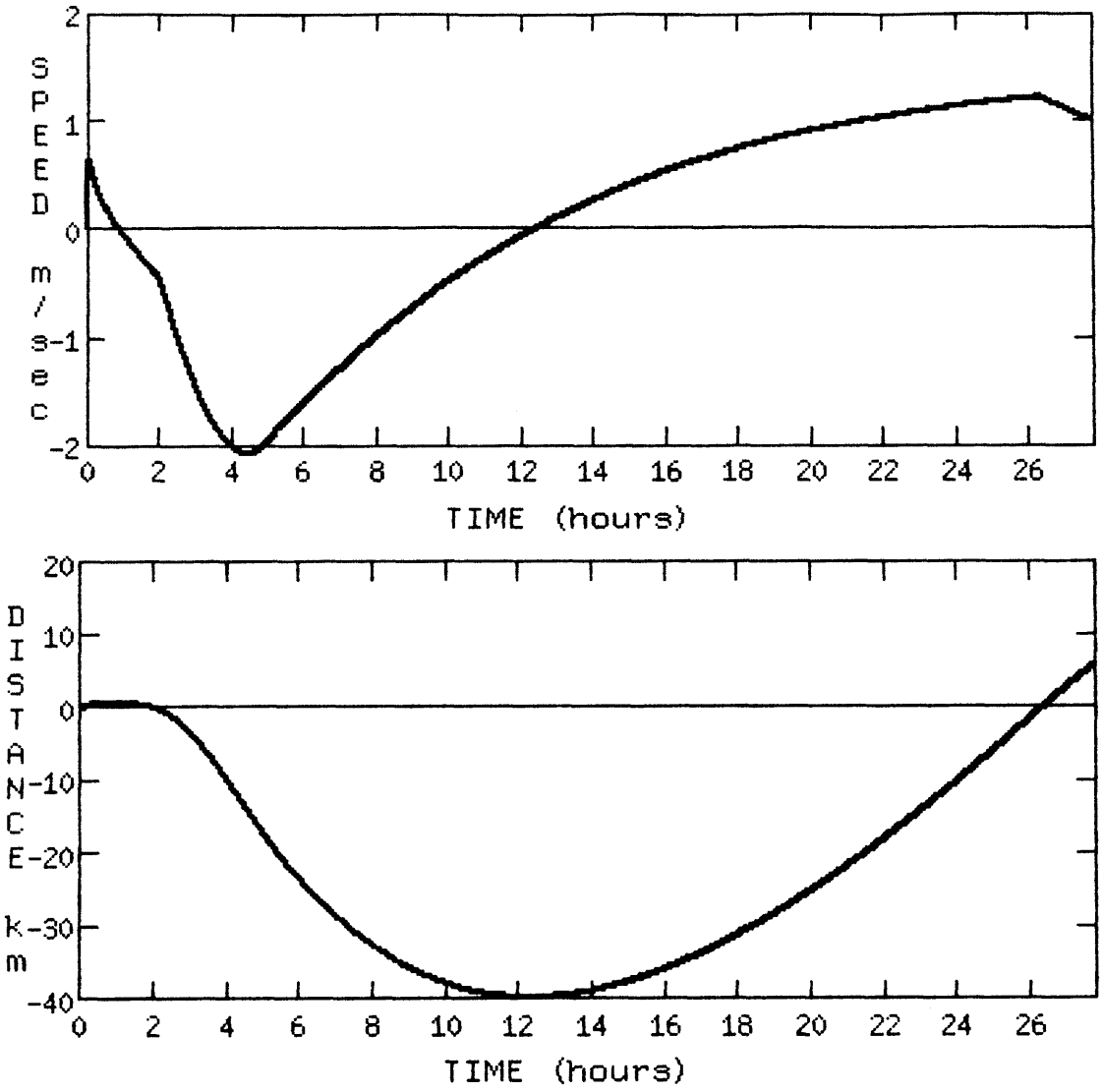

Fig. 3.15 As in Fig. 3.10, but with period of 90 degree windshift equal to 5 hours.

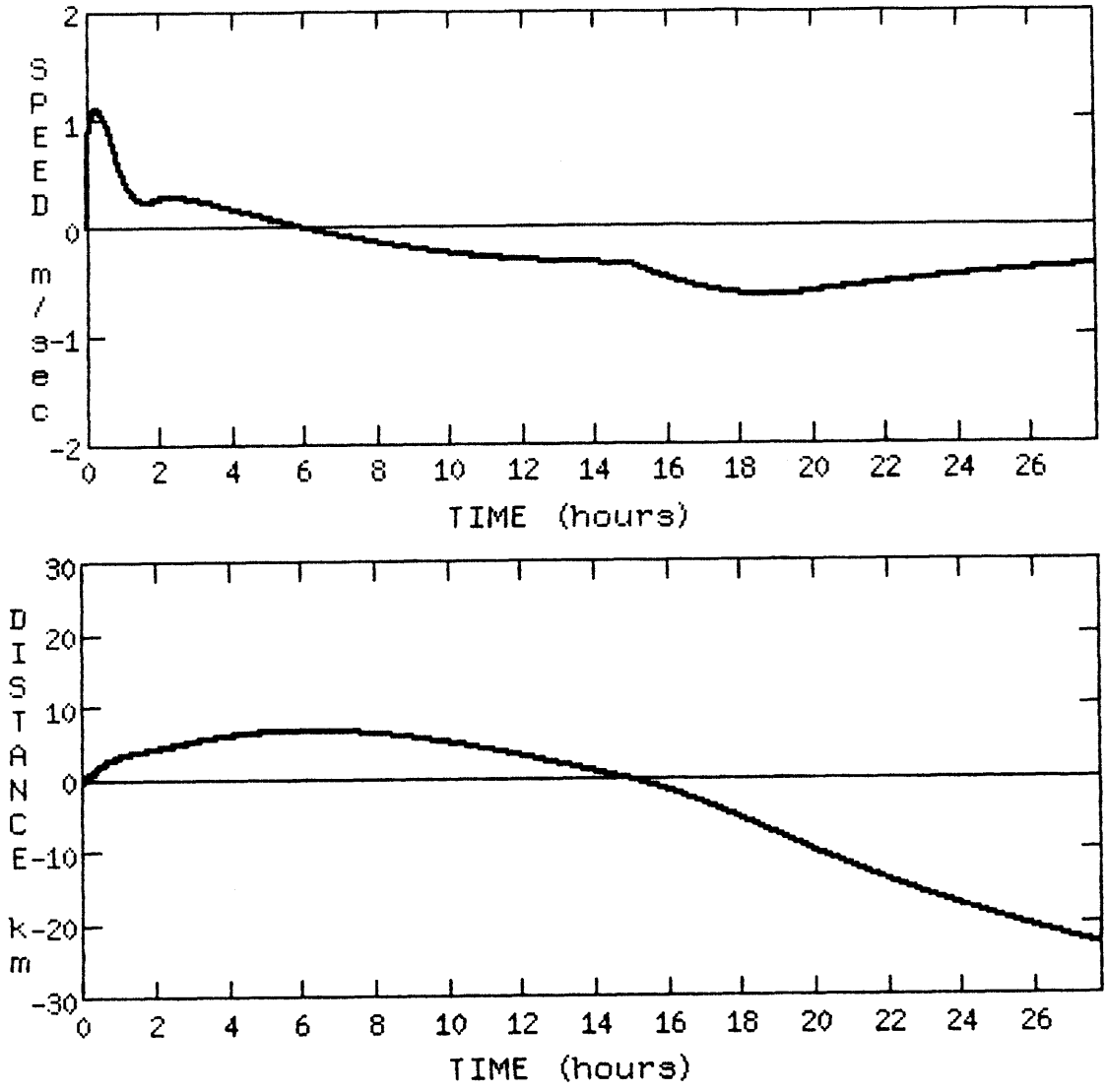

Fig. 3.16 As in Fig. 3.10, but with period of 90 degree windshift equal to 20 hours and air-sea temperature difference of 5 K.

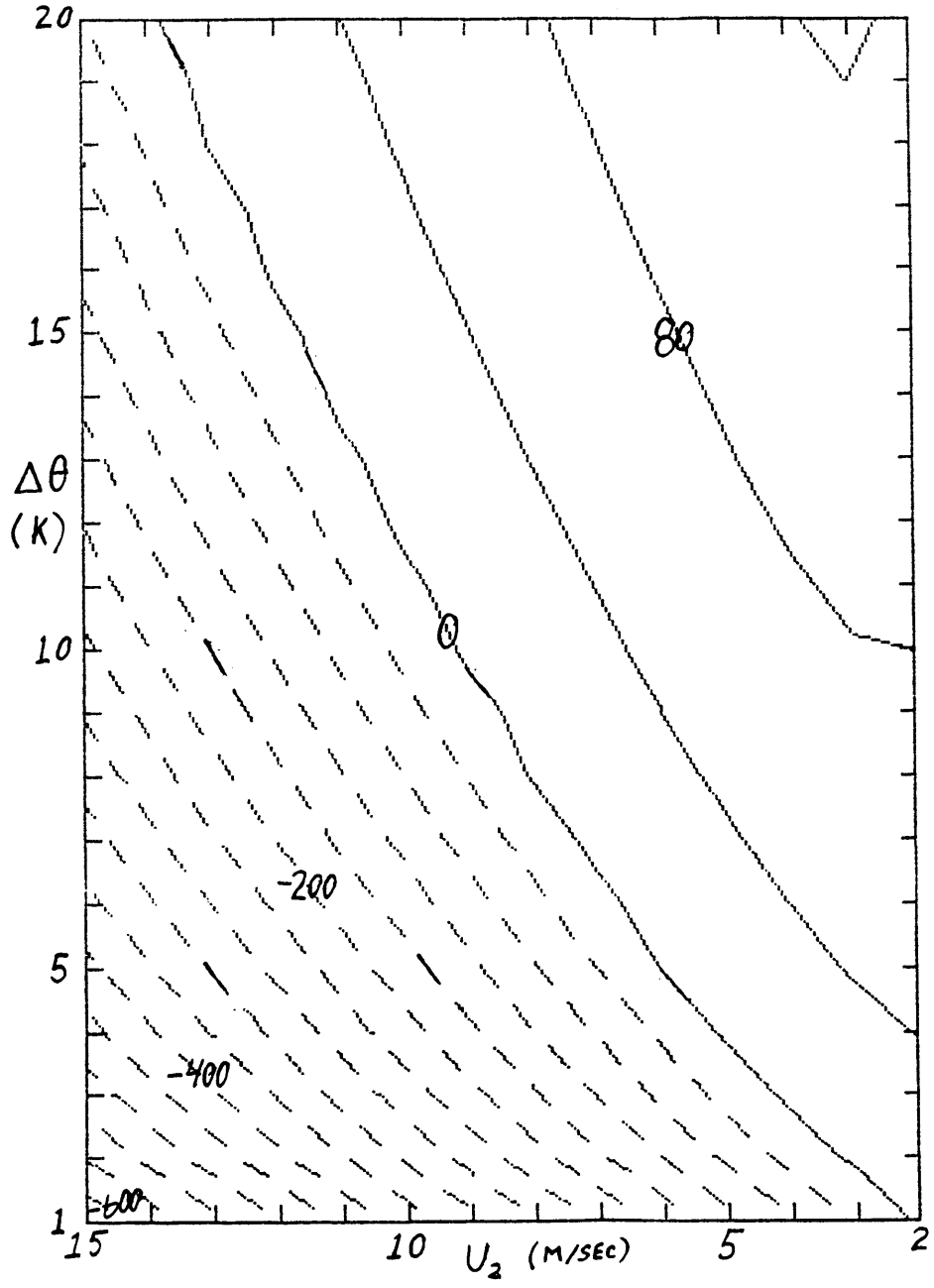

Fig. 3.17 Density current positions after 18 hours (positive offshore, contour interval = 40 km) as a function of warm air wind speed (m/s) and air-sea temperature difference (K), as calculated by density current model.

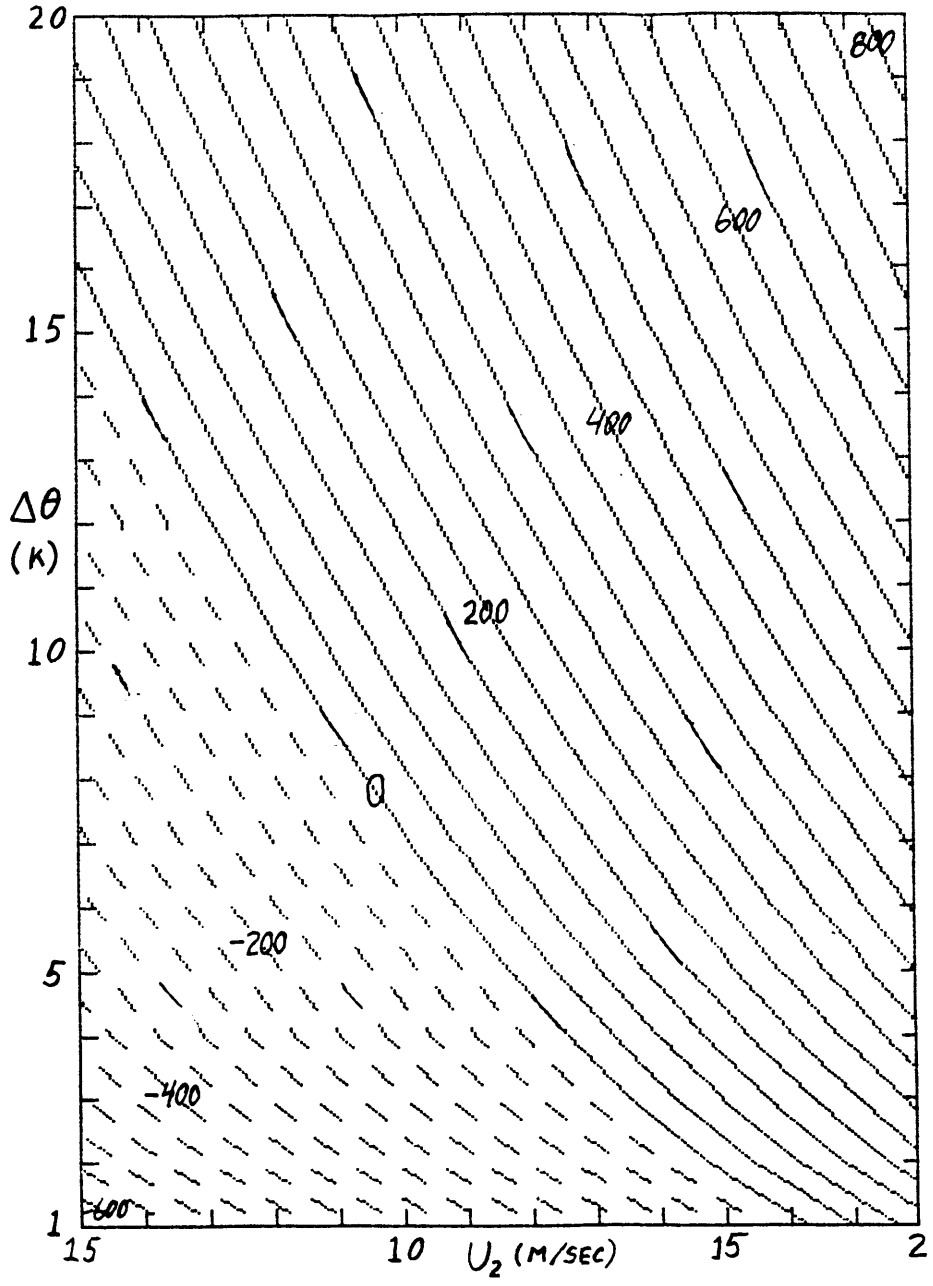

Fig. 3.18 As in Fig. 3.17, but with warm air equal to sea temperature and zero surface heat flux.

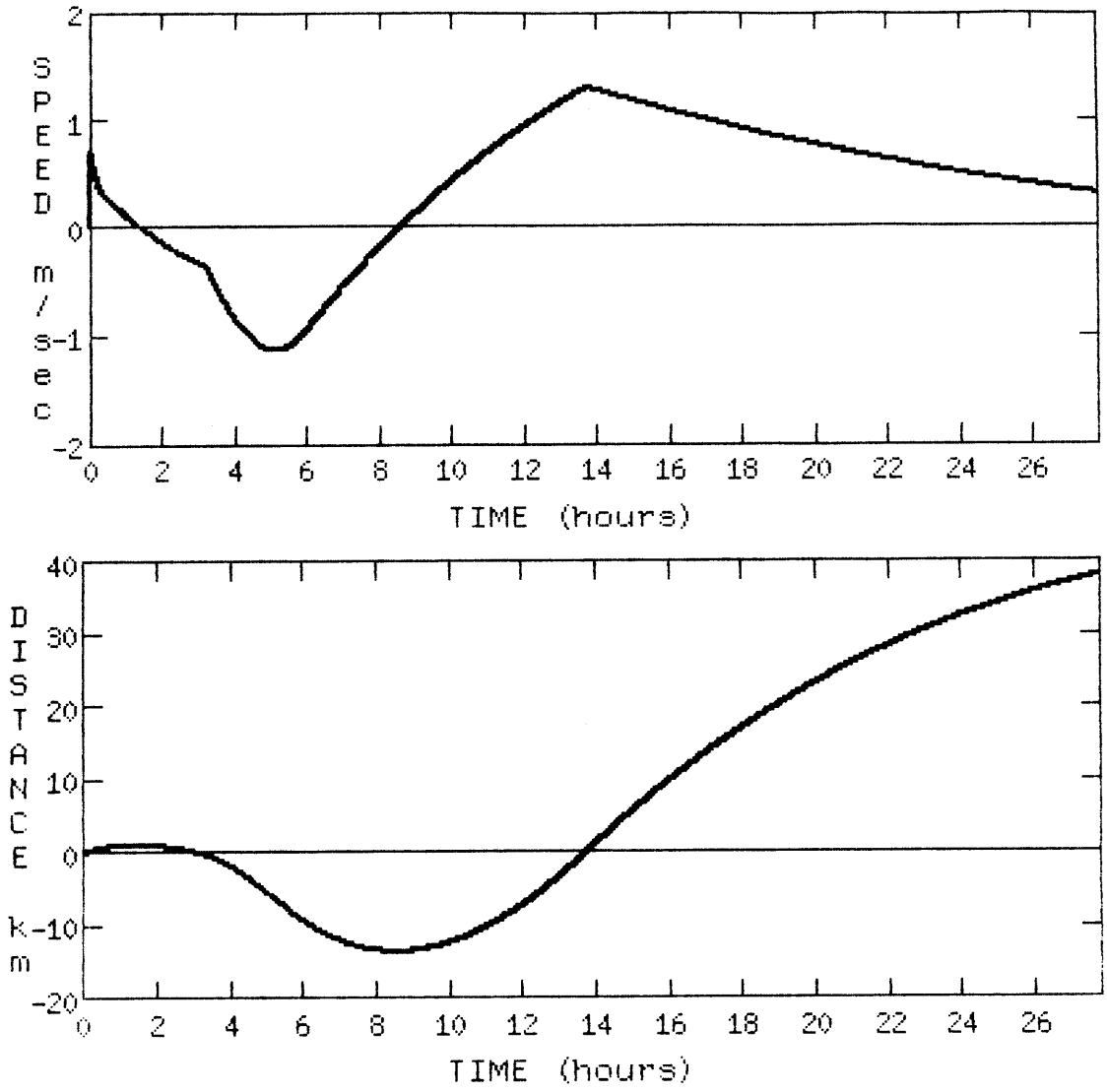

Fig. 3.19 As in Fig. 3.10, but with parameters appropriate to 4 Dec 1983 coastal front case. See text for details.

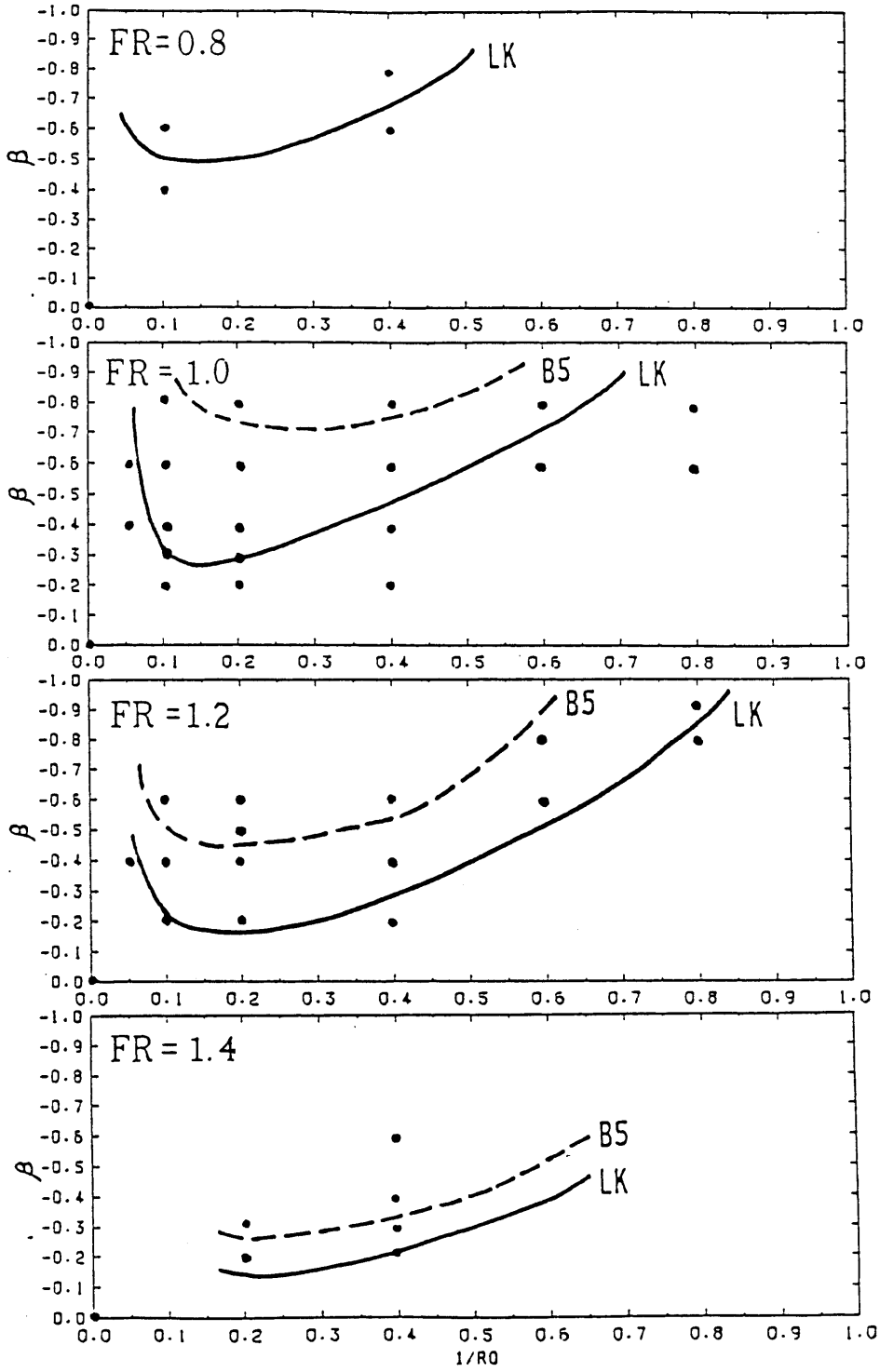

Fig. 4.1 a) Blocking criteria as a function of inverse Rossby number (1/Ro), β, and Froude number (Fr), for two asymmetric mountain profiles (dashed line = B5 profile, solid line = LK profile), as determined by numerical model. Blocking occurs for values of parameters located above the lines. See text for description of mountain profiles. From Garner (1986).

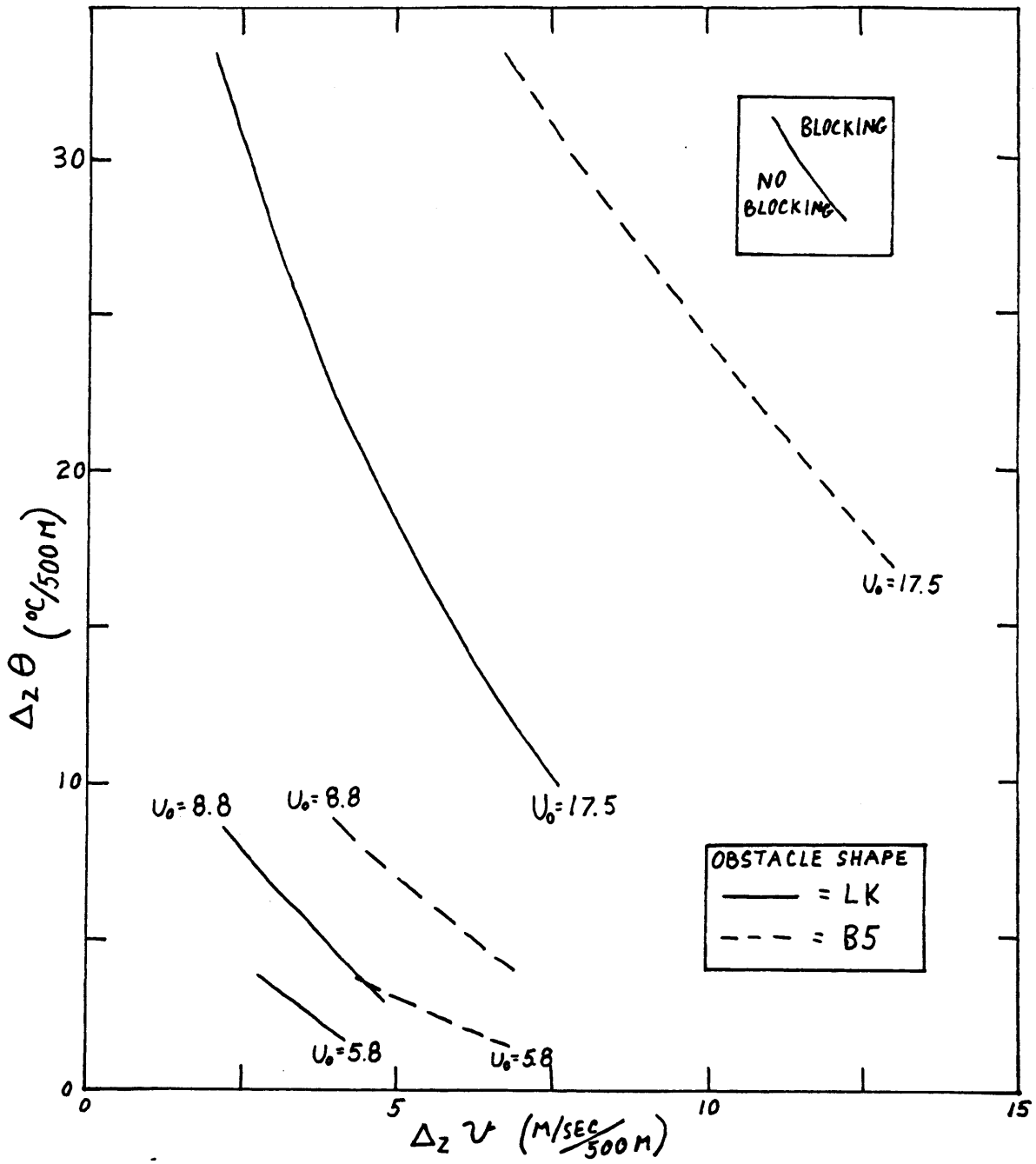

Fig. 4.1 b) Blocking criteria, as in a), but as a function of mountain-normal wind speed and vertical gradients of potential temperature and mountain-parallel wind. Derived from 4.1a) using external parameters appropriate to New England. Vertical derivatives are normalized by the assumed height of the obstacle. Blocking occurs for values of parameters located above the lines. See text for details.

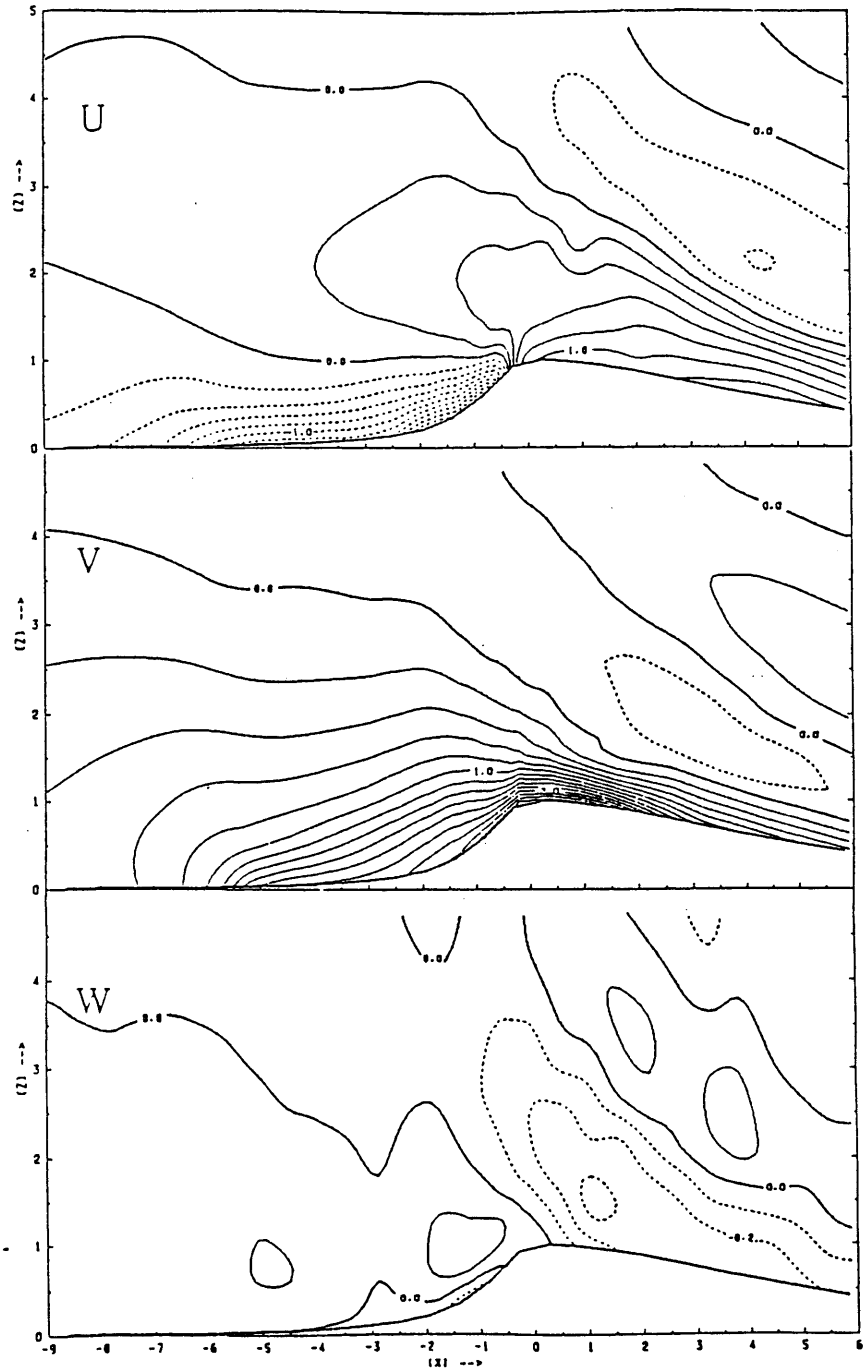

Fig. 4.2 Perturbation non-dimensional velocity components at t = 30 for strongly blocked flow simulation. From Garner (1986).

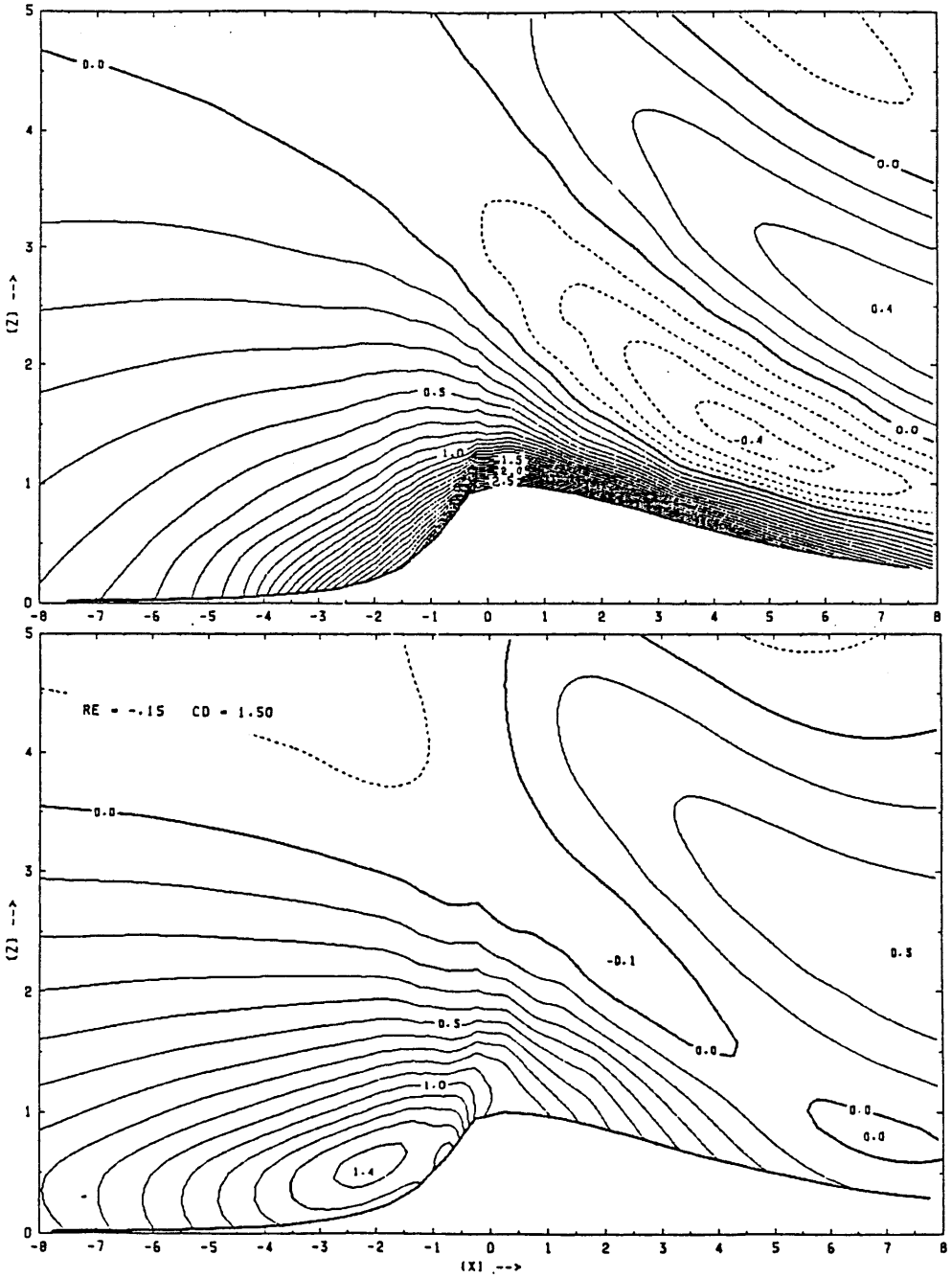

Fig. 4.3 Non-dimensional mountain-parallel velocity components at t = 30 for strongly blocked flow simulation. From Garner (1986). a) No surface friction b) Surface friction.

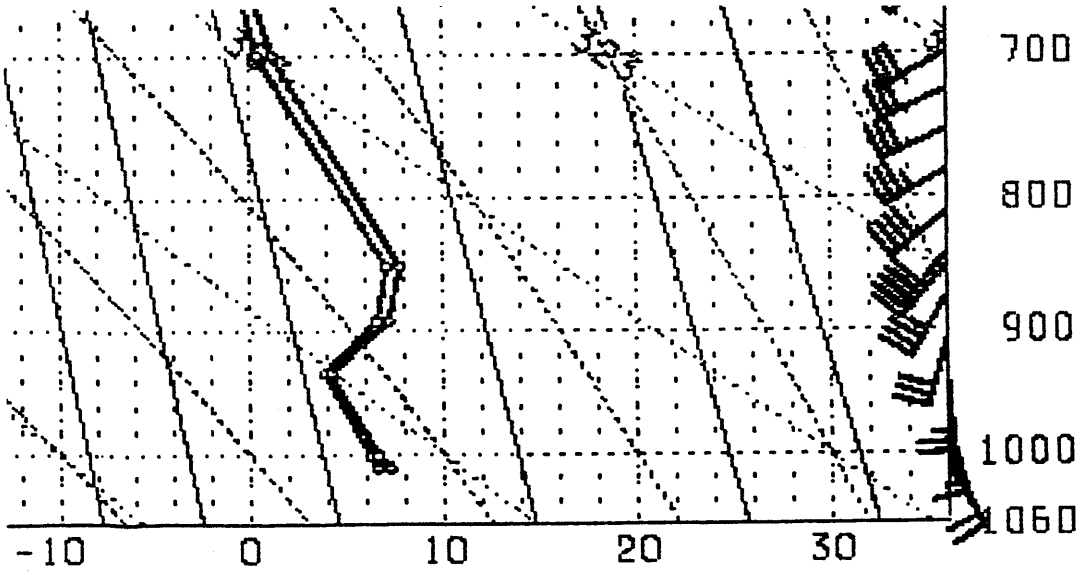

Fig. 4.4 Low-level sounding, as in 3.1, but for PWM, 0000 25 Nov 1983. Wind plots are conventional; long barb = 10 knots, short barb = 5 knots.

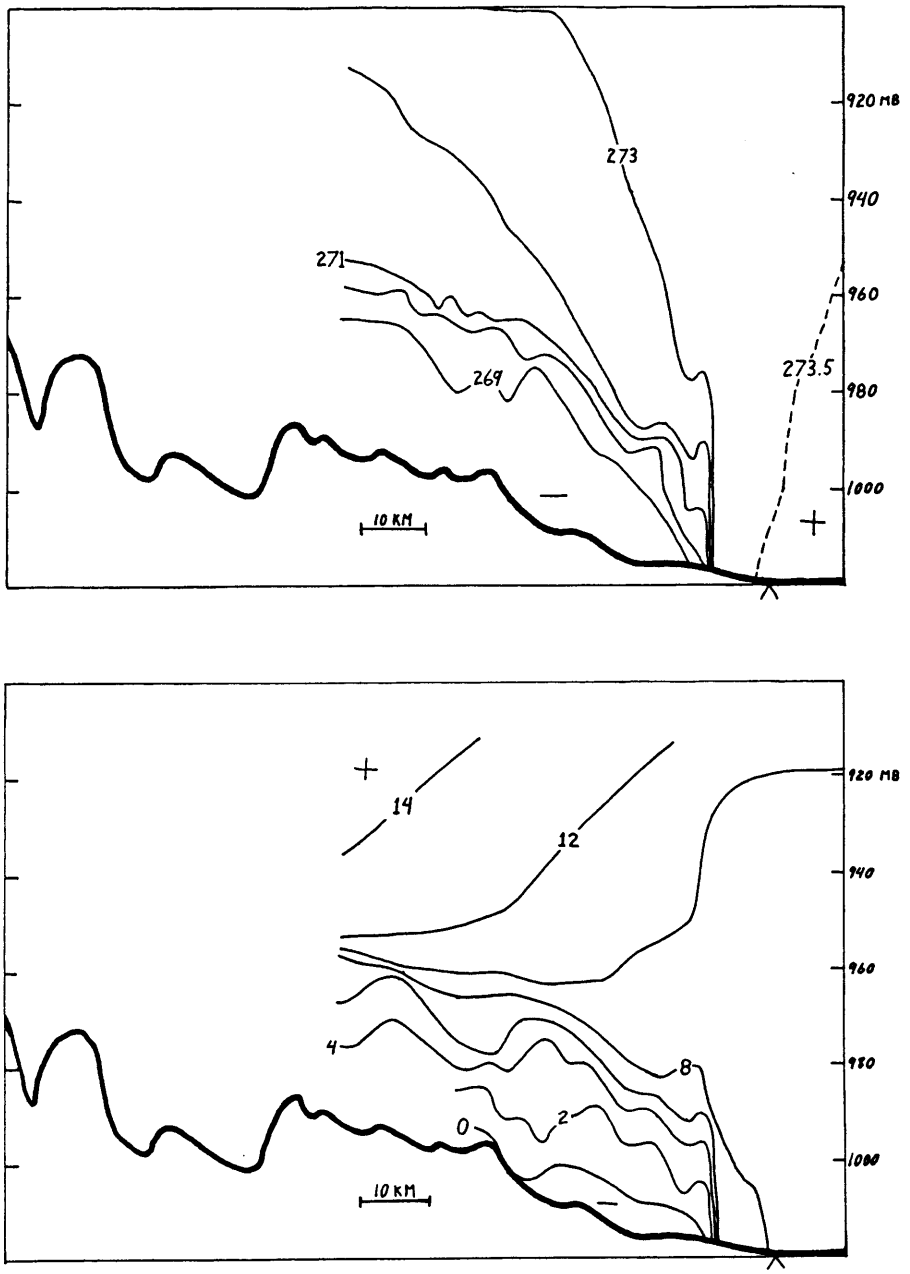

Fig. 4.5 Cross section through coastal front, 1500 4 Dec 1983. See text for details. Inverted 'V' shows approximate location of coast. a) Potential temperature, contour interval = 1 K b) Front-normal horizontal winds, contour interval = 2 m/s. Positive wind blows from right to left.

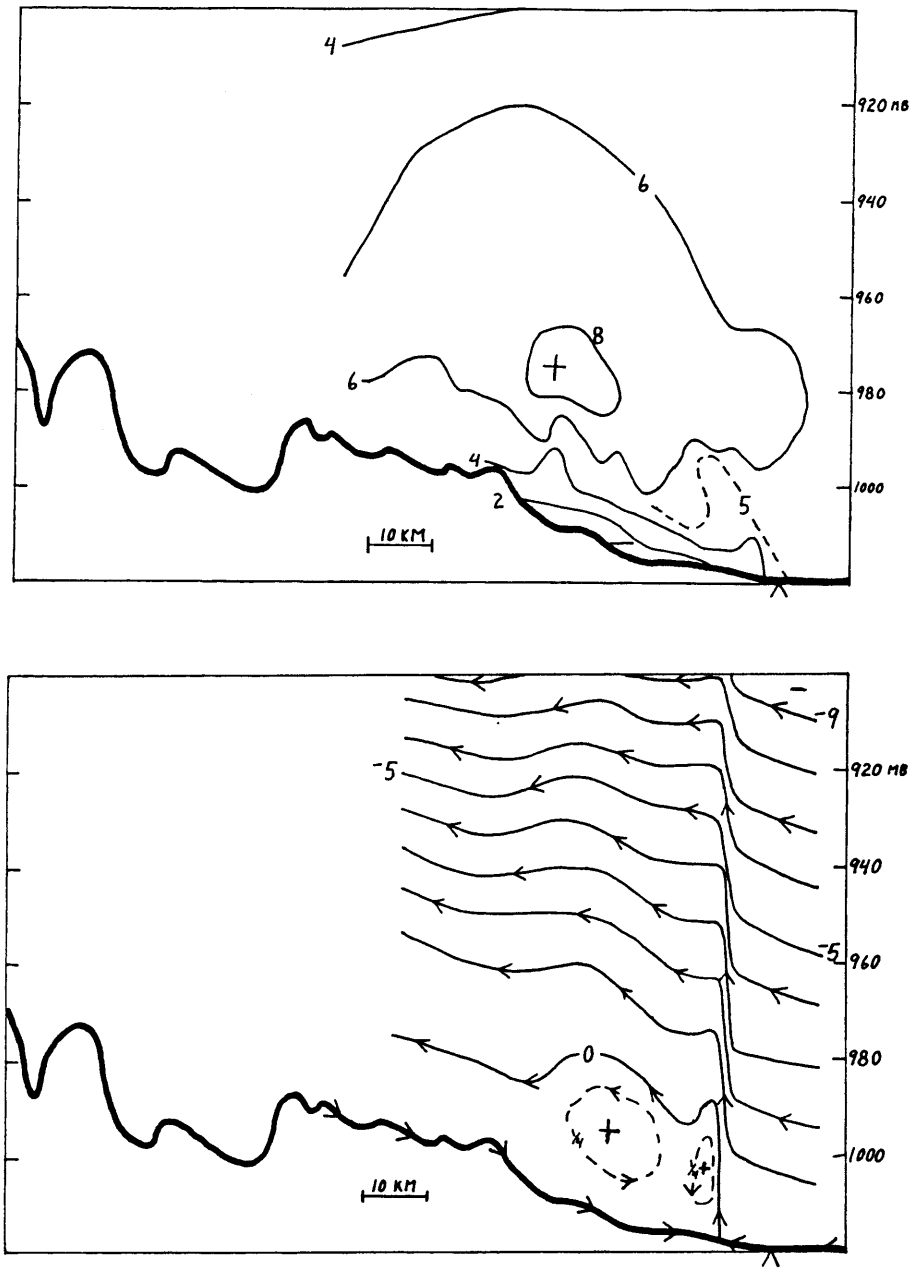

Fig. 4.6 As in Fig. 4.5. a) Front-parallel winds, contour interval = 2 m/s. Positive wind blows out of the page. b) Front-relative stream function, contour interval = 1 m/s/km. See text for details.

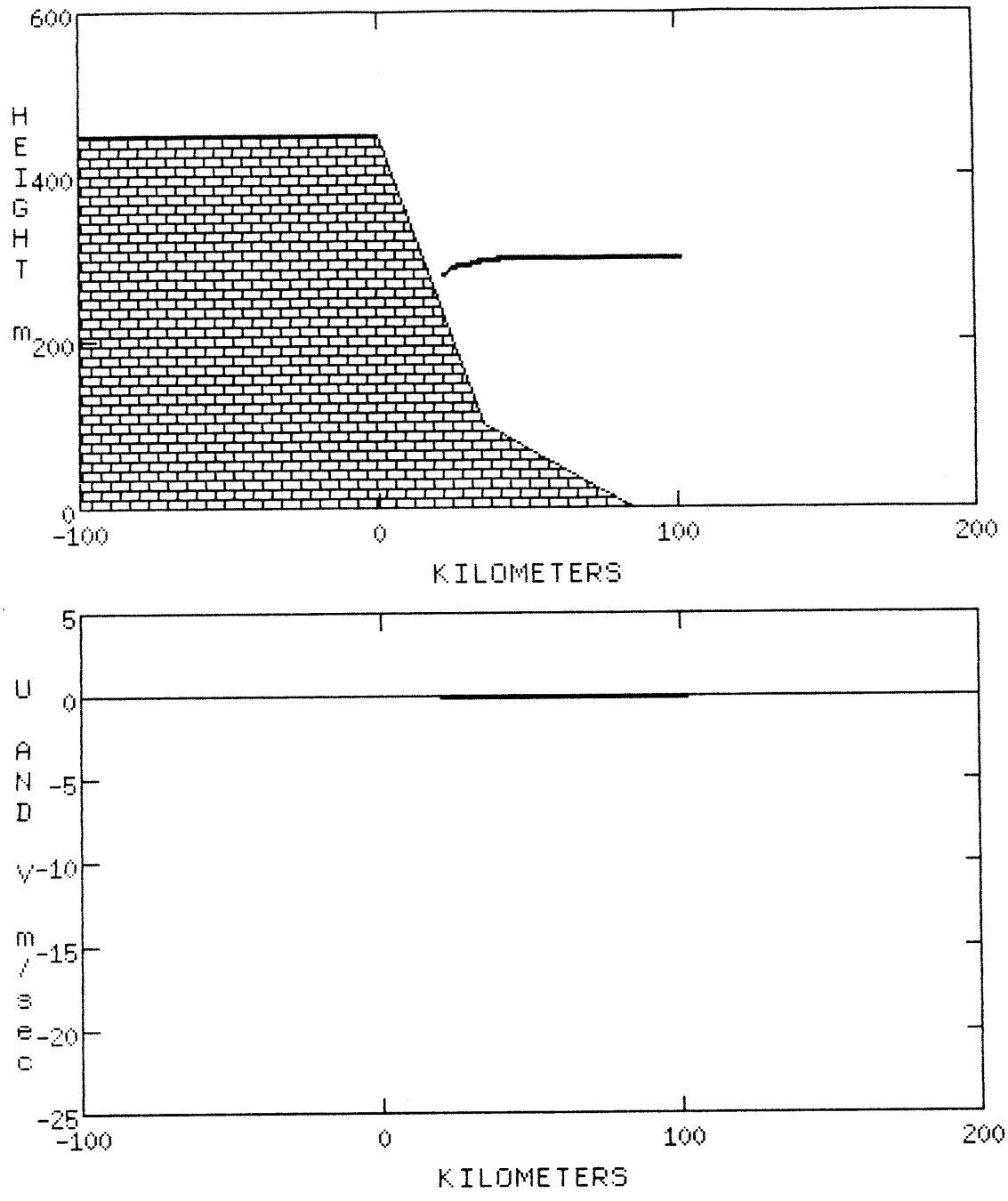

Fig. 4.7 Lagrangian model, initial conditions. a) Upper margin of dense fluid. b) Velocities within dense fluid. See text for details.

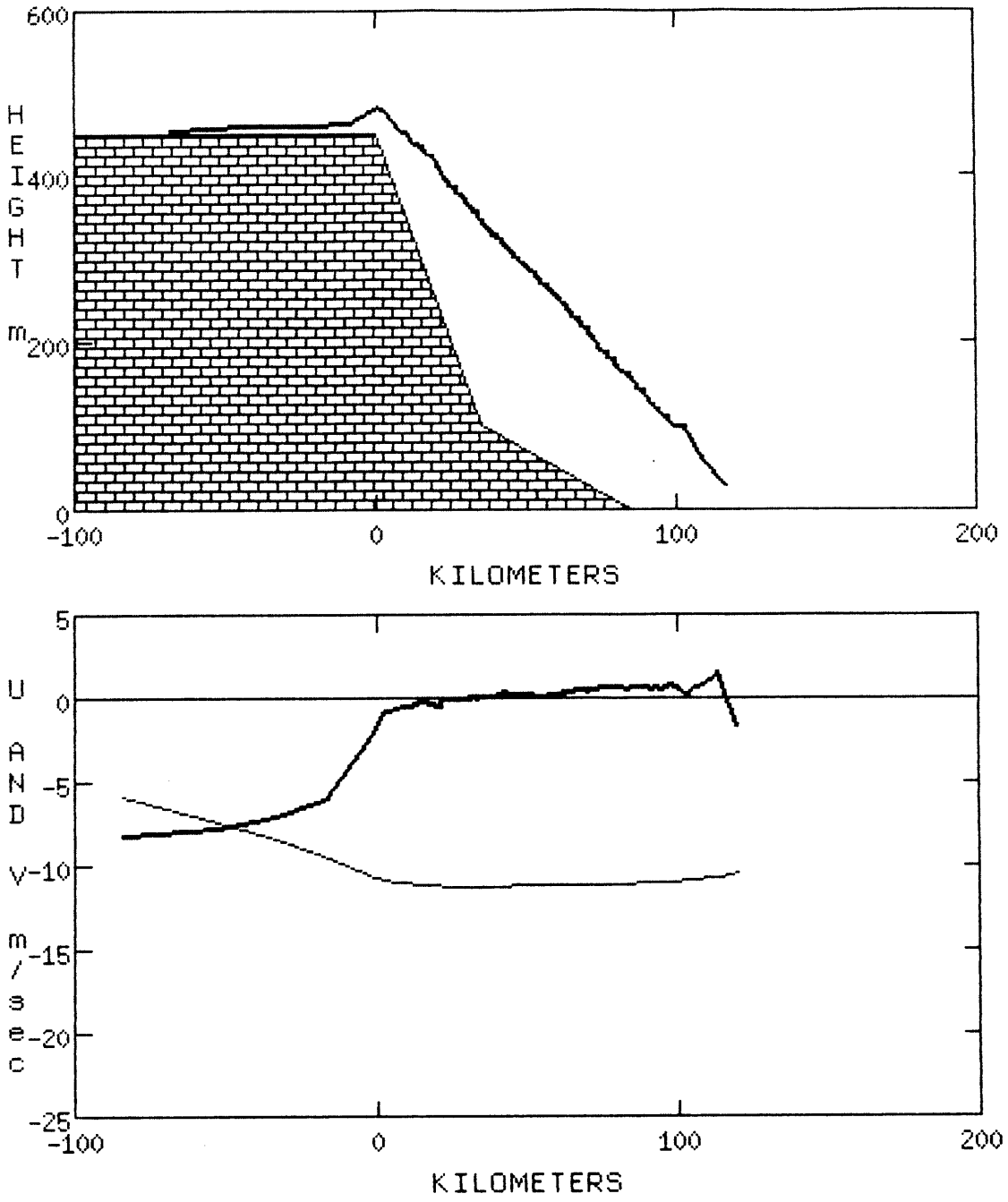

Fig. 4.8 As in Fig. 4.7, but for 12 hours after initialization, using control parameters (see text). Velocity component toward the right is thick line, component into the page is thin line.

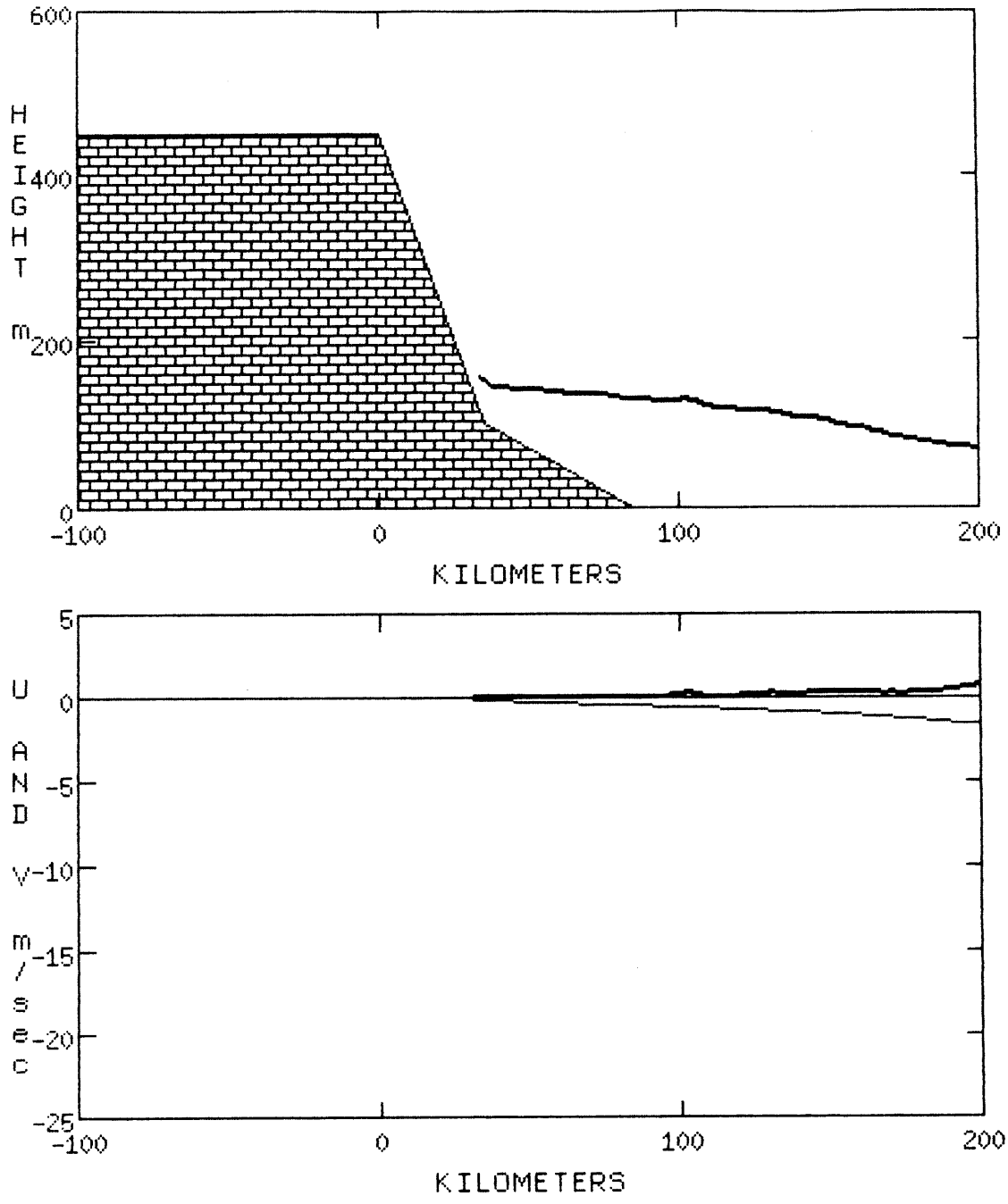

Fig. 4.9 As in Fig. 4.8, but with pressure gradient normal to obstacle equal to 0.0 mb/100 km.

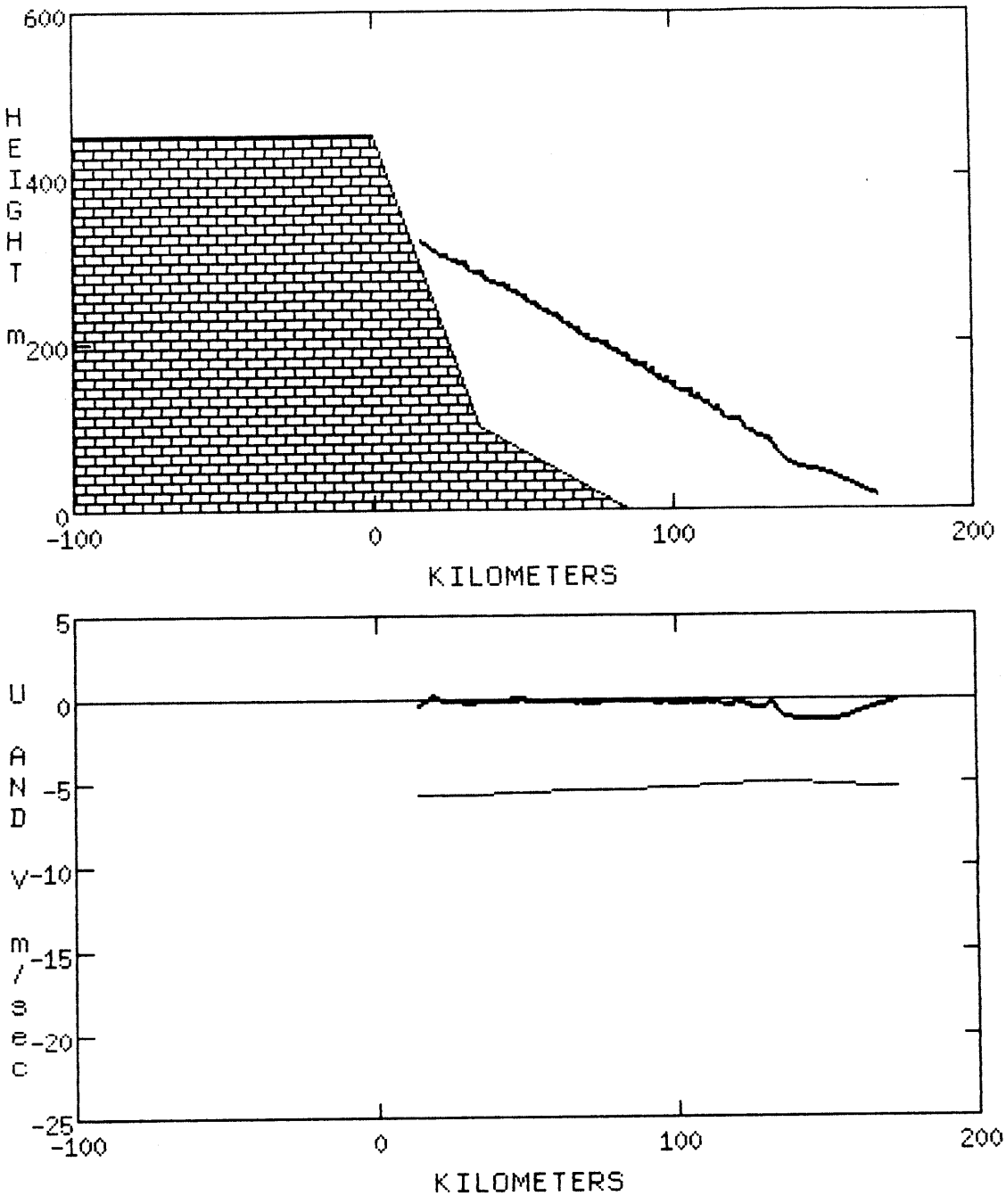

Fig. 4.10 As in Fig. 4.8, but with pressure gradient equal to 0.5 mb/100 km.

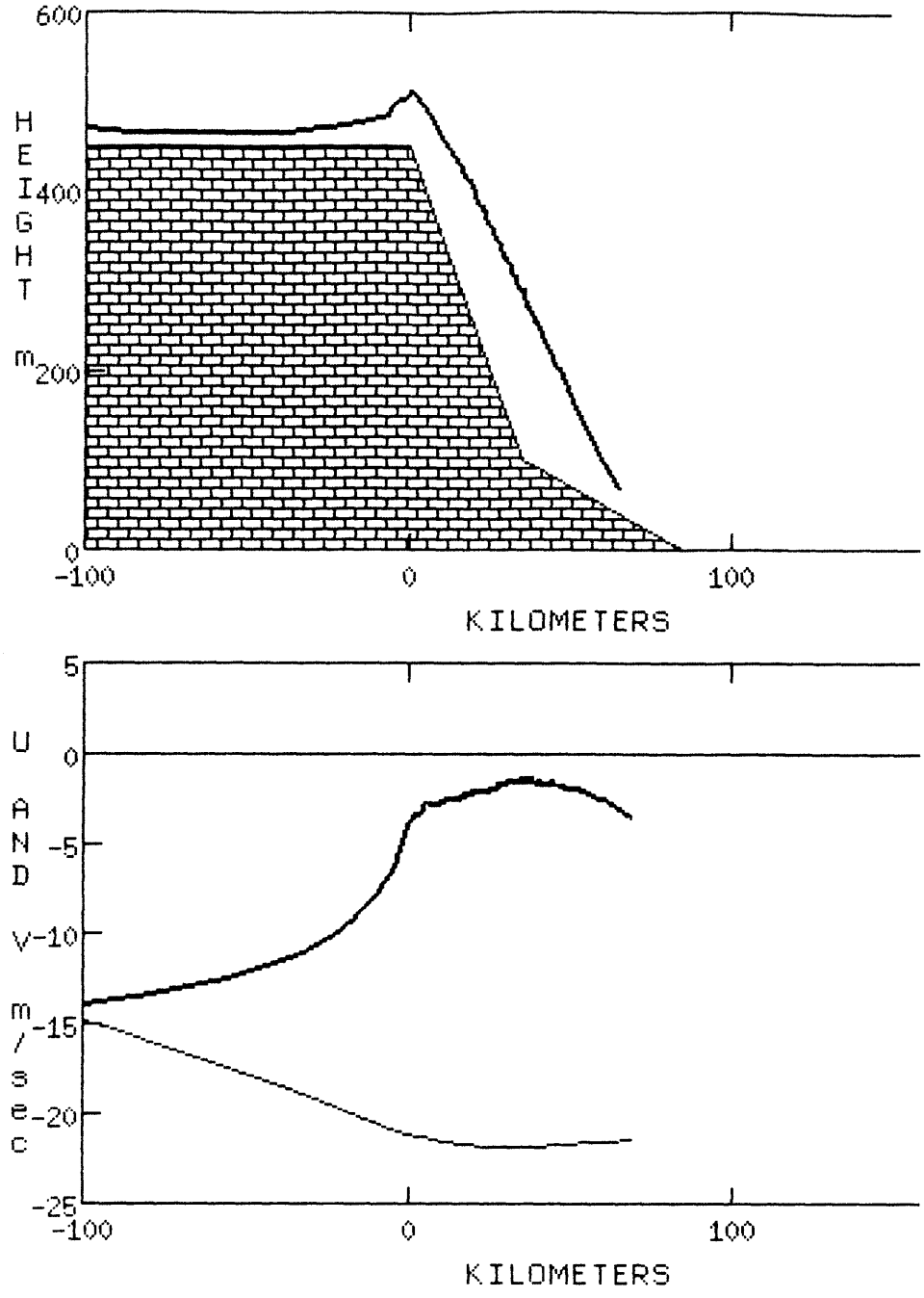

Fig. 4.11 As in Fig. 4.8, but with pressure gradient equal to 2.0 mb/100 km.

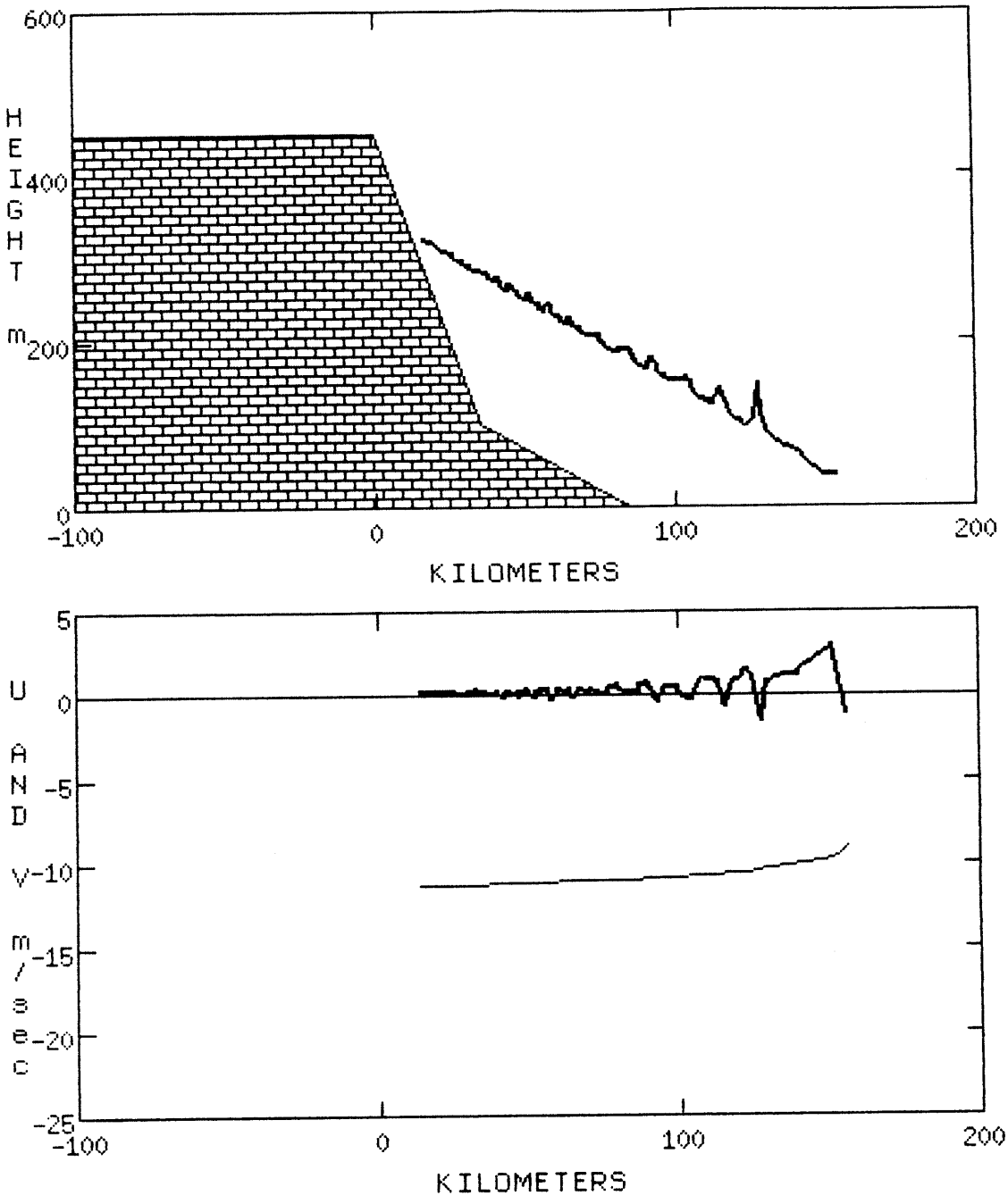

Fig. 4.12 As in Fig. 4.8, but with density difference equal to 6%.

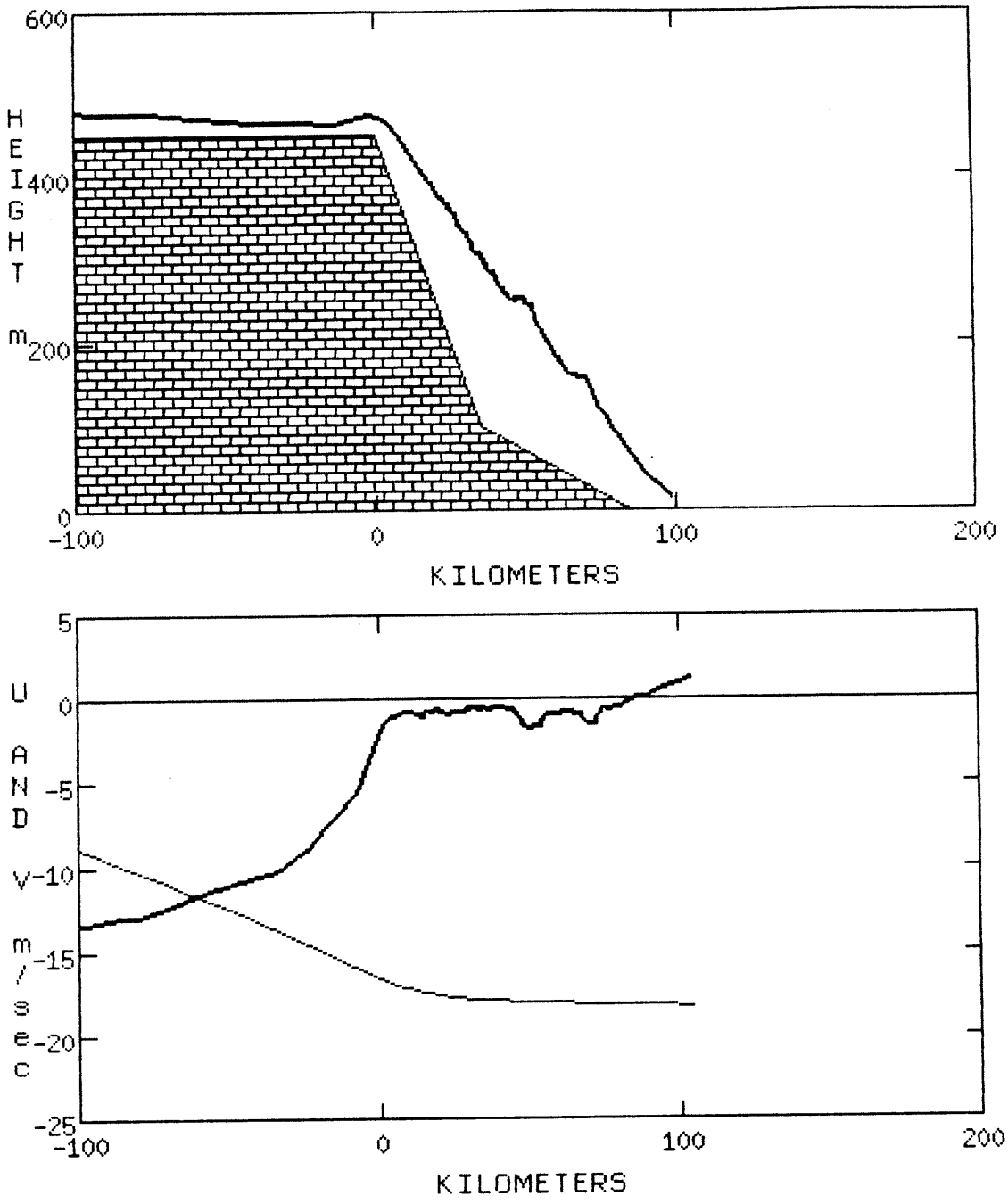

Fig. 4.13 As in Fig. 4.8, but with $C_d = 4.0 \times 10^{-5}\ s^{-1}$.

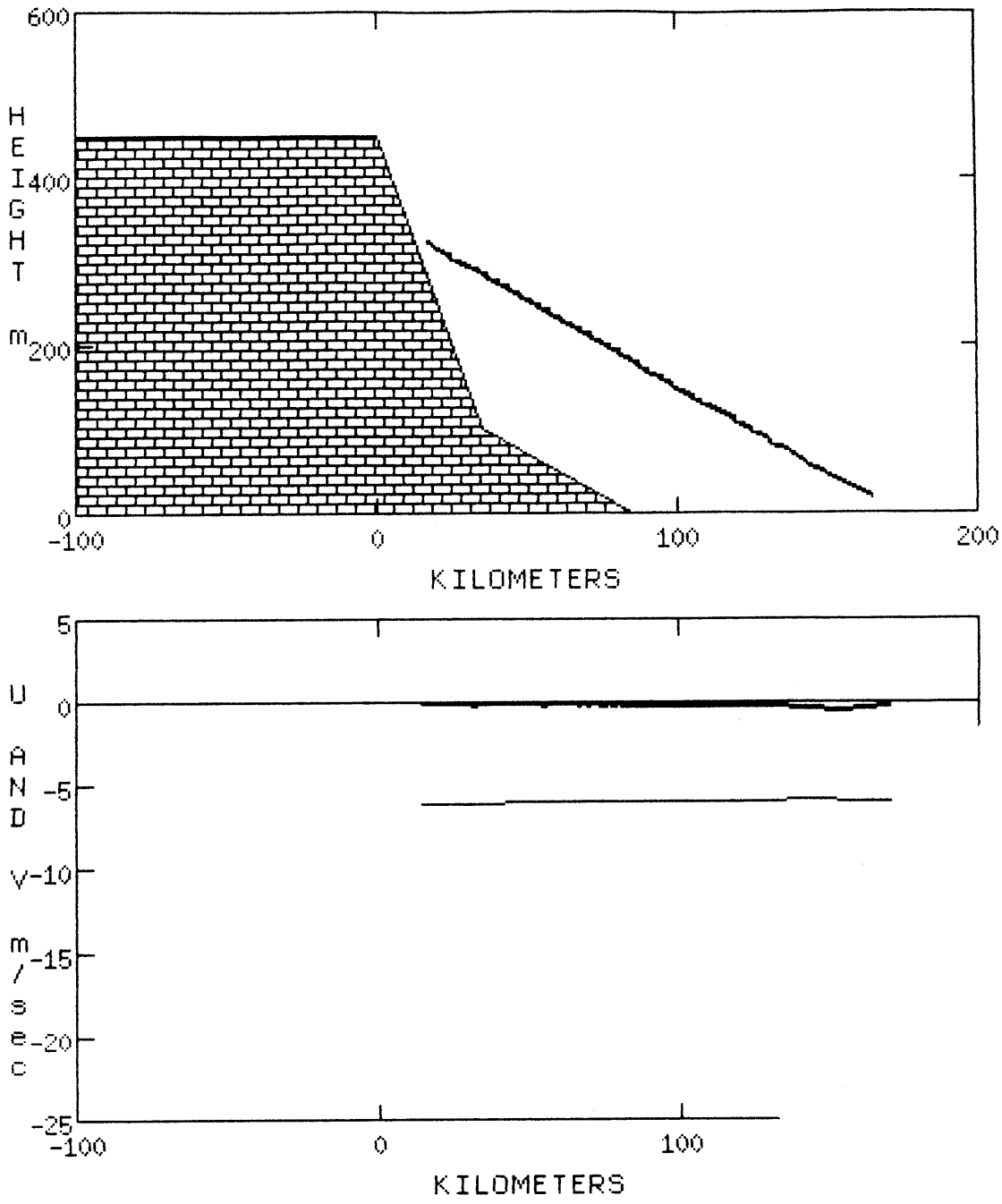

Fig. 4.14 As in Fig. 4.8, but with $C_d = 1.6 \times 10^{-4}\ s^{-1}$.

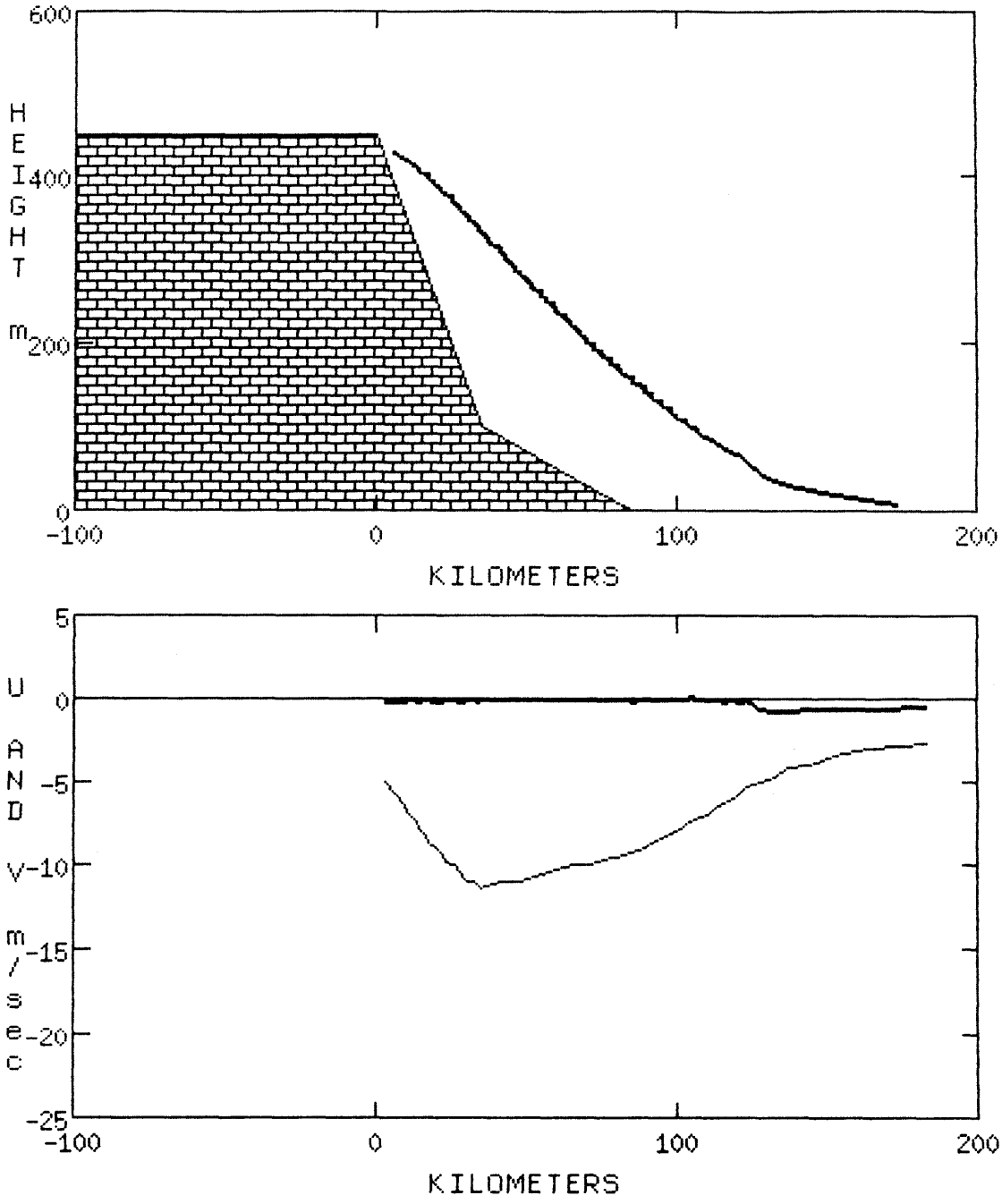

Fig. 4.15 As in Fig. 4.8, but with different friction parameterization, C_u= 1.8 x 10^{-3} (see text).

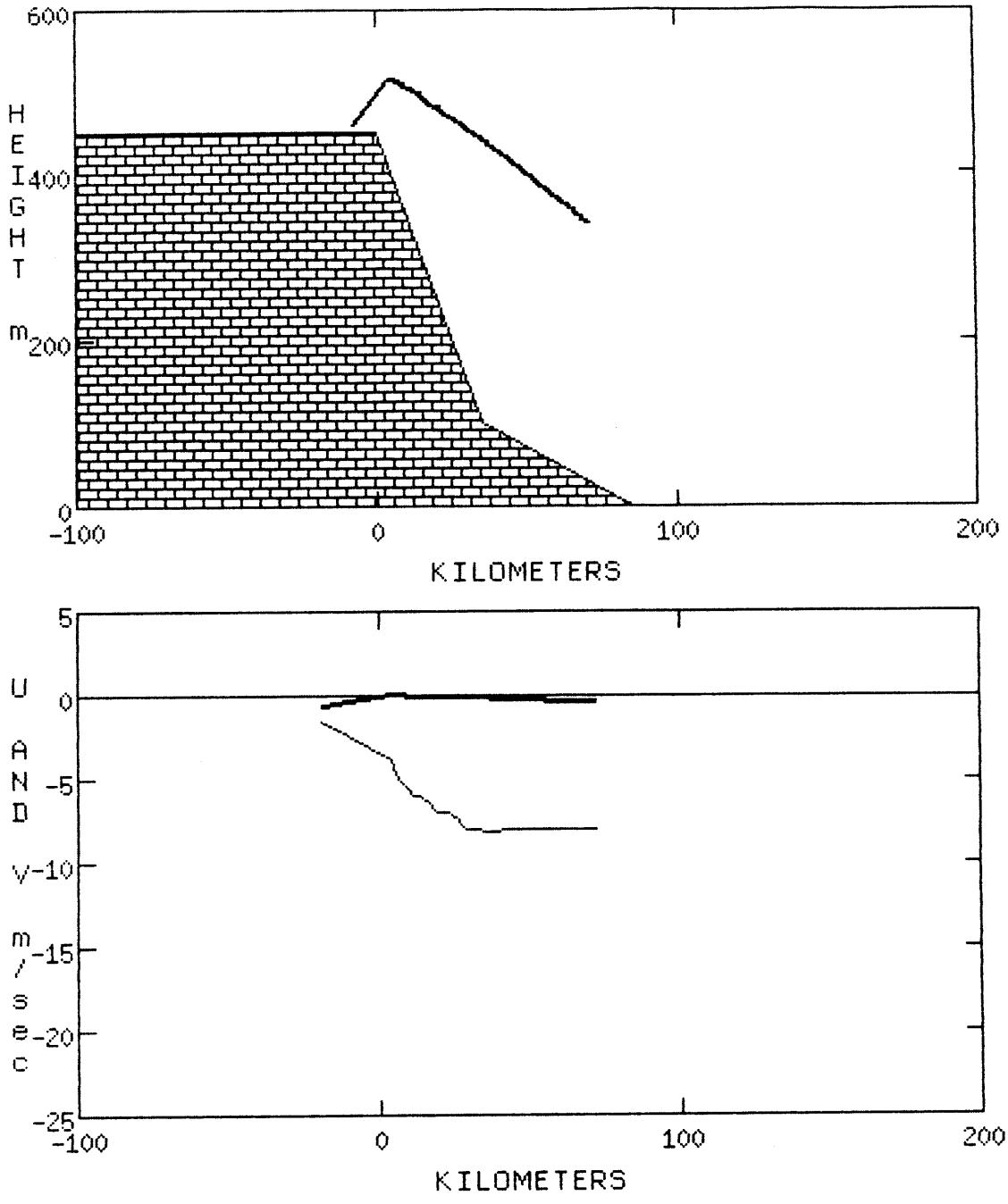

Fig. 4.16 As in Fig. 4.15, but with Cu = 5.0 x 10^{-3} and density current boundary condition (see text).

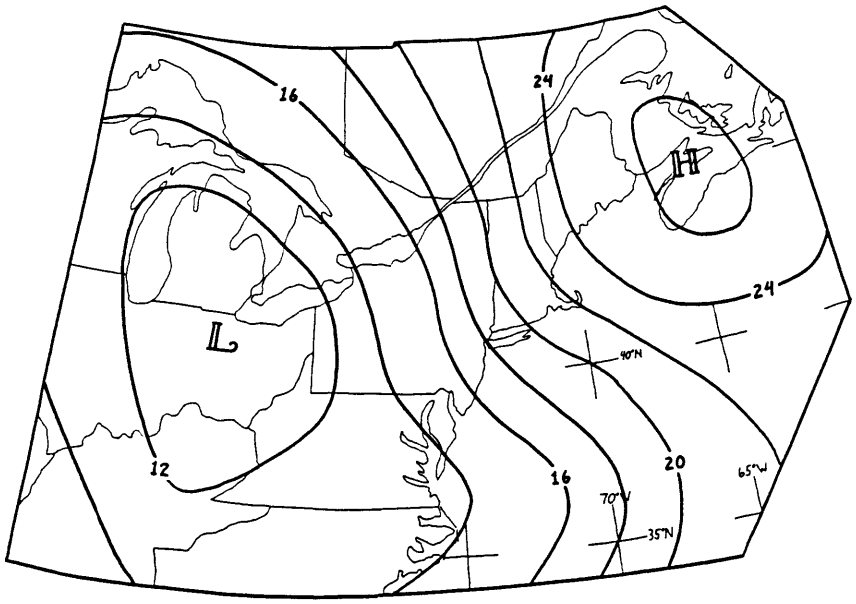

Fig. 5.1 Composite surface pressure at time of onset of coastal frontogenesis, redrawn from Bosart (1975).

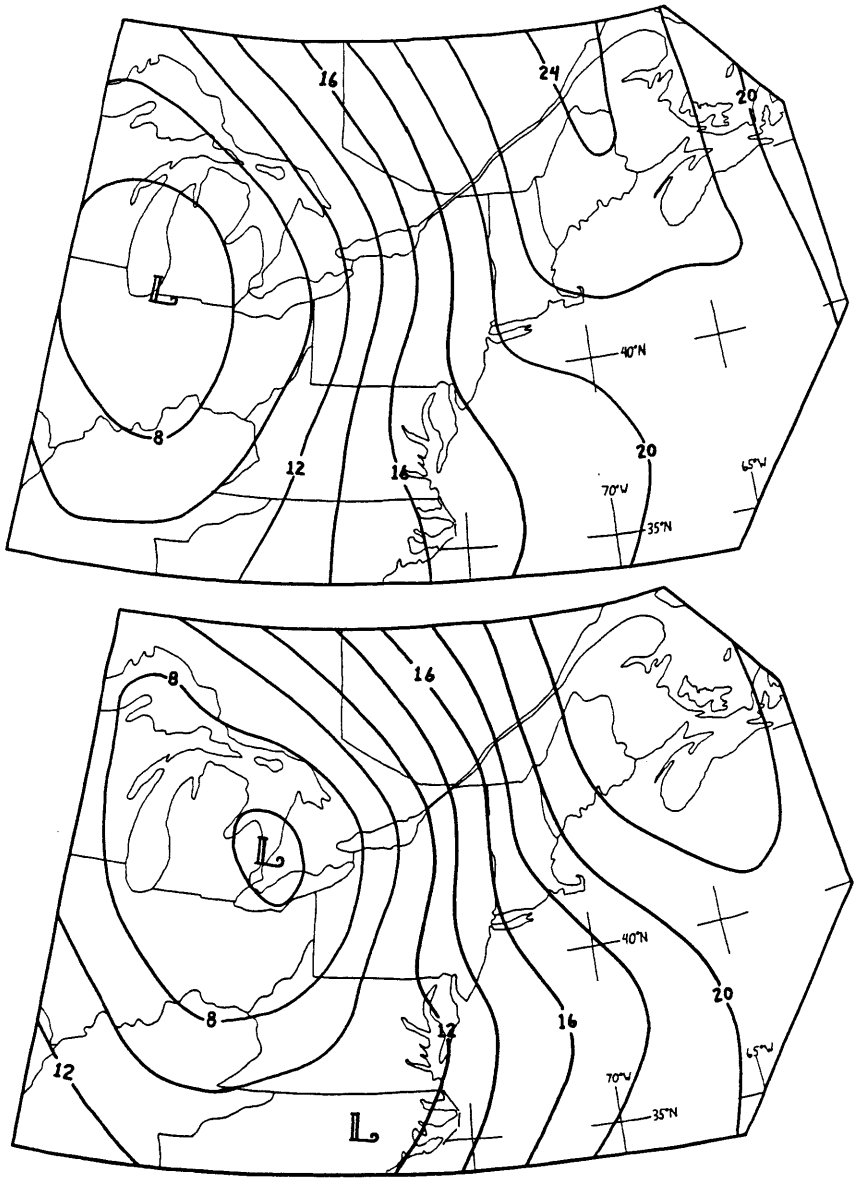

Fig. 5.2 Composite surface pressure analysis for 13 coastal front cases, Nov-Dec 1983. See text for details. a) 2-4 hours before onset of coastal frontogenesis b) 2-4 hours after coastal frontogenesis.

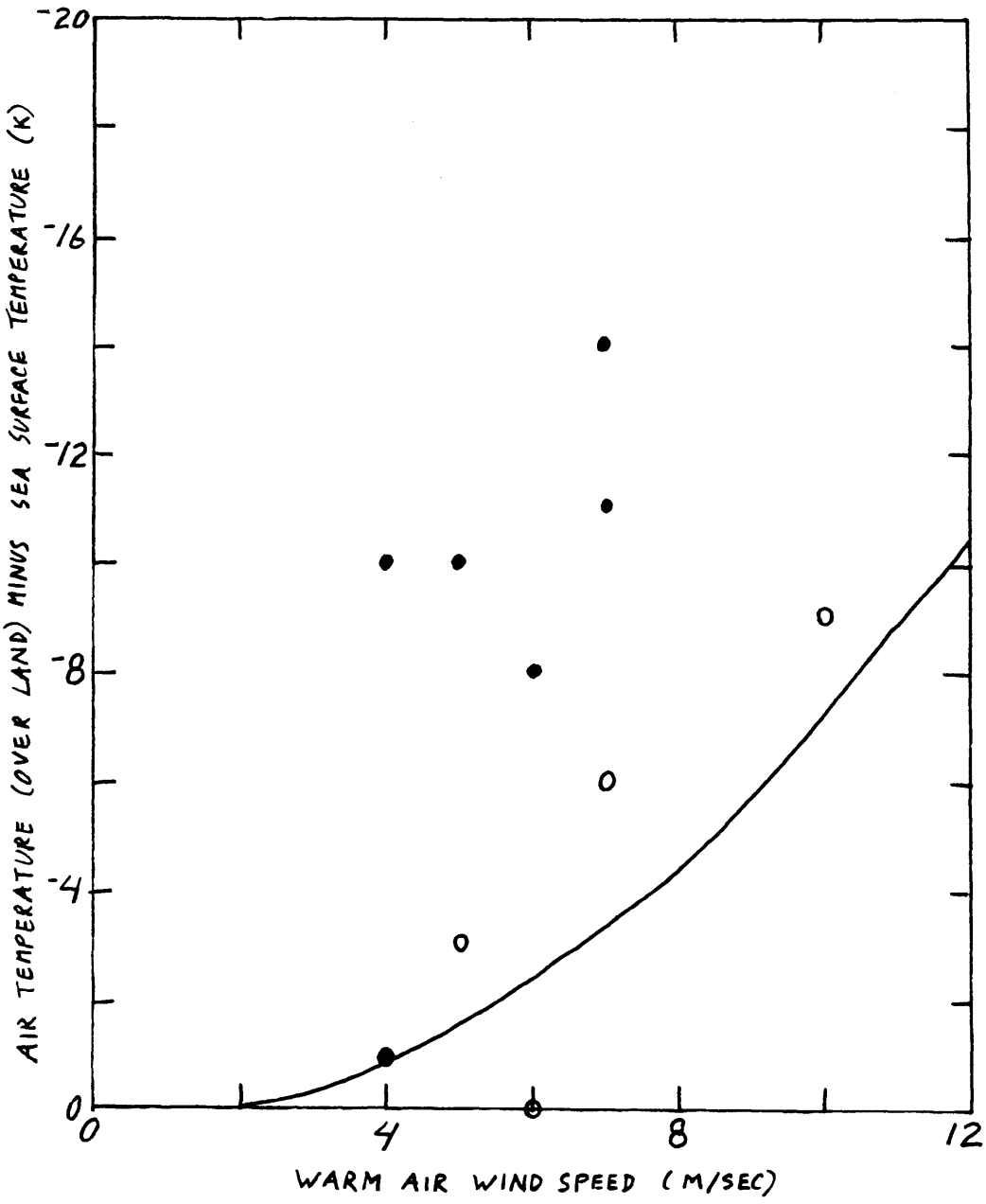

Fig. 5.3 Ridge passage events during NEWSEX as a function of wind speed over water and land-sea temperature contrast. Solid circles indicate events in which type A coastal fronts formed, open circles indicate events with no immediate coastal frontogenesis.

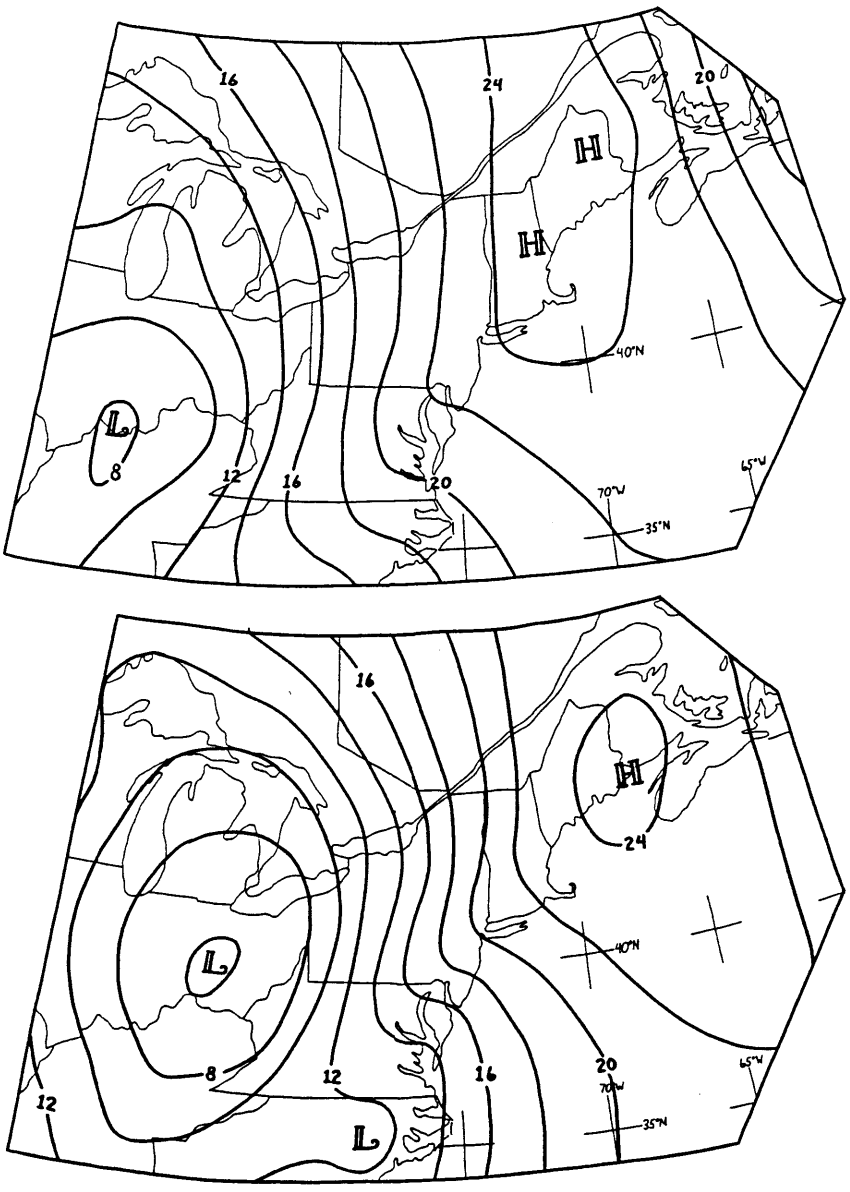

Fig. 5.4 As in Fig. 5.2, but for 6 type A coastal fronts only.

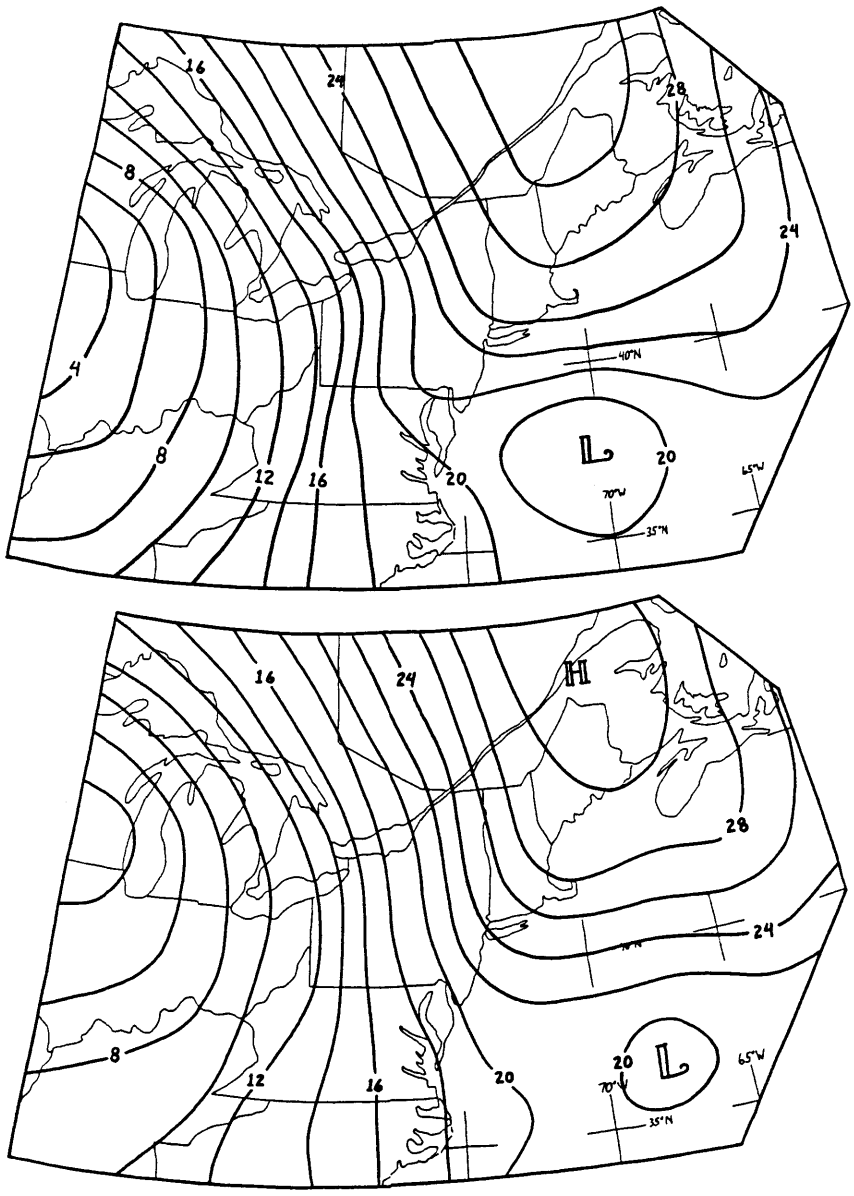

Fig. 5.5 As in Fig. 5.2, but for 3 type B coastal fronts only.

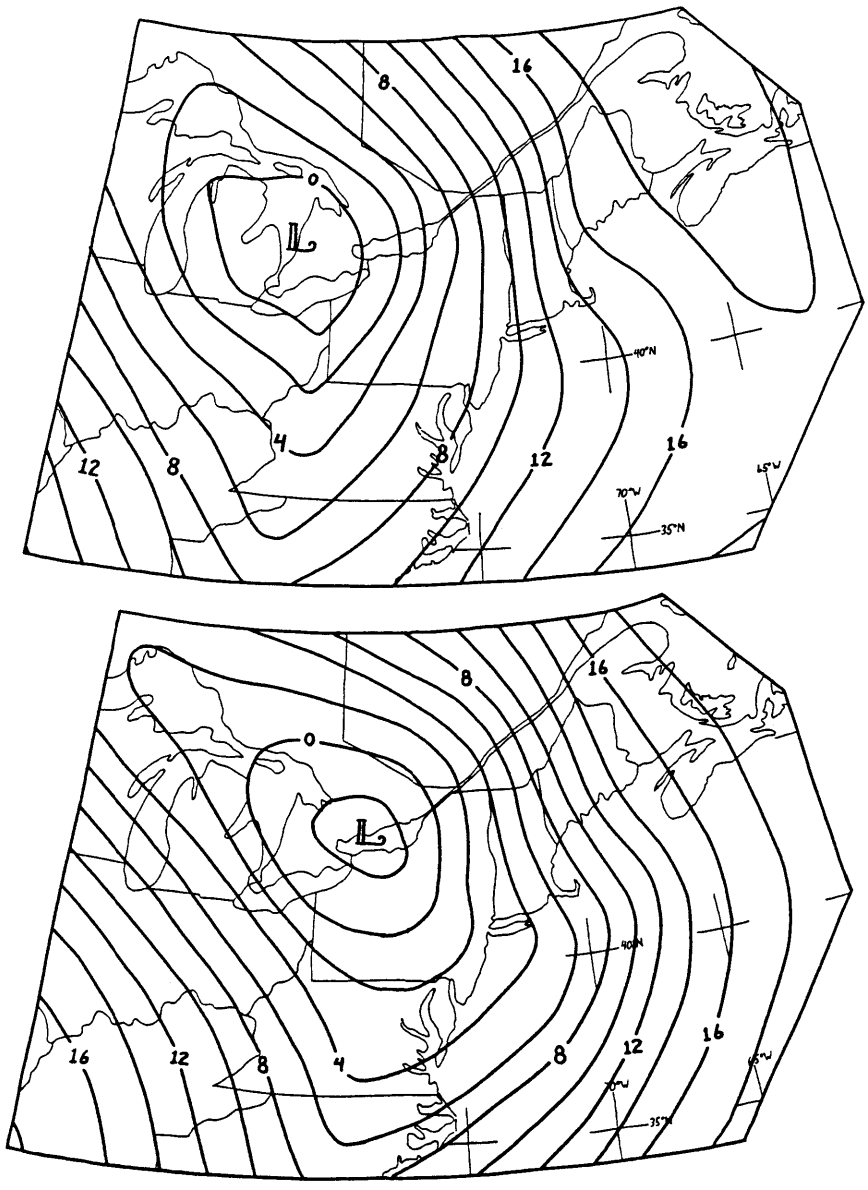

Fig. 5.6 As in Fig. 5.2, but for 4 type C coastal fronts only.

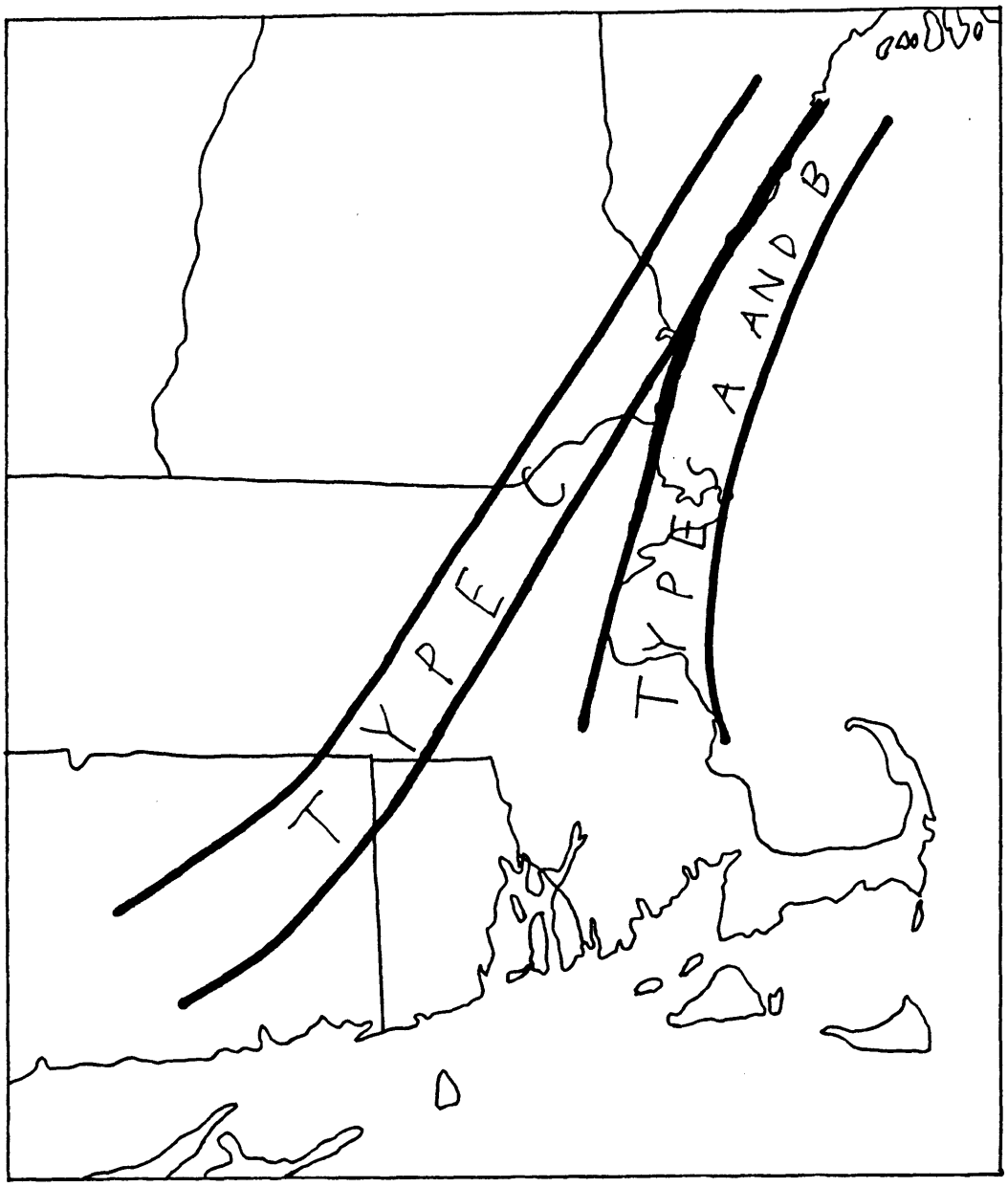

Fig. 5.7 Preferred locations for coastal frontogenesis observed during NEWSEX, stratified by type of frontogenesis.

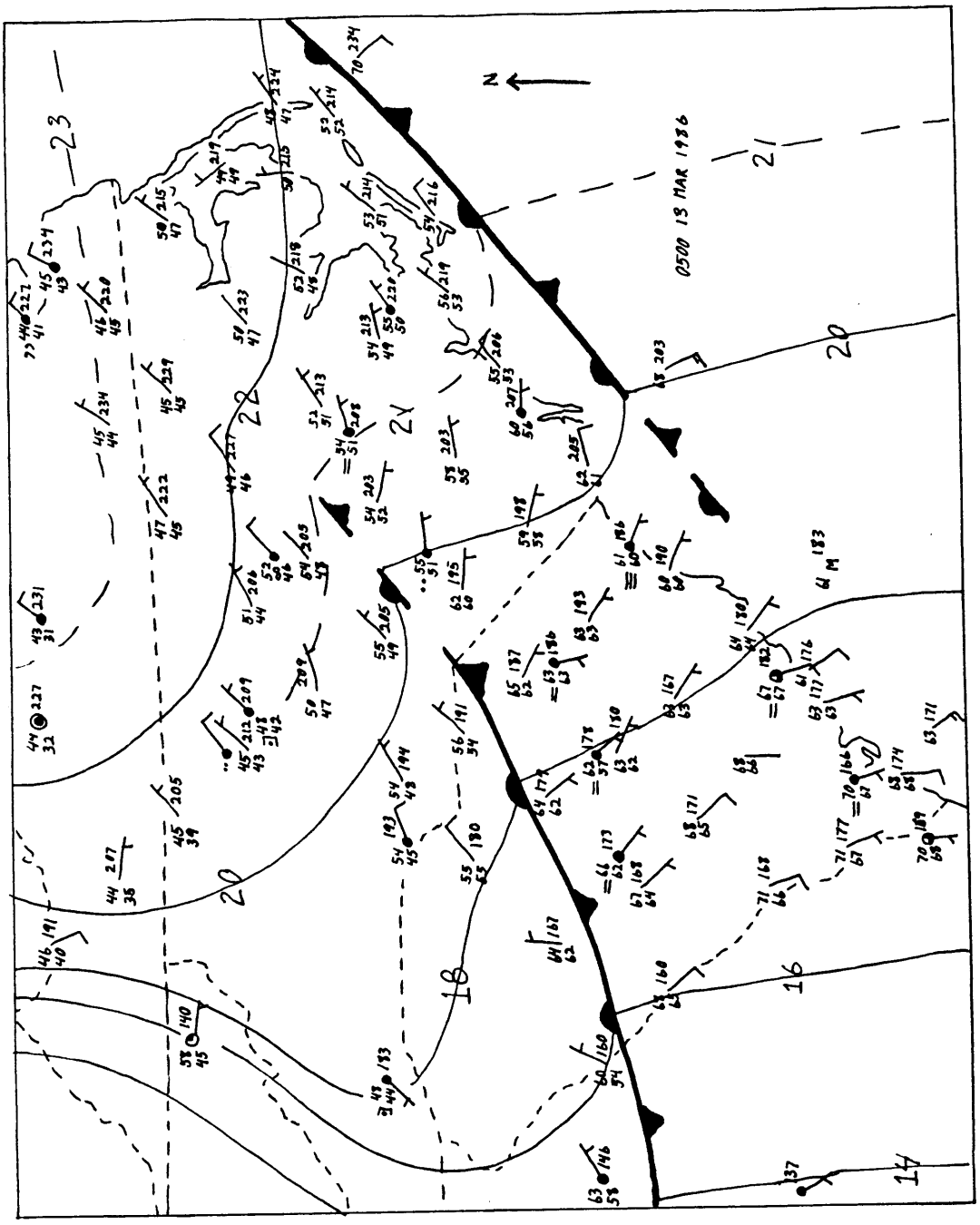

Fig. 6.1 Preliminary analysis of Carolinas, 0500 13 Mar 1986, showing simultaneous existence of two coastal fronts.